DESIGN, SYNTHESIS AND GAS ADSORPTION STUDY OF POROUS ORGANIC POLYMERS (POPS) AND COVALENT ORGANIC FRAMEWORKS (COFS) THROUGH DYNAMIC COVALENT CHEMISTRY

by

Youlong Zhu

B.S., Nanjing University, China, 2011

A thesis submitted to the

Faculty of the Graduate School of the

University of Colorado Boulder in partial fulfillment

of the requirement for the degree of

Doctor of Philosophy

Department of Chemistry and Biochemistry

2016

This thesis entitled:

Design, Synthesis and Gas Adsorption Study of Porous Organic Polymers (POPs) and Covalent Organic Frameworks (COFs) Through Dynamic Covalent Chemistry

written by Youlong Zhu

has been approved for the Department of Chemistry and Biochemistry

_____

(Wei Zhang, Ph.D.)

_____

(Douglas L. Gin, Ph.D.)

Date_____

The final copy of this thesis has been examined by the signatories, and we find that both the content and the form meet acceptable presentation standards of scholarly work in the above mentioned discipline.

Thesis Abstract

Zhu, Youlong

(Department of Chemistry and Biochemistry)

Design, Synthesis and Gas Adsorption Study of Porous Organic Polymers (POPs) and Covalent Organic Frameworks (COFs) Through Dynamic Covalent Chemistry

Thesis supervised by Prof. Dr. Wei Zhang

Porous organic polymers (POPs) as a new class of porous materials have received tremendous research interest in the past decade. POPs are constructed from lightweight elements through strong covalent bonds; as a result, they possess high specific surface area, porosity, high physiochemical stability, and tunable pore structure, etc. POPs have great potential for application in many different fields, such as gas adsorption, separation, heterogeneous catalysis, energy storage, chemical sensing, optoelectronics, etc. This thesis is mainly focused on the design, synthesis, and property study of POPs through different types of dynamic covalent chemical reactions, with a particular focus on investigating their application in gas adsorption and separation.

In chapter 1, the current development of POPs is reviewed. The classification of POPs, synthetic strategies, and their various potential applications will be discussed.

In chapter 2, the synthesis of a series of imine-linked porous polymer frameworks (PPFs) through dynamic imine condensation is reported. The resulting PPFs exhibit high specific surface area and high physical stability. Gas adsorption studies revealed that these types of materials have high H_2, CH_4, C_2H_2, and CO_2 adsorption capacity and high CO_2/N_2 adsorption selectivity, which can be used as potential gas storage and separation materials.

In chapter 3, porous poly (aryleneethynylene) networks (PAEs) were prepared through both reversible alkyne metathesis and irreversible Sonogashira cross coupling reactions. The PAEs prepared through dynamic alkyne metathesis consistently show higher surface area than those prepared through Sonogashira cross coupling, thus indicating the advantage of dynamic alkyne metathesis in the porous organic polymer synthesis.

In chapter 4, the photoresponsive azobenzene moiety was incorporated into POPs, and a series of photoresponsive POPs were synthesized. These photoresponsive POPs exhibit permanent porosity. Gas adsorption studies revealed that their pore size distribution and CO_2 adsorption behavior is responsive to the ultraviolet visible light (UV) irradiation, and the process is highly reversible even after a few cycles.

In chapter 5, the desymmetrized vertex design strategy was employed in the synthesis of covalent organic frameworks (COFs), which show an alternative heterogeneous hexagonal pore structure as expected. Both experimental data and theoretical models confirm the heterogeneous pore structure COFs. This new synthetic method will provide a new possibility for the synthesis of complicated COFs containing heterogeneous pore structures.

Chapter 6 describes the perspective and near future work based on the current research progress. The construction of COFs with heterogeneous pore structures from other aromatic building blocks is explored. Given the geometry of the building blocks used, COFs with up to three different pore sizes or alternating tetragonal and octagonal pores are expected. The synthesis and characterization of these COFs with new topology are currently being pursued.

DEDICATION

To my family

Acknowledgments

First and foremost, I would like to express my deepest gratitude to my thesis advisor, Professor Wei Zhang, for his guidance in the past five years. I could not have made this journey without his suggestive advice, continuing support, and consistent encouragement. His passion and creativity in chemistry laid the foundation for me how to be a good chemist. What's more, his advising, mentorship, and friendship penetrate into both my chemical research and daily life, inspiring me to be a better chemist as well as a better person.

I would also like to acknowledge all my thesis committee members, -Professor Douglas Gin, Professor David Walba, Professor Garret Miyake from the department of chemistry & biochemistry, and Dr. Hai Long from the National Renewable Energy Laboratory (NREL)-for their insightful contributions. Their helpful suggestions and insights make my dissertation better. In addition, Professor Douglas Gin, Professor Richard Noble, and Professor Steven George served as my oral examination committee. I thank them all for their help.

None of this work would have been possible without the support and help of the Zhang's group members, both past and present. In particular, I would thank Dr. Yinghua (Alice) Jin for helping me to run organic reactions, purify compounds using flashing chromatography columns, and write manuscripts. During the past five years, I learned a lot from other group members. We shared ideas in chemistry, solved challenging problems in research, and more importantly, they help me to become a better chemist and a better person as well. So I thank Dr. Yinghua Jin, Dr. Haishen Yang, Dr. Ya Du, Dr. Jyothish Kuthanapillil, Dr. Chenxi Zhang, Dr. Qi Wang, Dr. Chao Yu, Dr. Philip Taynton, Dr. Kenji Okochi, Dr. Guolong Lu, Prof. Huagang Ni, Prof. Dazhi Tan, Ryan Denman, Ryan McCraffrey, Michael Ortiz, Chengpu Zhu, Yu Gong, Lili Tan, Xinyu Hu,

Kun Xu, David Tran, Shouhong Fan, Setareh Azarnoush, Gun Su Han, Devon Trahan, Qian Feng, Yuliang Liu and Alice Hearn for their support.

I am so lucky that I have a lot of great collaborators. They helped me with the research a lot and made my research into a higher level. Particularly, I would thank Prof. Richard Shoemaker from the department of chemistry and biochemistry for his help with solid state NMR characterization of the porous organic materials. I would also thank Dr. Hai Long from the National Renewable Energy Laboratory and Dr. Shun Wan from *Storagenergy Technologies, Inc.* They helped me to optimize the geometry structure and simulation of the porous organic polymers and covalent organic frameworks. The research in chapter 3 would not have been possible without the assistance of Dr. Haishen Yang from the Zhang group. He helped me find stable and efficient catalysts for the synthesis of porous poly (aryleneethynylene) networks through dynamic alkyne metathesis. Dr. Guolong Lu did a lot of electrochemical characterizations for our materials as well, I thank him for his kind help.

From the other side of Pacific Ocean, my parents and younger brother have always supported me in pursuing my dreams. I would not have got my Ph.D. without their unyielding support.

I would also thank the financial support from the National Science Foundation (NSF), MAST center. In particular, I would also thank the Eugene H. Hoffman fellowship from the department of chemistry and biochemistry for partial financial support in the summer of 2014. And I would also like to thank the travel grants from the UGGS and graduate school at the University of Colorado Boulder for the support of my 251st ACS national meeting.

Contents

List of Tables

List of Figures

List of Schemes

CHAPTER 1

Introduction to Porous Organic Polymers (POPs) and Their Potential Applications

1.1. Introduction

Porous organic polymers (POPs) are an emerging class of porous organic materials with unprecedented structure and properties that have received considerable research interest in the past decade.[1-3] Given their porosity, tunable pore structure, high stability, structure diversity and ease of functionalization, POPs have great potential applications in gas adsorption[4-6], separation[7,8], heterogeneous catalysis[9,10], chemical sensing[11], optoelectronics[12], proton and ion conduction[13-15], etc. In general, POPs include crystalline covalent organic frameworks (COFs)[16-18], covalent triazine frameworks (CTFs)[19,20] and amorphous polymers of intrinsic microporosity (PIMs)[21,22], conjugated microporous polymers (CMPs)[23-28], hyper cross-linked polymers (HCPs)[29], porous aromatic frameworks (PAFs)[30-34], porous polymer networks (PPNs)[6,35-38], microporous organic polymers (MOPs)[4,5], and so on. POPs are constructed through strong covalent bonds between lightweight elements, such as H, B, C, N, O, etc., which gives them low density and high physical and chemical stability. In addition, they possess high specific surface areas, ranging from a few hundred square meters per gram to a few thousand square meters per gram; the highest surface area reported for POPs exceeds 6400 m^2 g^{-1} by Zhou *et al.*[6] in 2011. They also possess micro- or meso- pore structures and large pore volumes, which make them ideal materials for gas storage as well as heterogeneous catalysis. Moreover, there are a variety of organic building blocks and chemical reactions that can be used for the construction of POPs, and these building blocks can also be further functionalized to make POP structures even more diverse.

1.2. Classifications and structure properties

According to their morphology, POPs can be classified as crystalline or amorphous. Crystalline POPs are structurally more ordered and the pore size is more uniform. However, amorphous POPs are much more common than crystalline POPs. The synthesis of amorphous POPs is much easier since the crystallization process for the preparation of highly ordered crystalline POPs is very difficult. Crystalline POPs are generally synthesized from building blocks with high symmetry, while the selection of building blocks for the synthesis of amorphous POPs is more diverse.

1.2.1. Amorphous POPs

Most of the POPs reported are amorphous since the crystallization process is challenging. There are many different types of amorphous POPs, such as PIMs, CMPs, PAFs, PPNs, MOPs, etc. The diversity of amorphous POPs derives from abundant organic building blocks and a large number of chemical reactions available for synthesis of amorphous POPs. Amorphous POPs play an important role in the development of porous materials as well as functional materials design. Tremendous efforts have been devoted to the design and synthesis of amorphous POPs for various applications, especially on gas adsorption/separation, and heterogeneous catalysis.

1.2.1.1 Polymer of intrinsic microporosity (PIMs)

PIMs are derived from soluble polymers through inefficient packing. Since their building blocks have randomly contorted shapes, they can prevent the efficient packing between polymer chains, by creating voids and pores inside the polymer, as reported by McKeown *et al*[21,39]. The structure of PIMs generally comprises the spirobisindane based catechol derivatives or other non-planar catechols and different linkers. The spiro-center has a sp^3 hybridized carbon, which

provides the nonlinear shape, and the fused ring structure controls the required rigidity. The design strategy creates inefficient packing, and generates pores inside the polymers. Later, the spiro-center was extended to other rigid molecules, as shown in Figures 1.2 and 1.3[40]. These types PIMs have relatively high specific surface, in the range of 500-1000 m^2 g^{-1}. Since PIMs are soluble polymers and easy to fabricate, they can be used as membrane for gas separation, heterogeneous catalysis, adsorption of organic molecules, etc.

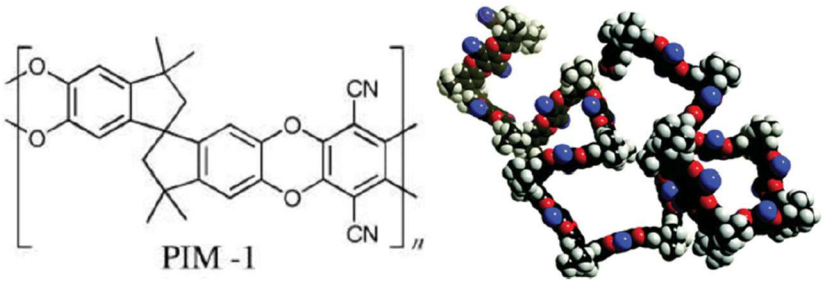

Figure 1.1. Chemical structure and modeling of PIM-1 (Reprinted with permission from Ref. 21. Copyright (2004) Royal Society of Chemistry.)

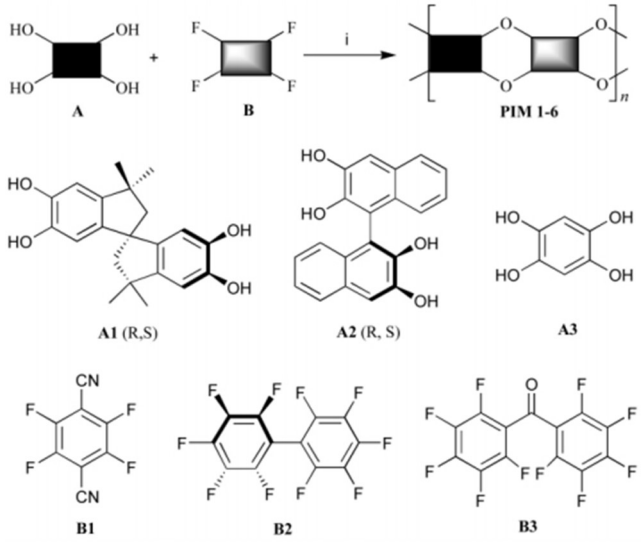

Figure 1.2. Building blocks and synthesis of PIMs **1-6**.

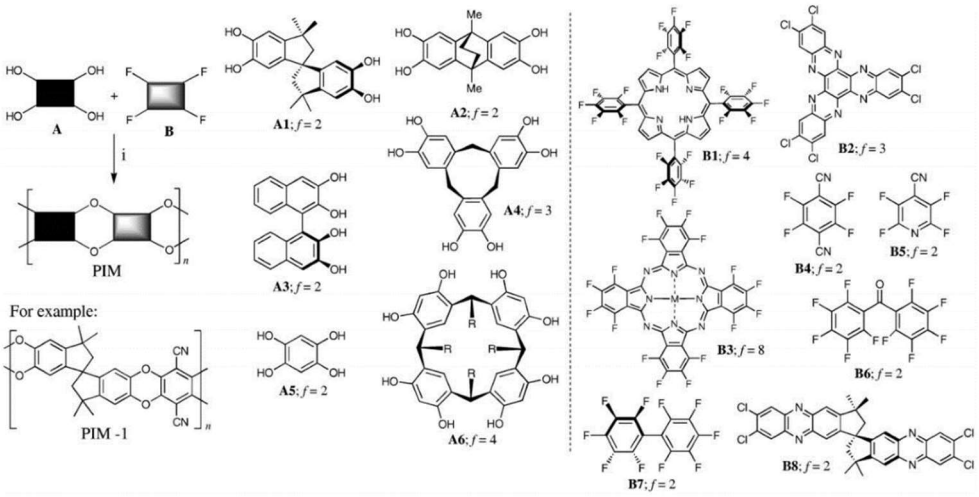

Figure 1.3. Building blocks for the synthesis of PIMs.

1.2.1.2. Conjugated microporous polymers (CMPs)

CMPs are a class of materials with unique properties, such as extended conjugation and microporosity. There is a huge diversity for the synthesis of CMPs which offer topological control of their structure and properties. Cooper *et al.*[23,27] reported a series of CMPs and investigated their porosity and gas adsorption properties. These CMPs are connected through aromatic rings and triple bonds, which can extend the conjugation of the system. Figure 1.4 shows some typical structures for the CMPs. CMPs can be used as gas adsorption materials, by incorporating functional groups into the CMPs. They can also be used for gas separation [41] and heterogeneous catalysis[42]. In addition, considering their conjugation nature, they can also be considered as semiconducting materials.

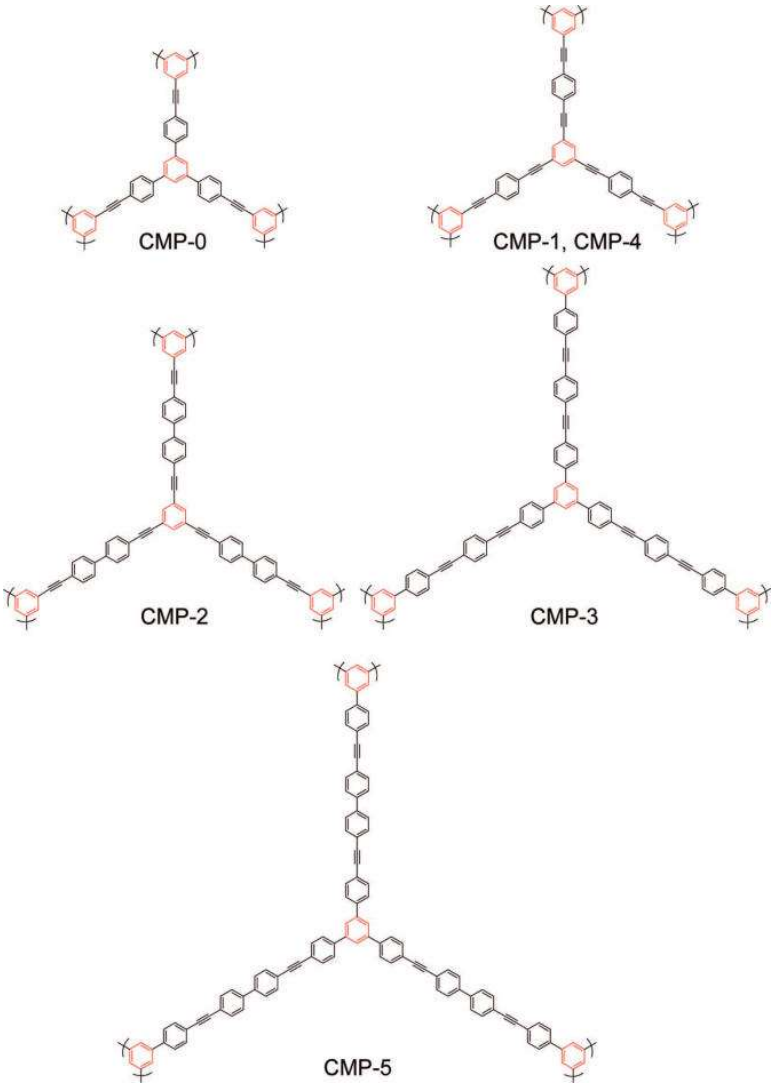

Figure 1.4. Typical structures of CMP series. (Reprinted with permission from Ref. 27. Copyright (2008) American Chemical Society.)

1.2.1.3. Porous Aromatic Frameworks (PAFs)

Porous aromatic frameworks are porous polymers connected by aromatic rings. In 2009, Qiu and Zhu *et al.*[30] reported the first example of PAFs. They used tetrakis(4-bromo-phenyl)methane as the building block to construct a diamond type PAF-1 through nickel(II) catalyzed Yamamoto Ullman cross coupling reaction. The resulting PAF exhibited an exceptional high specific surface

area, up to 5640 m^2g^{-1}, and high adsorption capacity for hydrogen, methane and carbon dioxide. More importantly, PAF-1 has exceptional physiochemical stability, and it doesn't decompose until 400 °C. Later, various building blocks have been utilized in 2D and 3D PAFs synthesis, as shown in Figure 1.5[31,43,44]. More recently, a large number of PAFs have been reported, and they have been used in gas storage, heterogeneous catalysis, etc.

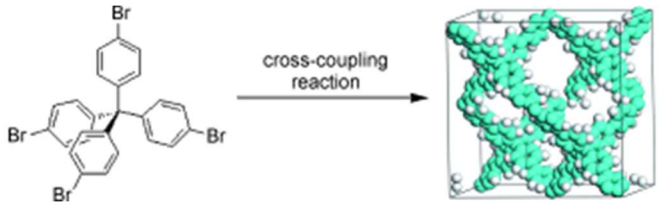

Figure 1.5. Synthesis and structure of PAF-1. (Reprinted with permission from Ref. 34. Copyright (2010) John Wiley & Sons, Inc.)

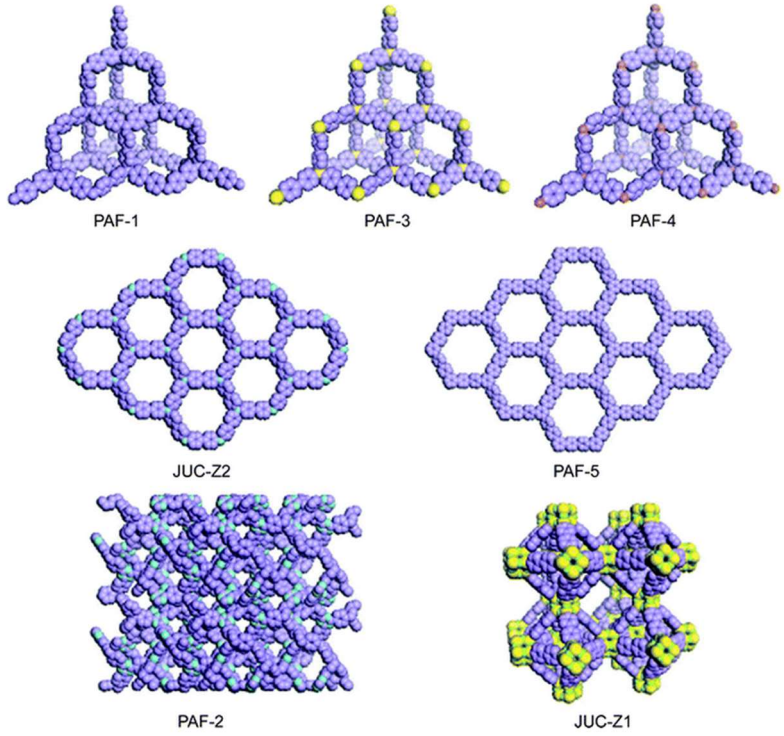

Figure 1.6. Structure model of synthesized and simulated PAF series. (Reprinted with permission from Ref. 42. Copyright (2011) Royal Society of Chemistry.)

1.2.2. Crystalline POPs

Crystalline POPs are not as common as amorphous ones since the synthesis of crystalline POPs is much more challenging and the selection of building blocks is limited. The synthesis of crystalline POPs usually requires highly symmetric building blocks, reversible chemical reactions, and a relatively slow crystallization process, thus making only a few reversible chemical reactions good candidates, such as imine condensation/metathesis, boronic acid self-condensation, and boronic acid-diol condensation. In addition, the material synthesis usually requires rigid and symmetric building blocks. The advantage of these types of reversible reactions would allow "error-correction" during the reaction, which can form more ordered and thermodynamically stable materials. In recent years, quite a few examples of crystalline POPs have been reported, such as COFs and CTFs, which have long-range order with regular and uniform pore structures.

1.2.2.1. Covalent organic frameworks (COFs)

COFs are the first examples of crystalline porous organic polymers and were first reported by Yaghi *et al.* in 2005[16]. They used phenyl diboronic acid as the building blocks, under solvothermal conditions. Through the acid catalyzed trimerization reaction, they are able to get crystalline materials COF-1 connected through boroxine. In addition, they also reported COF-5 prepared through the co-condensation of phenyl diboronic acid and hexahydroxytriphenylene. Gas adsorption studies showed both COF-1 and COF-5 have permanent porosity, the BET surface areas are up to 1670 m^2 g^{-1}. Powder X-Ray diffraction experiment revealed both materials have strong signals in the small angle range. Using the computer modeling, they are able to simulate the topological structure and the simulated PXRD derived from the models matched well with the experimental one. In 2007, they also reported the first example of 3D

COFs[17] by co-condensation reactions of tetrahedral tetra(4-dihydroxyborylphenyl) methane or tetra(4-dihydroxyborylphenyl) silane and triangular 2,3,6,7,10,11-hexahydroxytriphenylene. Compared to the 2D COFs, 3D COFs have much higher BET surface areas, which can reach up to 4000 m^2 g^{-1}. Since these materials are constructed entirely through covalent bonds, they have high thermal stabilities. In 2009, they also reported an example of imine linked COFs[45] by using a tetrahedral shaped amine and linear dialdehyde. The resulting COFs have diamond type topology and have permanent porosity. Compared to the boroxine and borate ester, the imine linked COFs are more stable. Given their high porosity and BET surface areas, COFs are widely used as gas adsorption and separation materials. In addition, considering their structure properties and long range order, they are also employed as semiconducting materials, optoelectronic materials, etc.

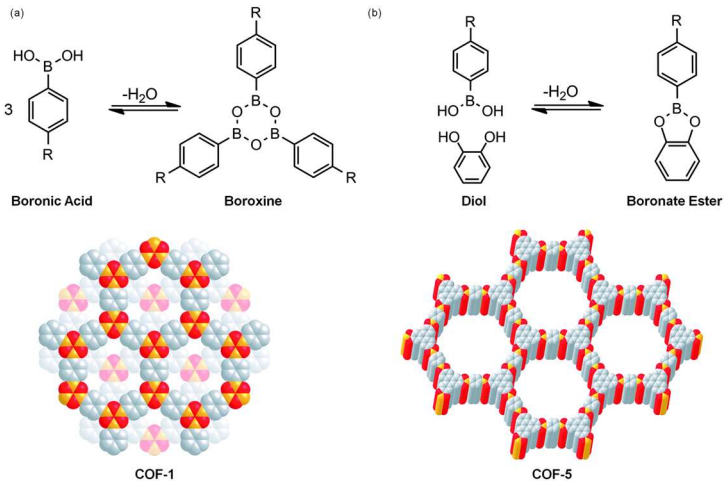

Figure 1.7. Condensation reactions and structure of COF-1 and COF-5. (Reprinted with permission from Ref. 16. Copyright (2005) American Association for the Advancement of Science.)

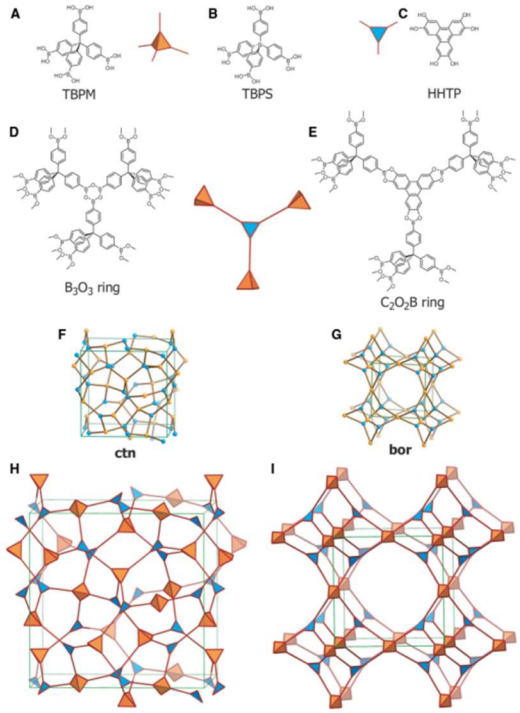

Figure 1.8. Building blocks for the constructions of 3D COFs and the topological structures. (Reprinted with permission from Ref. 17. Copyright (2007) American Association for the Advancement of Science.)

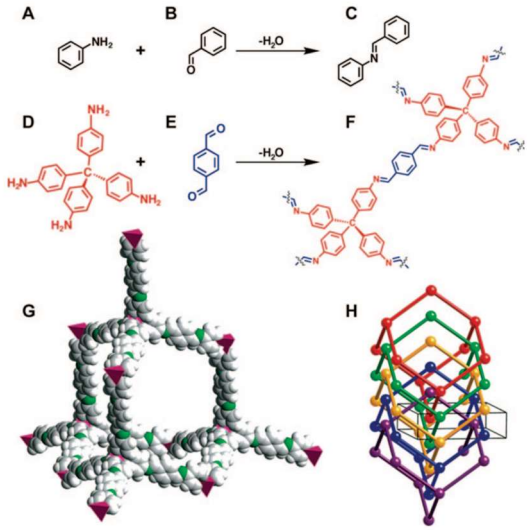

Figure 1.9. Structure of imine-linked COFs. (Reprinted with permission from Ref. 44. Copyright (2009) American Chemical Society.)

Until now, the COFs reported are basically polycrystalline or microcrystalline powders, there is also a single crystal structure reported by Wuest *et al.*[46]. They used tetranitroso based monomers through dimerization to grow single crystals. The resulting crystals show a diamondoid topological structure. This is the only example of single crystal COFs reported. Although the structure is not very stable, it represents a milestone toward constructing single crystal COFs.

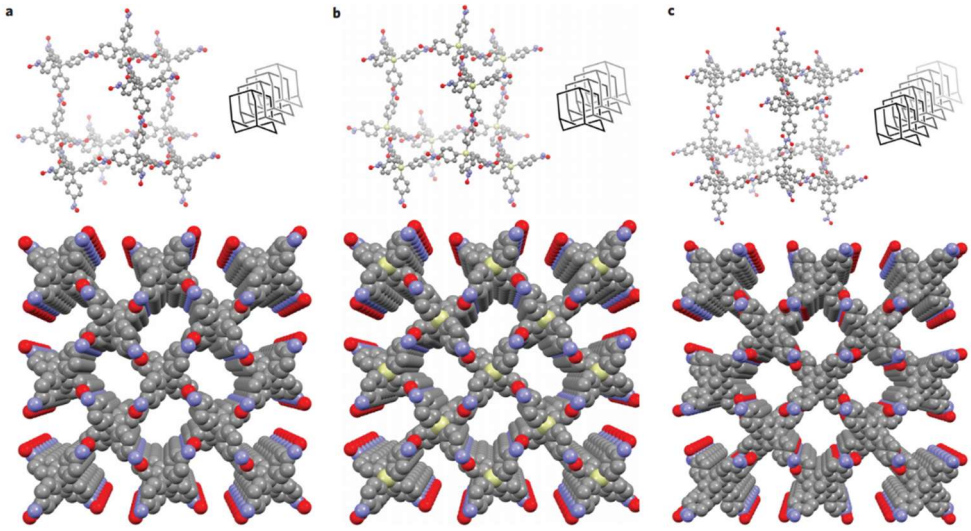

Figure 1.10. Representations of the structures of crystals of covalent organic networks NPN-1, NPN-2 and NPN-3. (Reprinted with permission from Ref. 45. Copyright (2013) Nature Publishing Group.)

1.2.2.2. Covalent triazine frameworks (CTFs)

The cyano group can undergo trimerization in molten $ZnCl_2$ and form oligomers and frameworks. Molten $ZnCl_2$ can act as both solvent and catalyst, this type of reaction usually requires high temperature (400-700 °C). By using this chemical reaction, Thomas *et al.*[19] reported a series of CTFs by using di- or tri-cyano based small building blocks. These types of CTFs usually display good crystallinity and permanent porosity. The BET surface area can

exceed 3000 m^2 g^{-1}, thus making them promising gas adsorption materials. Since this reaction doesn't require precious metal catalysts, it makes them appealing to scale up. CTFs are connected through strong triazine moieties, which make them physiochemically stable. They can be used for gas adsorption and separation. More recently, they are also explored as heterogeneous catalysts[47] and fluorescent materials[48].

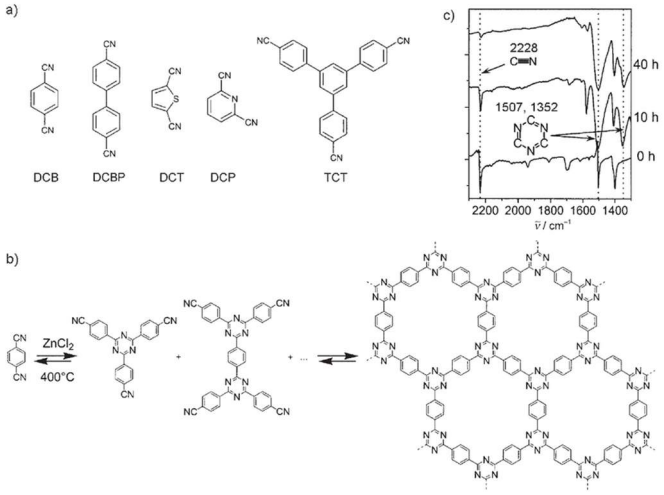

Figure 1.11. (a) Cyano based building blocks; (b) synthesis of triazine frameworks; (c) IR spectra of CTFs showing the formation of triazine ring. (Reprinted with permission from Ref. 19. Copyright (2008) John Wiley & Sons, Inc.)

1.3. Synthesis

POPs are synthesized through both irreversible covalent bond formation and reversible dynamic covalent chemistry. Generally, amorphous POPs can be synthesized by both irreversible and reversible reactions; however, synthetic approaches for crystalline POPs are basically limited to reversible chemical reactions. A variety of chemical reactions have been used for the preparation of POPs, such as acid catalyzed imine condensation, transition metal catalyzed Suzuki coupling, Sonogashira coupling, alkyne metathesis, etc., Figure 1.12 gives the summary

of chemical reactions used for the synthesis of POPs. Controlling the reaction thermodynamics and kinetics is the key to forming highly porous organic materials. In particular, the reaction conditions such as temperature, solvent combination/polarity, catalysts loading and reaction time should also be taken into consideration for the formation of stable POPs. Most of the POPs are synthesized in traditional solution reactions, in which monomers are mixed with solvents and catalysts, and reacted for a certain time (a few hours to few days) to form POPs. For synthesis of crystalline POPs, the synthetic conditions are more important, and in order to form ordered POPs, the kinetics should be well controlled. The classical method to synthesize crystalline POPs is the solvothermal reaction, in which the reaction is run under certain temperatures in sealed tubes. Recently, many other synthetic methods have also been developed for the synthesis of POPs, such as microwave synthesis[48-51], mechanical chemical synthesis[52], etc.

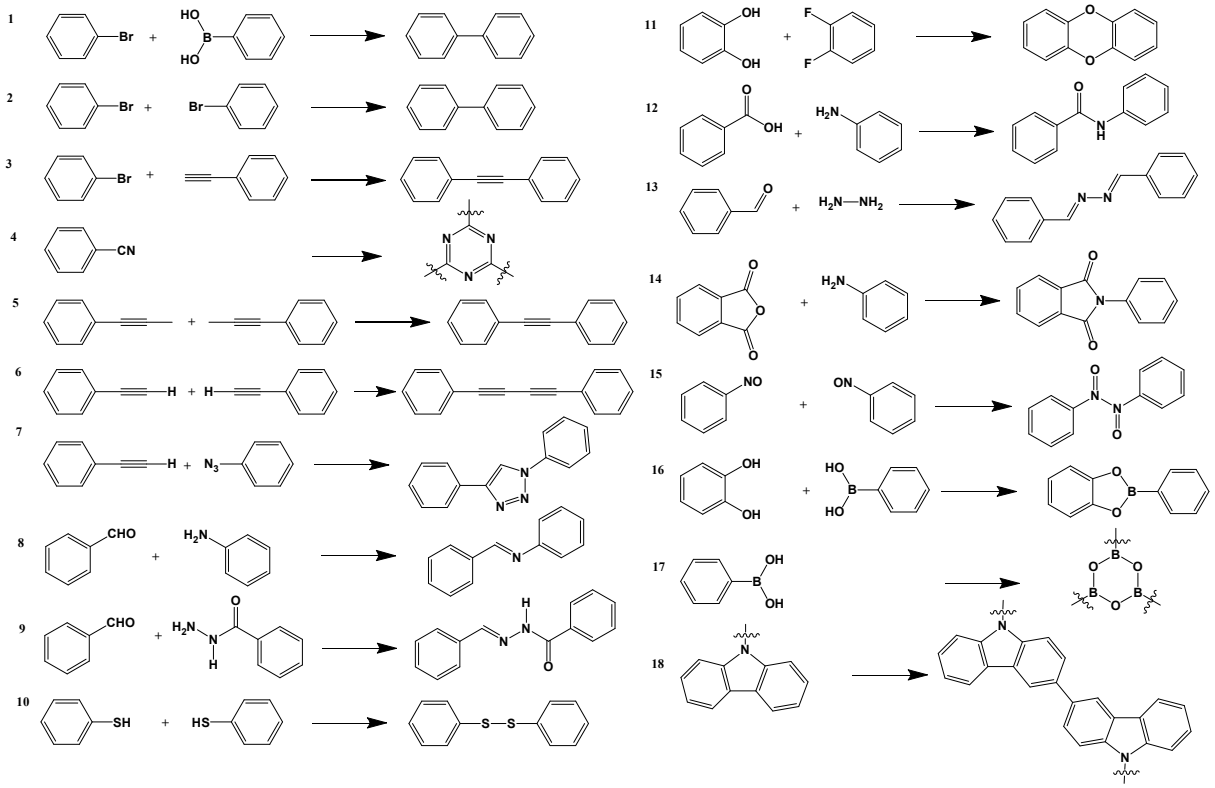

Figure 1.12. Summary of chemical reactions utilized to form POPs.

The diversity of POPs is not only derived from the chemical reactions to synthesize them, but also from many synthetic strategies to functionalize them. In general, there are two approaches to incorporate functional groups into the frameworks, which are "post-functionalization" and "bottom up" synthesis. As shown in Figure 1.13, in post synthesis strategy, the functional groups were introduced after the POPs were synthesized, while in bottom up synthesis, functional groups were introduced into the starting building blocks, then the POPs were synthesized using these functional building blocks. Both synthetic strategies allow the synthesis of POPs for advanced applications.

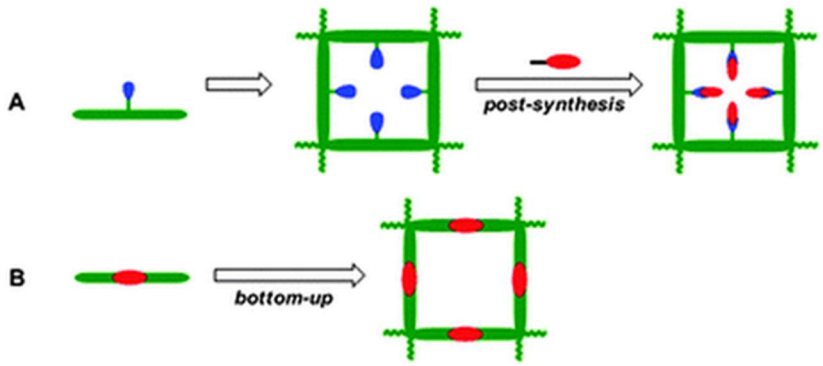

Figure 1.13. Bottom up synthesis and post functionalization strategies to introduce functional groups into POPs. (Reprinted with permission from book chapter "Porous Organic Frameworks" Copyright (2015) John Wiley & Sons, Inc.)

1.4. Applications

1.4.1. Gas adsorption and separation

Due to their ultra-high specific surface area, porosity and tunable pore structures, POPs are widely considered as gas storage and separation materials. They have been mainly used for storage of energy gas such as H_2, CH_4, C_2H_2, capture of greenhouse gas CO_2, and CO_2/N_2

separation. They can also be used as absorbent for small hydrocarbons, organic vapors, organic dyes, etc.

1.4.1.2. Hydrogen storage

Hydrogen gas (H_2) is proposed as an alternative to traditional fossil fuels due to its high energy density and zero pollution since it only generates water during combustion. However, large-scale storage and transportation of hydrogen remains a challenge since both the boiling point and molecular weight of hydrogen gas are low. Therefore, development of a safe and reliable method for the storage of hydrogen gas at ambient conditions is desired. One strategy is using physisorption. POPs with high specific surface areas have been investigated for hydrogen storage. They can uptake and release hydrogen gas very quickly, and are also safe for storage application. A variety of POPs have been reported as hydrogen storage materials, both at atmosphere pressure and at high pressure. Although tremendous progress has been made in this area, it is still a challenge to synthesize high storage capacity materials for hydrogen storage. **Table 1.1** lists the capacities of hydrogen gas storage of POPs.

Table 1.1. Hydrogen gas storage capacities in POPs.

Materials	S_{BET} (m^2/g)	P (bar)	T (K)	H_2 wt %	References
PIM-1	850	1	77	0.95	[53]
PAF-1	5640	1	77	1.66	[30]
PAF-3	2932	1	77	2.07	[31]
PAF-4	2246	1	77	1.5	[31]
PAF-1-Li	479	1	77	2.79	[54]
CMP-1	834	1	77	1.14	[27]

CMP-2	634	1	77	092	[27]
COF-1	750	1	77	1.46	[55]
COF-5	1670	35	77	3.54	[55]
COF-8	1350	35	77	3.46	[55]
COF-10	1760	35	77	3.88	[55]
COF-102	3620	35	77	7.24	[55]
COF-103	3530	35	77	7.05	[55]
CPOP-1	2220	1	77	2.8	[7]
EOF-1	780	1	77	0.94	[56]
POP-1	1031	1	77	2.78	[57]
PPN-4	6461	55	77	9.1	[6]
PPF-1	1740	1	77	2.75	[58]
PPF-2	1470	1	77	2.28	[58]
ICOF-1	1258	1	77	3.11	[15]

1.4.1.2. Methane storage

Besides hydrogen gas, methane is also considered as a rising star for clean energy with a relatively high energy density of 15.5 $kW \cdot h \cdot kg^{-1}$. Methane generally comes from natural gas, is available in large quantities, and is also environmentally preferable to other fossil fuels because it generates less emissions. For large scale usage, it is very important to find a safe and economical way to storage methane. One approach is using physisorption, which can provide energy density comparable to compressed gas at a relatively lower pressure (35-40 bar)[5]. The department of energy (DOE) has set a target for methane storage capacity at ambient conditions,

which is 180/1 (v/v) at 35 bar and 298K. Many porous materials have been used as methane storage materials, among them, POPs are one of the most promising due to their high surface area and high storage capacity for methane. POPs have a few advantages for methane storage. First, they are connected by lightweight elements, making them low density; second, there are a large number of synthetic strategies to incorporate chemical functional groups into POPs, such as functional groups that can enhance methane affinities. **Table 1.2** is a brief summary of current status of POPs with high methane storage capacities.

Table 1.2. Methane storage capacities in POPs.

Materials	S_{BET} (m^2/g)	P (bar)	T (K)	CH_4 wt %	References
PAF-1	5640	1	273	1.12	[30]
PAF-1-Li	479	1.22	273	1.3	[54]
PPF-1	1740	1	273	2.43	[58]
PPF-2	1470	1	273	2.31	[58]
PAF-41	1119	1	273	1.04	[59]
BILP-3	1306	1	273	1.50	[60]
BILP-4	1135	1	273	1.63	[61]
PPN-1	1249	70	295	6.25	[35]
PPN-2	1746	70	295	9.40	[35]
PPN-3	4221	70	295	12.20	[35]
PPN-4	6461	55	295	17.10	[6]
COF-1	750	35	298	4.0	[55]
COF-5	1670	35	298	8.9	[55]

COF-102	3620	35	298	18.7	[55]
COF-103	3530	35	298	17.5	[55]
ALP-1	1235	1	273	2.60	[62]
ALP-3	975	1	273	1.72	[62]

1.4.1.3. Capture of carbon dioxide (CO_2) and CO_2/N_2 separation

CO_2 has long been regarded as the major greenhouse gas. Since the industrial revolution, the CO_2 concentration in the atmosphere has doubled. Currently the CO_2 concentration in the atmosphere is more than 400 ppm, which leads to numerous negative effects on global warming. The capture and sequestration of CO_2 by selective adsorption using porous materials have been an effective way to mitigate CO_2 emissions by power plants, cars, fossil fuel combustion, etc. Recently, POPs have emerged as a potential candidate for CO_2 capture due to their high surface area, high stability, tunable pore size and high CO_2 adsorption capacity. In addition, many CO_2-philic functional groups, such as amine group can be introduced into the POPs. Another important criterion for materials used for CO_2 capture is the CO_2/N_2 adsorption selectivity. CO_2 has a smaller kinetic diameter compared to N_2. By controlling the pore size, POPs can show very high CO_2 adsorption selectivities versus N_2. A large number of POPs have been reported with high CO_2 capture and also with high CO_2/N_2 adsorption selectivity. **Table 1.3** is brief summary of some POPs with high CO_2 capture capacities.

Table 1.3. CO_2 capture capacities in POPs.

Materials	S_{BET} (m^2/g)	P (bar)	T (K)	CO_2 mmol/g	References
PAF-1	5640	1	298	2.05	[30]

PPF-1	1740	1	273	6.07	[58]
PPF-2	1470	1	273	5.55	[58]
BILP-1	1172	1	273	4.27	[63]
BILP-2	708	1	273	3.39	[61]
BILP-3	1306	1	273	5.11	[60]
BILP-4	1135	1	273	5.34	[61]
PPN-1	1249	60	295	11	[35]
PPN-2	1746	60	295	19	[35]
PPN-3	4221	60	295	25.3	[35]
PPN-4	6461	50	295	48.2	[6]
PPN-6-SO_3H	1254	1	295	3.6	[64]
PPN-6-SO_3Li	1186	1	295	3.7	[64]
PPN-6-SO_3NH_4	593	1	295	3.7	[37]
PPN-6-CH_2DETA	555	1	295	4.3	[36]
CMP-1	837	1	273	2.05	[41]
CMP-1-CH_3	899	1	273	1.64	[41]
CMP-1-NH_2	710	1	273	1.64	[41]
CMP-1-OH	1043	1	273	1.80	[41]
CMP-1-COOH	522	1	273	1.60	[41]
COF-1	750	55	298	5.2	[55]
COF-5	1670	55	298	19.8	[55]
COF-102	3620	55	298	27.3	[55]
COF-103	3530	55	298	27.0	[55]
CPOP-1	2220	1	273	4.82	[7]

1.4.2. Chemical sensing

POPs are attractive candidates for chemical sensing materials because they possess high specific surface area which can provide a broad interaction with analytes. In addition, POPs synthesized from conjugated building blocks have remarkable π-conjugation and photofluorescence properties. Jiang *et al.*[65] reported a carbazole based CMP which can detect a series of aromatic compounds. They used a carbazole based building block under oxidation coupling and the resulting CMPs had strong blue luminescence. Compared to the linear analogue, these porous and conjugated CMPs had enhanced detection sensitivity.

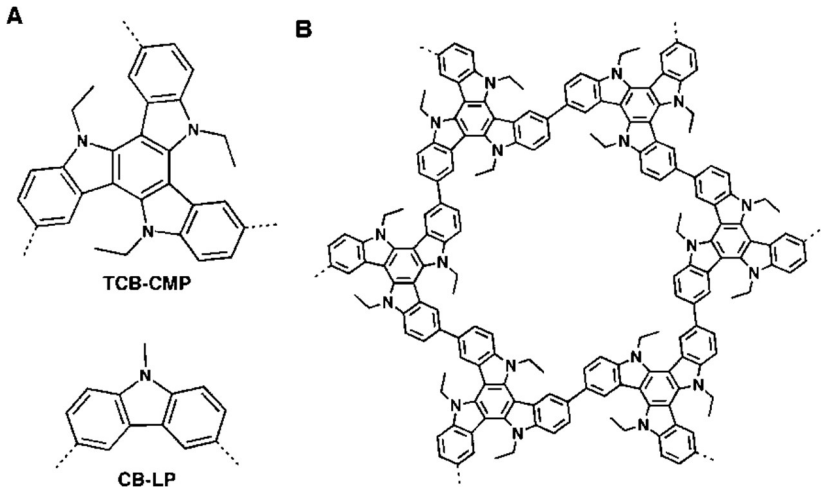

Figure 1.14. Structure of fluorescent CMPs.

More recently, Dichtel *et al.*[66] reported POPs with strong fluorescence can be used to detect explosives, such as RDX (1,3,5-Trinitroperhydro-1,3,5-triazine) vapor. The cross-linked POPs are highly fluorescent; they can be quenched by the RDX solution or vapor. The polymer network also responds to TNT and PETN similarly introduced from the solution or vapor phase.

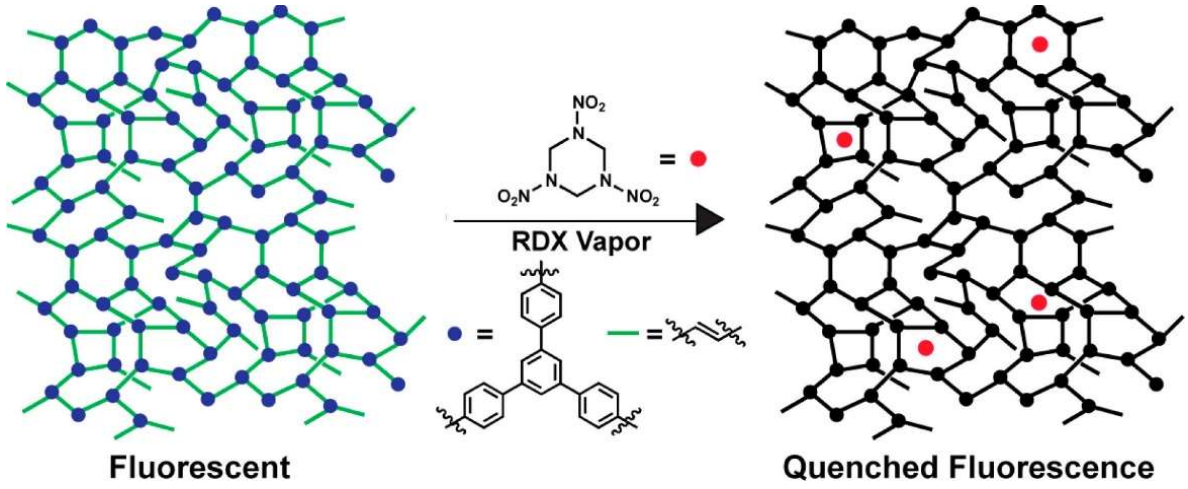

Figure 1.15. Cross-linked POPs as explosive sensor materials. (Reprinted with permission from Ref. 65. Copyright (2013) American Chemical Society.)

1.4.3. Heterogeneous catalysis

Given their high surface area, high stability, tunable pore size and ease of functionalization, POPs are also widely considered as heterogeneous catalysts[9,10]. Through building block modifications and introducing catalytic centers, POPs with catalytical performance can be achieved. Compared to traditional catalysts, POP based catalysts can provide a much higher density of catalytic centers and higher efficiency. Many POP based heterogeneous catalysts have been reported with high TON, TOF for catalysis. There are mainly two strategies to achieve catalytical applications of POPs, which are "bottom up synthesis" and "post-functionalization" to introduce catalytic active groups. In "bottom up" synthesis, catalytic active groups are incorporated into the building blocks, while in the "post functionalization" method, the catalytic units are introduced after the POPs are synthesized. In this section, a few examples of POPs for catalysis applications will be introduced.

1.4.3.1 Bottom up synthesis of POPs for heterogeneous catalysis

A iron(III) porphyrin based building block was incorporated into CMPs and used as efficient heterogeneous catalyst, which was reported by Jiang *et al.*.[67] Through Suzuki-Miyaura cross coupling, the iron(III) porphyrin was successfully introduced into the CMPs. The resulting CMPs (FeP-CMP) are 2D frameworks with a major pore size of 2.69 nm, and the surface area is 1270 m^2 g^{-1}. This rational design with metalloporphyrin allows for the high loading of catalytic centers. It can be used as an efficient and selective heterogeneous catalyst to convert various sulfides to sulfoxides. Compared to the monomer catalyst, FeP-CMP is much more efficient and very selective in converting various sulfides to sulfoxides and avoiding being over oxidized. The results reveal the advantage of incorporating catalytical sites into CMPs. In addition, the catalyst can be recycled and reused for at least three runs, indicating their high stability.

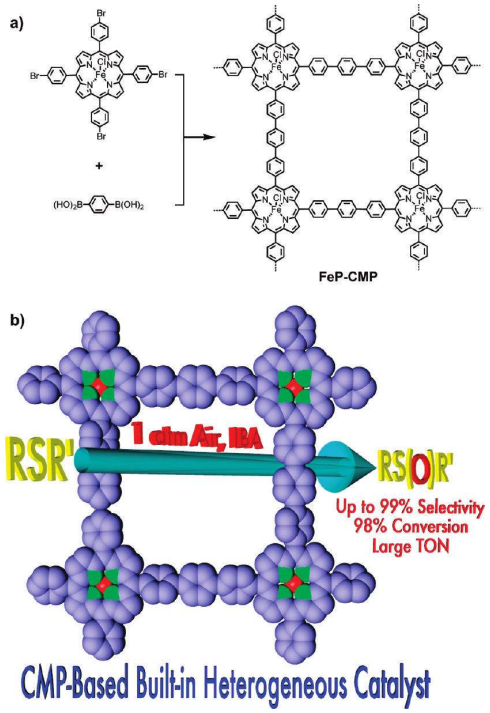

Figure 1.16. Synthesis of an iron(III) porphyrin CMPs based heterogeneous catalyst. (Reprinted with permission from Ref. 66. Copyright (2011) American Chemical Society.)

1.4.3.2. Post functionalization of POPs for heterogeneous catalysis

Recently Jiang *et al.* also reported attaching chiral catalytic centers to the POPs through post functionalized strategy.[68] In this work, they first prepared a stable POP, which has high specific surface area, then the chiral catalytic sites were installed on the framework. The resulting framework shows excellent stability and can be used as a stereo selectivity catalyst. Since the catalyst has high surface area and high density of catalytic centers, it is very efficient to catalyze the stereoselective reaction.

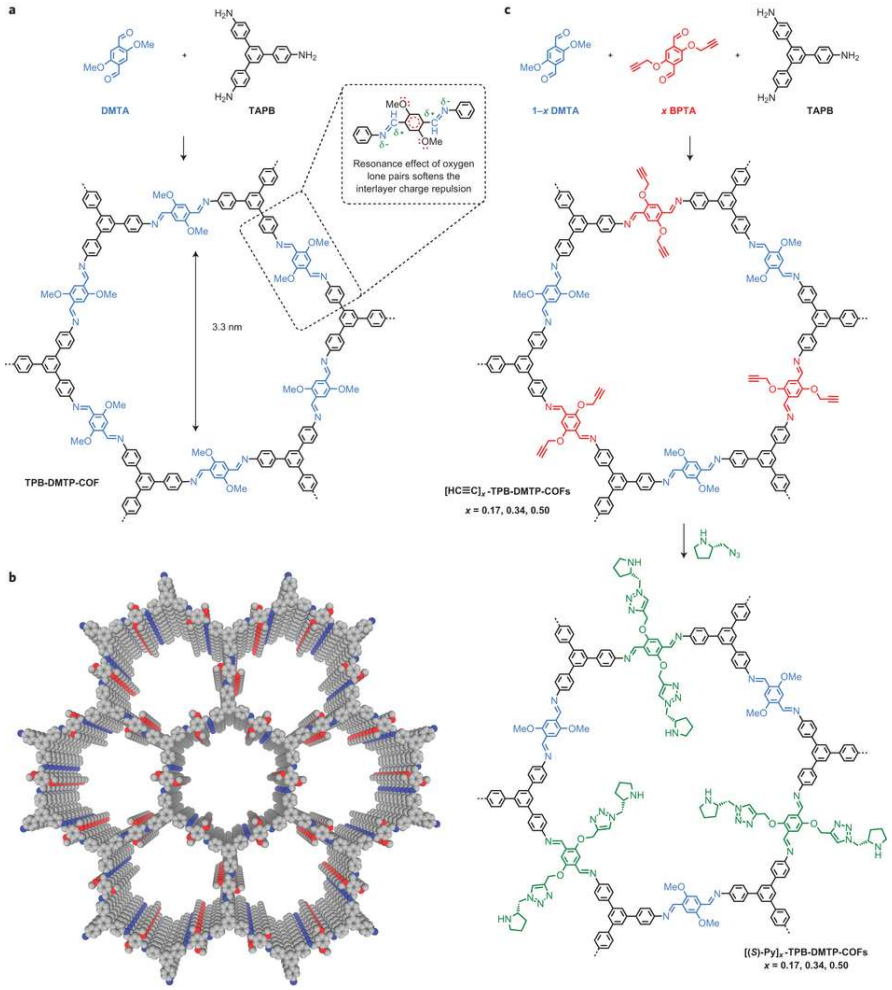

Figure 1.17. Synthesis and structure of COFs with chiral catalytic sites. (Reprinted with permission from Ref. 67. Copyright (2015) Nature Publish Group.)

1.4.4 Semiconductor applications

POPs with large conjugation represent a class of interesting materials for electronic and optoelectronic applications. This was demonstrated by Jiang *et al.* in 2008[69]. They designed a π-electronic 2D TP-COF consisting of interlocking hexagons made from HTTP molecules at the vertices and pyrene-2,7-diboronic acid (PDBA) groups at the edges. Interestingly, upon excitation of the pyrene units of the COF, TP-COF emitted a strong blue luminescence, and the emission is only from the pyrene moiety. This result indicates the strong conjugation in the COFs. The COFs can absorb a wide range of photons from the ultraviolet range to the visible regions and convert them to a brilliant blue luminescence. So this TP-COF is semiconducting, and further *I–V* curve measurements confirm the hole transport and is capable of the on–off switching of the electric current.

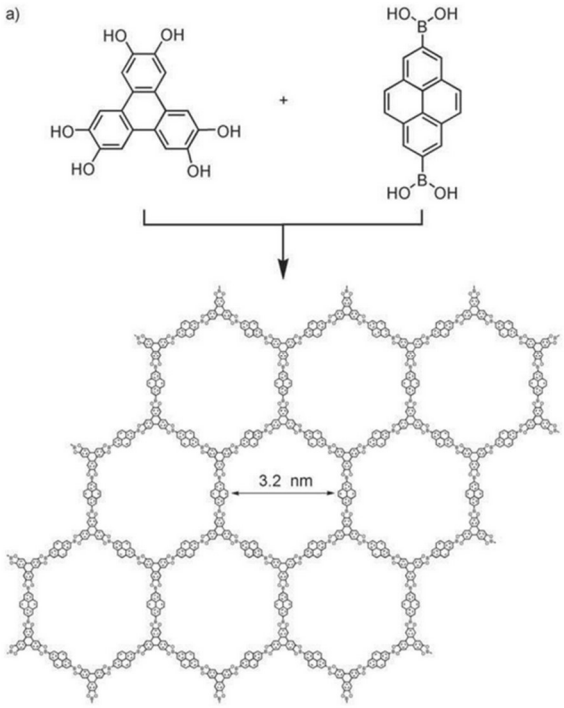

Figure 1.18. Synthesis and structure of a semiconduction COFs. (Reprinted with permission from Ref. 68. Copyright (2008) John Wiley & Sons, Inc.)

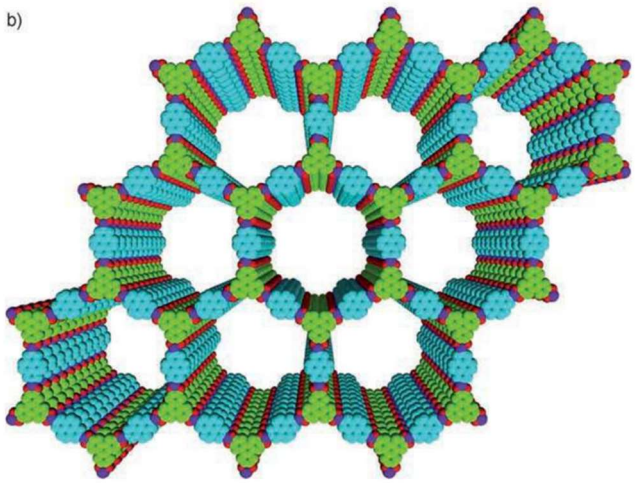

Figure 1.19. Schematic representation of the AA stacked structure of TP-COFs with preorganized and built-in π columns. (Reprinted with permission from Ref. 68. Copyright (2008) John Wiley & Sons, Inc.)

1.4.5. Electrochemical energy storage applications

POPs can be functionalized with different chemical groups. By incorporating redox active groups, it can be used for electrochemical applications. Recently, Dichtel *et al.* reported a POP that can be used for electrochemical energy storage[70]. They incorporated redox active 2,6-diaminoanthraquinone (**DAAQ**) moieties into the 2D COFs linked by ketoenamines. The DAAQ can be reduced to 9,10-dihydroxyanthracenes upon two-electron, two-proton reduction in a protic electrolyte. Electrodes with this redox-active COF incorporated show higher capacitance than those modified with a similar non-redox-active COF, and the electrode is very stable even after 5000 charge−discharge cycles. These findings opened a new door for exploring the potential of POPs.

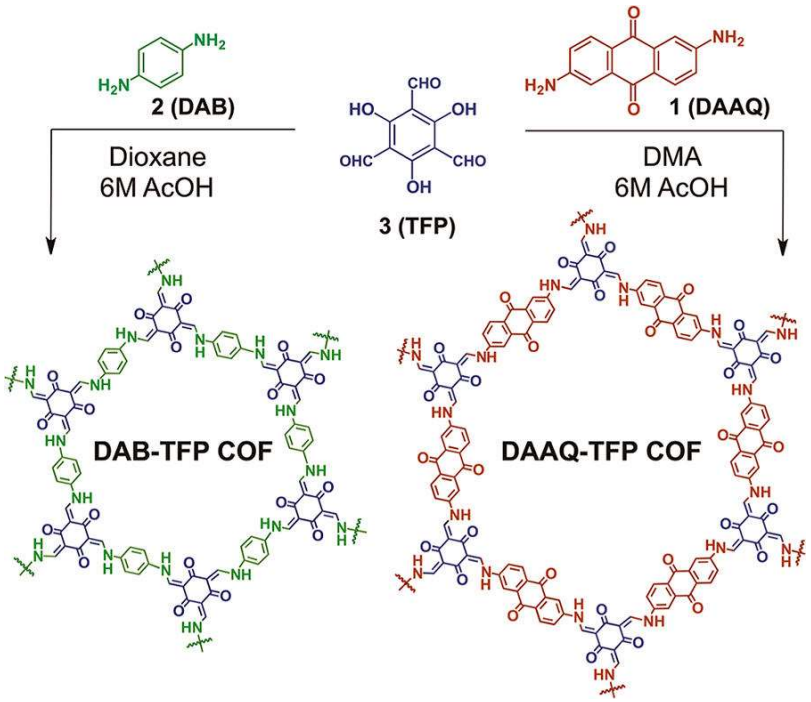

Figure 1.20. Synthesis and structure of redox active porous COFs. (Reprinted with permission from Ref. 69. Copyright (2013) American Chemical Society.)

1.4.6. Proton conduction and ion conduction

Proton and ion conduction materials are very important in fuel cells, sensors, and electronics device applications. Although POPs for proton and ion conduction are not well explored, there are a few examples using POPs as proton and ion conduction materials.[13-15,71]

1.4.6.1. Proton conducting materials using POPs

Nafion-based proton conducting membranes are considered as the dominant materials in this field for fuel cells production, yet the high cost of this type of materials always encourages researchers to find alternative materials for proton conduction. Banerjee and his coworkers reported a phosphoric acid loaded azo COFs for proton conduction application.[13] In this work, azo group was introduced into the COFs. Azo group can act as receptors for phosphoric acid,

which can immobilize the phosphoric acid in the porous framework and thus increase the proton conduction. The materials can facilitate the proton conduction in both the hydrous ($\sigma = 9.9 \times 10^{-4}$ S cm^{-1}) and anhydrous state ($\sigma = 6.7 \times 10^{-5}$S cm^{-1}). This work represented the first example of proton conduction for COFs, which further extended the applications of POPs.

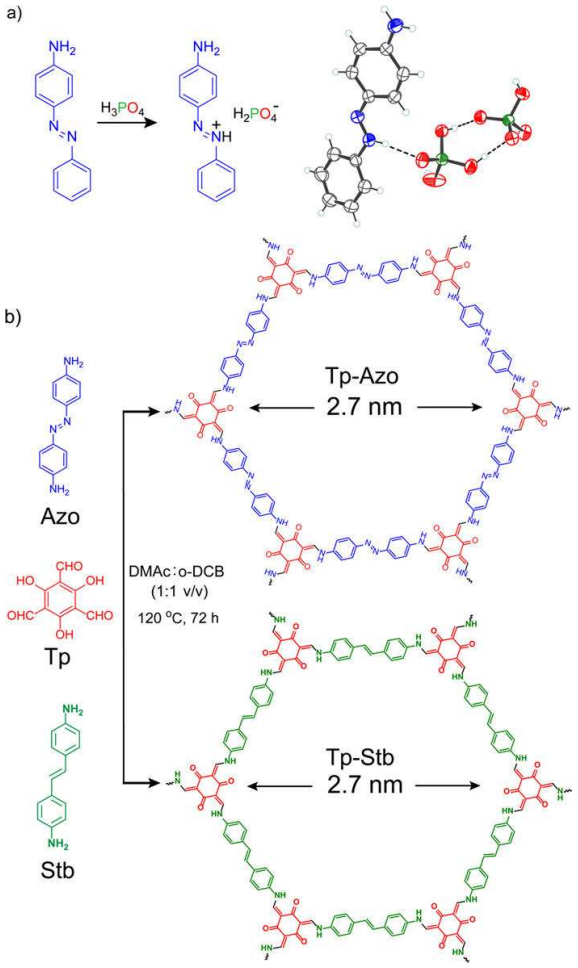

Figure 1.21. Structure of proton conducting COFs. (Reprinted with permission from Ref. 13. Copyright (2013) American Chemical Society.)

1.4.6.2. Ion conducting materials using POPs

Ion conduction is also a very important process in batteries, especially lithium ion batteries. With the development of the lithium ion battery, more stable and high performance electrolytes

are desired. Long *et al.* reported tetraarylborate polymer networks as lithium ion conducting solid electrolytes[14]. They used a tetrahedral-shape based boron anion building block to couple with linear linker. The resulting framework is negative charged and can bind the cations, such as Li^+. Indeed, they observed promising conductivity metrics in room temperature, up to 2.7×10^{-4} S cm^{-1} and high lithium ion transport numbers (up to 0.93).

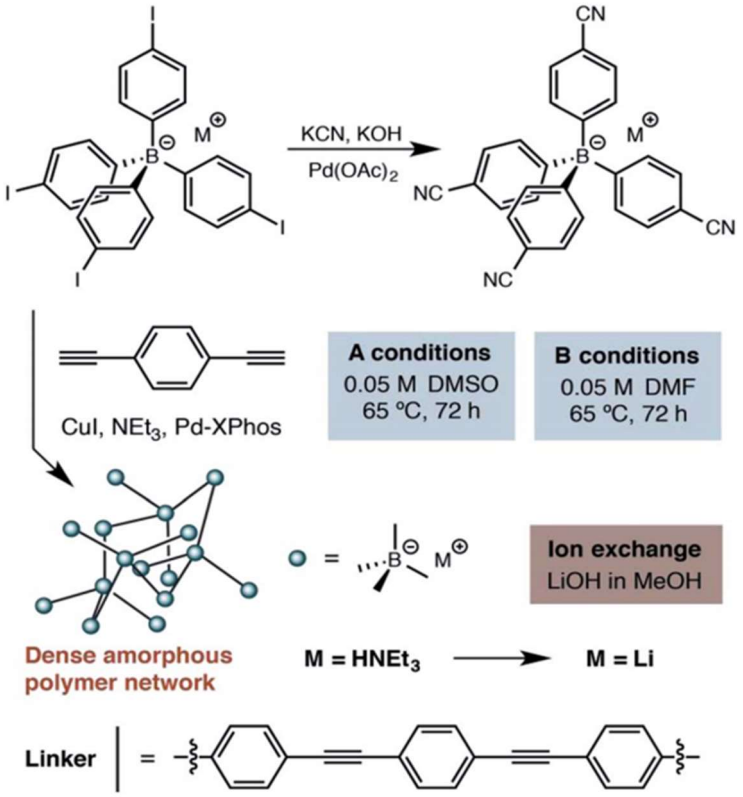

Figure 1.22. Synthesis and structure of tetraarylborate polymer networks as an ion conducting electrolyte. (Reprinted with permission from Ref. 14. Copyright (2015) Royal Society of Chemistry.)

Recently, Zhang *et al.* reported an ionic covalent organic framework (ICOF) with spiroborate linkage[15]. The sp^3 hybridization boron in the spiroborate center is negatively charged, which makes the framework bearing with negative charge. After the ion exchange, the lithium

ions are distributed inside the frameworks, which can be used as lithium conducting materials. The presence of permanently immobilized ion centers in ICOFs enables the transportation of lithium ions with a room temperature lithium-ion conductivity of 3.05×10^{-5} S cm^{-1} and an average Li^+ transference number value of about 0.80.

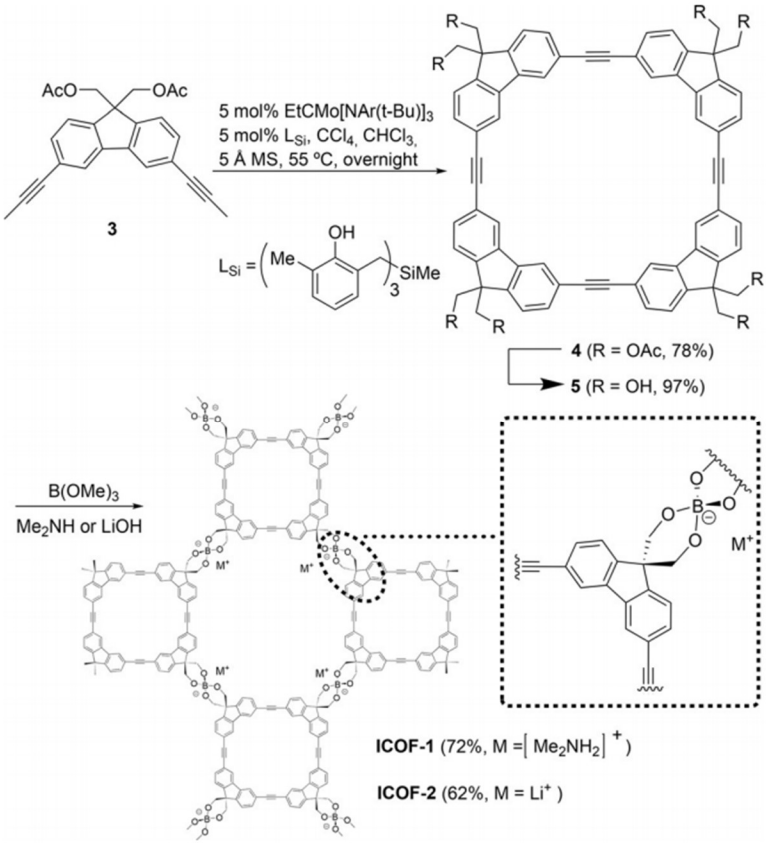

Figure 1.23. Synthesis and structure of ICOF-1,2. (Reprinted with permission from Ref. 15. Copyright (2016) John Wiley & Sons, Inc.)

1.5. Conclusion and outlook

In conclusion, within the past decade, porous organic polymers have achieved tremendous progress and exhibited many potential applications in various fields, such as gas adsorption, gas separation, oil-water separation, heterogeneous catalysis, optoelectronics, electrochemical energy

storage, semiconduction, ion and proton conducting materials, etc. Their unique structure features, such as flexible building block design, micro or meso porosity, and tunable pore size and pore structure, pore surface decoration and engineering, and the functionalization of building blocks promise that this field, although currently still in its early stage, will quickly grow into a rich and broad research area of great importance in the near future. Development of new synthetic methods, introducing new functional groups, linkages, and structures using novel building blocks would be very important for the design and synthesis of POPs with desired structure and functionality. In addition, with the development of structure characterization techniques, the structure property relationship investigation would be much easier, which will further advance the function design for the development of porous organic polymers.

1.6. References

(1) Wu, D. C.; Xu, F.; Sun, B.; Fu, R. W.; He, H. K.; Matyjaszewski, K. *Chem. Rev.* **2012**, *112*, 3959.

(2) Ding, S. Y.; Wang, W. *Chem. Soc. Rev.* **2013**, *42*, 548.

(3) Xiang, Z. H.; Zhou, X.; Zhou, C. H.; Zhong, S.; He, X.; Qin, C. P.; Cao, D. P. *J. Mater. Chem.* **2012**, *22*, 22663.

(4) Dawson, R.; Stockel, E.; Holst, J. R.; Adams, D. J.; Cooper, A. I. *Energy & Environmental Science* **2011**, *4*, 4239.

(5) Wood, C. D.; Tan, B.; Trewin, A.; Su, F.; Rosseinsky, M. J.; Bradshaw, D.; Sun, Y.; Zhou, L.; Cooper, A. I. *Adv. Mater.* **2008**, *20*, 1916.

(6) Yuan, D. Q.; Lu, W. G.; Zhao, D.; Zhou, H. C. *Adv. Mater.* **2011**, *23*, 3723.

(7) Chen, Q.; Luo, M.; Hammershoj, P.; Zhou, D.; Han, Y.; Laursen, B. W.; Yan, C. G.; Han, B. H. *J. Am. Chem. Soc.* **2012**, *134*, 6084.

(8) Chang, Z.; Zhang, D. S.; Chen, Q.; Bu, X. H. *Phys. Chem. Chem. Phys.* **2013**, *15*, 5430.

(9) Zhang, Y. G.; Riduan, S. N. *Chem. Soc. Rev.* **2012**, *41*, 2083.

(10) Kaur, P.; Hupp, J. T.; Nguyen, S. T. *ACS Catal.* **2011**, *1*, 819.

(11) Dalapati, S.; Jin, S. B.; Gao, J.; Xu, Y. H.; Nagai, A.; Jiang, D. L. *J. Am. Chem. Soc.* **2013**, *135*, 17310.

(12) Ding, X. S.; Guo, J.; Feng, X. A.; Honsho, Y.; Guo, J. D.; Seki, S.; Maitarad, P.; Saeki, A.; Nagase, S.; Jiang, D. L. *Angew. Chem., Int. Ed.* **2011**, *50*, 1289.

(13) Chandra, S.; Kundu, T.; Kandambeth, S.; BabaRao, R.; Marathe, Y.; Kunjir, S. M.; Banerjee, R. *J. Am. Chem. Soc.* **2014**, *136*, 6570.

(14) Van Humbeck, J. F.; Aubrey, M. L.; Alsbaiee, A.; Ameloot, R.; Coates, G. W.; Dichtel, W. R.; Long, J. R. *Chem. Sci.* **2015**, *6*, 5499.

(15) Du, Y.; Yang, H. S.; Whiteley, J. M.; Wan, S.; Jin, Y. H.; Lee, S. H.; Zhang, W. *Angew. Chem., Int. Ed.* **2016**, *55*, 1737.

(16) Cote, A. P.; Benin, A. I.; Ockwig, N. W.; O'Keeffe, M.; Matzger, A. J.; Yaghi, O. M. *Science* **2005**, *310*, 1166.

(17) El-Kaderi, H. M.; Hunt, J. R.; Mendoza-Cortes, J. L.; Cote, A. P.; Taylor, R. E.; O'Keeffe, M.; Yaghi, O. M. *Science* **2007**, *316*, 268.

(18) Feng, X.; Ding, X. S.; Jiang, D. L. *Chem. Soc. Rev.* **2012**, *41*, 6010.

(19) Kuhn, P.; Antonietti, M.; Thomas, A. *Angew. Chem., Int. Ed.* **2008**, *47*, 3450.

(20) Kuhn, P.; Forget, A.; Su, D. S.; Thomas, A.; Antonietti, M. *J. Am. Chem. Soc.* **2008**, *130*, 13333.

(21) Budd, P. M.; Ghanem, B. S.; Makhseed, S.; McKeown, N. B.; Msayib, K. J.; Tattershall, C. E. *Chem. Commun.* **2004**, 230.

(22) McKeown, N. B.; Budd, P. M. *Chem. Soc. Rev.* **2006**, *35*, 675.

(23) Jiang, J. X.; Su, F.; Trewin, A.; Wood, C. D.; Campbell, N. L.; Niu, H.; Dickinson, C.; Ganin, A. Y.; Rosseinsky, M. J.; Khimyak, Y. Z.; Cooper, A. I. *Angew. Chem., Int. Ed.* **2007**, *46*, 8574.

(24) Cooper, A. I. *Adv. Mater.* **2009**, *21*, 1291.

(25) Dawson, R.; Laybourn, A.; Clowes, R.; Khimyak, Y. Z.; Adams, D. J.; Cooper, A. I. *Macromolecules* **2009**, *42*, 8809.

(26) Xu, Y. H.; Jin, S. B.; Xu, H.; Nagai, A.; Jiang, D. L. *Chem. Soc. Rev.* **2013**, *42*, 8012.

(27) Jiang, J. X.; Su, F.; Trewin, A.; Wood, C. D.; Niu, H.; Jones, J. T. A.; Khimyak, Y. Z.; Cooper, A. I. *J. Am. Chem. Soc.* **2008**, *130*, 7710.

(28) Chen, L.; Honsho, Y.; Seki, S.; Jiang, D. L. *J. Am. Chem. Soc.* **2010**, *132*, 6742.

(29) Wood, C. D.; Tan, B.; Trewin, A.; Niu, H. J.; Bradshaw, D.; Rosseinsky, M. J.; Khimyak, Y. Z.; Campbell, N. L.; Kirk, R.; Stockel, E.; Cooper, A. I. *Chem. Mater.* **2007**, *19*, 2034.

(30) Ben, T.; Ren, H.; Ma, S. Q.; Cao, D. P.; Lan, J. H.; Jing, X. F.; Wang, W. C.; Xu, J.; Deng, F.; Simmons, J. M.; Qiu, S. L.; Zhu, G. S. *Angew. Chem., Int. Ed.* **2009**, *48*, 9457.

(31) Ben, T.; Pei, C. Y.; Zhang, D. L.; Xu, J.; Deng, F.; Jing, X. F.; Qiu, S. L. *Energy Environ. Sci.* **2011**, *4*, 3991.

(32) Ren, H.; Ben, T.; Wang, E. S.; Jing, X. F.; Xue, M.; Liu, B. B.; Cui, Y.; Qiu, S. L.; Zhu, G. S. *Chem. Commun.* **2010**, *46*, 291.

(33) Zhao, H. Y.; Jin, Z.; Su, H. M.; Jing, X. F.; Sun, F. X.; Zhu, G. S. *Chem. Commun.* **2011**, *47*, 6389.

(34) Trewin, A.; Cooper, A. I. *Angew. Chem., Int. Ed.* **2010**, *49*, 1533.

(35) Lu, W. G.; Yuan, D. Q.; Zhao, D.; Schilling, C. I.; Plietzsch, O.; Muller, T.; Brase, S.; Guenther, J.; Blumel, J.; Krishna, R.; Li, Z.; Zhou, H. C. *Chem. Mater.* **2010**, *22*, 5964.

(36) Lu, W. G.; Sculley, J. P.; Yuan, D. Q.; Krishna, R.; Wei, Z. W.; Zhou, H. C. *Angew. Chem., Int. Ed.* **2012**, *51*, 7480.

(37) Lu, W. G.; Verdegaal, W. M.; Yu, J. M.; Balbuena, P. B.; Jeong, H. K.; Zhou, H. C. *Energy Environ. Sci.* **2013**, *6*, 3559.

(38) Lu, W. G.; Wei, Z. W.; Yuan, D. Q.; Tian, J.; Fordham, S.; Zhou, H. C. *Chem. Mater.* **2014**, *26*, 4589.

(39) McKeown, N. B.; Makhseed, S.; Budd, P. M. *Chem. Commun.* **2002**, 2780.

(40) McKeown, N. B.; Budd, P. M.; Msayib, K. J.; Ghanem, B. S.; Kingston, H. J.; Tattershall, C. E.; Makhseed, S.; Reynolds, K. J.; Fritsch, D. *Chem.-Eur. J.* **2005**, *11*, 2610.

(41) Dawson, R.; Adams, D. J.; Cooper, A. I. *Chem. Sci.* **2011**, *2*, 1173.

(42) Jiang, J. X.; Li, Y. Y.; Wu, X. F.; Xiao, J. L.; Adams, D. J.; Cooper, A. I. *Macromolecules* **2013**, *46*, 8779.

(43) Ben, T.; Qiu, S. L. *CrystEngComm* **2013**, *15*, 17.

(44) Peng, Y.; Ben, T.; Xu, J.; Xue, M.; Jing, X. F.; Deng, F.; Qiu, S. L.; Zhu, G. S. *Dalton Trans.* **2011**, *40*, 2720.

(45) Uribe-Romo, F. J.; Hunt, J. R.; Furukawa, H.; Klock, C.; O'Keeffe, M.; Yaghi, O. M. *J. Am. Chem. Soc.* **2009**, *131*, 4570.

(46) Beaudoin, D.; Maris, T.; Wuest, J. D. *Nat. Chem.* **2013**, *5*, 830.

(47) Roeser, J.; Kailasam, K.; Thomas, A. *Chemsuschem* **2012**, *5*, 1793.

(48) Ren, S. J.; Bojdys, M. J.; Dawson, R.; Laybourn, A.; Khimyak, Y. Z.; Adams, D. J.; Cooper, A. I. *Adv. Mater.* **2012**, *24*, 2357.

(49) Dogru, M.; Sonnauer, A.; Gavryushin, A.; Knochel, P.; Bein, T. *Chem. Commun.* **2011**, *47*, 1707.

(50) Campbell, N. L.; Clowes, R.; Ritchie, L. K.; Cooper, A. I. *Chem. Mater.* **2009**, *21*, 204.

(51) Jin, Y. H.; Voss, B. A.; McCaffrey, R.; Baggett, C. T.; Noble, R. D.; Zhang, W. *Chem. Sci.* **2012**, *3*, 874.

(52) Chandra, S.; Kandambeth, S.; Biswal, B. P.; Lukose, B.; Kunjir, S. M.; Chaudhary, M.; Babarao, R.; Heine, T.; Banerjee, R. *J. Am. Chem. Soc.* **2013**, *135*, 17853.

(53) McKeown, N. B.; Budd, P. M.; Book, D. *Macromol. Rapid Comm.* **2007**, *28*, 995.

(54) Konstas, K.; Taylor, J. W.; Thornton, A. W.; Doherty, C. M.; Lim, W. X.; Bastow, T. J.; Kennedy, D. F.; Wood, C. D.; Cox, B. J.; Hill, J. M.; Hill, A. J.; Hill, M. R. *Angew. Chem., Int. Ed.* **2012**, *51*, 6639.

(55) Furukawa, H.; Yaghi, O. M. *J. Am. Chem. Soc.* **2009**, *131*, 8875.

(56) Rose, M.; Bohlmann, W.; Sabo, M.; Kaskel, S. *Chem. Commun.* **2008**, 2462.

(57) Yuan, S. W.; Dorney, B.; White, D.; Kirklin, S.; Zapol, P.; Yu, L. P.; Liu, D. J. *Chem. Commun.* **2010**, *46*, 4547.

(58) Zhu, Y. L.; Long, H.; Zhang, W. *Chem. Mater.* **2013**, *25*, 1630.

(59) Li, L. N.; Ren, H.; Yuan, Y.; Yu, G. L.; Zhu, G. S. *J. Mater. Chem. A* **2014**, *2*, 11091.

(60) Rabbani, M. G.; Reich, T. E.; Kassab, R. M.; Jackson, K. T.; El-Kaderi, H. M. *Chem. Commun.* **2012**, *48*, 1141.

(61) Rabbani, M. G.; El-Kaderi, H. M. *Chem. Mater.* **2012**, *24*, 1511.

(62) Arab, P.; Rabbani, M. G.; Sekizkardes, A. K.; Islamoglu, T.; El-Kaderi, H. M. *Chem. Mater.* **2014**, *26*, 1385.

(63) Rabbani, M. G.; El-Kaderi, H. M. *Chem. Mater.* **2011**, *23*, 1650.

(64) Lu, W. G.; Yuan, D. Q.; Sculley, J. L.; Zhao, D.; Krishna, R.; Zhou, H. C. *J. Am. Chem. Soc.* **2011**, *133*, 18126.

(65) Liu, X. M.; Xu, Y. H.; Jiang, D. L. *J. Am. Chem. Soc.* **2012**, *134*, 8738.

(66) Gopalakrishnan, D.; Dichtel, W. R. *J. Am. Chem. Soc.* **2013**, *135*, 8357.

(67) Chen, L.; Yang, Y.; Jiang, D. L. *J. Am. Chem. Soc.* **2010**, *132*, 9138.

(68) Xu, H.; Gao, J.; Jiang, D. L. *Nat. Chem.* **2015**, *7*, 905.

(69) Wan, S.; Guo, J.; Kim, J.; Ihee, H.; Jiang, D. L. *Angew. Chem., Int. Ed.* **2008**, *47*, 8826.

(70) DeBlase, C. R.; Silberstein, K. E.; Truong, T. T.; Abruna, H. D.; Dichtel, W. R. *J. Am. Chem. Soc.* **2013**, *135*, 16821.

(71) Shinde, D. B.; Aiyappa, H. B.; Bhadra, M.; Biswal, B. P.; Wadge, P.; Kandambeth, S.; Garai, B.; Kundu, T.; Kurungot, S.; Banerjee, R. *J. Mater. Chem. A* **2016**, *4*, 2682.

CHAPTER 2

Imine-Linked Porous Polymer Frameworks with High Small Gas (H_2, CO_2, CH_4, C_2H_2) uptake and CO_2/N_2 selectivity

(A paper was published for this chapter: Zhu, Y.; Long, H.; Zhang, W. " Imine-linked Porous Polymer Frameworks with High Small Gas (H_2, CO_2, CH_4, C_2H_2) Uptake and CO_2/N_2 Selectivity" *Chem. Mater.* **2013**, *25 (9)*, 1630-1635)

2.1 Abstract

A series of novel porous polymer frameworks (PPFs) with [3 + 4] structure motif has been synthesized from readily accessible tetra-amine and tri-aldehyde building blocks *via* imine condensation, and the dependence of gas adsorption properties on the building block dimensions and functionalities was studied. The resulting imine-linked frameworks exhibit high surface area, the Brunauer−Emmett−Teller (BET) specific surface area up to 1740 $m^2\ g^{-1}$, and a Langmuir surface area up to 2157 $m^2\ g^{-1}$. More importantly, the porous frameworks exhibit outstanding H_2 (up to 2.75 wt %, 77 K, 1 bar), CO_2 (up to 26.7 wt %, 273 K, 1 bar), CH_4 (up to 2.43 wt %, 273 K, 1 bar), and C_2H_2 (up to 17.9 wt %, 273 K, 1 bar) uptake, which are among the highest reported for organic porous materials. PPFs exhibit good ideal selectivities for CO_2/N_2 (14.5/1−20.4/1), and CO_2/CH_4 adsorption (8.6/1− 11.0/1), and high thermal stabilities (up to 500 °C), thus showing a great potential in gas storage and separation applications.

2.2 Introduction

Recently, there has been explosive growth in the research of novel porous materials, which have shown great promise for applications in gas storage and separation. Porous materials play key roles in carbon capture and sequestration technology, and safe storage of clean energy (e.g., hydrogen) and explosive industrial gases (e.g., acetylene). A notable achievement in porous materials research is the development of porous metal-organic frameworks (MOFs),[1] highly ordered crystalline materials constructed through reticular chemistry from metal ions or clusters and organic linkers. Several of these fascinating materials have the highest surface area and gas uptake capacity reported so far among all porous materials. However, despite greater flexibility in design and phenomenal success in synthesis of highly diverse 3-D structures, MOFs invariably contain a large amount of metal centers and relatively labile coordination bonds that may limit their applications. Recently purely organic porous materials have received increasing attention and they have shown great potential in a variety of applications, such as gas storage and separation,[2-5] heterogeneous catalysis,[6-8] chemical sensing,[9] etc. Two types of organic porous materials have been developed in the past decade, including discrete porous organic molecules[10-12] and infinite porous organic polymer networks such as crystalline COFs[13-15] and CTFs,[16-18] or amorphous HCPs[19], PAFs,[20,21] PPNs,[22,23] CMPs[24,25] and OCFs[26] etc. Both of these two types of materials are constructed from light-weight elements through strong covalent bonding. These materials generally possess permanent porosity, low mass densities, synthetic diversification and high physicochemical stability, which make them highly competitive in gas storage and separation applications.[5,23,27,28]

Although significant progress has been made in the area of organic porous materials, only limited dimensionality, framework connectivity, and topologies of these promising materials have been explored. In addition, better understanding on the effect of building block features on the target framework structures and properties is still highly desired. Continuing our effort of seeking high-performance organic porous materials,[12,26,29] we have developed high-yielding and cost-effective syntheses of a series of porous polymer frameworks (**PPFs**) through imine condensation, which show high H_2, CO_2, CH_4, and C_2H_2 storage capacity as well as good CO_2/N_2 adsorption selectivity. The structure-property relationship was studied using various building blocks of different size and functionality. We found decoration of the framework **PPF-1** with electron-donating groups enhanced the uptake of C_2H_2 significantly, from 9.4 wt % to 17.9 wt %, which is the highest C_2H_2 capacity reported so far for organic porous materials, and comparable or superior to those of MOFs.

2.3 Results and discussion

A few chemical transformations have been applied to the syntheses of organic porous materials, among which Schiff-base chemistry is the most widely used. We choose imine condensation reaction to connect the building blocks for the following reasons: 1) imine condensation is an efficient well-established process and does not require expensive catalysts; 2) the reversibility of the reaction offers error-correction features, thus possibly producing highly-ordered crystalline materials; 3) it can introduce imine bonds into the structure that can promote CO_2 binding. In general, 3-D frameworks provide higher surface area compared to 2-D frameworks. We searched Reticular Chemistry Structure Resource (RCSR) database for potential candidate 3-D topology. A highly symmetric *ctn* topological structure,[30] which can be constructed from tritopic and tetratopic

building blocks, appeared to be an interesting target (**Scheme 2.1a**). Although various examples of porous polymers or covalent organic frameworks (COFs) have been reported through imine condensation,[8,31-35] surprisingly, the [3+4] structure motif has never been explored. We used tetra-(4-anilyl)-methane as the tetratopic building block. In order to investigate the structure-property relationship, we choose a series of trialdehydes (**2-5**) with different sizes (distance between two aldehyde moieties ranging from 4.99 Å to 12.37 Å) as the tritopic building blocks (**Scheme 2.1**). It has been reported that attempts to increase the pores sizes of topologically identical MOFs by using lager organic linkers commonly result in interpenetration, leading to porosity decrease.[36] One of our goals is to explore the effect of geometrical features of building blocks on the pore size distribution and surface area of these purely organic frameworks with [3+4] motif. 1,3,5-Triformylphloroglucinol (**3**) was synthesized as the analog of aldehyde **2** to study the influence of hydroxyl substituents on the gas adsorption properties.

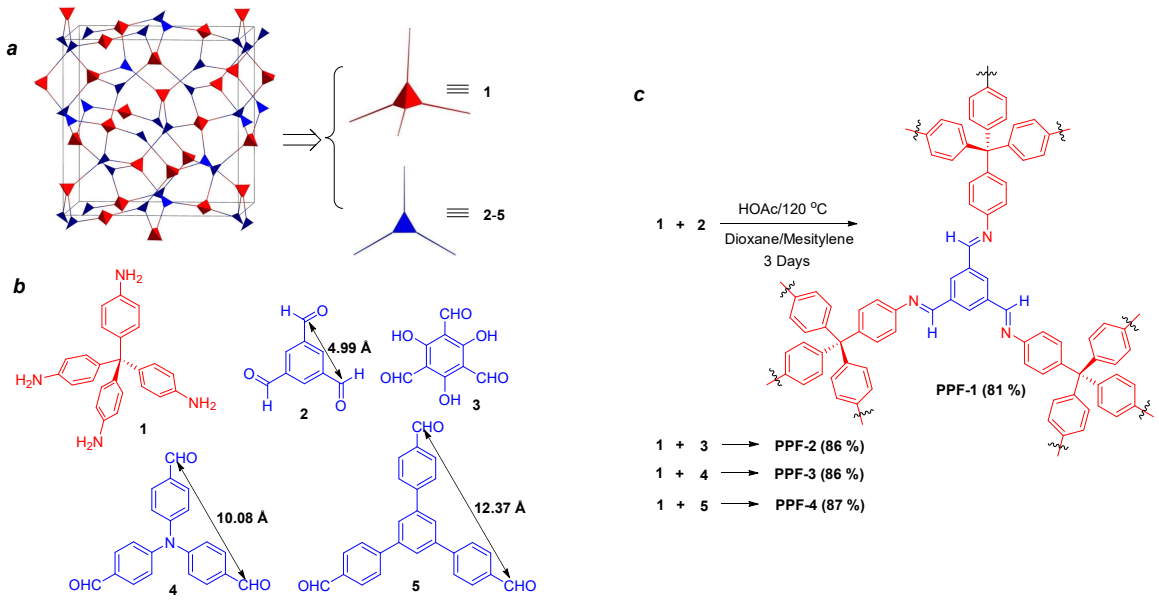

Scheme 2.1. **(a)** *ctn* topological structure from trigonal building block and tetrahedral building block; (b) Building blocks for PPFs; **(c)** The synthesis of PPF series.

PPFs were synthesized in good yields (81-89 %) by reacting tetraamine **1** with various trialdehydes (**2-5**) in a 1:1 (*v/v*) mixture of 1, 4-dioxane and mesitylene, in the presence of 6 M acetic acid under solvothermal conditions. Multiple attempts to synthesize crystalline frameworks failed and all materials were obtained as amorphous solids. Preparation of crystalline COF materials is not trivial, and usually requires enormous efforts in screening of various reaction conditions. The structures of PPFs were characterized by FT-IR, and solid state NMR. FT-IR spectra of **PPF-1, PPF-3**, and **PPF-4** show the characteristic C=N stretching band around 1623 cm^{-1}, which is overlapped with aromatic ring stretching band around 1589 cm^{-1} (Figure 2.7-2.15). The ^{13}C cross-polarization magic angle spinning (CP-MAS) NMR spectra of **PPF-1,3,4** showed the imine carbon resonance around 157 ppm, supporting the imine bond formation (Figure 2.55). There exist incompletely converted free amine and aldehyde functional groups, evidenced by the N-H stretching band around 3442 cm^{-1}, C=O stretching band around 1700 cm^{-1} in the IR spectra, as well as the aldehyde carbon resonance around 189 ppm in the ^{13}C-NMR spectra.

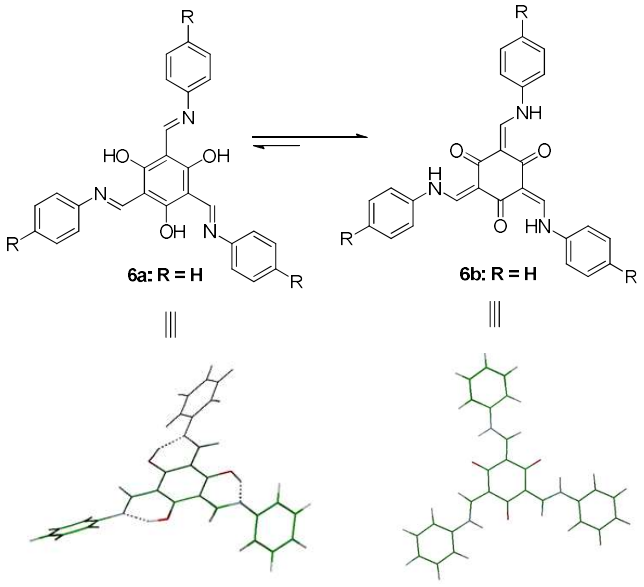

Scheme 2.2. Tautomers of model compound **6** (top), and their optimized structures (bottom).

For **PPF-2**, there are two possible tautomers, enol-imine form **PPF-2a** or keto-enamine form **PPF-2b**, which might coexist under equilibrium. Interestingly, the ^{13}C CP-MAS NMR spectra of **PPF-2** shows negligible imine carbon resonance peak around 157 ppm, which is present in other imine-linked frameworks **PPF-1, 3, 4**. It suggests **PPF-2** exists predominantly as keto-enamine form instead of enol-imine form. The appearance of new resonance peaks around 184, and 107 ppm in the ^{13}C CP-MAS NMR spectra of **PPF-2**, which are characteristic resonances of carbonyl carbon and α-carbon of keto-enamine isomer, further supports **PPF-2b** is the predominant tautomer in the solid state. IR spectrum of **PPF-2** shows strong absorption band at 1578 cm-1 arising from C=C stretching, together with the C=O stretching band at 1616 cm^{-1} and aromatic ring stretching band around 1595 cm^{-1} as broad shoulders, supporting the keto-enamine form of **PPF-2**.

We also performed theoretical calculations using Amber 11.0 molecular dynamics program package to optimize the structure and compare their relative energies of simple model compound **6**. We used the general Amber force field (GAFF field) with the charge parameters computed by AM1-BCC method. The computer calculations show that the keto-enamine form **6b** is totally flat and 18 kcal/mol more stable than the enol-imine form **6a.** Our modeling study is consistent with the report and X-ray crystal structure of similar compound (**6**, R = ^{t}BOC) by MacLachlan, in which only keto-enamine form was observed in both solution and solid state.[37] Given such significant energy difference between two tautomers, and the absence of imine characters in the IR and NMR spectra, irreversible conversion of **PPF-2a** to **PPF-2b** is suggested. The IR and ^{13}C NMR spectrum of framework **PPF-2b** match well with the reported data of the similar 2-D COF **TpPa-1** and **TpPa-2** constructed from of 1,3,5-triformylphloroglucinol (**3**) and *p*-phenylenediamine or 2,5-dimethyl-p-phenylenediamine, respectively.[38]

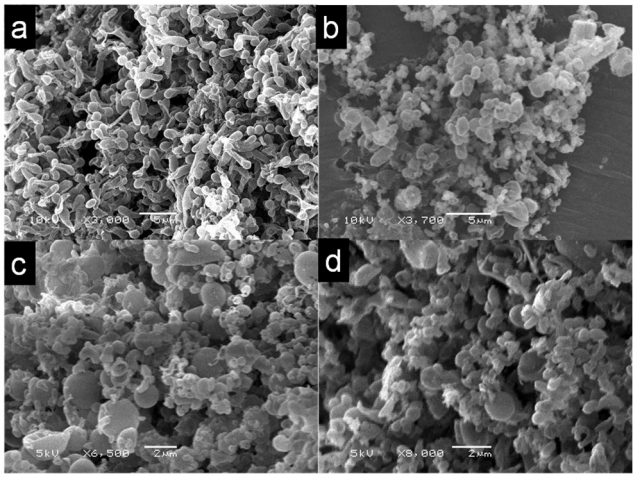

Figure 2.1: SEM images of **PPF-1** (a), **PPF-2** (b), **PPF-3** (c), and **PPF-4** (d).

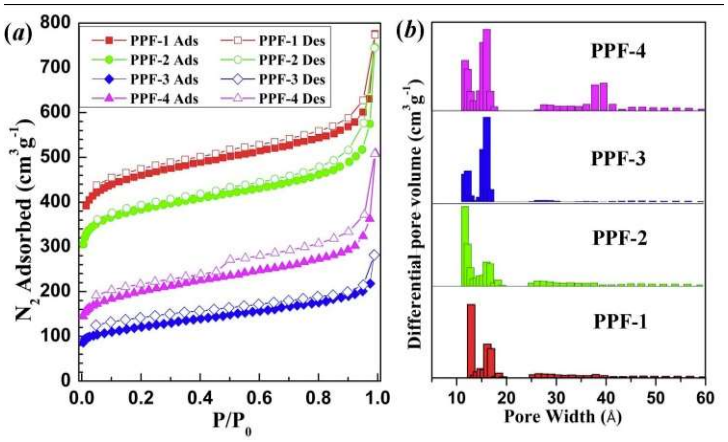

Figure 2.2. (a) N_2 adsorption (solid) and desorption (hollow) isotherms at 77 K of PPFs; (b) pore size distribution of PPFs series.

All the frameworks are stable under ambient conditions and we did not observe any decomposition during purification and handling. Scanning electron microscopy (SEM) images showed that **PPF-1** consists of mostly uniform sea anemone-shaped particles, whereas **PPF-2**, **PPF-3**, and **PPF-4** are composed of particles of various size, ranging from hundred nanometers to several micrometers (Figure 2.1). The materials are insoluble in most common organic solvents.

PPF-1, **PPF-3**, and **PPF-4** showed superior thermal stability with the onset decomposition temperatures of >501 °C (Figure 2.5). **PPF-2** decomposes at relatively lower temperature (400 ºC).

The permanent porosities of **PPFs (1-4)** were characterized by nitrogen adsorption/desorption isotherms of freshly activated samples at 77 K. The fully reversible adsorption-desorption of nitrogen depicted in Figure 2.2 shows type **I** isotherm character with a rapid uptake at low relative pressure (P/P_0 = 0-0.1), indicating a permanent micro-porosity nature of all the PPFs. According the IUPAC classification, all of the PPFs are typical microporous materials.[39] The gradual increase in nitrogen adsorption under relatively high pressure (P/P_0 = 0.1-0.9) and the sharp increase above P/P_0 = 0.9 are presumably due to the presence of interparticular void.[40] The isotherms in the low relative pressure range (P/P_0 = 0-0.1) shows decrease in N_2 uptake in the order of **PPF-1**<**PPF-2**<**PPF-4**<**PPF-3**. The pore size distribution (PSD) analysis based on the nonlocal density functional theory (NLDFT) model shows smaller micropores (pore width < 1.5 nm) are dominant in **PPF-1** and **PPF-2**, whereas relatively bigger micropores (pore width > 1.5 nm) are predominant in **PPF-3**, and **PPF-4**, and significant amount of mesopores in **PPF-4**. In general, the micropore size distribution of final framework is shifted to the larger pores when bigger building blocks were used. These results indicate the pore size distribution of the frameworks can be controlled by varying the size of building blocks.

All of the PPFs showed a small hysteresis in the whole range of relative pressure suggesting relative strong gas binding on the pore surface. The N_2 isotherms of **PPF-4** shows both type I and type IV character with significant hysteresis, consistent with the presence of pronounced amount of mesopores. The calculated Brunauer-Emmett-Teller (BET) specific surface area of PPF series are 1740 $m^2\ g^{-1}$, 1470 $m^2\ g^{-1}$, 419 $m^2\ g^{-1}$, and 726 $m^2\ g^{-1}$ for **PPF-1**, **PPF-2**, **PPF-3**, and **PPF-4**

respectively, and the Langmuir surface area is 2157 m^2 g^{-1}, 1918 m^2 g^{-1}, 598 m^2 g^{-1}, and 1162 m^2 g^{-1}, respectively (corresponding to P/P_0 = 0.4) (**Table 2.1**). These surfaces are comparable or higher than previously reported organic porous materials constructed through imine-condensation.

It is interesting to note that the surface area was dramatically decreased (from SA_{BET} 1740 m^2 g^{-1} of **PPF-1** to 419 m^2 g^{-1} of **PPF-3**) when the size of aldehyde building block was increased from 4.99 Å to 10.08 Å (distance between two aldehyde moieties). The network entanglement might be one possible reason for this porosity decrease. It has been documented that interpenetration occurs commonly, thus reducing the effective size of the pores, when larger building blocks are used to increase the pore dimensions.[22] One such example is the imine-linked 3D COF-300, reported by Yaghi.[41] However, when even larger aldehyde building block **5** (distance 12.37 Å) was used, we observed increase in surface area (from SA_{BET} 419 m^2 g^{-1} to 726 m^2 g^{-1}). The structure of aldehyde **5** shares the same geometrical features as aldehyde **4** with a sp^2-hybridization planar configuration for the nitrogen atom and propeller-like arrangement for the three phenyl rings. Therefore, similar building block connectivity in **PPF-3** and **PPF-4** is assumed. SEM images of **PPF-3** and **PPF-4** show similar morphological features, both consisting of mostly spheres of various sizes. Due to the lack of more detailed 3-D structural information on these amorphous materials, we do not have a clear explanation at present for the lowest surface area of **PPF-3**.

Given the microporous nature and the narrow pore size distribution of PPFs series, we next investigated their gas uptake capacities of small molecules (CO_2, H_2, CH_4, and C_2H_2) (Figure 2.3). In general, increased gas uptake capacities were observed with increased porosity, i.e. uptakes of CO_2, H_2, and CH_4, are in the order of **PPF-1**>**PPF-2**>**PPF-4**>**PPF-3**, consistent with the order of SA_{BET} of these frameworks. **PPF-1** with highest SA_{BET} adsorbs 136 cm^3 g^{-1} (26.7 wt %) of CO_2 at

273 K and 1 bar; 305 cm^3 g^{-1} (2.75 wt %) of H_2 at 77 K and 1 bar, and 34 cm^3 g^{-1} (2.43 wt %) of CH_4 at 273 K and 1 bar. To our knowledge, the adsorption capacities of **PPF-1** toward CO_2 H_2, and CH_4 are among the highest in all organic porous materials that have been reported (see **Table 2.3**), and even competitive with the best reported MOFs under the same conditions.[42] At 195 K and 1 bar, the CO_2 uptake reached to an impressive amount of 444 cm^3 g^{-1} (87.2 wt %) (Figure 2.19). **PPF-2** also shows excellent gas adsorption capabilities, albeit it adsorbs slightly less amount of CO_2, H_2, CH_4 compared to **PPF-1** under the same conditions. The CO_2 H_2, and CH_4 uptake of **PPF-3** and **PPF-4** are almost reduced by half under identical conditions, compared to **PPF-1**, and **PPF-2**, which is consistent with their significantly reduced specific surface areas.

Table 2.1. Summary of porosity and pore volume data for the PPF series.

Polymer	SA_{BET}[a]	$SA_{Langmuir}$[b]	V_{Total}[c]
PPF-1	1740	2157	1.18
PPF-2	1470	1918	1.14
PPF-3	419	598	0.37
PPF-4	726	1162	0.77

[a]Surface area (m^2 g^{-1}) calculated from the nitrogen adsorption based on the BET model; [b]Surface area (m^2 g^{-1}) calculated from the nitrogen adsorption isotherms based on the Langmuir model; [c]The total pore volume (cm^3 g^{-1}) calculated at $P/P_0 = 0.99$.

In addition to CO_2, H_2, and CH_4 storage by porous materials, extensive research efforts have been devoted to acetylene (C_2H_2) storage. Acetylene is the most common starting material in various industries such as petrochemical industry, and serves as an important building block in organic syntheses. Acetylene is also considered as an important alternative energy source.

However, acetylene is explosive when it is compressed to above 30 psi or 15 psi at room temperature even in the

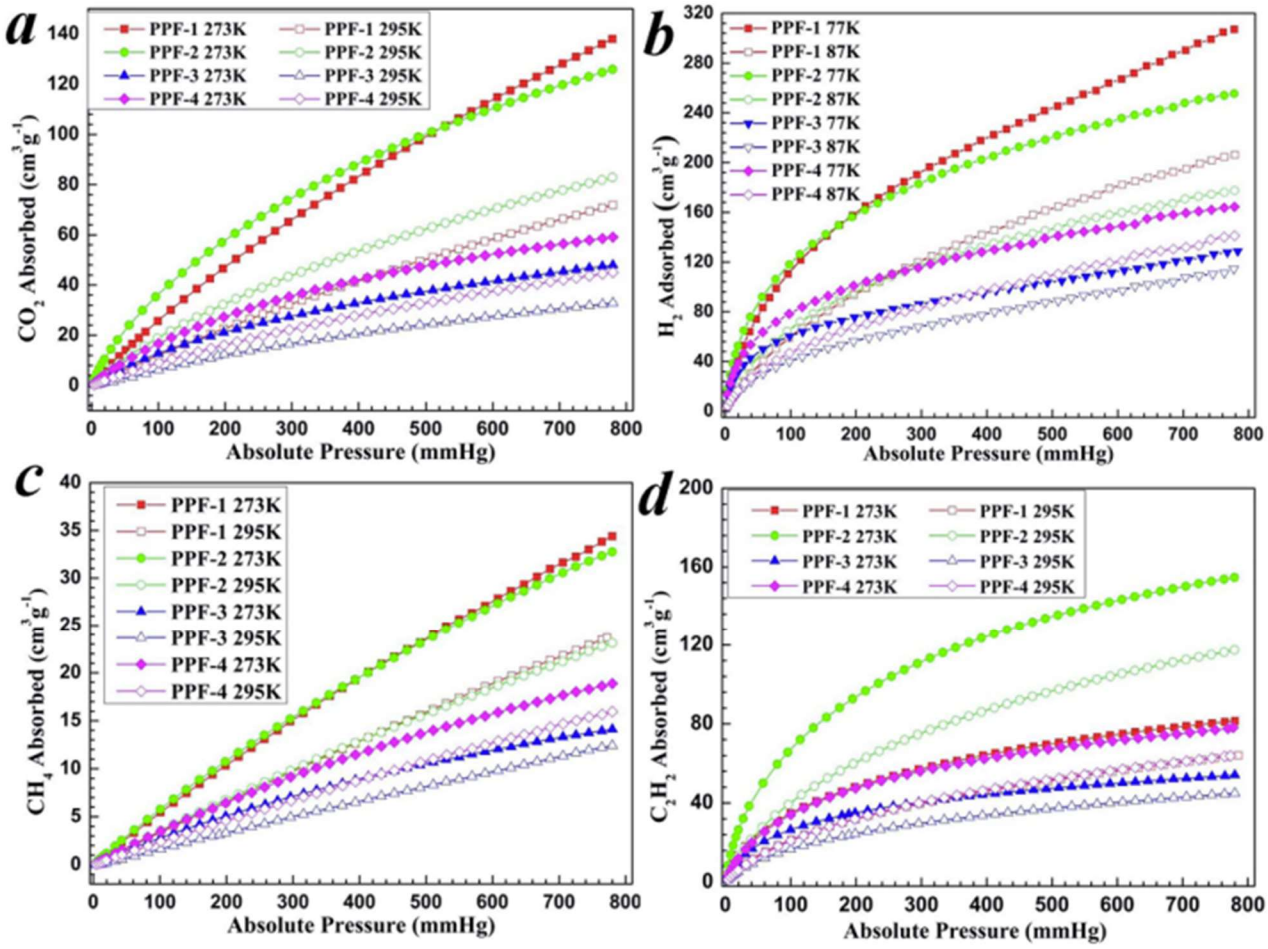

Figure 2.3. (a) CO_2 adsorption of the PPF series at 273 K and 295 K; (b) H_2 adsorption of the PPF series at 77 K and 87 K; (c) CH_4 adsorption of the PPF series at 273 K and 295 K; (d) C_2H_2 adsorption of the PPF series at 273 K and 295 K.

Table 2.2. Summary of gas adsorption properties of the PPF series at low pressure.

Porous Polymer	CO_2 Uptake[a]		H_2 Uptake[b]		CH_4 Uptake[a]		C_2H_2		Selectivity[c]	
	wt %	Q_{st}	wt %	Q_{st}	wt %	Q_{st}	wt %	Q_{st}	CO_2/N_2	CO_2/CH_4
PPF-1	26.7	25.6	2.75	6.8	2.43	15.1	9.38	27.9	14.5	11.0
PPF-2	24.4	29.2	2.28	7.5	2.31	15.9	17.9	31.6	15.4	10.6
PPF-3	9.2	21.8	1.14	8.2	1.00	19.4	6.23	29.7	20.4	9.2
PPF-4	11.4	25.1	1.47	8.1	1.32	13.9	8.97	23.9	15.0	8.6

[a] 273K and 1 bar, and unit of Q_{st}: kJ mol^{-1} ; [b] 77K and 1bar, and unit of Q_{st}: kJ mol^{-1}; [c] Adsorption selectivity at 273K and 1bar.

Table 2.3. Summary of gas adsorption properties of organic porous materials at low pressure.

Porous polymer	SA_{BET}[a]	SA_{Lang}[a]	V_{pore}[b]	CO_2 Uptake[c]		H_2 Uptake[d]		Ref.
				Wt %	Q_{st}	Wt %	Q_{st}	
PPF-1	1740	2157	1.18	26.7	25.6	2.75	6.8	**This work**
BILP-4	1135	1486	0.65	23.5	28.7	2.30	7.8	[27]
CPOP-1	2220	2508	1.293	21.2	27.0	2.80	N/A	[5]
PAF-3	2932	3857	1.54	15.3	19.2	2.07	6.6	[43]
COF-102	3620	4650	1.55	5.3	N/A	1.20	N/A	[44]
A1-B2	1521	N/A	1.13	N/A	N/A	1.50	3.0	[33]

[a]unit: m^2 g^{-1}; [b] unit: cm^3 g^{-1}; [c] 273 K. 1 bar; unit of Q_{st}: kJ mol^{-1}; [d] 77 K. 1 bar; unit of Q_{st}: kJ mol^{-1}

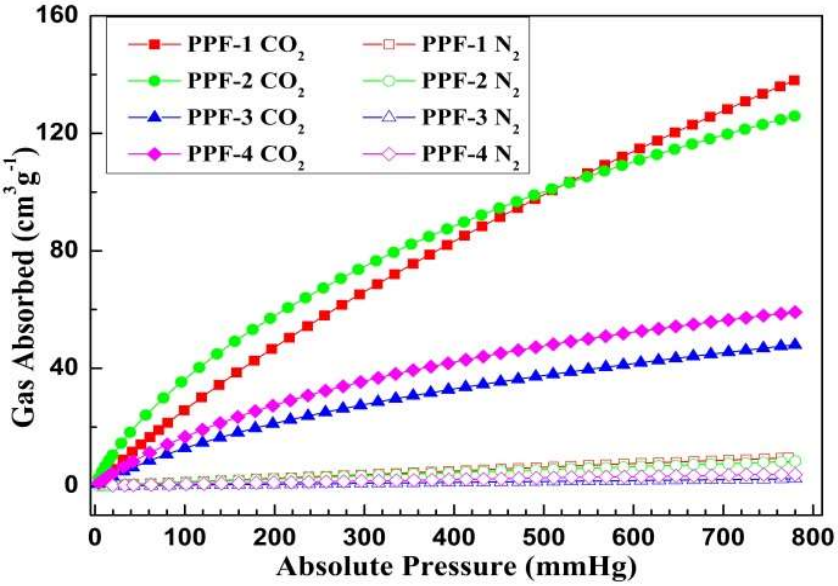

Figure 2.4. Single-component gas adsorption isotherms for CO_2 and N_2 at 273 K.

absence of oxygen. The safe storage and transportation of acetylene gas in porous materials is recommended as a promising technology.[45] However, only limited organic porous materials have been reported for acetylene adsorption. Our frameworks showed excellent C_2H_2 adsorption capacities (6.23-17.9 wt %) at 273 K and 1 bar. The impressive C_2H_2 uptake of 17.9 wt % in **PPF-2** is the highest reported so far for all organic porous materials. Although our experimental data suggests the CO_2, H_2 and CH_4 uptake are proportional to the surface area (**PPF-1** is the highest), interestingly, **PPF-2** shows the highest C_2H_2 uptake (153 cm^3 g^{-1} at 273K and 1bar), almost two-fold higher than **PPF-1** (80 cm^3 g^{-1}). Given the structural similarity of **PPF-1** and **PPF-2**, the increased acetylene adsorption is presumably due to the electron-donating substituents in framework **PPF-2**. The stronger polarizing effect induced by carbonyls and secondary amines in **PPF-2** presumably enables its stronger interactions with C_2H_2.[46] It has been reported that electron-rich benzene rings have stronger C-H…π interactions with acetylene compared to electron-deficient ones.[47]

To further understand the gas adsorption properties, the isosteric heats (Q_{st}) of adsorption for different gases were calculated from the gas adsorption isotherms at two different temperatures by fitting the data to virial equation (Figure 2.2 and Figure 2.15-2.47). A summary of Q_{st} for different gases were shown in **Table 2.2**. At zero-coverage, the highest Q_{st} for CO_2, CH_4 and C_2H_2 were observed for **PPF-2:** 29.2 kJ mol^{-1}, 15.9 kJ mol^{-1} and 31.6 kJ mol^{-1}, respectively, all of which are the highest among the reported values for organic porous polymers.[22,44,48] The Q_{st} of PPFs for H_2 is between 6.8 to 8.2 kJ mol^{-1}, which are comparable or even higher than other polymers previously reported (**Table 2.3**). The impressive isosteric heat of 31.6 kJ/mol further indicates the strong interaction of **PPF-2** with acetylene guest molecule. It should be noted that **PPF-2**, the functionalized analogue of **PPF-1** generally shows higher Q_{st} than unfunctionalized **PPF-1**, which supports the notion that incorporating polar groups inside the pore surface can enhance the gas binding of porous materials.[4,28]

To assess the potential applications of these frameworks in post-combustion CO_2 capture under ambient pressure, single-component gas adsorption isotherms were carried out on CO_2 and N_2 under 273 K and up to 780 mmHg (**Figure 2.4**). CO_2/N_2 selectivities were calculated by using ideal adsorption solution theory (IAST)[49] method at 273 K and 1 bar. Good adsorption selectivities CO_2/N_2 were observed for all the frameworks: 14.5, 15.4, 20.4 and 15.0 for **PPF-1**, **PPF-2**, **PPF-3** and **PPF-4**, respectively (**Table 2.2**). High CO_2 adsorption capacity as well as CO_2/N_2 adsorption selectivities are the two key parameters for evaluating the potential of porous materials in carbon capture applications. PPFs also showed good adsorption selectivities (8.6-11.2) toward CO_2 over CH_4 at 273 K, and 1 bar, further highlighting the great potential of these PPFs in gas separation applications.

2.4 Conclusion

In conclusion, we have successfully synthesized a series of microporous polymer frameworks with novel [3+4] structure motif through the imine condensation. The BET surface area of these PPFs is up to 1740 $m^2 g^{-1}$. Owing to the narrow pore size distribution and electron-rich pore surface, PPFs exhibit exceptionally high H_2 uptake of 2.75 wt % (77 K and 1 bar), C_2H_2 uptake of 17.9 wt % (273 K, and 1 bar) and CO_2 uptake of 26.7 wt % (273 K and 1 bar). Moreover, **PPF-2** shows a good CO_2/N_2 adsorption ideal selectivity (20.4/1), as well as CO_2/CH_4 selectivity (up to 11.2/1), at 273 K and 1 bar. Collectively, along with the relatively low cost for large-scale manufacturing of these porous polymers, these results open up a strategy to prepare organic porous polymers highly competitive in gas storage and separation applications. Extended research of this series of materials is ongoing in our lab.

2.5 Experimental section

2.5.1. Materials and measurements

All chemical reagents were commercially available and used without further purification. Tetrakis-(4-nitrophenyl)-methane, 1, 3, 5-benzenetricarboxaldehyde, 2,4,6-trihydroxybenzene-1,3,5-tricarbaldehyde, Tris(p-formylphenyl)amine, and 1,3,5-Tris(4-formylphenyl)benzene were synthesized following the published procedures[22,50,51,33,52-54].

Flash column chromatography was performed by using a 100-150 times the weight excess of flash silica gel 32-63 μm from Dynamic Absorbants, Inc. Fractions were analyzed by TLC using TLC silica gel F254 250 μm precoated-plates from Dynamic Absorbants Inc.

NMR spectra were taken using Inova 400 and Inova 500 spectrometers. Solid-state cross polarization magic angle spinning (CP-MAS) NMR spectra were recorded on an Inova 400 NMR spectrometer.

Powder X-Ray Diffraction (PXRD) was obtained from Inel CPS 120 diffraction system, using monochromated Cu K_α (λ=1.542 Å) radiation.

The FT-IR spectra of starting materials and as synthesized PPF-1 were obtained from Thermo Nicolet Avatar-370 spectrometer using KBr pellets.

Elemental analyses were taken at Huffman Laboratories, Inc.

Thermogravimetric analyses (TGA) were performed on a thermogravimetric/differential thermal analyzer by heating the samples at 10 °C min^{-1} to 800 °C in the atmosphere of nitrogen.

The Quantachrome Autosorb ASiQ automated gas sorption analyzer was used to measure N_2, H_2, CO_2 C_2H_2, and CH_4 adsorption isotherms. The sample was heated at 160 °C and kept at this temperature for at least 22 hours under vacuum for activation. Ultra high purity grade (99.999% purity) N_2, CO_2, H_2, CH_4, C_2H_2 and He, oil-free valves and gas regulators were used for all free space corrections and measurements. For all of the gas adsorption measurements, the temperatures were controlled by using a refrigerated bath of liquid N_2 (77K), liquid Ar (87K), dry ice-acetone (195K), ice water (273K) and water (295K).

Scanning Electron Microscopy images (SEM) were recorded using a JSM-6480LV (LVSEM) at 5.0 kV. Sample was sputter coated with gold prior to analysis.

2.5.2. General synthetic routes

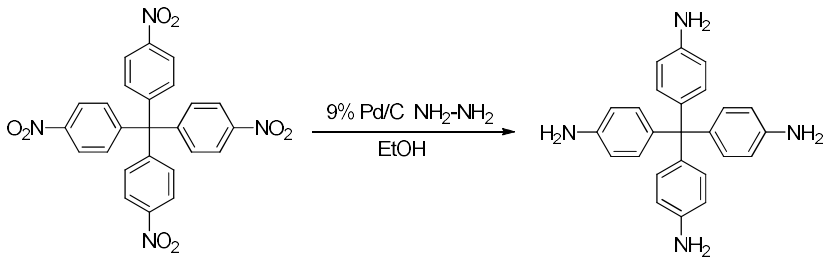

Synthesis of tetra-(4-anilyl)-methane: Tetrakis-(4-nitrophenyl)-methane (0.50 g, 1.0 mmol) was placed in a 100 mL schlenk tube, and anhydrous ethanol (35 mL) was added as the solvent, followed by Pd/C (60 mg, 9 %). A hydrazine hydrate solution (2 mL of 80 %) was then added dropwise with vigorous stirring. The resulting mixture was heated to reflux for 16 hours. After the solution was cooled to room temperature, the crude product was collected by vacuum filtration. After purification by running a flash column chromatography (with 9 % ethanol in dichloromethane as the eluent), the pure product was collected as a white solid (0.36 g, 96 %): ^{1}H-NMR (d_6-DMSO, 500 MHz): δ 6.65 (d, 8H, J = 8.5 Hz), 6.38 (d, 8H, J = 8.5 Hz), 4.85 (s, 8H); ^{13}C-NMR (d_6-DMSO, 101 MHz): δ 146.4, 136.5, 131.7, 113.2, 61.8 ppm. The NMR data are consistent with the literature reported.[55]

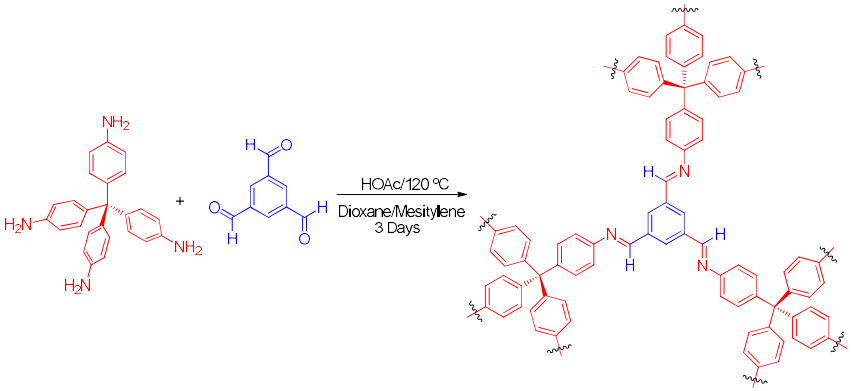

Synthesis of PPF-1: A 25 mL schlenk tube was charged with tetra-(4-anilyl)-methane (36 mg, 0.095 mmol), 1, 3, 5-benzenetricarboxaldehyde (17.2 mg, 0.079 mmol), anhydrous 1, 4-dioxane

(5 mL) and mesitylene (5 mL). The resulting mixture was sonicated for a few minutes until the solid was completely dissolved. The solution was then bubbled with nitrogen for 5 minutes, and 6 M acetic acid (0.2 mL) was added. The schlenk tube was flash frozen at 77 K using the liquid nitrogen bath, evacuated to the internal pressure of 300 mTorr for 5 minutes. Then the tube was sealed by Teflon valve and heated at 120 °C for 3 days under nitrogen atmosphere. After cooling to room temperature, the light yellow precipitate was collected by vacuum filtration, washed with anhydrous THF and dried in vacuo overnight to provide PPF-1 (34 mg, 81 % based on the aldehyde): Elemental analysis for $C_{111}H_{72}N_{12}\cdot 7H_2O$: Calcd. C, 78.42 %; H, 5.10 %; N, 9.89 %. Found. C, 77.79 %; H, 5.31 %; N, 9.83 %. (Since the materials are polymers instead of pure compounds, their elemental analysis results are just used as a reference, not to determine their purity.)

Synthesis of PPF-2: This polymer was synthesized following the similar method as described above for the synthesis of PPF-1 by using 2,4,6-trihydroxybenzene-1,3,5-tricarbaldehyde (33 mg, 0.16 mmol) and tetra-(4-anilyl)-methane (50 mg, 0.16 mmol). After drying in the vacuum overnight, the PPF-1-OH was obtained as an orange powder solid. (62 mg, 89 % based on the aldehyde): Elemental analysis for $C_{111}H_{72}O_{12}N_{12}\cdot 12H_2O$: Calcd. C, 67.26 %; H, 4.88 %; N, 8.48 %. Found. C, 67.20 %; H, 4.46 %; N, 8.15 %. (Since the materials are polymers instead of pure compounds, their elemental analysis results are just used as a reference, not to determine their purity.)

Synthesis of PPF-3: This polymer was synthesized following the similar method as described above for the synthesis of PPF-1 by using tris(p-formylphenyl)amine (35 mg, 0.11 mmol) and tetra-(4-anilyl)-methane (30 mg, 0.094 mmol). After drying in the vacuum overnight, the PPF-2

was obtained as a yellow powder solid. (51 mg, 86 % based on the aldehyde): Elemental analysis for $C_{159}H_{108}N_{16}\cdot 10H_2O$: Calcd. C, 78.82 %; H, 5.32 %; N, 9.25 %. Found. C, 78.86 %; H, 5.10 %; N, 9.13 %. (Since the materials are polymers instead of pure compounds, their elemental analysis results are just used as a reference, not to determine their purity.)

Synthesis of PPF-4: This polymer was synthesized following the similar method as described above for the synthesis of PPF-1 by using 1,3,5-tris(4-formylphenyl)benzene (41 mg, 0.11 mmol) and tetra-(4-anilyl)-methane (36 mg, 0.11 mmol). After drying in the vacuum overnight, the PPF-3 was obtained as a tan powder solid. (57 mg, 87 % based on the aldehyde): Elemental analysis for $C_{183}H_{120}N_{12}\cdot 12H_2O$: Calcd. C, 81.31 %; H, 5.37 %; N, 6.22 %. Found. C, 81.23 %; H, 4.90 %; N, 6.45 %. (Since the materials are polymers instead of pure compounds, their elemental analysis results are just used as a reference, not to determine their purity.)

2.5.3. Thermal gravimetric analysis of PPF series

Samples were run on a TA Instruments Q-500 series thermal gravimetric analyzer with samples held in a platinum pan under nitrogen atmosphere. A 10 K min^{-1} ramp rate was used. The materials show a good thermal stability up to at least 400 °C.

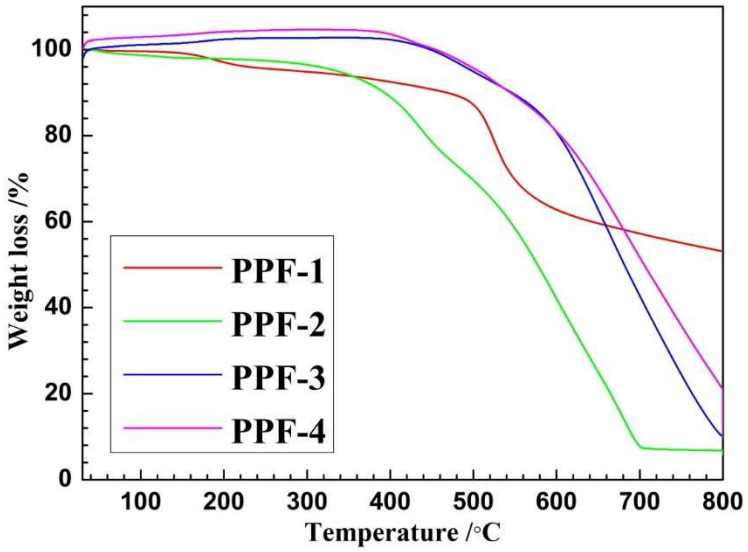

Figure 2.5. TGA profiles of the PPF series.

2.5.4. FT-IR of starting materials and PPF series

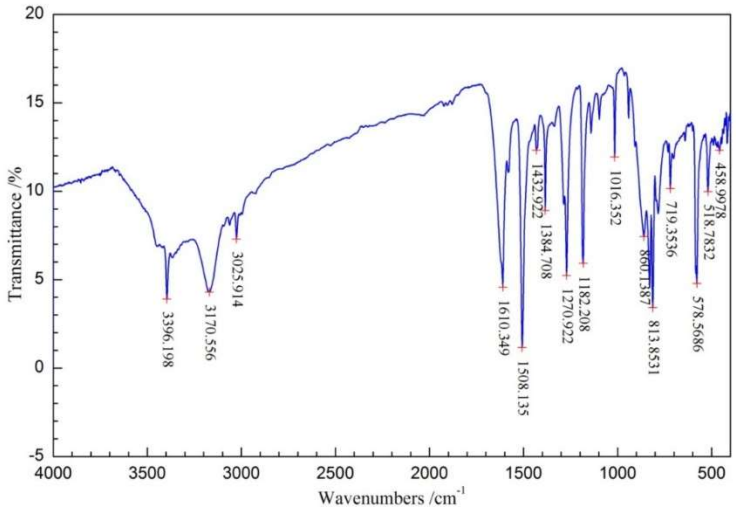

Figure 2.6. FT-IR spectrum of tetra-(4-anilyl)-methane.

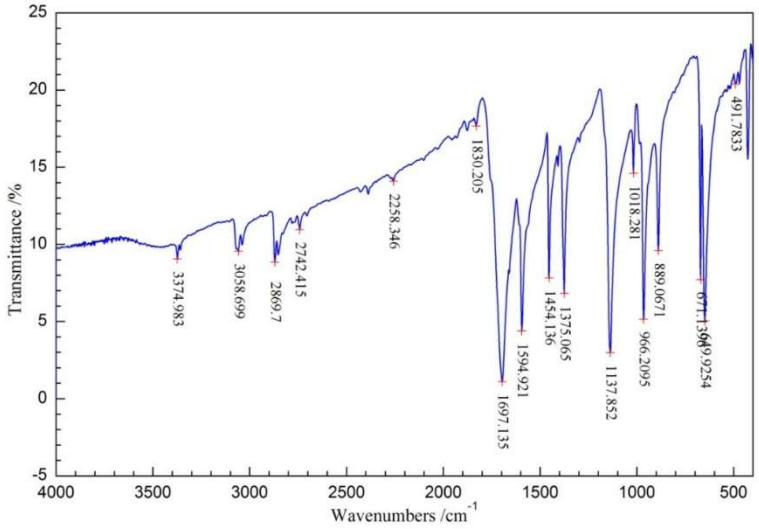

Figure 2.7. FT-IR spectrum of 1, 3, 5-benzenetricarboxaldehyde.

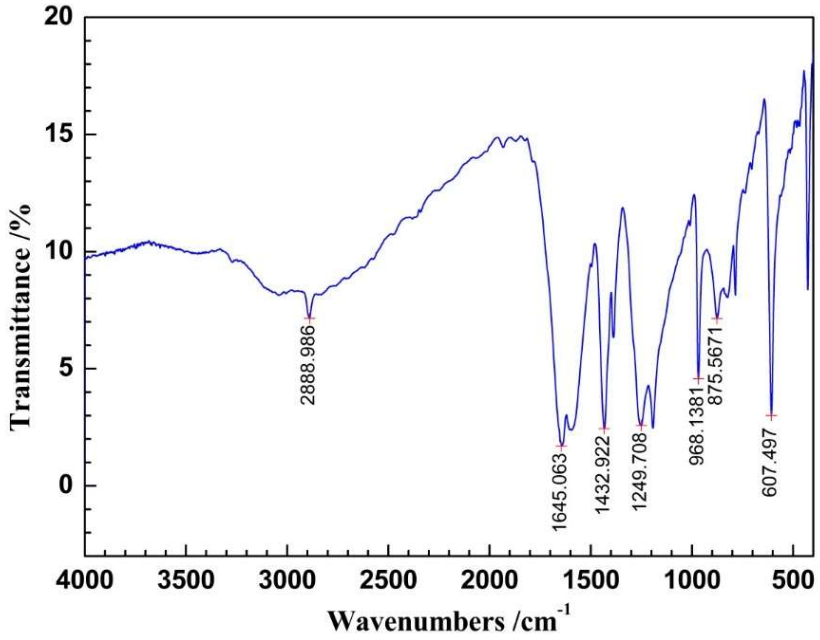

Figure 2.8. FT-IR spectrum of 2,4,6-trihydroxybenzene-1,3,5-tricarbaldehyde.

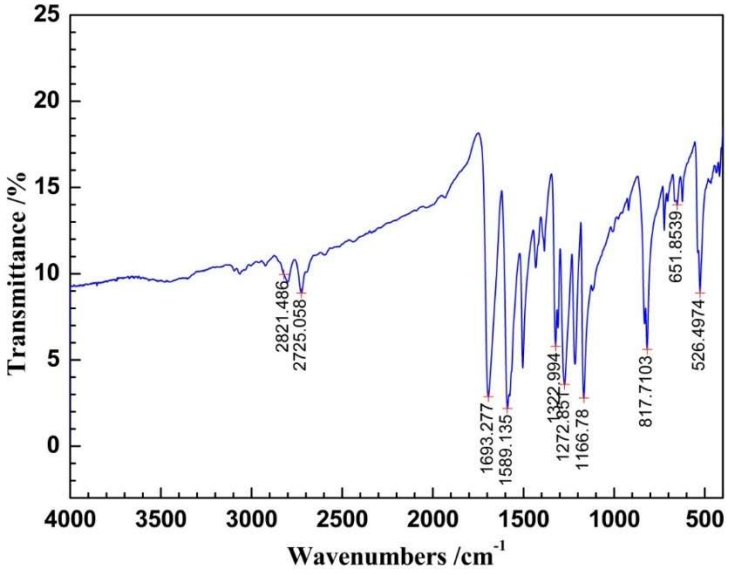

Figure 2.9. FT-IR spectrum of tris(p-formylphenyl)amine.

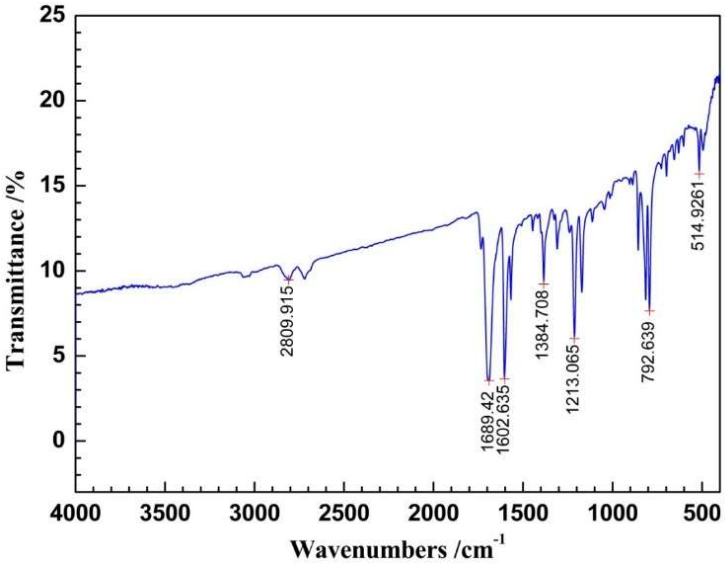

Figure 2.10. FT-IR spectrum of 1,3,5-tris(4-formylphenyl)benzene.

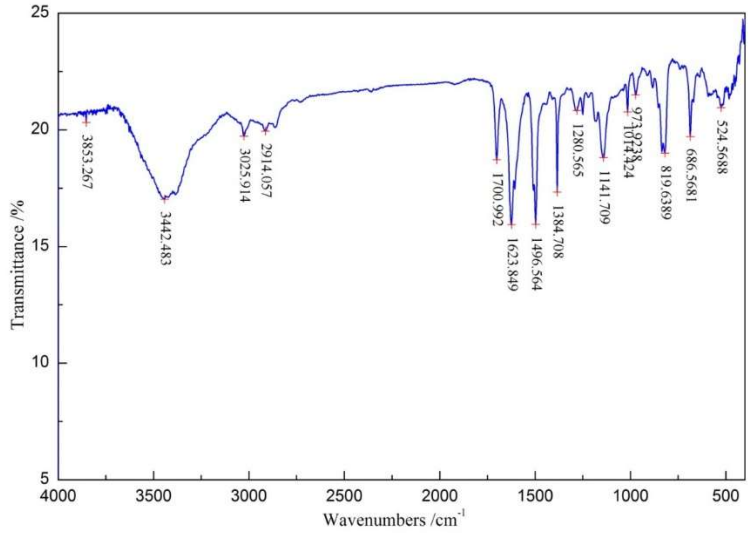

Figure 2.11. FT-IR spectrum of as-synthesized PPF-1.

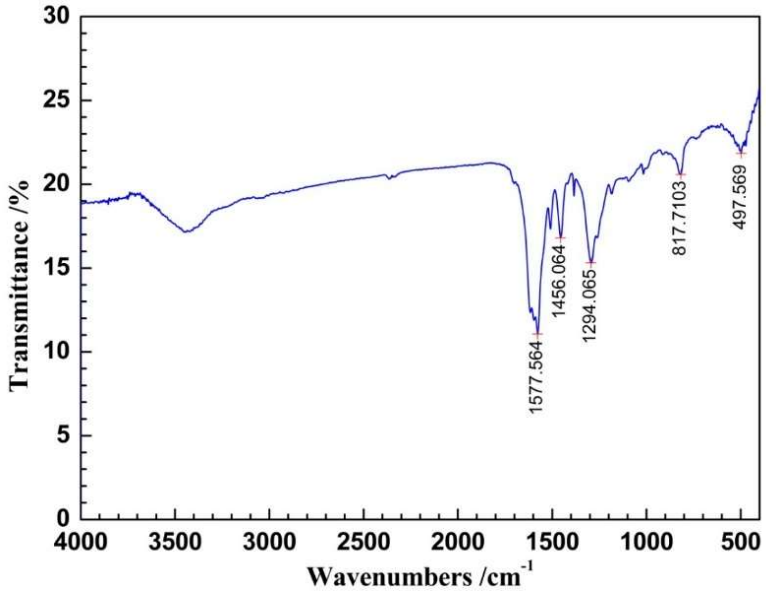

Figure 2.12. FT-IR spectrum of as-synthesized PPF-2.

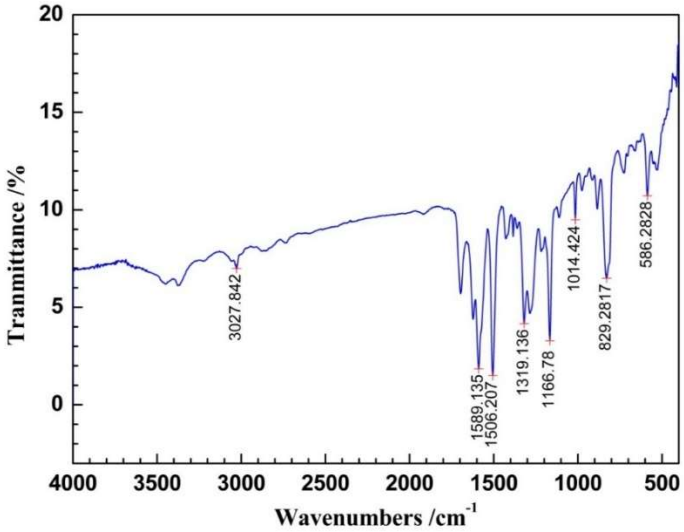

Figure 2.13. FT-IR spectrum of as-synthesized PPF-3.

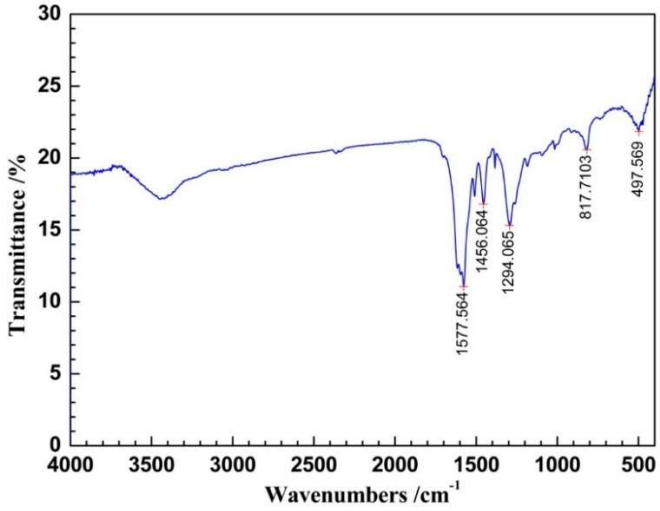

Figure 2.14. FT-IR spectrum of as-synthesized PPF-4.

2.5.5. Estimation of the Isosteric Heats of Gas (CO_2, H_2, CH_4 and C_2H_2) Adsorption

To determine the binding affinity of PPF series for different gases (CO_2, CH_4 and H_2), we calculated the Q_{st} for different gases using the virial method[56] based on two independent temperature gas adsorption isotherms. In each case, the data were fitted using the following equation:

$$\mathrm{Ln}P = \mathrm{Ln}N + \frac{1}{T}\sum_{i}^{m} a_i N^i + \sum_{i}^{n} b_i N^i$$

Here, P is pressure expressed in mmHg; N is the adsorption capacity expressed in mg/g; T is the absolute temperature expressed in K; a_i and b_i are virial coefficients, and m and n are the number of coefficients to describe the adsorption isotherms, usually m≤6 and n≤3. The isosteric heat of adsorption is calculated through the following expression:

$$Q_{st} = -R\sum_{i}^{m} a_i N^i$$

Where R is universal gas constant, in this manuscript, Q_{st} is based the gas adsorption from 0 to 780 mmHg.

2.5.5.1 Isosteric Heats of Gas (CO_2, H_2, CH_4 and C_2H_2) for PPF-1

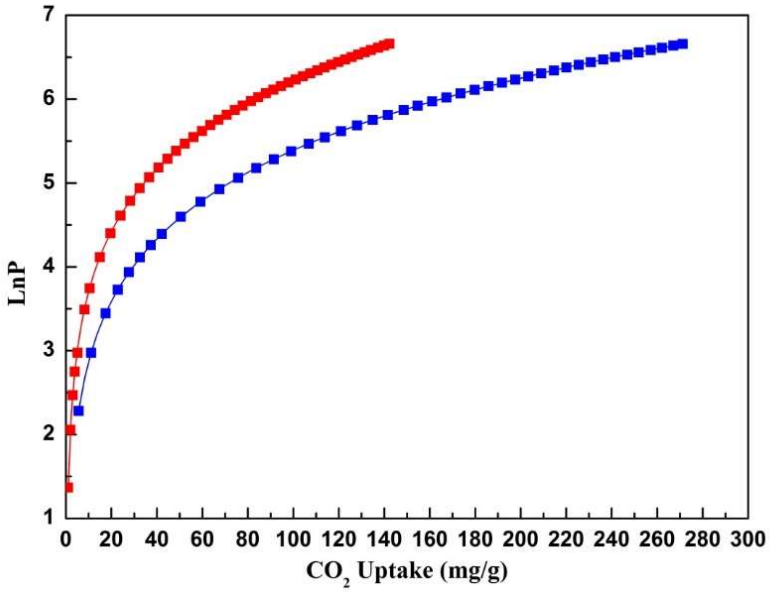

Figure 2.15. Virial analysis of CO_2 adsorption isotherms at 273 K (**red**) and 295 K (**blue**).

Table 2.4. Virial equation fitting results of CO_2 adsorption for PPF-1.

a_0	a_1	a_2	a_3	a_4	a_5	b_0	b_1	b_2	R^2
3074.3785	0.93013	0.00352	4.5800E-5	2.0535E-7	3.0435E-10	11.79985	9.18074E-4	2.30998E-5	0.99996

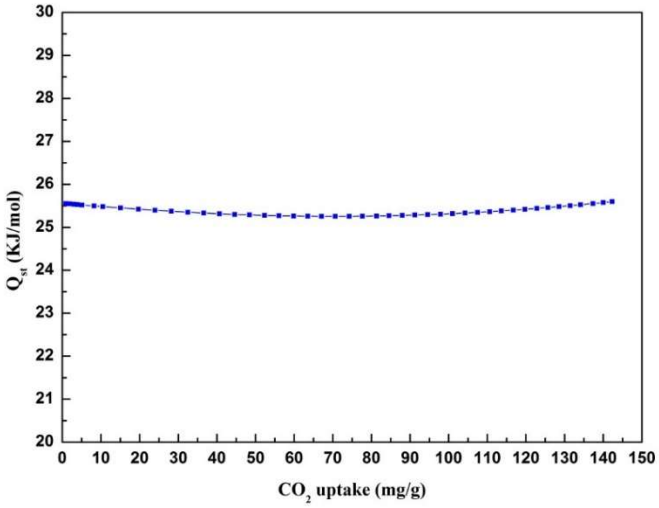

Figure 2.16. Isosteric heat of CO_2 adsorption for PPF-1.

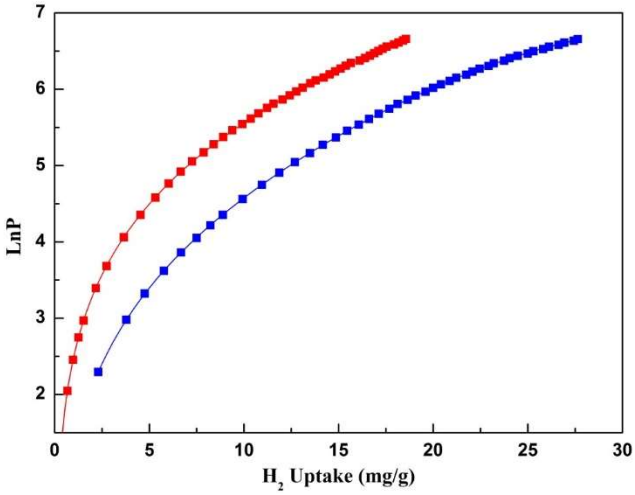

Figure 2.17. Virial analysis of H_2 adsorption isotherms at 77 K (**red**) and 87 K (**blue**).

Table 2.5. Virial equation fitting results of H_2 adsorption for PPF-1.

a_0	a_1	a_2	a_3	a_4	a_5	b_0	b_1	b_2	R^2
830.9810	21.1384	0.63325	0.03437	9.9440E-4	1.0129E-5	11.90755	0.10794	1.56327E-4	0.99998

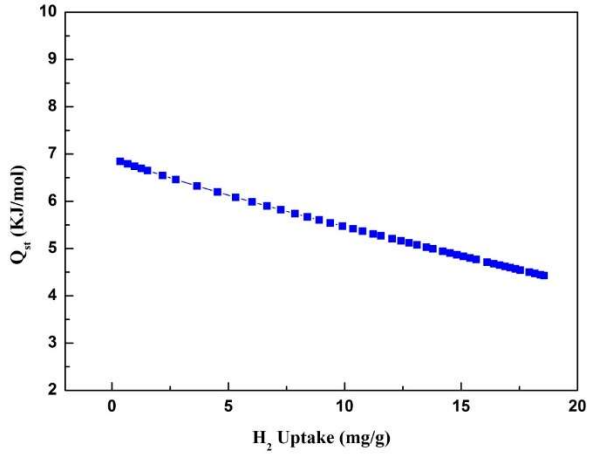

Figure 2.18. Isosteric heat of H_2 adsorption for PPF-1.

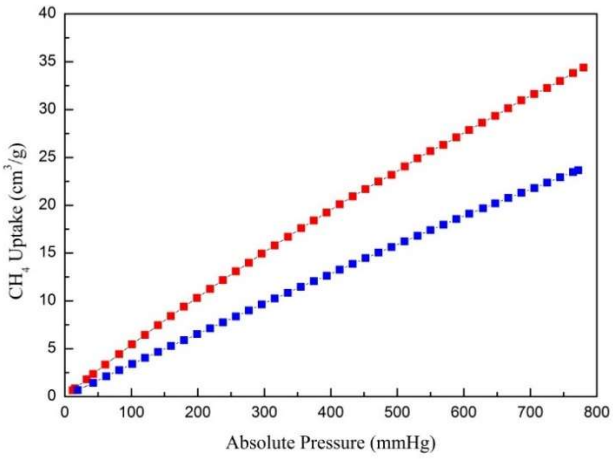

Figure 2.19. CH_4 adsorption for PPF-1 at different temperatures (red for 273 K and blue for 295 K).

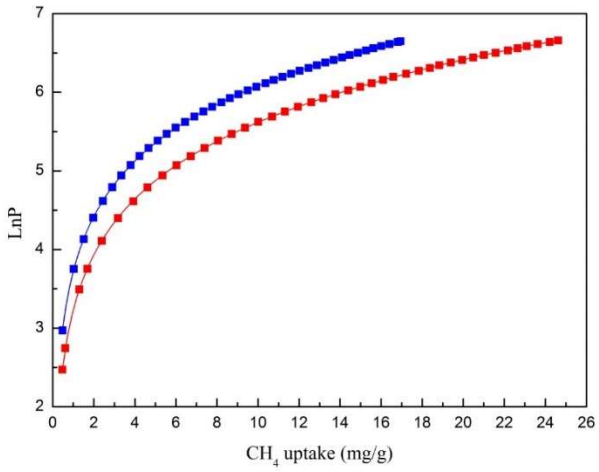

Figure 2.20. Virial analysis of CH_4 adsorption isotherms at 273 K (**red**) and 295 K (**blue**).

Table 2.6. Virial equation fitting results of CH_4 adsorption for PPF-1.

a_0	a_1	a_2	a_3	a_4	a_5	b_0	b_1	b_2	R^2
1814.9119	6.79264	0.53361	0.01994	0.00105	1.93980E-5	8.8672	0.01763	0.00133	0.99998

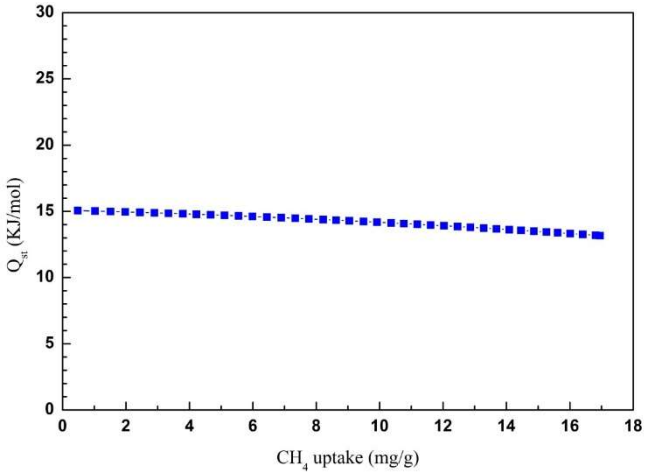

Figure 2.21. Isosteric heat of CH_4 adsorption for PPF-1.

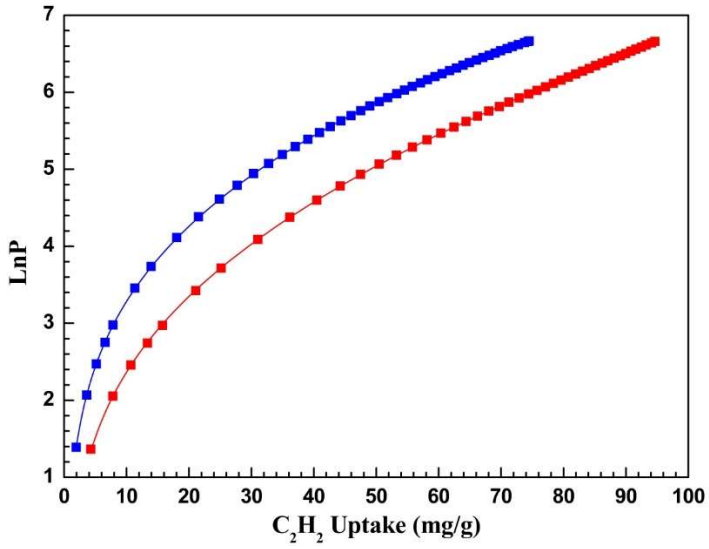

Figure 2.22. Virial analysis of CH_4 adsorption isotherms at 273 K (**red**) and 295 K (**blue**).

Table 2.7. Virial equation fitting results of C_2H_2 adsorption for PPF-1.

a_0	a_1	a_2	a_3	a_4	a_5	b_0	b_1	b_2	R^2
3352.7162	2.85125	0.19233	6.8997e-5	1.6974e-6	1.4348e-8	12.04067	0.04166	7.8488e-4	0.99998

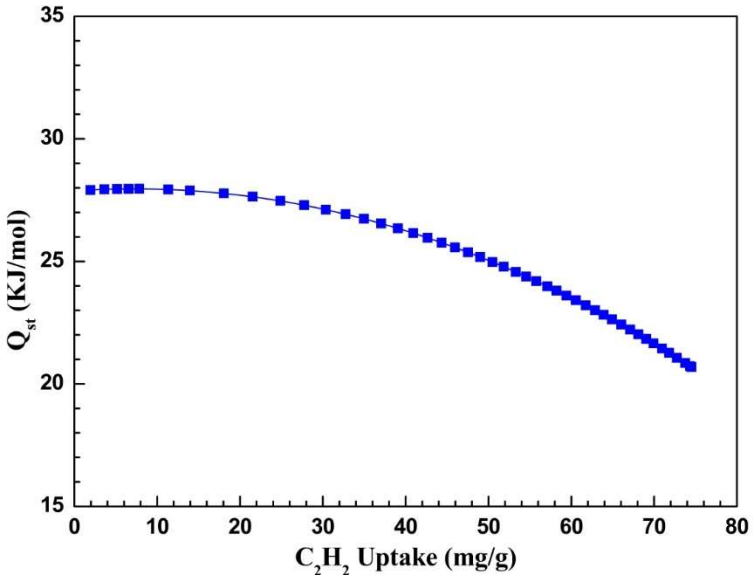

Figure 2.23. Isosteric heat of C_2H_2 adsorption for PPF-1.

2.5.5.2 Isosteric Heats of Gas (CO_2, H_2, CH_4 and C_2H_2) for PPF-2

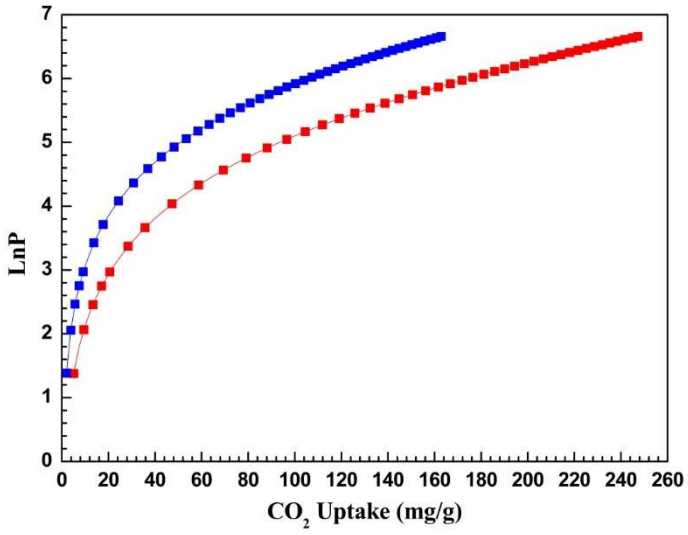

Figure 2.24. Virial analysis of CO_2 adsorption isotherms at 273 K (**red**) and 295 K (**blue**).

Table 2.8. Virial equation fitting results of CO_2 adsorption for PPF-2.

a_0	a_1	a_2	a_3	a_4	a_5	b_0	b_1	b_2	R^2
3516.1716	8.51652	0.04217	1.4323e-4	4.1455e-7	4.9472e-10	12.57446	0.01751	5.8612e-5	0.99999

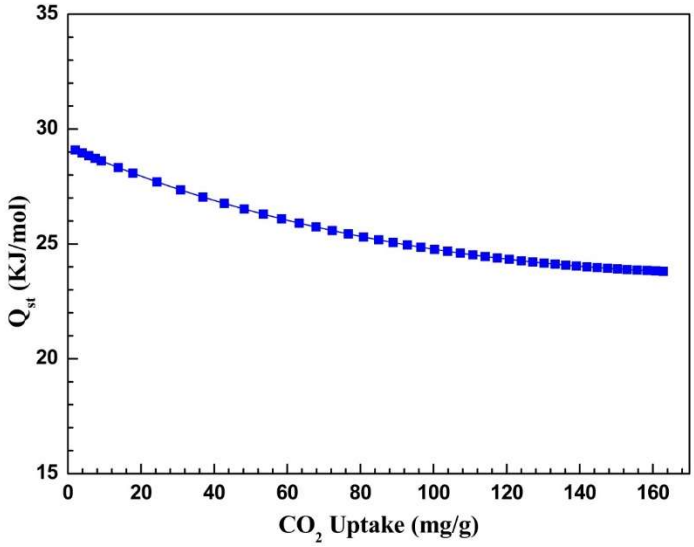

Figure 2.25. Isosteric heat of CO_2 adsorption for PPF-2.

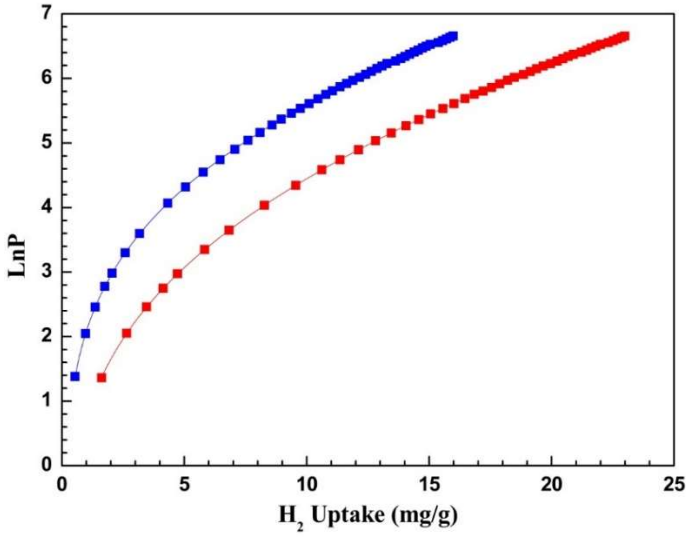

Figure 2.26. Virial analysis of H_2 adsorption isotherms at 77 K (**red**) and 87 K (**blue**).

Table 2.9. Virial equation fitting results of H_2 adsorption for PPF-2.

a_0	a_1	a_2	a_3	a_4	a_5	b_0	b_1	b_2	R^2
901.93864	18.11982	0.82484	0.04998	0.00171	2.31613e-5	12.26403	0.01238	2.21953e-4	0.99998

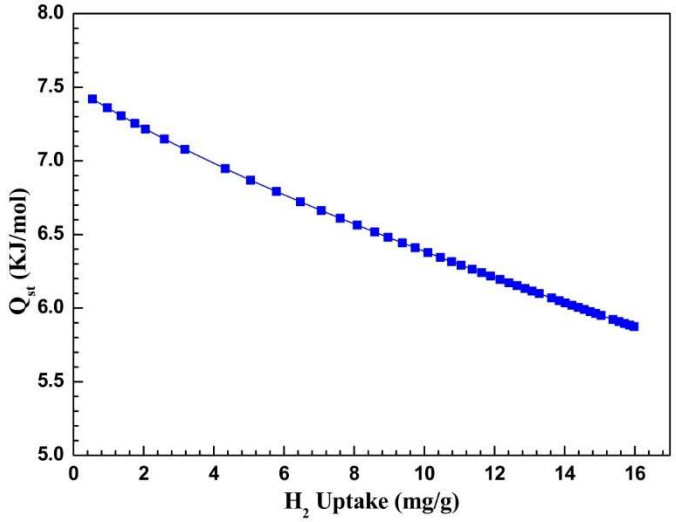

Figure 2.27. Isosteric heat of H_2 adsorption for PPF-2.

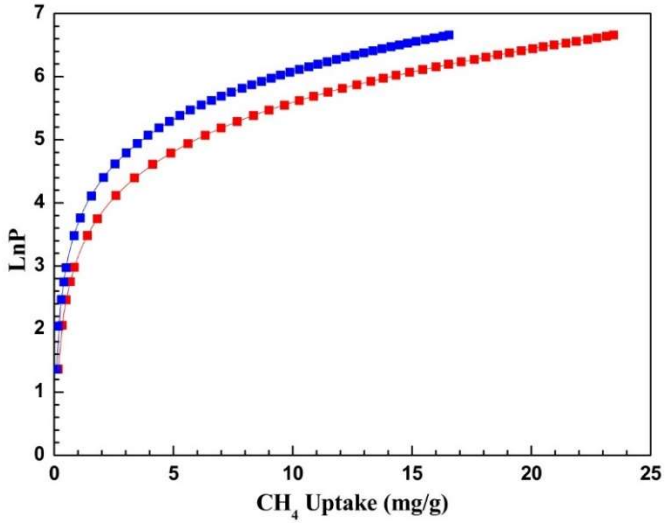

Figure 2.28. Virial analysis of CH_4 adsorption isotherms at 273 K (**red**) and 295 K (**blue**).

Table 2.10. Virial equation fitting results of CH_4 adsorption for PPF-2.

a_0	a_1	a_2	a_3	a_4	a_5	b_0	b_1	b_2	R^2
1915.2523	3.37537	1.8673	0.1573	0.0065	9.78398e-5	10.17328	0.02258	7.38374e-4	0.99995

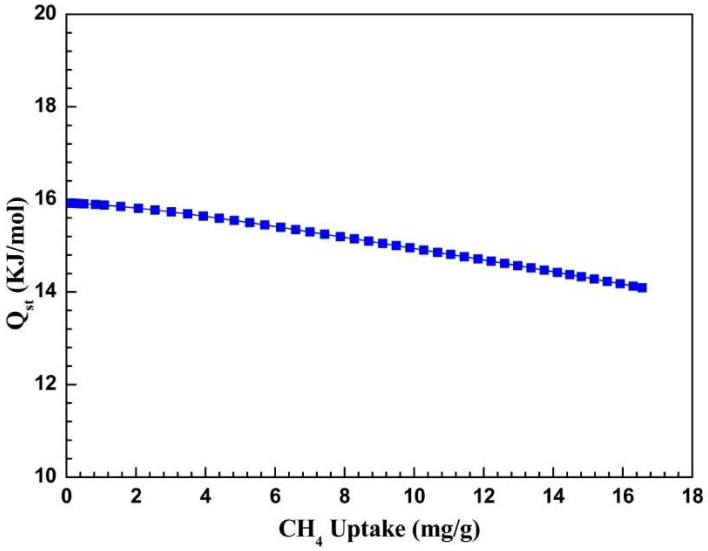

Figure 2.29. Isosteric heat of CH_4 adsorption for PPF-2.

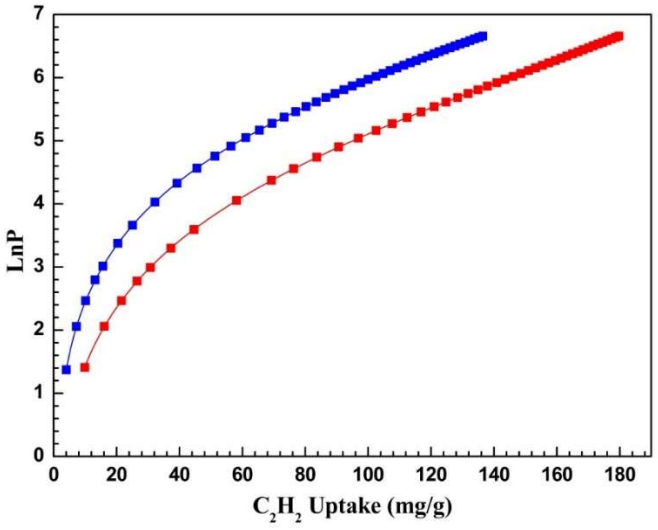

Figure 2.30. Virial analysis of C_2H_2 adsorption isotherms at 273 K (**red**) and 295 K (**blue**).

Table 2.11. Virial equation fitting results of C_2H_2 adsorption for PPF-2.

a_0	a_1	a_2	a_3	a_4	a_5	b_0	b_1	b_2	R^2
3801.7395	11.21537	0.09493	7.4471e-4	3.3020e-6	6.02529e-9	12.77169	0.00993	2.7911e-5	0.99999

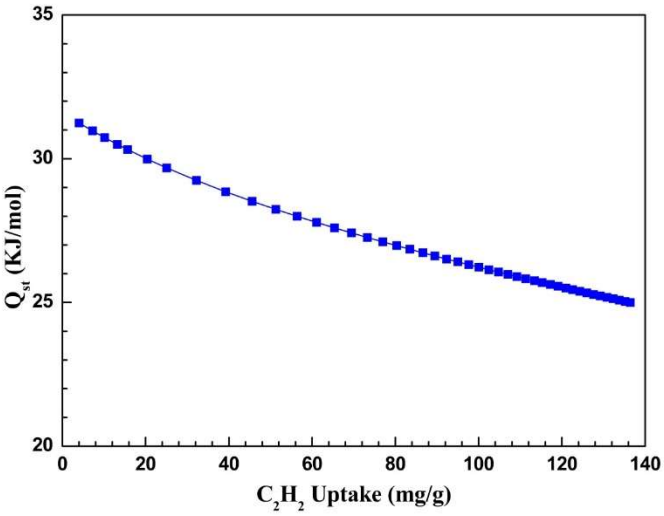

Figure 2.31. Isosteric heat of C_2H_2 adsorption for PPF-2.

2.5.5.3 Isosteric Heats of Gas (CO_2, H_2, CH_4 and C_2H_2) for PPF-3

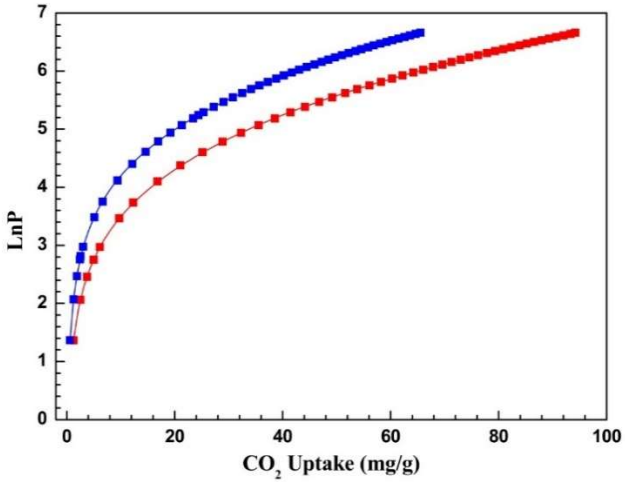

Figure 2.32. Virial analysis of CO_2 adsorption isotherms at 273 K (**red**) and 295 K (**blue**).

Table 2.12. Virial equation fitting results of CO_2 adsorption for PPF-3.

a_0	a_1	a_2	a_3	a_4	a_5	b_0	b_1	b_2	R^2
2622.3386	3.4796	0.11602	0.00369	3.774e-5	1.4172e-7	10.72787	0.01061	1.4546e-4	0.99997

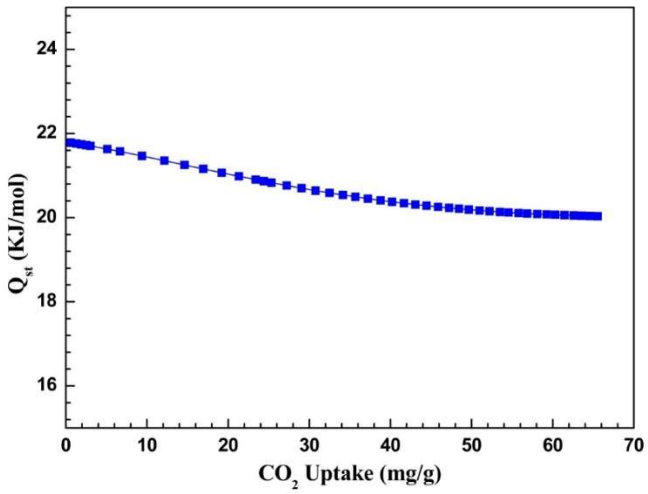

Figure 2.33. Isosteric heat of CO_2 adsorption for PPF-3.

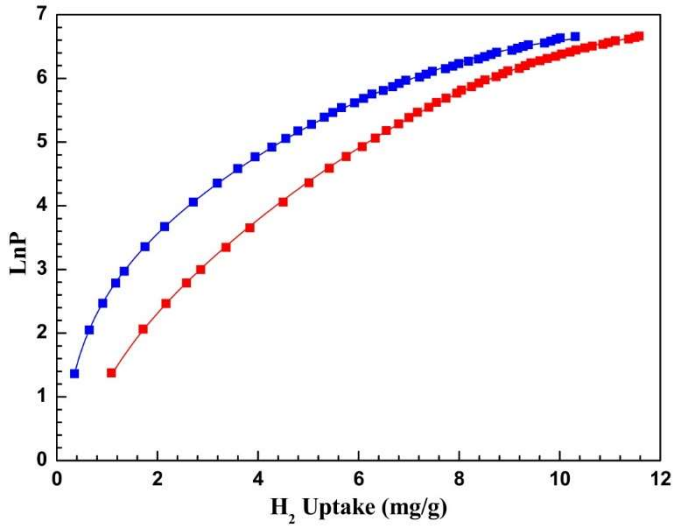

Figure 2.34. Virial analysis of H_2 adsorption isotherms at 77 K (**red**) and 87 K (**blue**).

Table 2.13. Virial equation fitting results of H_2 adsorption for PPF-3.

a_0	a_1	a_2	a_3	a_4	a_5	b_0	b_1	b_2	R^2
992.27046	75.03685	1.38949	0.07283	0.01782	6.294e-4	13.71569	0.57859	0.01967	0.99985

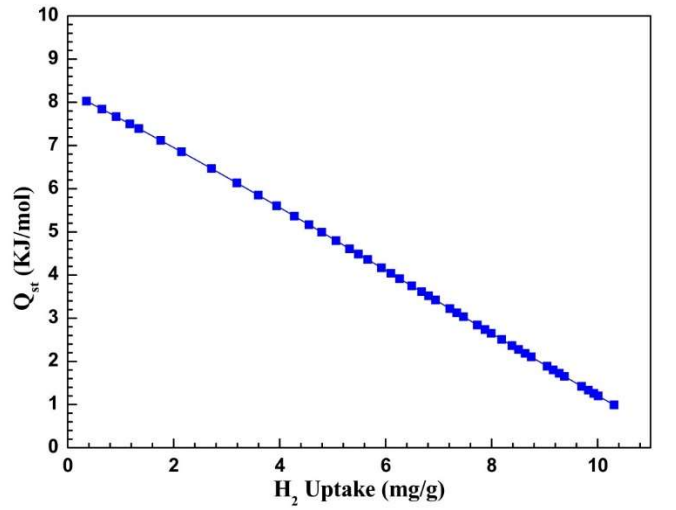

Figure 2.35. Isosteric heat of H_2 adsorption for PPF-3.

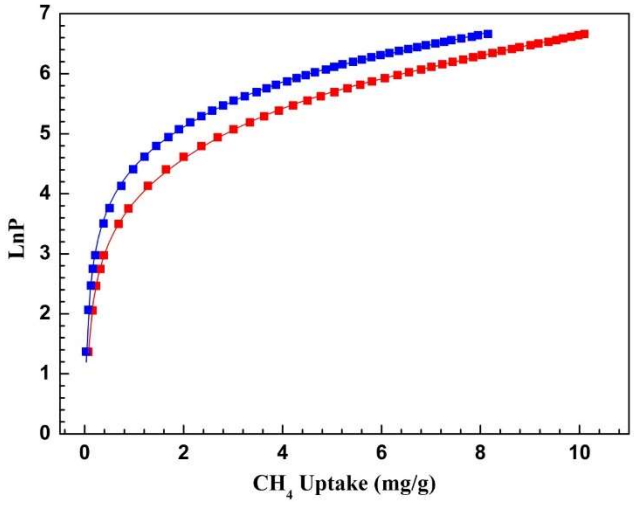

Figure 2.36. Virial analysis of CH_4 adsorption isotherms at 273 K (**red**) and 295 K (**blue**).

Table 2.14. Virial equation fitting results of CH_4 adsorption for PPF-3.

a_0	a_1	a_2	a_3	a_4	a_5	b_0	b_1	b_2	R^2
2337.3348	168.9132	25.51239	8.58201	0.80947	0.02794	12.53971	0.85639	0.05416	0.99957

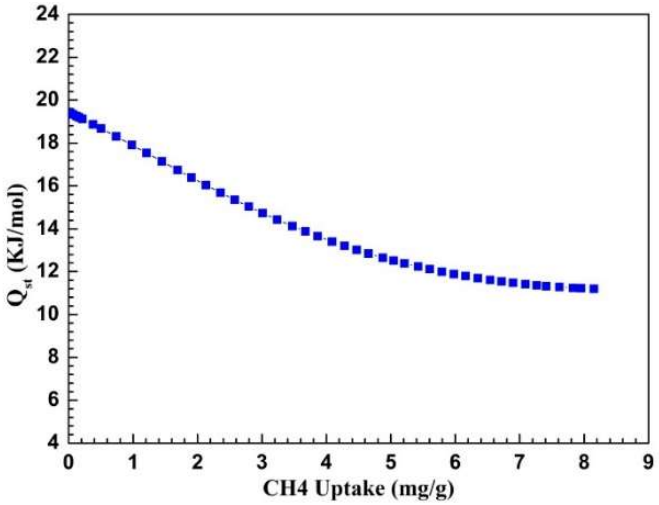

Figure 2.37. Isosteric heat of CH_4 adsorption for PPF-3.

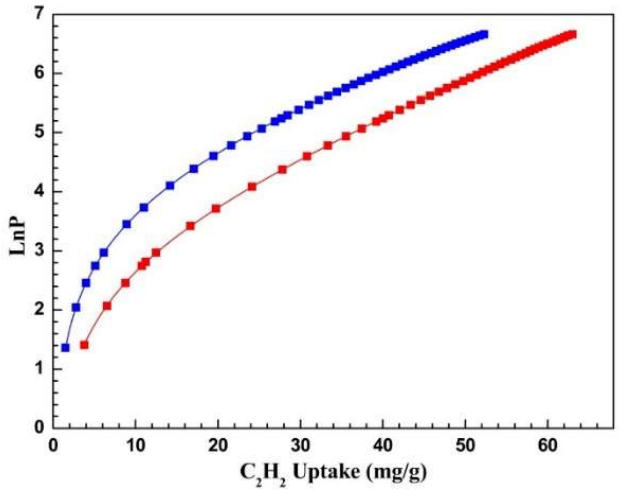

Figure 2.38. Virial analysis of C_2H_2 adsorption isotherms at 273 K (**red**) and 295 K (**blue**).

Table 2.15. Virial equation fitting results of C_2H_2 adsorption for PPF-3.

a_0	a_1	a_2	a_3	a_4	a_5	b_0	b_1	b_2	R^2
3577.5881	1.72907	0.36718	0.00194	1.893e-5	4.0912e-8	13.03415	0.03626	0.00158	0.99999

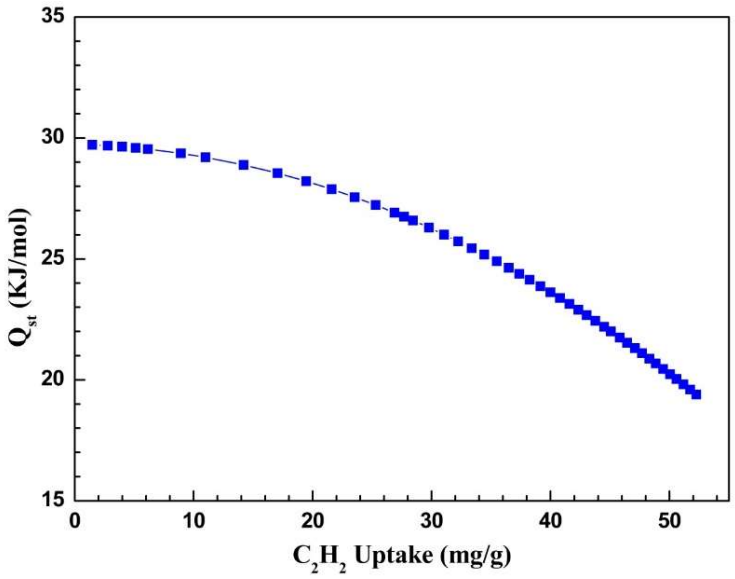

Figure 2.39. Isosteric heat of C_2H_2 adsorption for PPF-3.

2.5.5.4 Isosteric Heats of Gas (CO_2, H_2, CH_4 and C_2H_2) for PPF-4

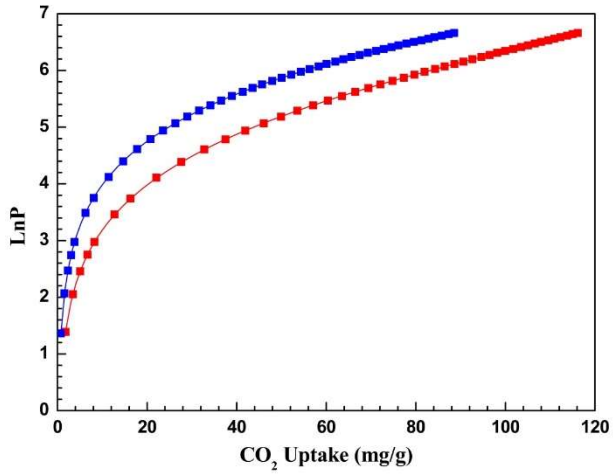

Figure 2.40. Virial analysis of CO_2 adsorption isotherms at 273 K (**red**) and 295 K (**blue**).

Table 2.16. Virial equation fitting results of CO_2 adsorption for PPF-4.

a_0	a_1	a_2	a_3	a_4	a_5	b_0	b_1	b_2	R^2
3022.7118	9.50424	0.04708	7.2653e-4	6.5993e-6	2.035e-8	11.86309	0.02652	6.1583e-5	0.99999

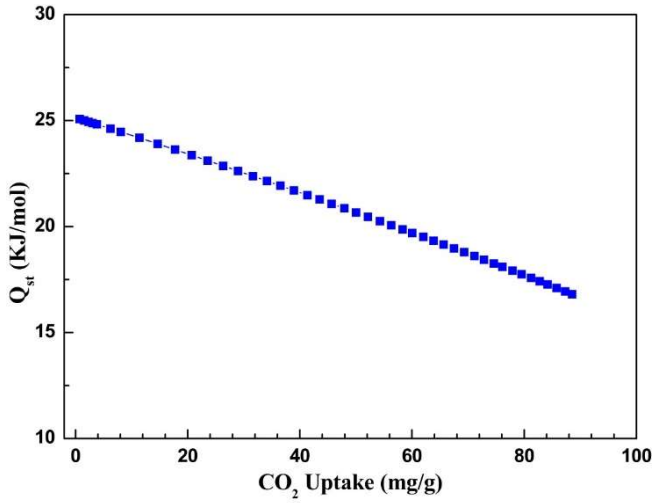

Figure 2.41. Isosteric heat of CO_2 adsorption for PPF-4.

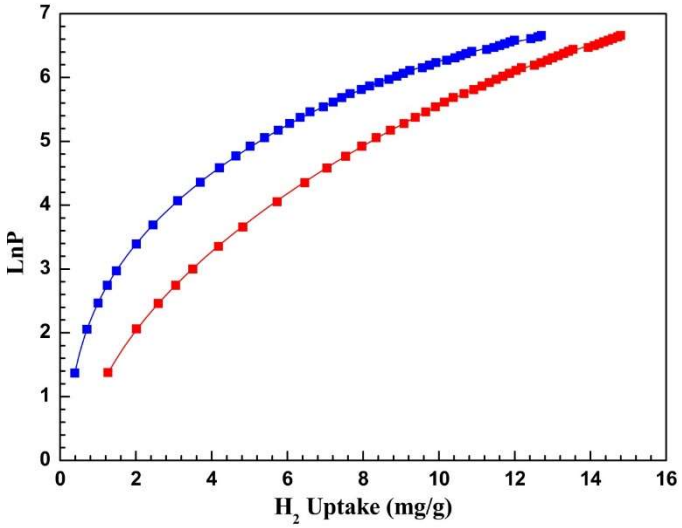

Figure 2.42. Virial analysis of H_2 adsorption isotherms at 77 K (**red**) and 87 K (**blue**).

Table 2.17. Virial equation fitting results of H_2 adsorption for PPF-4.

a_0	a_1	a_2	a_3	a_4	a_5	b_0	b_1	b_2	R^2
977.4333	30.28096	2.30862	0.03576	0.00234	8.0122e-5	13.46031	0.10117	0.03164	0.99992

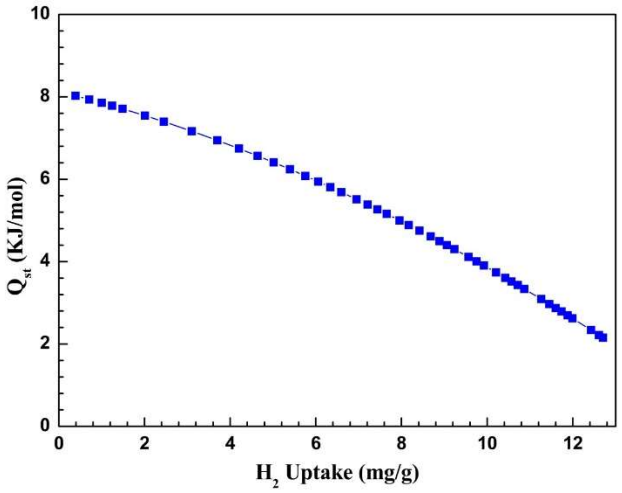

Figure 2.43. Isosteric heat of H_2 adsorption for PPF-4.

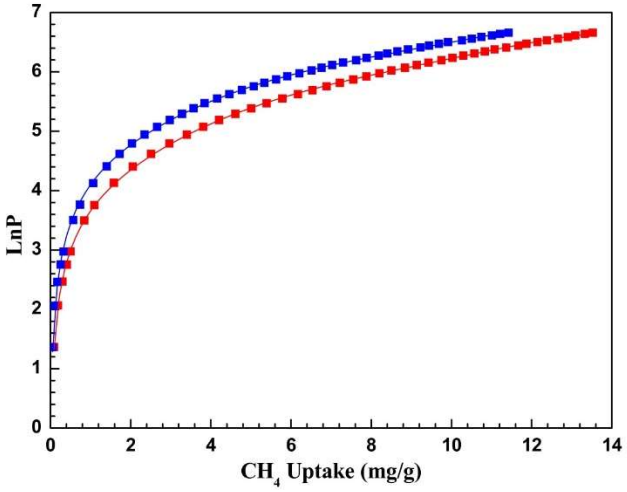

Figure 2.44. Virial analysis of CH_4 adsorption isotherms at 273 K (**red**) and 295 K (**blue**).

Table 2.18. Virial equation fitting results of CH_4 adsorption for PPF-4.

a_0	a_1	a_2	a_3	a_4	a_5	b_0	b_1	b_2	R^2
1668.0504	34.48768	19.26501	3.47985	0.25598	0.00688	9.8634	0.28578	0.00597	0.99964

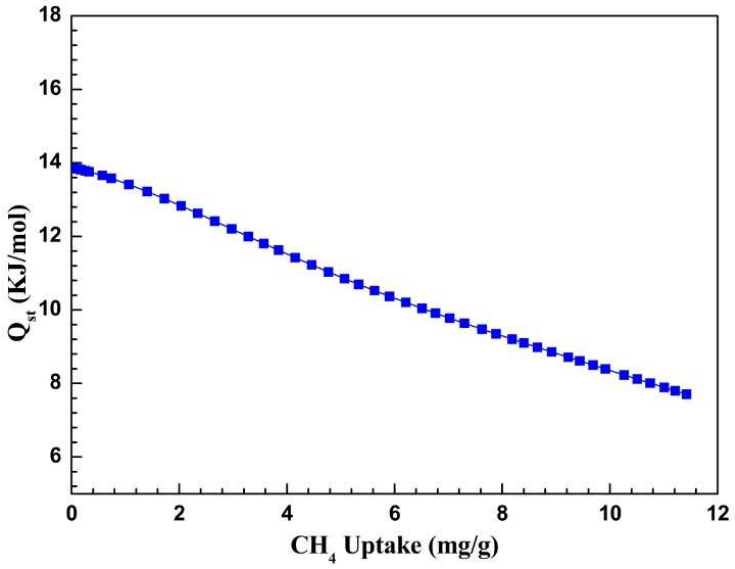

Figure 2.45. Isosteric heat of CH_4 adsorption for PPF-4.

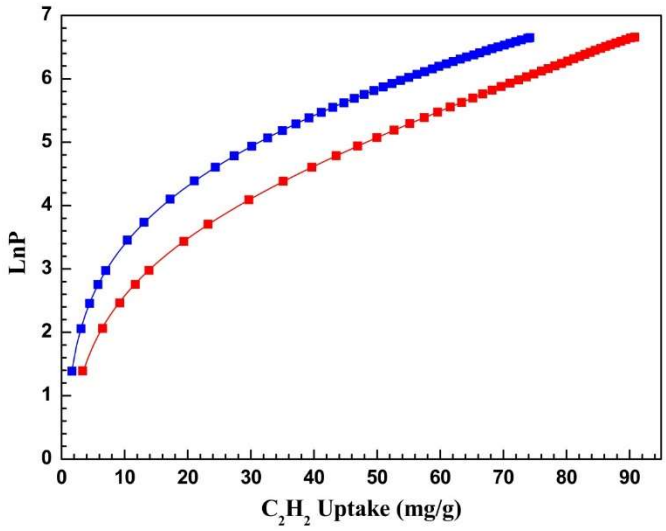

Figure 2.46. Virial analysis of C_2H_2 adsorption isotherms at 273 K (**red**) and 295 K (**blue**).

Table 2.19. Virial equation fitting results of C_2H_2 adsorption for PPF-4.

a_0	a_1	a_2	a_3	a_4	a_5	b_0	b_1	b_2	R^2
2873.9937	14.67741	0.37079	0.00166	1.9246e-5	8.135e-8	10.61354	0.07035	0.00109	0.99998

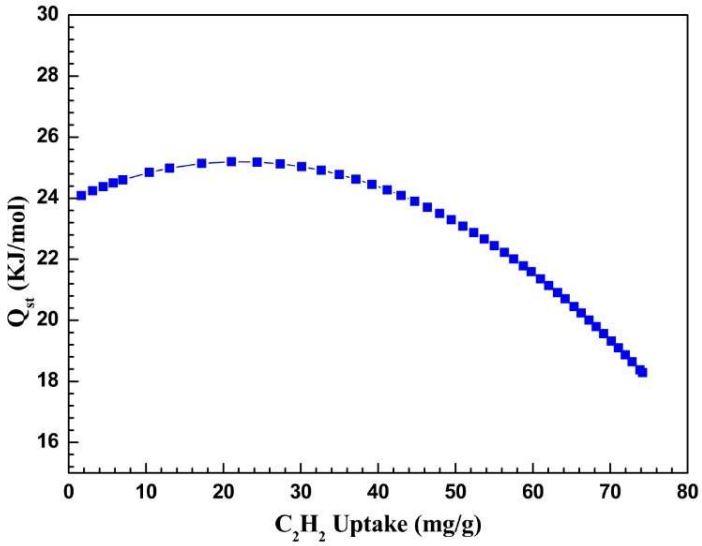

Figure 2.47. Isosteric heat of C_2H_2 adsorption for PPF-4.

2.5.6. Solid-State ^{13}C CP-MAS

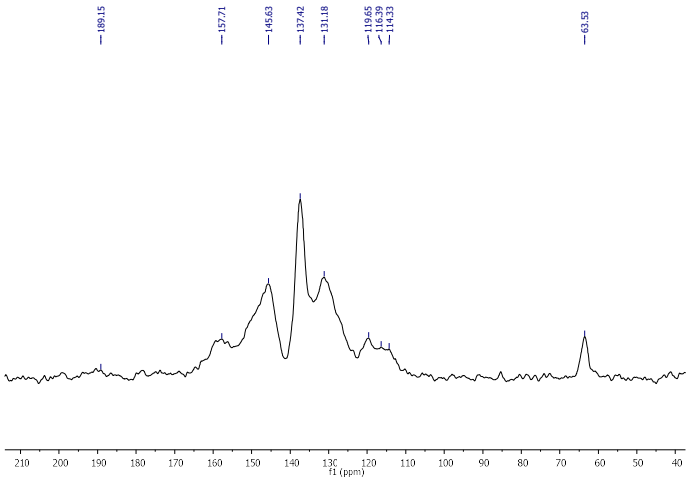

Figure 2.48. ^{13}C CP-MAS NMR spectrum of PPF-1.

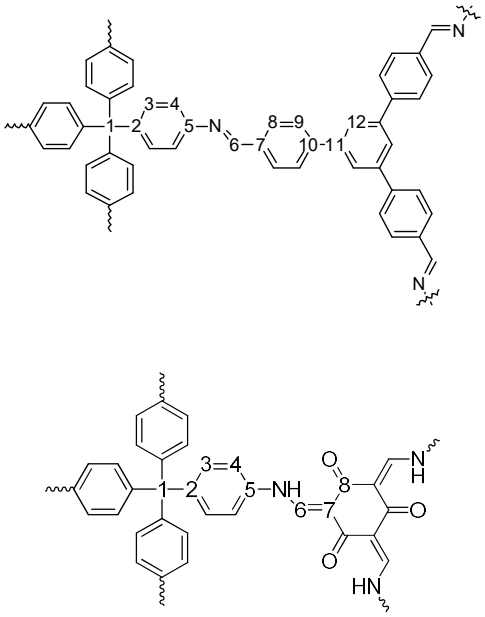

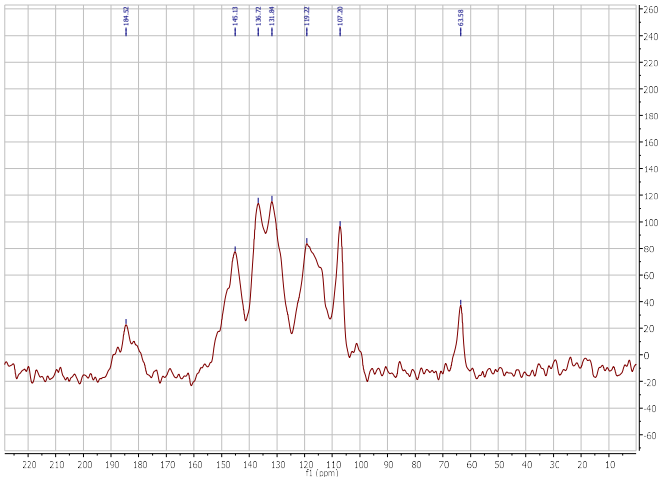

Figure 2.49. ^{13}C CP-MAS NMR spectrum of PPF-2.

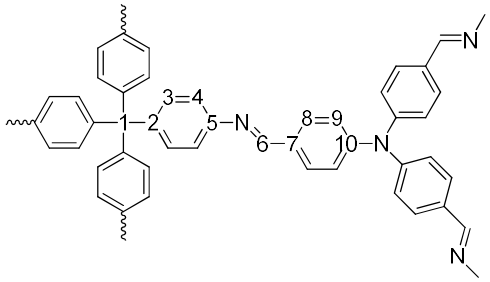

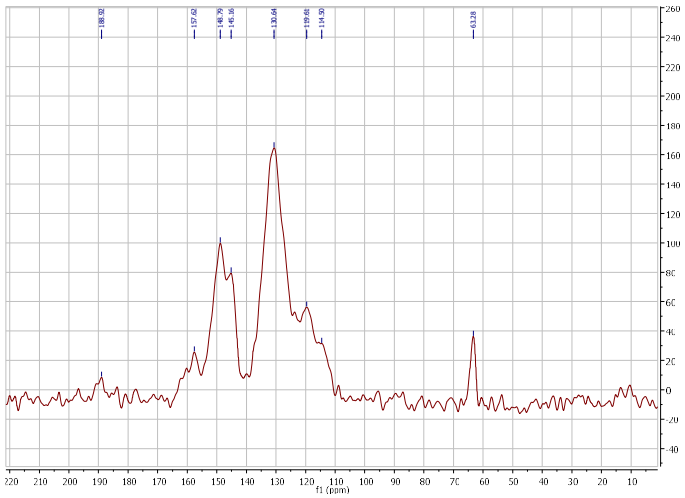

Figure 2.50. ^{13}C CP-MAS NMR spectrum of PPF-3.

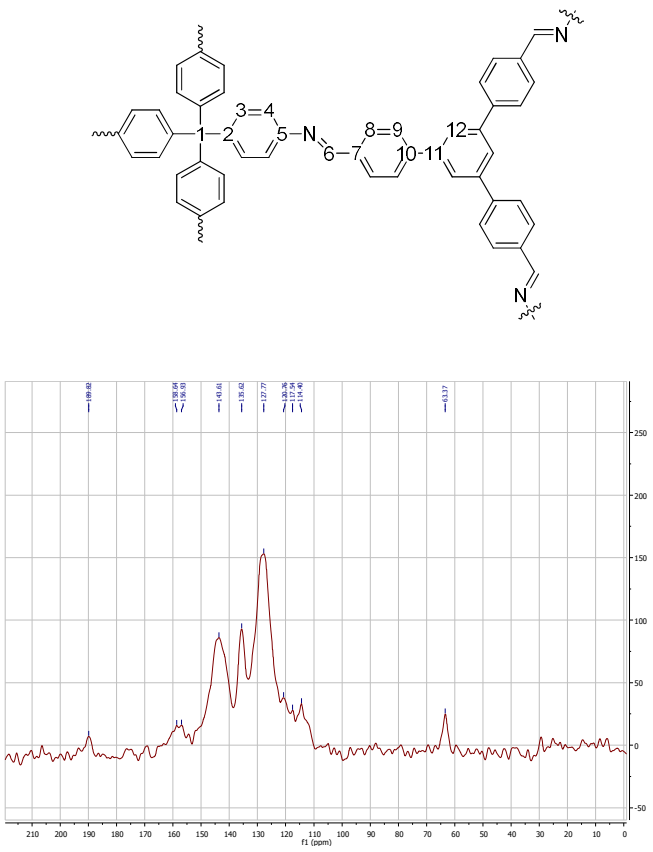

Figure 2.51. ^{13}C CP-MAS NMR spectrum of PPF-4.

2.6 References

(1) Zhou, H. C.; Long, J. R.; Yaghi, O. M. *Chem. Rev.* **2012**, *112*, 673.

(2) Wood, C. D.; Tan, B.; Trewin, A.; Su, F.; Rosseinsky, M. J.; Bradshaw, D.; Sun, Y.; Zhou, L.; Cooper, A. I. *Adv. Mater.* **2008**, *20*, 1916.

(3) Han, S. S.; Furukawa, H.; Yaghi, O. M.; Goddard, W. A. *J. Am. Chem. Soc.* **2008**, *130*, 11580.

(4) Dawson, R.; Adams, D. J.; Cooper, A. I. *Chem. Sci.* **2011**, *2*, 1173.

(5) Chen, Q.; Luo, M.; Hammershoj, P.; Zhou, D.; Han, Y.; Laursen, B. W.; Yan, C. G.; Han, B. H. *J. Am. Chem. Soc.* **2012**, *134*, 6084.

(6) Wang, C.; Xie, Z. G.; deKrafft, K. E.; Lin, W. B. *Acs Appl. Mater. Inter.* **2012**, *4*, 2288.

(7) Xie, Z. G.; Wang, C.; deKrafft, K. E.; Lin, W. B. *J. Am. Chem. Soc.* **2011**, *133*, 2056.

(8) Ding, S. Y.; Gao, J.; Wang, Q.; Zhang, Y.; Song, W. G.; Su, C. Y.; Wang, W. *J. Am. Chem. Soc.* **2011**, *133*, 19816.

(9) Zhao, C.; Danish, E.; Cameron, N. R.; Kataky, R. *J. Mater. Chem.* **2007**, *17*, 2446.

(10) Tozawa, T.; Jones, J. T. A.; Swamy, S. I.; Jiang, S.; Adams, D. J.; Shakespeare, S.; Clowes, R.; Bradshaw, D.; Hasell, T.; Chong, S. Y.; Tang, C.; Thompson, S.; Parker, J.; Trewin, A.; Bacsa, J.; Slawin, A. M. Z.; Steiner, A.; Cooper, A. I. *Nature Mater.* **2009**, *8*, 973.

(11) Tian, J.; Thallapally, P. K.; Dalgarno, S. J.; McGrail, P. B.; Atwood, J. L. *Angew. Chem., Int. Ed.* **2009**, *48*, 5492.

(12) Jin, Y. H.; Voss, B. A.; Noble, R. D.; Zhang, W. *Angew. Chem., Int. Ed.* **2010**, *49*, 6348.

(13) Cote, A. P.; Benin, A. I.; Ockwig, N. W.; O'Keeffe, M.; Matzger, A. J.; Yaghi, O. M. *Science* **2005**, *310*, 1166.

(14) El-Kaderi, H. M.; Hunt, J. R.; Mendoza-Cortes, J. L.; Cote, A. P.; Taylor, R. E.; O'Keeffe, M.; Yaghi, O. M. *Science* **2007**, *316*, 268.

(15) Spitler, E. L.; Colson, J. W.; Uribe-Romo, F. J.; Woll, A. R.; Giovino, M. R.; Saldivar, A.; Dichtel, W. R. *Angew. Chem., Int. Ed.* **2012**, *51*, 2623.

(16) Kuhn, P.; Antonietti, M.; Thomas, A. *Angew. Chem., Int. Ed.* **2008**, *47*, 3450.

(17) Kuhn, P.; Forget, A.; Su, D. S.; Thomas, A.; Antonietti, M. *J. Am. Chem. Soc.* **2008**, *130*, 13333.

(18) Ren, S. J.; Bojdys, M. J.; Dawson, R.; Laybourn, A.; Khimyak, Y. Z.; Adams, D. J.; Cooper, A. I. *Adv. Mater.* **2012**, *24*, 2357.

(19) Wood, C. D.; Tan, B.; Trewin, A.; Niu, H. J.; Bradshaw, D.; Rosseinsky, M. J.; Khimyak, Y. Z.; Campbell, N. L.; Kirk, R.; Stockel, E.; Cooper, A. I. *Chem. Mater.* **2007**, *19*, 2034.

(20) Ben, T.; Ren, H.; Ma, S. Q.; Cao, D. P.; Lan, J. H.; Jing, X. F.; Wang, W. C.; Xu, J.; Deng, F.; Simmons, J. M.; Qiu, S. L.; Zhu, G. S. *Angew. Chem., Int. Ed.* **2009**, *48*, 9457.

(21) Ren, H.; Ben, T.; Wang, E. S.; Jing, X. F.; Xue, M.; Liu, B. B.; Cui, Y.; Qiu, S. L.; Zhu, G. S. *Chem. Commun.* **2010**, *46*, 291.

(22) Lu, W. G.; Yuan, D. Q.; Zhao, D.; Schilling, C. I.; Plietzsch, O.; Muller, T.; Brase, S.; Guenther, J.; Blumel, J.; Krishna, R.; Li, Z.; Zhou, H. C. *Chem. Mater.* **2010**, *22*, 5964.

(23) Yuan, D. Q.; Lu, W. G.; Zhao, D.; Zhou, H. C. *Adv. Mater.* **2011**, *23*, 3723.

(24) Jiang, J. X.; Su, F.; Trewin, A.; Wood, C. D.; Campbell, N. L.; Niu, H.; Dickinson, C.; Ganin, A. Y.; Rosseinsky, M. J.; Khimyak, Y. Z.; Cooper, A. I. *Angew. Chem., Int. Ed.* **2007**, *46*, 8574.

(25) Jiang, J. X.; Su, F.; Trewin, A.; Wood, C. D.; Campbell, N. L.; Niu, H.; Dickinson, C.; Ganin, A. Y.; Rosseinsky, M. J.; Khimyak, Y. Z.; Cooper, A. I. *Angew. Chem., Int. Ed.* **2008**, *47*, 1167.

(26) Jin, Y. H.; Voss, B. A.; McCaffrey, R.; Baggett, C. T.; Noble, R. D.; Zhang, W. *Chem. Sci.* **2012**, *3*, 874.

(27) Rabbani, M. G.; El-Kaderi, H. M. *Chem. Mater.* **2012**, *24*, 1511.

(28) Lu, W. G.; Yuan, D. Q.; Sculley, J. L.; Zhao, D.; Krishna, R.; Zhou, H. C. *J. Am. Chem. Soc.* **2011**, *133*, 18126.

(29) Jin, Y. H.; Voss, B. A.; Jin, A.; Long, H.; Noble, R. D.; Zhang, W. *J. Am. Chem. Soc.* **2011**, *133*, 6650.

(30) http://rcsr.anu.edu.au/nets/ctn

(31) Schwab, M. G.; Fassbender, B.; Spiess, H. W.; Thomas, A.; Feng, X. L.; Mullen, K. *J. Am. Chem. Soc.* **2009**, *131*, 7216.

(32) Uribe-Romo, F. J.; Hunt, J. R.; Furukawa, H.; Klock, C.; O'Keeffe, M.; Yaghi, O. M. *J. Am. Chem. Soc.* **2009**, *131*, 4570.

(33) Pandey, P.; Katsoulidis, A. P.; Eryazici, I.; Wu, Y. Y.; Kanatzidis, M. G.; Nguyen, S. T. *Chem. Mater.* **2010**, *22*, 4974.

(34) Laybourn, A.; Dawson, R.; Clowes, R.; Iggo, J. A.; Cooper, A. I.; Khimyak, Y. Z.; Adams, D. J. *Polym. Chem.* **2012**, *3*, 533.

(35) Jin, Y. H.; Zhu, Y. L.; Zhang, W. *CrystEngComm* **2013**, *15*, 1484.

(36) Yaghi, O. M. *Nat. Mater.* **2007**, *6*, 92.

(37) Chong, J. H.; Sauer, M.; Patrick, B. O.; MacLachlan, M. J. *Org. Lett.* **2003**, *5*, 3823.

(38) Kandambeth, S.; Mallick, A.; Lukose, B.; Mane, N. V.; Heine, T.; Banerjee, R. *J. Am. Chem. Soc.* **2012**, *134*, 19524.

(39) Rouquerol, J.; Avnir, D.; Fairbridge, C. W.; Everett, D. H.; Haynes, J. H.; Pernicone, N.; Ramsay, J. D. F.; Sing, K. S. W.; Unger, K. K. *Pure. Appl. Chem.* **1994**, *66*, 1739.

(40) Weber, J.; Schmidt, J.; Thomas, A.; Bohlmann, W. *Langmuir* **2010**, *26*, 15650.

(41) Uribe-Romo, F. J.; Hunt, J. R.; Furukawa, H.; Klock, C.; O'Keeffe, M.; Yaghi, O. M. *J Am Chem Soc* **2009**, *131*, 4570.

(42) Sumida, K.; Rogow, D. L.; Mason, J. A.; McDonald, T. M.; Bloch, E. D.; Herm, Z. R.; Bae, T. H.; Long, J. R. *Chem. Rev.* **2012**, *112*, 724.

(43) Ben, T.; Pei, C. Y.; Zhang, D. L.; Xu, J.; Deng, F.; Jing, X. F.; Qiu, S. L. *Energy Environ. Sci.* **2011**, *4*, 3991.

(44) Furukawa, H.; Yaghi, O. M. *J. Am. Chem. Soc.* **2009**, *131*, 8875.

(45) Zhang, Z. J.; Xiang, S. C.; Chen, B. L. *CrystEngComm* **2011**, *13*, 5983.

(46) Li, J. R.; Kuppler, R. J.; Zhou, H. C. *Chem. Soc. Rev.* **2009**, *38*, 1477.

(47) Mishra, B. K.; Karthikeyan, S.; Ramanathan, V. *J. Chem. Theory Comput.* **2012**, *8*, 1935.

(48) Wang, Z. G.; Zhang, B. F.; Yu, H.; Sun, L. X.; Jiao, C. L.; Liu, W. S. *Chem. Commun.* **2010**, *46*, 7730.

(49) Myers, A. L.; Prausnitz, J. M. *AiChe J.* **1965**, *11*, 121.

(50) Ganesan, P.; Yang, X. N.; Loos, J.; Savenije, T. J.; Abellon, R. D.; Zuilhof, H.; Sudholter, E. J. R. *J. Am. Chem. Soc.* **2005**, *127*, 14530.

(51) Yelamaggad, C. V.; Achalkumar, A. S.; Rao, D. S. S.; Prasad, S. K. *J. Org. Chem.* **2009**, *74*, 3168.

(52) Mallegol, T.; Gmouh, S.; Meziane, M. A. A.; Blanchard-Desce, M.; Mongin, O. *Synthesis* **2005**, 1771.

(53) Kathiresan, M.; Walder, L.; Ye, F.; Reuter, H. *Tetrahedron. Lett.* **2010**, *51*, 2188.

(54) Kotha, S.; Shah, V. R. *Synthesis* **2007**, 3653.

(55) Plietzsch, O.; Schilling, C. I.; Tolev, M.; Nieger, M.; Richert, C.; Muller, T.; Brase, S. *Org. Biomol. Chem.* **2009**, *7*, 4734.

(56) Rowsell, J. L. C.; Yaghi, O. M. *J. Am. Chem. Soc.* **2006**, *128*, 1304.

CHAPTER 3

Synthesis of Porous Poly(aryleneethynylene) Networks through Dynamic Alkyne Metathesis

(A paper was published for this chapter: Zhu, Y.*; Yang, H.*; Jin, Y.; Zhang, W. "Porous Poly(aryleneethynylene) Networks through Alkyne Metathesis" *Chem. Mater.* **2013**, *25*, 3718-3723.)

3.1 Abstract

The development of new synthetic methods has been a central challenge in the field of organic porous materials. In this chapter, the first application of dynamic alkyne metathesis to the synthesis of highly porous poly(aryleneethynylene) (PAE) networks was presented. The permanent porosity of as-synthesized PAEs was confirmed by N_2 adsorption/desorption studies, and high Brunauer-Emmett-Teller (BET) specific surface areas (P/P_0 = 0.01-0.1) up to 2312 $m^2 \cdot g^{-1}$ were observed. PAE networks with the same chemical connectivity were also prepared through palladium-catalyzed Sonogashira cross-coupling under similar reaction conditions. The networks prepared through alkyne metathesis at three different temperatures (40 °C, 55 °C, and 75 °C) consistently exhibit higher specific surface area and higher thermal stability, suggesting alkyne metathesis is advantageous in the preparation of highly porous organic materials. Our study demonstrates the feasibility of employing alkyne metathesis in the preparation of porous polymer networks, and serves to expand the synthetic tool box for this emerging class of porous materials.

3.2 Introduction

Purely organic porous materials have emerged as promising candidates for gas storage and separation applications.[1-9] The advantages of organic porous materials include low density and high chemical and thermal stability, since they are constructed through robust covalent bonds between light-weight elements, such as B, C, N, O, etc., and free of heavy metal centers. Various irreversible chemical transformations, including Friedel-Crafts alkylations,[10] and transition metal-catalyzed cross-coupling reactions, *e.g.*

Sonogashira cross-coupling,[11-13] Yamamoto cross-coupling,[5] etc., have been applied to the synthesis of amorphous porous organic polymers. Ordered crystalline organic materials, such as covalent organic frameworks (COFs),[14-19] have been developed recently by employing dynamic covalent reactions. With well-defined and tunable structures, functional diversity, and high stability, COFs have found interesting applications in gas adsorption,[14,15] heterogeneous catalysis,[20,21] and optoelectronics.[22-25] In contrast to the rich variety of irreversible reactions, the dynamic covalent reactions that have been explored in the synthesis of porous materials are mainly limited to Schiff-base chemistry, boronic acid-diol condensation and boronic acid self-condensation, providing materials linked by relatively labile C=N or B-O bonds.[14,15] Although these methodologies will remain important in the development of porous organic materials, the need to design and develop other synthetic approaches providing robust chemical linkages will become increasingly important as the challenges and requirements for new materials become more complex.

Alkyne metathesis is an emerging dynamic covalent reaction that provides rigid and robust ethynylene linkages. The significance of the reversibility of alkyne metathesis has been widely recognized in thermodynamically-controlled dynamic process, which has led to numerous successful construction of various complex molecular architectures, such as shape-persistent 2-D macrocycles,[26-37] and 3-D covalent organic polyhedrons[38]. Similar to other dynamic covalent reactions applied to the synthesis of COFs, dynamic alkyne metathesis has the potential to create well-ordered porous crystalline networks. As the first key step toward this goal, we have explored the possibility of utilizing such reaction in the preparation of porous organic materials. Various ethynylene-linked porous polymer networks have previously been prepared via Sonogashira cross coupling reactions.[11-13,39] However, moderate surface areas, typically in the range of 500-800 $m^2 \cdot g^{-1}$, were observed, with highest 1018 $m^2 \cdot g^{-1}$ for networks containing 1,3,5-trisubstituted benzene monomers, and 1213 $m^2 \cdot g^{-1}$ for neworks containing tetrahedral monomers. Herein, we present the first example of successful preparation of highly porous poly(aryleneethynylene) (PAE) networks through alkyne metathesis, which exhibit specific surface areas exceeding the previously reported similar materials.

3.3 Results and Discussion

Our group has recently developed a series of highly active multidentate molybdenum carbyne catalysts for alkyne metathesis.[35,36,40] They exhibit high catalytic activity, broad substrate scope, fast reaction rate, and long lifetime. Additionally, these catalysts showed excellent catalytic performance with the aid of 5 Å molecular sieves as small alkyne by-product scavengers. We envisioned that our catalysts could enable the efficient preparation of poly(aryleneethynylene) networks through alkyne metathesis. Herein, we prepared rigid ethynylene-linked networks, **PAE-8-RAM**, and **PAE-9-RAM**, through reversible alkyne metathesis (RAM) of **2** or **3**. Alternatively, the networks with the same chemical connectivity, **PAE-8-ICC**, and **PAE-9-ICC**, were also prepared through irreversible cross-coupling (ICC) of **4** and **5** or **6** and **7** (**Scheme 3.1**). We found the networks prepared through alkyne metathesis at three different temperatures (40 °C, 55 °C, and 75 °C) consistently exhibit higher specific surface area, and higher thermal stability.

We first explored the synthesis of network **PAE-8-RAM** from monomer **2**. In order to drive the metathesis reaction to completion, the efficient removal of 2-butyne by-product is required. Initially, we tested the alkyne metathesis of **2** under widely practiced dynamic vacuum conditions (Table 3.1, entry 1, and 2).[41-44] Either chloroform or toluene could be used as the reaction solvent since in both of which the starting material has good solubility and the metathesis catalyst **1** is active. A solution of monomer **2** in $CHCl_3$ (or toluene) was added to the *in situ* generated catalyst **1** in CCl_4. The reaction mixture was then exposed to vacuum for five times at 30 min intervals across 2.5 hours at the beginning of the reaction. The solvent evaporated during the vacuum exposure was compensated and the reaction vessel was sealed. After stirring for 22 h at 55 °C, the network was obtained as gray gel-like materials, which were treated with acetone, concentrated ammonium hydroxide solution, and water to give final network **PAE-8-RAM** as a yellow powder in quantitative yield.

To evaluate the permanent porosity of such as-synthesized PAE networks, nitrogen gas (N_2) adsorption/desorption studies were conducted on the freshly activated samples. As shown in **Figure 3.1**, the N_2 adsorption isotherms at 77 K show a rapid uptake at low relative pressure (P/P_0 below 0.1) and typical type I adsorption behaviour, indicating the permanent micro-porous nature of the network. **PAE-8-RAM** also shows a slight hysteresis loop, indicating the presence of some mesopores. The gradual nitrogen adsorption of the networks under relatively high pressure ($P/P_0 > 0.1$) may be due to the presence of interparticular void[45] and some meso- as well as macro-pores. The Brunauer-Emmett-Teller (BET) specific surface area within the pressure range of $P/P_0 = 0.01$-0.1 was found to be 1373 $m^2 \cdot g^{-1}$ (Table 3.1, entry 1), which surpasses those of poly(aryleneethynylene) networks previously reported.

Table 3.1. The synthesis of 2-D network PAE-8-RAM.

Entry	Method	Temp (°C)	Solvent[a]	Cat. (mol %)	S_{BET} ($m^2 \cdot g^{-1}$)
1	A	55	$CHCl_3$	4.5	1373
2	A	55	Toluene	4.5	1170
3	B	55	$CHCl_3$	1.5	1191
4	B	55	$CHCl_3$	4.5	1439
5	B	55	Toluene	4.5	1183
6	B	40	Toluene	4.5	1284
7	B	75	Toluene	4.5	1269

Method A: dynamic vacuum; Method B: 5 Å molecular sieves (pellet, 8-12 mesh); [a]contains 20% CCl_4 (v/v).

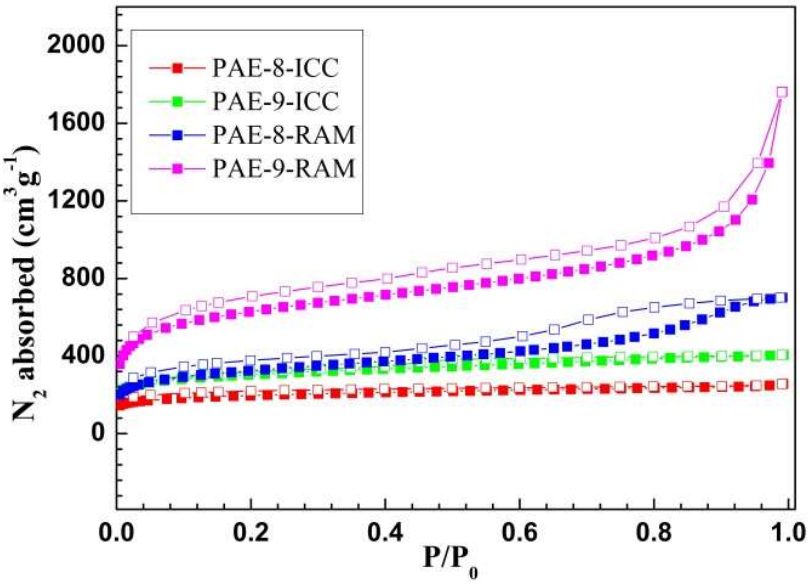

Figure 3.1. N_2 adsorption (solid) and desorption (hollow) isotherms of networks at 77 K: **PAE-8-ICC** (55 °C), **PAE-9-ICC** (55 °C), **PAE-8-RAM** (Table 3.1, entry 4), **PAE-9-RAM** (Table 3.2, entry 5).

Although vacuum-driven alkyne metathesis works well, the potential drawback of this method is the requirement of the stringent moisture- and air-free vacuum system and also solvent refill. In order to make this methodology more user-friendly and further improve the material properties, we explored the feasibility of conducting metathesis reactions in a closed system. Previously, we have demonstrated that 2-butyne can be removed under dynamic vacuum or using 5 Å molecular sieves (powder form) as a scavenger.[40] In this study, we used 5 Å molecular sieves (8–12 mesh pellets), as the butyne scavenger in order to ensure easy separation of the molecular sieves from gel-like network product. Various reaction conditions, solvent, temperature, and catalyst loadings were explored to optimize the reaction conditions. The optimal synthetic procedure is quite simple. Instead of exposing the reaction mixture to vacuum, molecular sieves were added and the reaction was heated in a closed system without stirring at various temperatures for 22 h. Upon completion, the product was treated with acetone. The pellets of molecular sieves stayed at the bottom of the flask, and were easily separated from the acetone suspension containing network particles. The highest surface area (S_{BET} = 1439 $m^2 \cdot g^{-1}$) was observed for the network prepared at 55 °C using 4.5% catalyst loading in $CHCl_3$ (Table 3.1, entry 4). Apparent decrease of BET surface

area of networks was observed when the catalyst loading was decreased from 4.5% to 1.5%. It appears that chloroform is a better solvent compared to toluene, producing materials with somewhat higher surface areas (entry 1 vs. 2; entry 4 vs. 5 in Table 3.1). The reaction temperature seems to have little effect on the porosity of the final materials (40 °C→ 75 °C). Considering 3-D networks usually display higher specific surface area compared to 2-D networks, we next examined the self-reaction of tetrahedral building block **3** through alkyne metathesis. Various reaction conditions were explored including solvent and temperature to produce **PAE-9-RAM.** The network with the highest BET surface area, 2312 $m^2 g^{-1}$, was obtained in chloroform at 55 °C using molecular sieves as the 2-butyne scavenger (Table 3.2, entry 2). Similar to the synthesis of network **PAE-8-RAM**, chloroform seems to be a better solvent than toluene for the formation of high porosity materials. Interestingly, significant temperature effect was observed when toluene was used as the solvent. We observed evident increase of BET surface area by 56%, when the reaction temperature was raised from 40 °C to 55 °C. However, further increasing the temperature to 75 °C has adverse effect, decreasing the specific surface area by 32%. In chloroform, the temperature effect was not as significant as in toluene, showing only a slight decrease of specific surface area (8%) when the temperature was increased from 55 °C to 75 °C. This pronounced temperature effect in the synthesis of network **PAE-9-RAM** is in great contrast to the preparation of **PAE-8-RAM**, in which little temperature effect on the final product porosity was observed. The solubility of metathesis substrate and polymeric intermediates as well as the substrate reactivity in the reaction solvent might explain the observed temperature dependency.

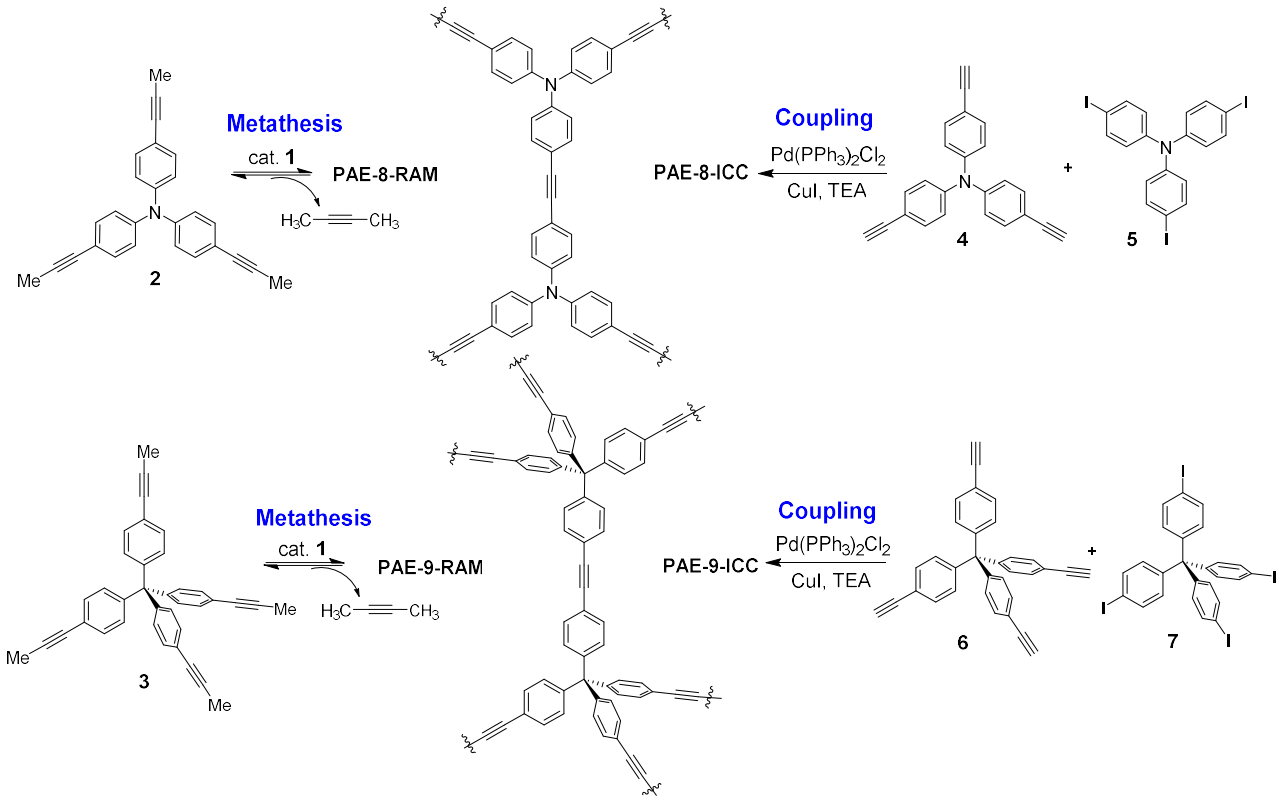

Scheme 3.1. Synthesis of PAE-8 and PAE-9 networks through alkyne metathesis and cross coupling reactions.

Table 3.2. The synthesis of 3-D network PAE-9-RAM.

Entry	Method	Temp (°C)	Solvent[a]	S_{BET} ($m^2.g^{-1}$)
1	A	55	Toluene	1998
2	B	55	$CHCl_3$	2312
3	B	75	$CHCl_3$	2123
4	B	40	Toluene	1474
5	B	55	Toluene	2299
6	B	75	Toluene	1561

Method A: dynamic vacuum, 6% Cat. loading; Method B: 5 Å molecular sieves (pellet, 8-12 mesh), 6% Cat. loading; [a]contains 14% CCl_4 (v/v).

Alkyne metathesis provides ethynylene linkage, which can also be formed through irreversible cross coupling chemistry. In order to explore how the networks obtained through alkyne metathesis are different from those obtained through irreversible cross coupling reactions in terms of gas adsorption properties, we next synthesized the networks **PAE-8-ICC** and **PAE-9-ICC** through irreversible palladium-catalyzed Sonogashira cross-coupling reactions. In order to exclude the solvent, and solubility effect, we used the same monomer concentration (0.04 M) in the same solvent (toluene). We are aware that it is difficult to provide totally unbiased reaction conditions, but we tried to avoid favoring either reaction. Although toluene is not the best solvent for alkyne metathesis, we choose toluene as the solvent since it is commonly used in Sonogashira cross-coupling reactions. We used the same mol % catalyst loadings, and we also screened a range of temperatures. Interestingly, compared to the gel-like network products observed during alkyne metathesis, the networks were formed as precipitates through the cross-coupling reactions.

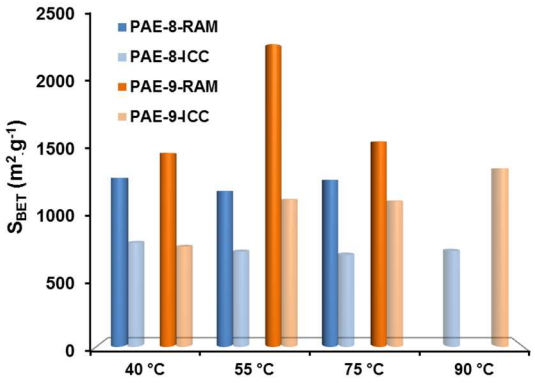

Figure 3.2. Comparison of BET surface areas of networks prepared through alkyne metathesis (**PAE-8-RAM**, and **PAE-9-RAM**) with the networks (**PAE-8-ICC**, and **PAE-9-ICC**) constructed through Sonogashira cross-coupling reactions.

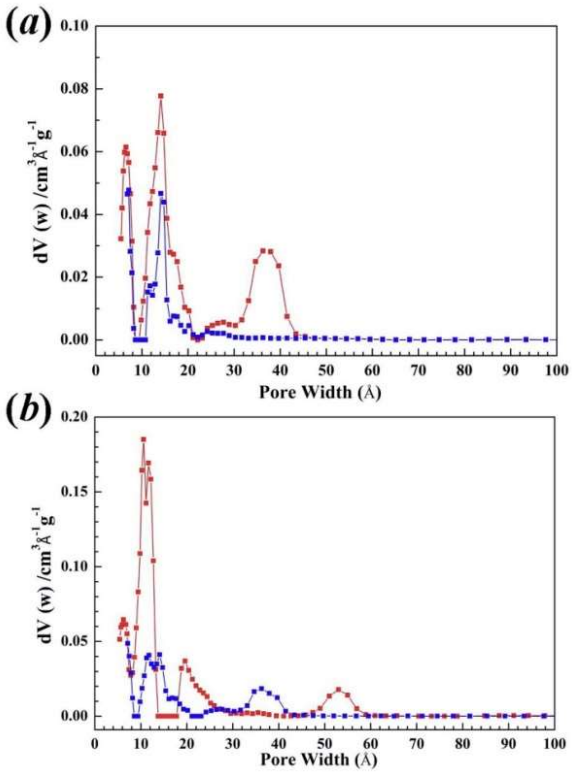

Figure 3.3. Pore size distribution of different networks: (a) top: **PAE-8-ICC** (55 °C), bottom: **PAE-8-RAM** (Table 3.1, entry 4); (b) top: **PAE-9-ICC** (55 °C), bottom: **PAE-9-RAM** (Table 3.2, entry 5).

The networks **PAE-8-RAM/ICC** and **PAE-9-RAM/ICC** were characterized by FT-IR, solid state ^{13}C NMR, TGA, SEM, and powder X-ray diffraction (PXRD). The ^{13}C cross-polarization magic angle spinning (CP-MAS) NMR spectra of **PAE-8-RAM** and **PAE-8-ICC** show resonances at 148, 133, 121, 91 ppm, corresponding to Ar-C-, Ar-CH, Ar-C-N, and -C≡C- carbons. **PAE-9-RAM** and **PAE-9-ICC** show three aromatic carbon signals at 147, 131, 123 ppm, ethynylene carbon at 91 ppm, and quaternary carbon at 66 ppm (Figure 3.12-3.15). The FT-IR spectra of **PAE-8-RAM /ICC** and **PAE-9-RAM/ICC** show similar aromatic resonance peaks as monomers **2**, and **3**, respectively. We observed the characteristic two C≡C stretch bands of asymmetric ethynylene bond around 2250 cm^{-1} in the FT-IR spectra of monomers **2** and **3**. However, a negligible amount of these resonances was observed in the spectra of **PAE-8-RAM /ICC** and **PAE-9-RAM /ICC**, indicating the formation of symmetrical C≡C bond, further supporting the network structures (Figure 3.8-3.9). All network materials show good thermal stability based on thermal gravimetric analyses (TGA). Interestingly, networks, **PAE-8-RAM** and **PAE-9-RAM**, prepared through alkyne metathesis show considerably higher thermal stability (T_{dec} > 600 °C) than **PAE-8-ICC** and **PAE-9-ICC**, which start to decompose around 400 °C (Figure 3.7). **PAE-8-RAM** shows some crystallinity (Figure 3.10). However, due to the poor quality of PXRD data, we were unable to deduce the topology of this presumably hexagonal 2-D COF. All other networks are completely amorphous.

Although the networks (**PAE-8-RAM** and **PAE-9-RAM**) constructed through alkyne metathesis are amorphous, at each reaction temperature (40 °C, 55 °C, and 75 °C), they showed significantly higher BET surface areas than **PAE-8-ICC** and **PAE-9-ICC**. Specifically, almost two-fold higher BET surface area was observed for **PAE-9-RAM** at 55 °C, compared to **PAE-9-ICC** obtained through Sonogashira cross coupling at the same temperature (**Figure 3.2**). The cross

coupling reactions were also conducted at elevated temperature (90 °C). However, only little increase in network porosity was observed for both **PAE-8-ICC** and **PAE-9-ICC**. Clearly, alkyne metathesis is advantageous in the preparation of high porosity materials. However, the nature of how reversibility of alkyne metathesis contributes to the higher porosity still needs further investigation.

To gain further insight into the porosity of these materials, the pore size distribution (PSD) analysis of the four polymer networks was also performed applying the nonlocal density functional theory (NLDFT) by using slit pore model supported by Quantachrome ASiQ program. All of the pore size distribution graphs are derived from the N_2 adsorption isotherms. For the networks from planar monomers, **PAE-8-RAM** and **PAE-8-ICC**, the pore size distribution in the micropore range (< 2.0 nm) is similar, although some mesopores are also observed in **PAE-8-RAM**. The colloidal phase separation might be responsible for the mesopores formation during alkyne metathesis reactions. For the networks from tetrahedral monomers, **PAE-9-RAM** shows narrower micropore size distribution, with the dominant pore width of 12 Å, thus indicating a more uniform pore structure of the network. In contrast, **PAE-9-ICC** exhibits a broader pore size distribution, which indicates a higher haphazardry of the network. It is interesting to note that the difference between the pore size distribution in **PAE-9-RAM**, and **PAE-9-ICC**, is more significant than the difference observed in **PAE-8-RAM**, and **PAE-8-ICC**. Presumably, the structural complexity of possible 2-D networks is less than that of 3-D networks, and the structures of more elaborate ones are more dependent on the synthetic conditions.

The reaction pathway to porous networks through alkyne metathesis presumably involves kinetic, and thermodynamic considerations, as well as gel-chemistry. Ordered crystalline organic frameworks have been prepared through solvent-mediated crystallization from a mixture of

reaction precursors via reversible reactions[14] The formation of ordered frameworks has been empirically developed and there are still significant synthetic challenges and the crystal growth is unpredictable and not always guaranteed even through reversible reactions. In our hand, alkyne metathesis approach failed to provide highly ordered materials. To gain better understanding on the reversibility of our reaction system, we subjected **PAE-8-ICC** prepared at 75 °C through cross coupling reactions to the standard alkyne metathesis conditions (55 °C, CH_3Cl, 22 h, 6% Cat. loading). We did not observe a significant change in the nitrogen gas adsorption isotherms at 77 K (S_{BET} 676 *vs.* 654 $m^2 \cdot g^{-1}$) (Figure 3.12). The pore size distribution of **PAE-8-ICC** after treatment under alkyne metathesis conditions shows the presence of some mesopores, which is presumably due to the phase separation (Figure 3.13). It should be noted that **PAE-8-ICC** network is in a precipitate form that is insoluble in the solvent (toluene) used for alkyne metathesis. This experiment therefore may not resemble the alkyne metathesis system in which the network materials stay as a gel throughout the reaction. We also prepared **PAE-8-RAM** through alkyne metathesis (55 °C, $CHCl_3$) in a closed system without removing butyne byproduct in hopes that butyne can assist the reversibility of the networks. However, we obtained amorphous networks with decreased surface area (S_{BET} =1039 $m^2 \cdot g^{-1}$). It is possible that the presence of free butyne interrupts the growth of polymer networks, by reversibly reacting with ethynylene linkages and chopping down the networks. The extent of reversibility of these species formation is still not clear and under investigation.

3.4 Conclusion

We have successfully synthesized poly(aryleneethynylene) networks with high BET surface area through dynamic alkyne metathesis. The networks with the same chemical connectivity were also prepared through irreversible cross-coupling reactions. Porous polymer networks prepared

through alkyne metathesis consistently displayed higher specific surface area and higher thermal stability compared to those networks prepared through Sonogashira cross-coupling under similar reaction conditions at various temperatures. Although the networks prepared through alkyne metathesis are amorphous at this stage, it is conceivable that such dynamic covalent approach could generate ordered materials in the future. The preparation of crystalline poly(aryleneethynylene) networks and investigation of the reversibility effect on the order of network structures are ongoing and the results will be reported in due course.

3.5 Experimental section

3.5.1 General Information.

Reagents and solvents were purchased from commercial suppliers and used without further purification, unless otherwise indicated. Ether, tetrahydrofuran (THF), toluene, CH_2Cl_2 and DMF are purified by MBRAUN solvent purification systems. Reagent-grade $CHCl_3$ and CCl_4 were purchased from Sigma-Aldrich and stored over molecular sieves. The alkyne metathesis reactions were conducted under argon atmosphere in the glovebox. All other reactions were conducted under dry nitrogen in oven-dried glassware. Flash column chromatography was performed by using a 100-150 times weight excess of flash silica gel 32-63 μm from Dynamic Absorbants Inc. Fractions were analyzed by TLC using TLC silica gel F254 250 μm precoated-plates from Dynamic Absorbants Inc. NMR spectra were taken on Inova 400 and Inova 500 spectrometers. Solid-state cross polarization magic angle spinning (CP/MAS) NMR spectra were recorded on an Inova 400 NMR spectrometer with the spinning rate of 11499 Hz. Powder X-Ray Diffraction (PXRD) was obtained from Inel CPS 120 diffraction system, using monochromated Cu K_α (λ=1.542 Å) radiation. The Fourier transform Infrared (FT-IR) spectra of starting materials and as synthesized PAE were obtained from Thermo Nicolet Avatar-370 spectrometer using KBr pellets. Elemental

analyses were taken at Huffman Laboratories, Inc. Thermogravimetric analyses (TGA) were performed in a thermogravimetric/differential thermal analyzer by heating the samples at 10 °C min^{-1} to 800 °C under the atmosphere of nitrogen. The Quantachrome Autosorb ASiQ automated gas sorption analyzer was used to measure N_2 adsorption/desorption isotherms. The sample was heated at 150 °C and kept at this temperature for at least 20 hours under the vacuum for activation. Ultra high purity grade (99.999% purity) N_2 and He, oil-free valves and gas regulators were used for all free space connections and measurements. For the adsorption measurements, the temperature was controlled by using a refrigerated bath of liquid N_2 (77K). Scanning Electron Microscopy images (SEM) were recorded using a JSM-6480LV (LVSEM) at 5.0 kV. Sample was sputter coated with gold prior to analysis.

3.5.2 Synthesis.

Tris(4-iodophenyl)amine, tris(4-ethynylphenyl)amine, tetrakis(4-iodophenyl)methane, tetrakis(4-ethynylphenyl)methane were synthesized following the published procedures.[46-49]

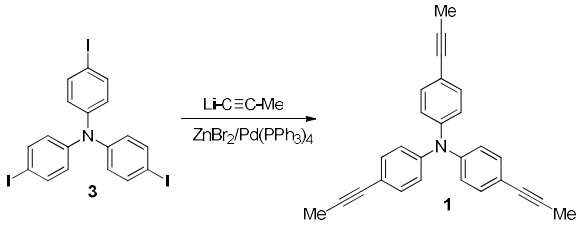

Synthesis of tris(4-(prop-1-yn-1-yl)phenyl)amine: A 25 mL schlenk tube was charged with tris(4-iodophenyl)amine (1.0 g, 1.59 mmol), and degassed three times. Then $Pd(PPh_3)_4$ (340 mg, 0.30 mmol) and anhydrous THF (2 mL) were added to this tube in the glove box. The mixture was stirred for a few minutes. A solution of $ZnBr_2$ (1.58 g, 7.0 mmol) and Lithium propyne (350 mg, 7.6 mmol) (add lithium propyne to $ZnBr_2$ slowly, the reaction is exothermic) in anhydrous THF (3 mL) was added dropwise to the mixture. The resulting mixture was sealed and heated at 80 °C

overnight. It was then cooled to room temperature. Dilute HCl (20 mL) was added to the mixture and the product was extracted with dichloromethane (3×60 mL). The combined organic layer was washed with water (100 mL) and brine (100 mL), and dried over anhydrous sodium sulfate. The solvent was removed under reduced pressure, and the residue was purified by flash column chromatography (15 %-30 % dichloromethane in hexanes as the eluent) to yield the pure compound **1** as a light yellow solid (0.57 g, 99 %): ^{1}H-NMR (500 MHz, $CDCl_3$) δ 7.26 (d, 6H, *J*=8.5 Hz), 6.96 (d, 6H, *J*=9.0 Hz), 2.05 (s, 9H). The proton NMR is consistent with the literature report.[50]

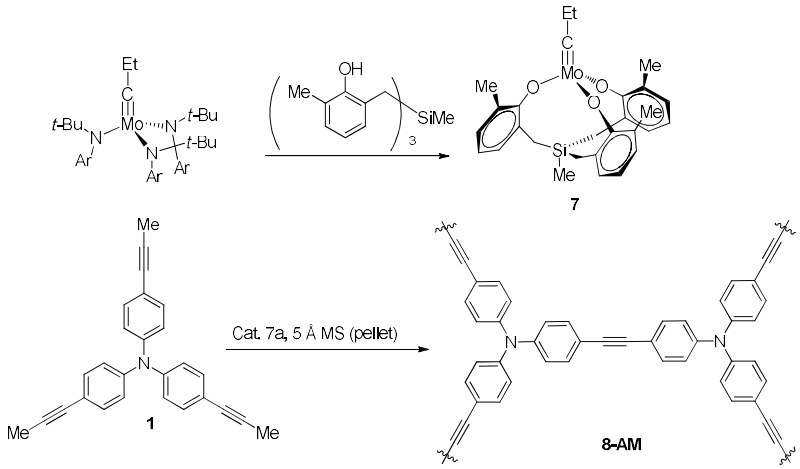

Typical procedure for the synthesis of 2D porous polymer frameworks through alkyne metathesis: The triphenolsilane (4.1 mg, 0.01 mmol) and molybdenum(VI) trisamide precursor (6.8 mg, 0.01 mmol) were premixed in dry CCl_4 (1 mL) for 15 minutes at rt to generate the catalyst **7** *in situ*. Subsequently, a solution of tetrakis(4-(prop-1-yn-1-yl)phenyl)methane (80 mg, 0.22 mmol) in $CHCl_3$ (4 mL) was added followed by 5 Å molecular sieves (1.0 g, pellet, 8 – 12 mesh). The reaction was heated at 55 °C for 22 h without stirring. Acetone (~ 100 mL) was added, and the gel like framework was broken into tiny pieces. The suspension was separated from the molecular sieves by decantation. The acetone suspension was centrifuged and most of the solvent

was removed. The resultant mixture was poured into conc. ammonium hydroxide (100 mL) with vigorous stirring. The yellow solid was collected by filtration, washed with water (2 x 30 mL), and dried under high vacuum overnight to yield the framework (60 mg, 97 %). Elemental analysis for $(C_{21}H_{12}N)_n$ Calcd. C, 90.62 %; H, 4.35 %; N, 5.03 %. Found. C, 84.43 %; H, 4.66 %; N, 4.43 %. (Since the materials are polymers instead of pure compounds, their elemental analysis results are just used as a reference, not to determine their purity)

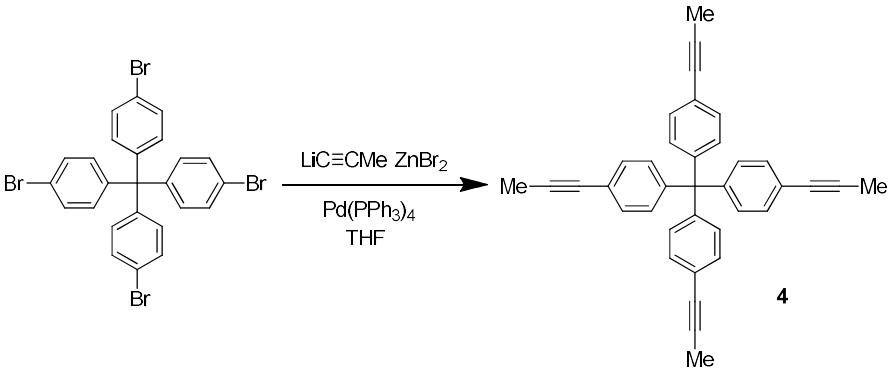

4

Synthesis of tetrakis(4-(prop-1-yn-1-yl)phenyl)methane: A 25 mL Schleck tube was charged with tetrakis(4-bromophenyl)methane (1.0 g, 1.57 mmol), and degassed three times. Then $Pd(PPh_3)_4$ (450 mg, 0.40 mmol) and anhydrous THF (2 mL) were added in the glove box. A solution of $ZnBr_2$ (2.1 g, 9.35 mmol) and Lithium propyne (470 mg, 10.0 mmol) in anhydrous THF (2 mL) was added dropwise. The resulting mixture was sealed and heated at 60 °C overnight. It was then cooled to room temperature. Water (20 mL) was added to the mixture and the product was extracted with dichloromethane (3×60 mL). The combined organic layer was washed with water (100 mL) and brine (100 mL), and then dried over anhydrous sodium sulfate. The solvent was removed under reduced pressure, and the crude product was purified by flash column chromatography (15 %-30 % dichloromethane in hexanes as the eluent) to yield the pure compound **4** as a light yellow solid (0.61 g, 82 %). The trace amount of triphenylphosphine was removed by using the merrified resin. The physical data for **4**: ^{1}H-NMR (500 MHz, $CDCl_3$) δ 7.26

(d, 8H, J = 8.5 Hz), 7.05 (d, 8H, J = 8.5 Hz), 2.04 (s, 12H); ^{13}C-NMR (100 MHz, $CDCl_3$) δ 145.27, 130.77, 130.71, 121.83, 86.09, 79.32, 64.42, 4.35; HR-MS (ESI): calcd. for $C_{37}H_{28}$ ([M+H$^+$]) 473.2269, found 473.2244.

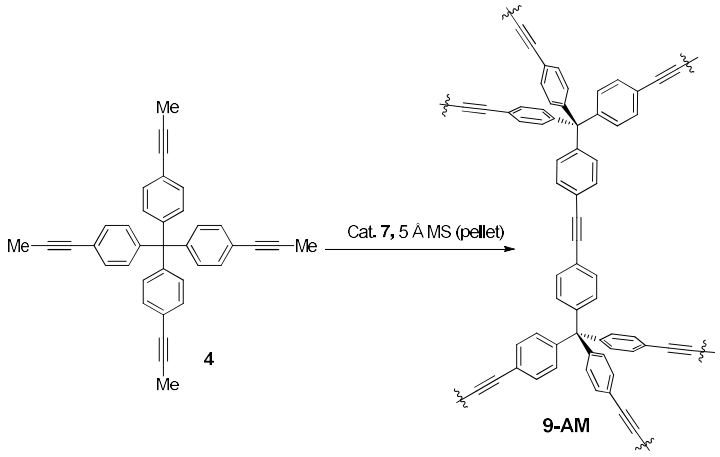

Typical procedure for the synthesis of 3D porous polymer frameworks through alkyne metathesis: The triphenolsilane (6.2 mg, 0.015 mmol) and the precursor (10.1 mg, 0.015 mmol) were premixed in dry CCl_4 (1 mL) for 15 minutes at rt to generate the catalyst **7** *in situ*. Subsequently, a solution of tetrakis(4-(prop-1-yn-1-yl)phenyl)methane (120 mg, 0.25 mmol) in $CHCl_3$ (6 mL) was added followed by 5 Å molecular sieves (1.5 g, pellet, 8 – 12 mesh). The reaction was heated at 55 °C for 22 h without stirring. Acetone (~ 100 mL) was added and. the gel like framework was broken into tiny pieces. The suspension was separated from the molecular sieves by decantation. The acetone suspension was centrifuged and most of the solvent was removed. The resultant mixture was poured into conc. ammonium hydroxide (100 mL) with vigorous stirring. The yellow solid was collected by filtration, washed with water (2 x 30 mL), and dried under high vacuum overnight to yield the framework **9-AM** as a white solid (98 mg, quantitative). Elemental analysis for $(C_{29}H_{16})_n$ Calcd. C, 95.57 %; H, 4.43 %. Found. C, 87.82 %; H, 4.92 %. (Since the materials are polymers instead of pure compounds, their elemental analysis

results are just used as a reference, not to determine their purity)

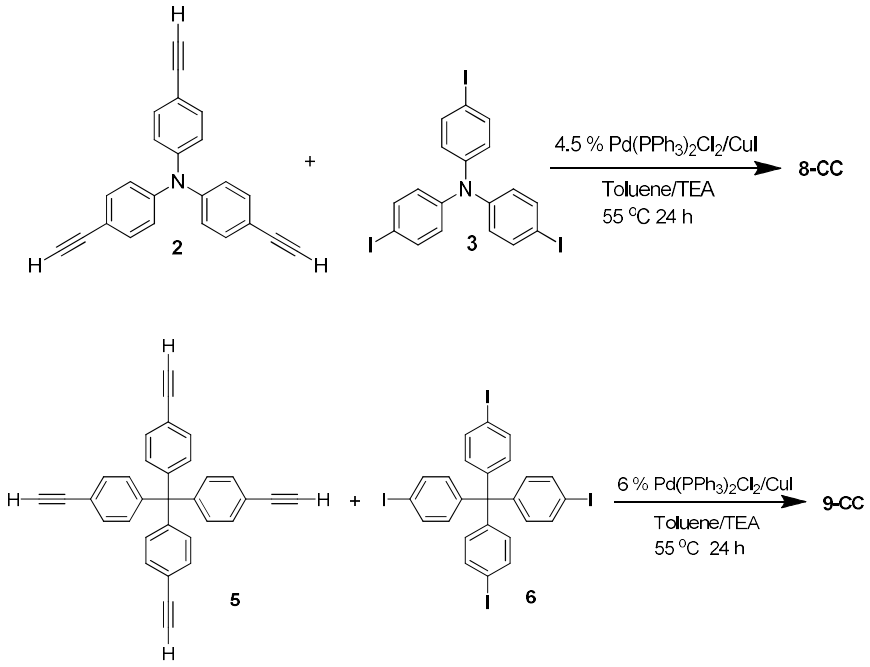

General procedure for the synthesis of 2D and 3D porous polymer frameworks: A 25 mL schlenk tube was charged with tris(4-iodophenyl)amine (118 mg, 0.19 mmol) and tris(4-(prop-1-yn-1-yl)phenyl)amine (60 mg, 0.19 mmol), then degassed three times. To this mixture, bis(triphenylphosphine)palladium(II) dichloride (6 mg, 0.0085 mmol) and CuI (2 mg, 0.010 mmol) were added, followed by anhydrous toluene (6.4 mL) and trienthylamine (2 mL). The mixture was degassed three times, then heated at 55 °C for 24 hours. After the mixture was cooled to room temperature, 6 M hydrochloric acid (6 mL) was added to the mixture and sonicated for 20 minutes. The product was collected by vacuum filtration, washed with water (10 mL), dichloromethane (20 mL), ethanol (20 mL) and acetone (20 mL), and dried under high vacuum overnight to yield framework **8-CC** as a yellow solid (155 mg, 90 %). Elemental analysis: 2D for $(C_{21}H_{12}N)_n$ Calcd. C, 90.62 %; H, 4.35 %; N, 5.03 %. Found. C, 76.72 %; H, 3.94 %; N, 4.09 %. 3D for $(C_{29}H_{16})_n$ Calcd. C, 95.57 %; H, 4.43 %. Found. C, 76.95 %; H, 3.96 %. (Since the materials are polymers

instead of pure compounds, their elemental analysis results are just used as a reference, not to determine their purity)

3.5.3. Thermal gravimetric analysis of PPF series

Samples were run on a TA Instruments Q-500 series thermal gravimetric analyzer with samples held in a platinum pan under nitrogen atmosphere. A 10 K min^{-1} ramp rate was used. The materials show a good thermal stability up to at least 400 °C. The cause of a slight weight increase at the beginning of TGA analysis of **8-CC** is unclear. We observed the same results in the multiple trials of TGA analysis **8-CC.**

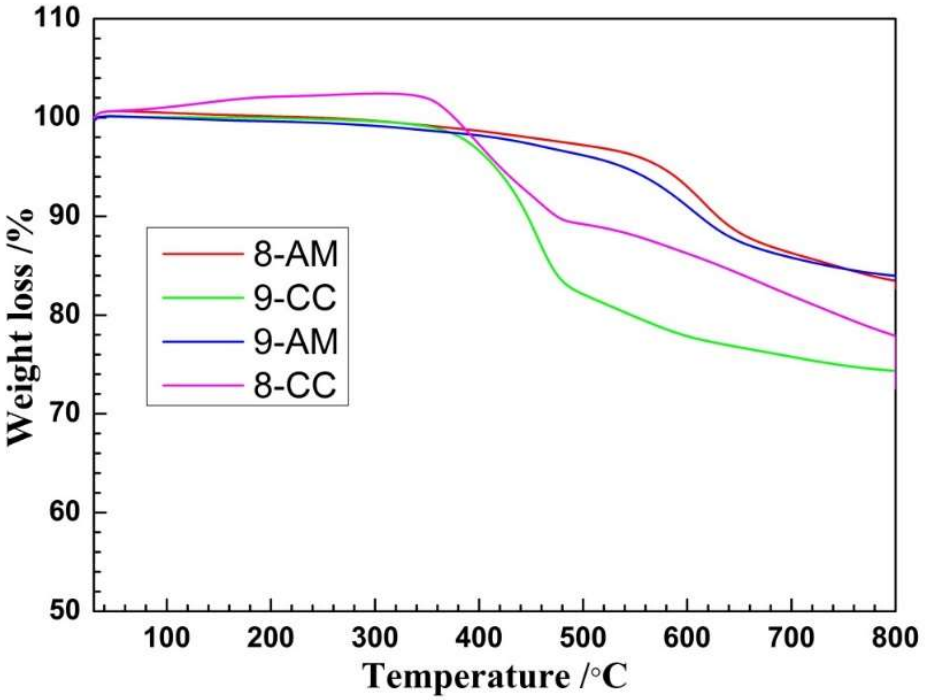

Figure 3.4. TGA profiles of the PAE series.

3.5.4. FT-IR of starting materials and PPF series

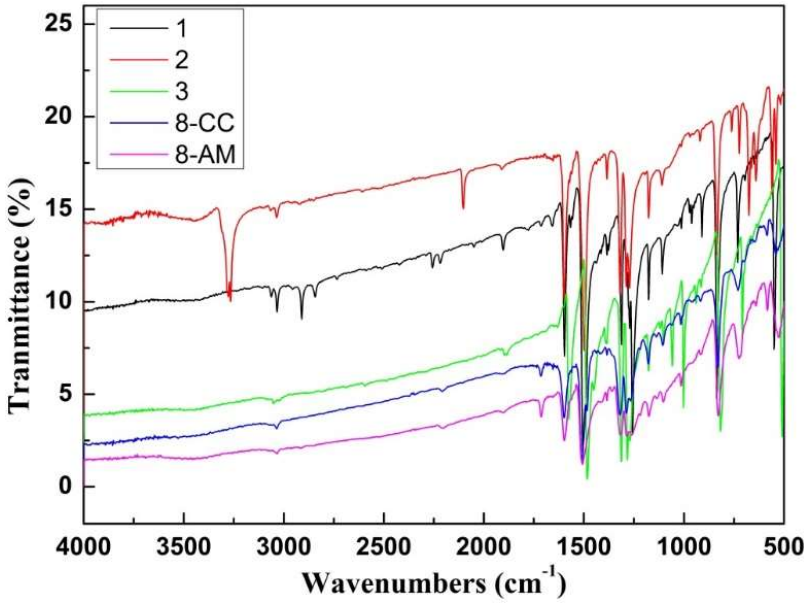

Figure 3.5. IR spectrum of starting materials (**1**-**3**) and as-synthesized **8-AM** and **8-CC**.

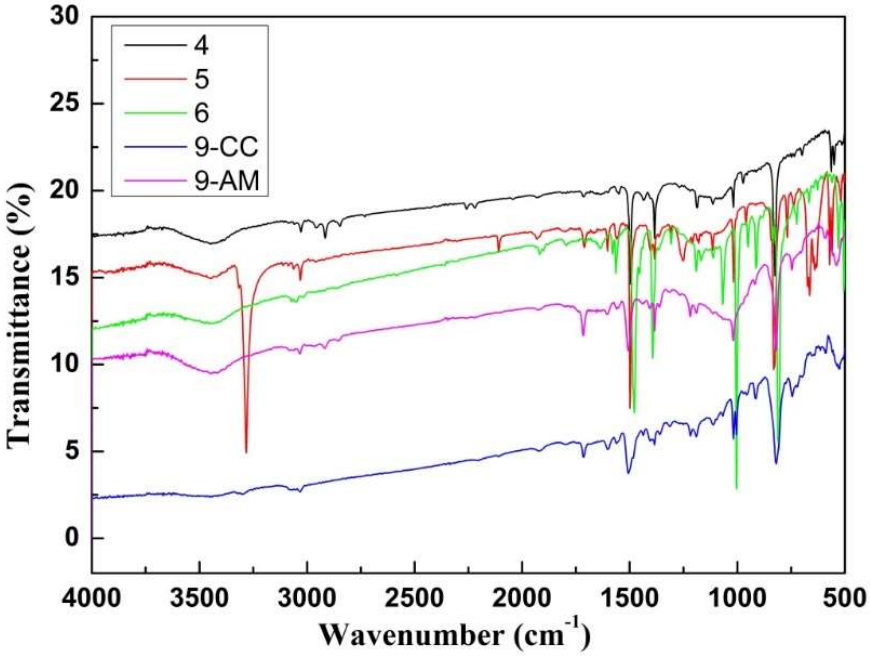

Figure 3.6. IR spectrum of starting materials (**4**-**6**) and as-synthesized **9-AM** and **9-CC**.

From the IR spectrum of the as synthesized frameworks, the C≡C vibration peak is disappeared since the framework has the symmetrical C≡C bond, with both phenyl groups in each side.

3.5.5. Powder X-Ray Diffraction of PPF series

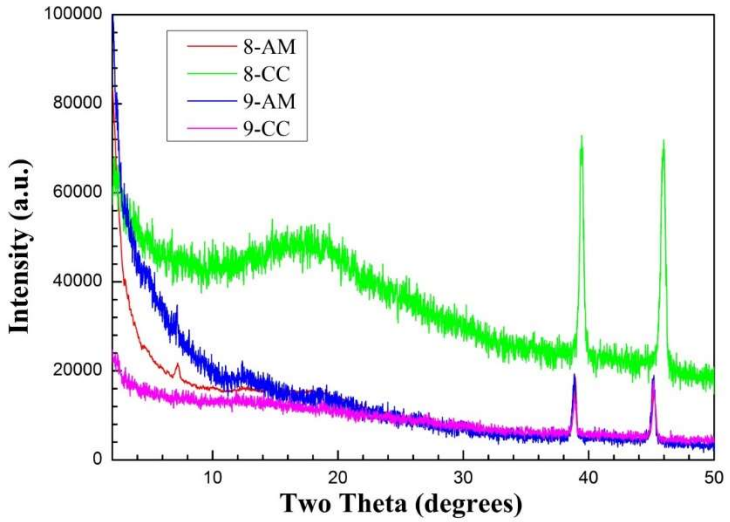

Figure 3.7. Powder X-ray diffraction profiles of 2D and 3D PPF prepared through different method.

Additional gas adsorption for the frameworks in different conditions.

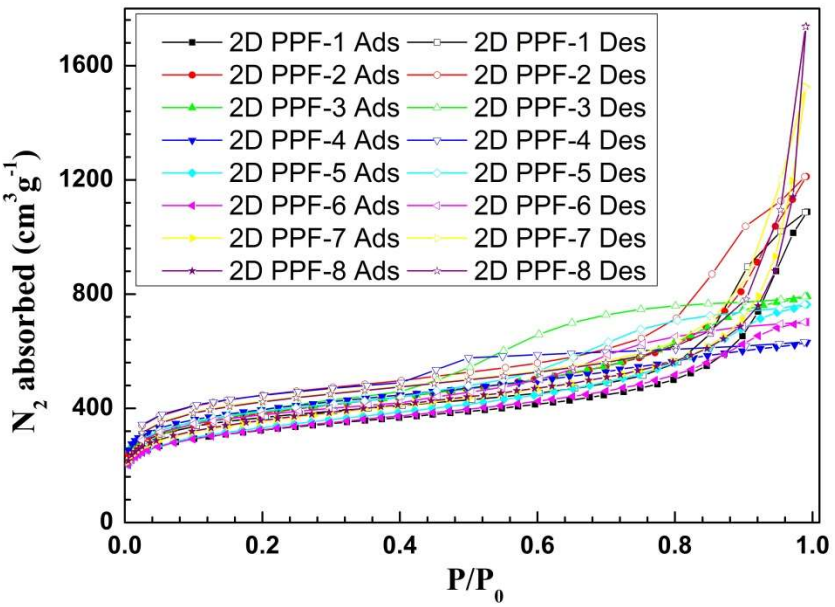

Figure 3.8. N_2 adsorption isotherms for 2D framework prepared through alkyne metathesis in different conditions. (black: 55 °C, toluene solvent, 4.5% catalyst loading; red: 55 °C, $CHCl_3$

solvent, 4.5% catalyst loading; green: 55 °C, $CHCl_3$ solvent, 4.5% catalyst loading and 4 Å molecular sieves; blue: 55 °C, $CHCl_3$ solvent, 4.5% catalyst loading and 5 Å molecular sieves; cyan: 55 °C, $CHCl_3$ solvent, 1.5% catalyst loading and 5 Å molecular sieves; magenta: 55 °C, toluene solvent, 4.5% catalyst loading and 5 Å molecular sieves; yellow: 75 °C, toluene solvent, 4.5% catalyst loading and 5 Å molecular sieves; purple: 40 °C, toluene solvent, 4.5% catalyst loading and 5 Å molecular sieves.)

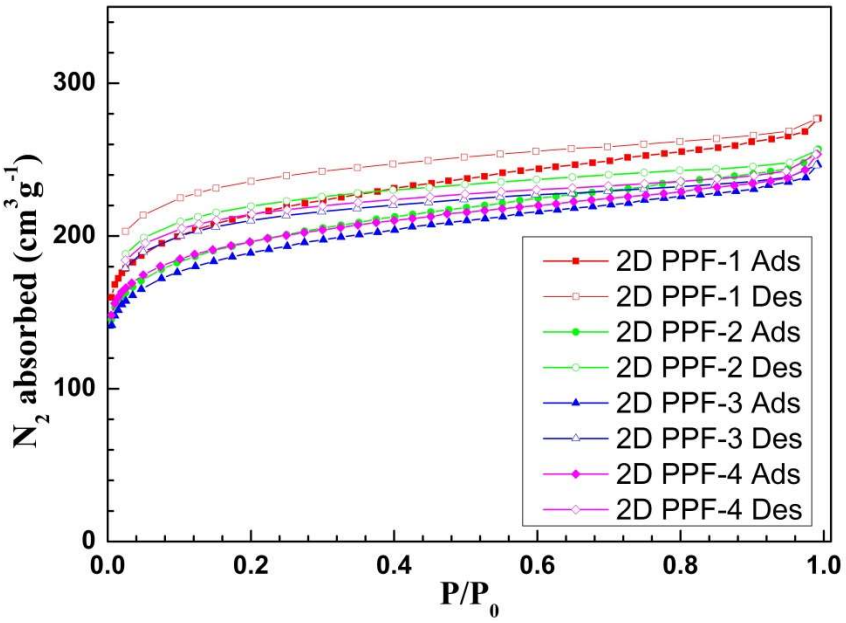

Figure 3.9. N_2 adsorption isotherms for 2D framework prepared through Sonogashira cross-coupling in different conditions. (red: 40 °C, toluene/TEA=6.4 mL/2.0 mL, 4.5% catalyst loading; green: 55 °C, toluene/TEA=6.4 mL/2.0 mL, 4.5% catalyst loading; blue: 75 °C, toluene/TEA=6.4 mL/2.0 mL, 4.5% catalyst loading; magenta: 90 °C, toluene/TEA=15 mL/10 mL, 4.5% catalyst loading.)

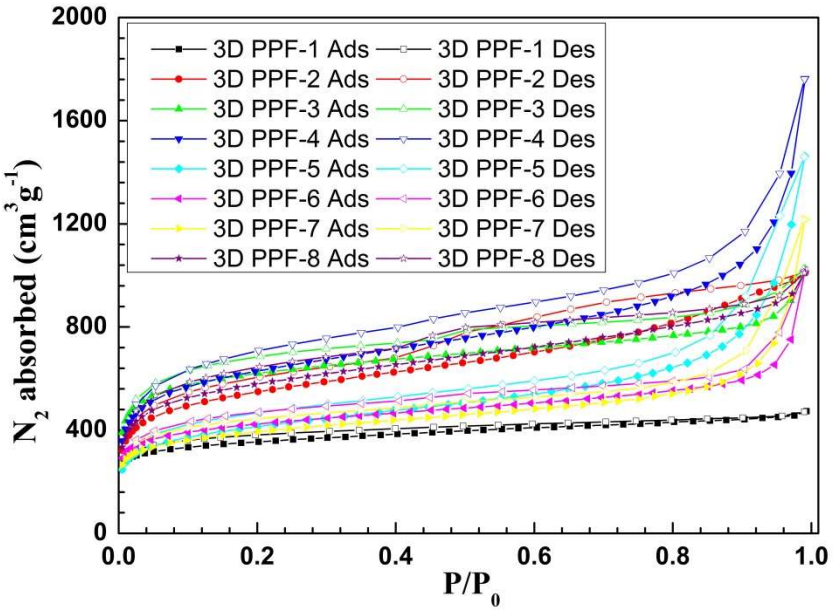

Figure 3.10. N_2 adsorption isotherms for 3D framework prepared through alkyne metathesis in different conditions. (black: 55 °C, toluene solvent, 6% catalyst loading; red: 55 °C, CCl_4 solvent, 2 % catalyst loading and 5 Å molecular sieves; green: 55 °C, $CHCl_3$ solvent, 6% catalyst loading and 5 Å molecular sieves; blue: 55 °C, toluene solvent, 6% catalyst loading and 5 Å molecular sieves; cyan: 40 °C, toluene solvent, 6% catalyst loading and 5 Å molecular sieves; magenta: 75 °C, toluene solvent, 6% catalyst loading and 5 Å molecular sieves; yellow: 75 °C, CCl_4, 6% catalyst loading and 5 Å molecular sieves; purple: 75 °C, $CHCl_3$, 6% catalyst loading and 5 Å molecular sieves.)

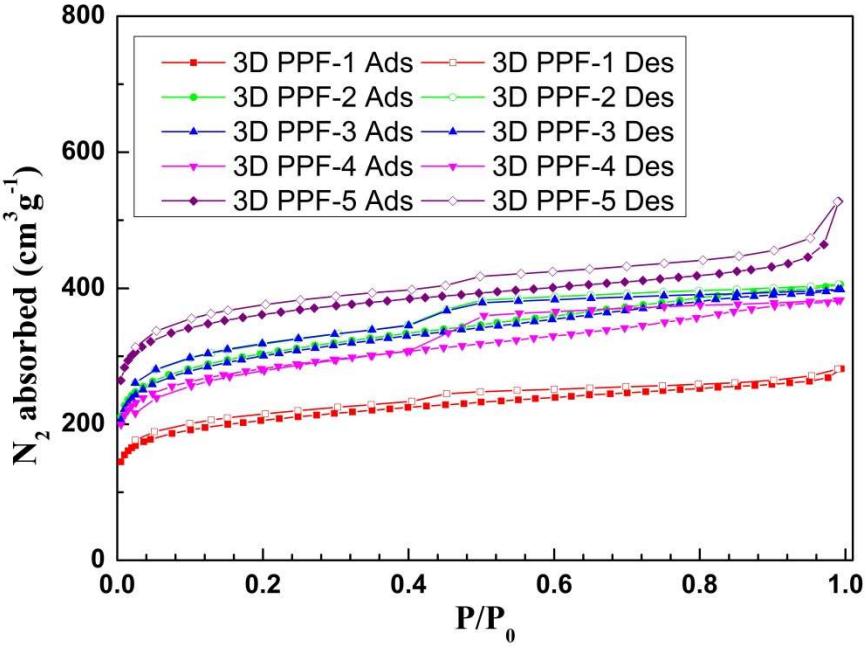

Figure 3.11. N_2 adsorption isotherms for 3D framework prepared through Sonogashira cross-coupling in different conditions. (red: 40 °C, toluene/TEA=6.4 mL/2.0 mL, 6% catalyst loading; green: 55 °C, toluene/TEA=6.4 mL/2.0 mL, 6% catalyst loading; blue: 75 °C, toluene/TEA=6.4 mL/2.0 mL, 6% catalyst loading; magenta: 55 °C, $CHCl_3$/TEA=6.4 mL/2.0 mL, 6% catalyst loading; purple: 90 °C, toluene/TEA=15 mL/10 mL, 6 % catalyst loading.)

3.5.7. Solid State NMR of the as synthesized frameworks

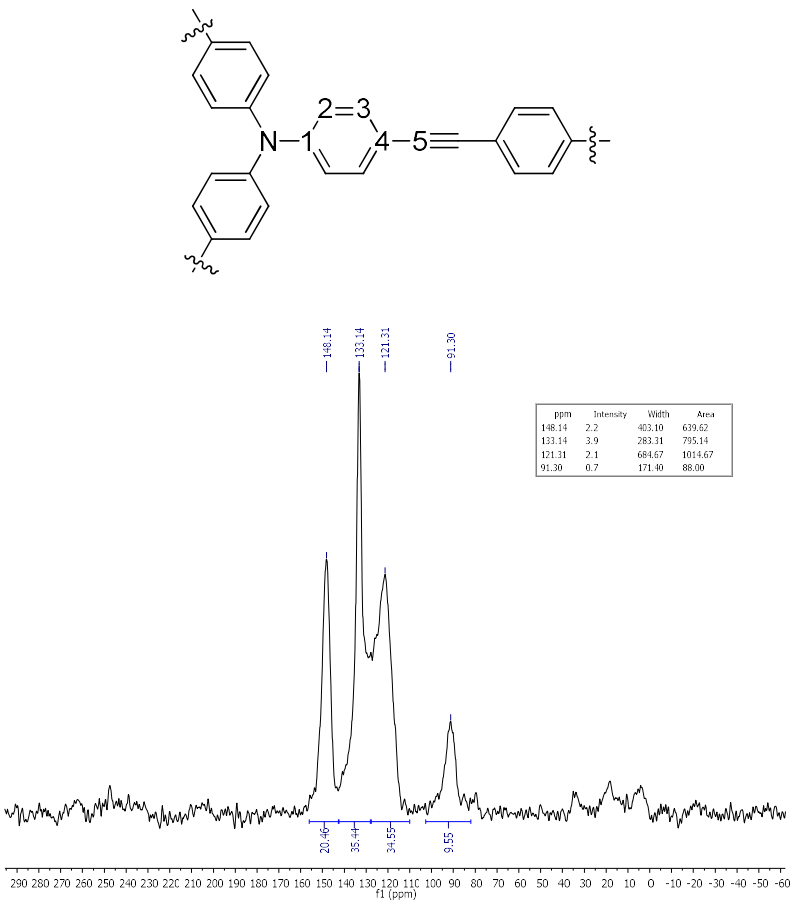

Figure 3.12. ^{13}C CP-MAS NMR spectrum of the **8-AM**.

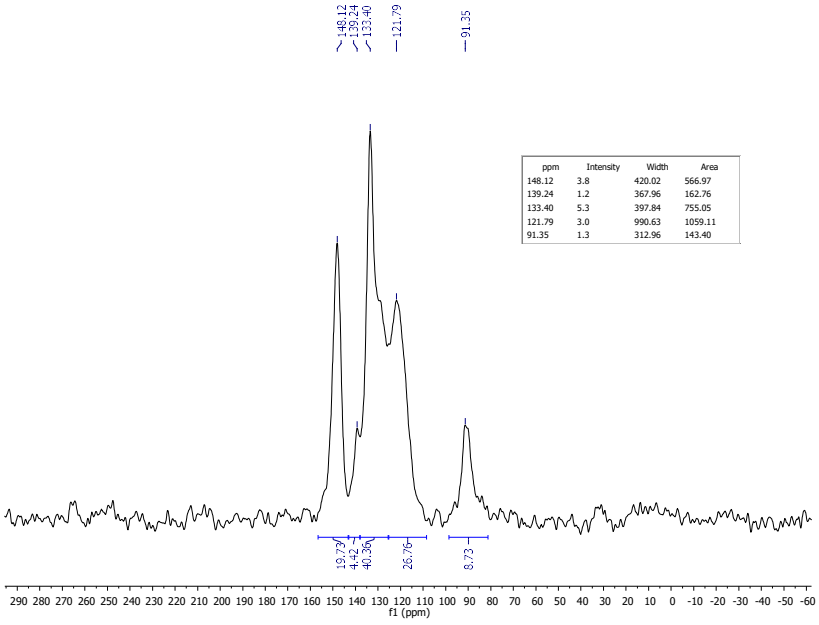

Figure 3.13. ^{13}C CP-MAS NMR spectrum of the **8-CC**.

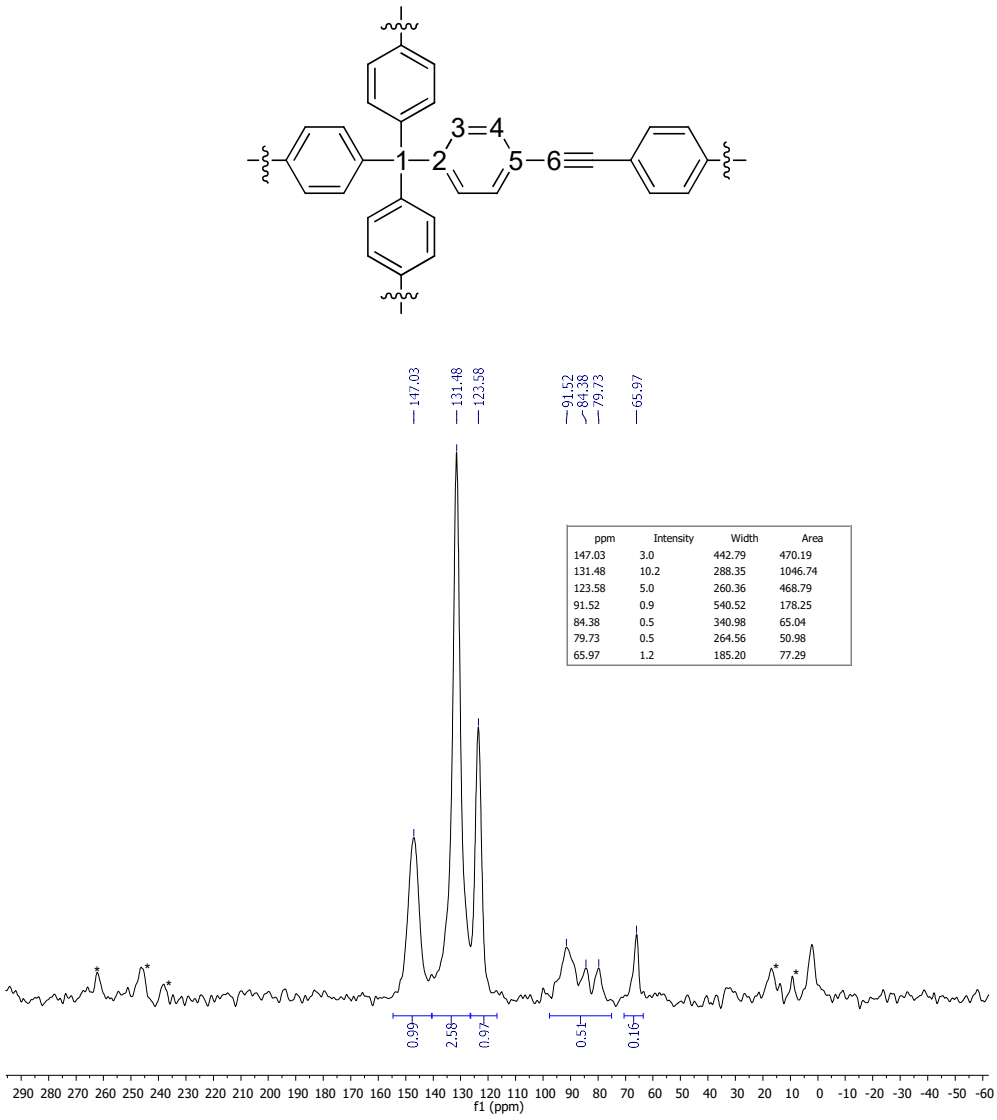

Figure 3.14. ^{13}C CP-MAS NMR spectrum of the **9-AM**.

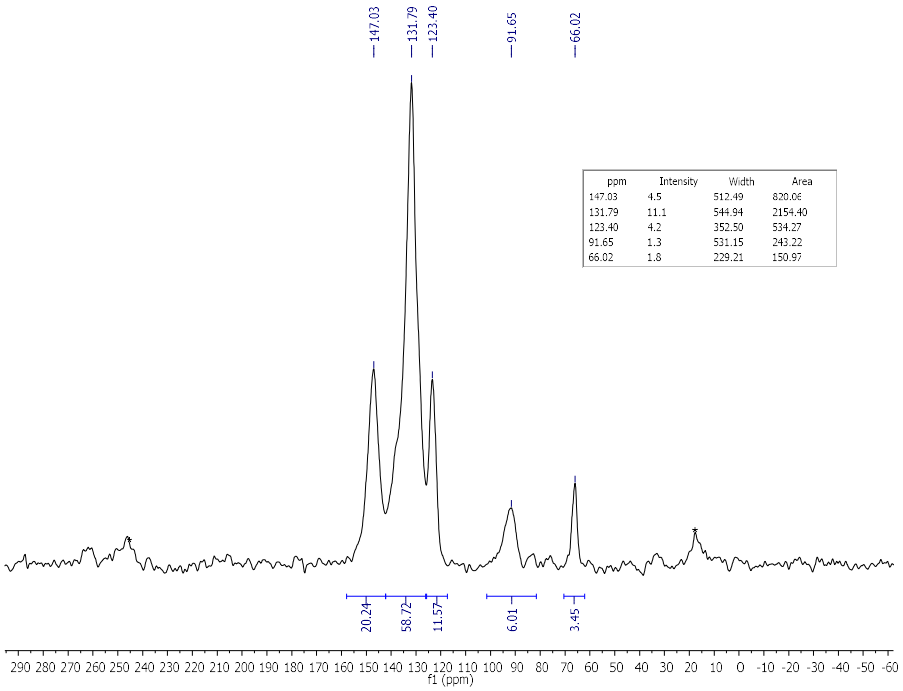

Figure 3.15. ^{13}C CP-MAS NMR spectrum of the **9-CC**.

3.5.8. SEM images of PPF series

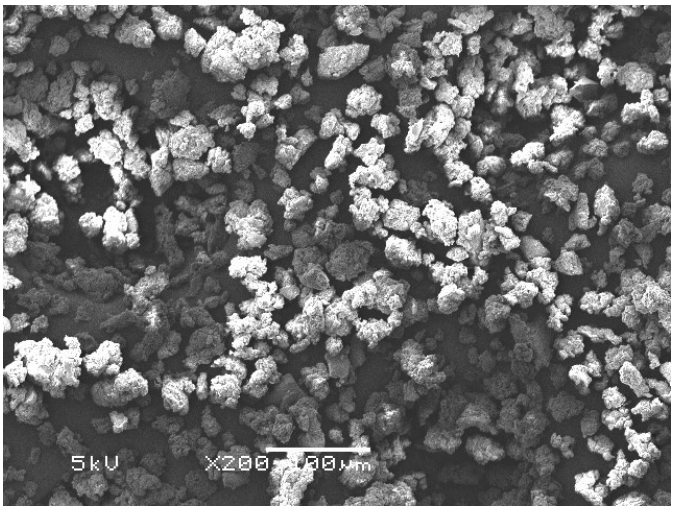

Figure 3.16. SEM image of **8-AM**.

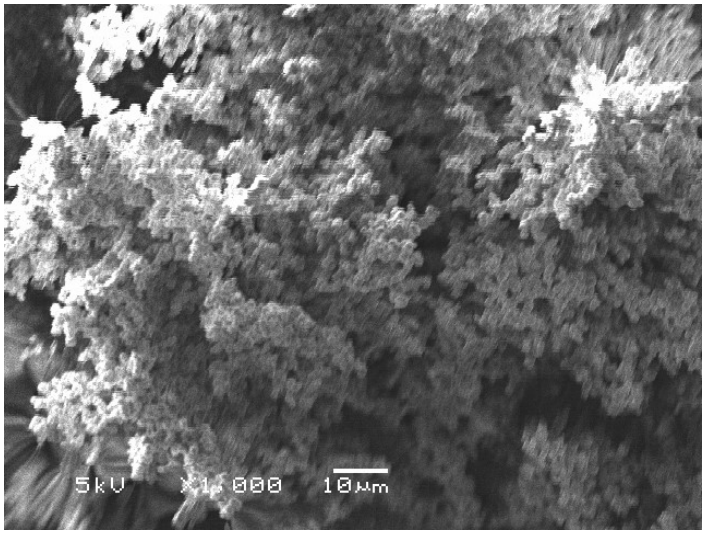

Figure 3.17. SEM image of **8-CC**.

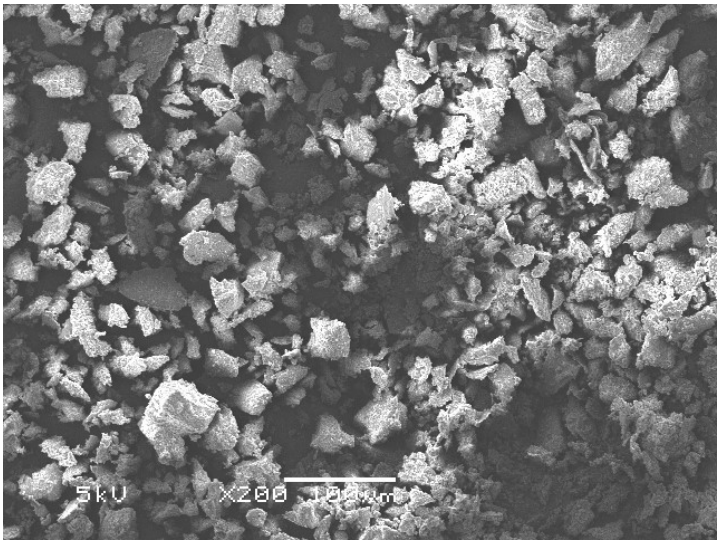

Figure 3.18. SEM image of **9-AM**.

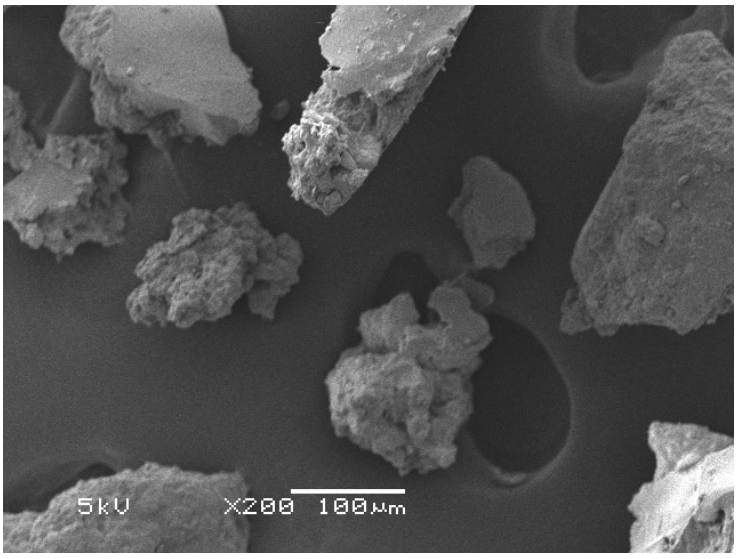

Figure 3.19. SEM image of **9-CC**.

3.6 References

(1) Wu, D. C.; Xu, F.; Sun, B.; Fu, R. W.; He, H. K.; Matyjaszewski, K. *Chem. Rev.* **2012**, *112*, 3959.

(2) Kuhn, P.; Antonietti, M.; Thomas, A. *Angew. Chem., Int. Ed.* **2008**, *47*, 3450.

(3) Wood, C. D.; Tan, B.; Trewin, A.; Su, F.; Rosseinsky, M. J.; Bradshaw, D.; Sun, Y.; Zhou, L.; Cooper, A. I. *Adv. Mater.* **2008**, *20*, 1916.

(4) Han, S. S.; Furukawa, H.; Yaghi, O. M.; Goddard, W. A. *J. Am. Chem. Soc.* **2008**, *130*, 11580.

(5) Ben, T.; Ren, H.; Ma, S. Q.; Cao, D. P.; Lan, J. H.; Jing, X. F.; Wang, W. C.; Xu, J.; Deng, F.; Simmons, J. M.; Qiu, S. L.; Zhu, G. S. *Angew. Chem., Int. Ed.* **2009**, *48*, 9457.

(6) Jin, Y. H.; Voss, B. A.; Noble, R. D.; Zhang, W. *Angew. Chem., Int. Ed.* **2010**, *49*, 6348.

(7) Yuan, D. Q.; Lu, W. G.; Zhao, D.; Zhou, H. C. *Adv. Mater.* **2011**, *23*, 3723.

(8) Jin, Y. H.; Voss, B. A.; McCaffrey, R.; Baggett, C. T.; Noble, R. D.; Zhang, W. *Chem. Sci.* **2012**, *3*, 874.

(9) Jin, Y. H.; Zhu, Y. L.; Zhang, W. *CrystEngComm* **2013**, *15*, 1484.

(10) Dawson, R.; Stevens, L. A.; Drage, T. C.; Snape, C. E.; Smith, M. W.; Adams, D. J.; Cooper, A. I. *J. Am. Chem. Soc.* **2012**, *134*, 10741.

(11) Jiang, J. X.; Su, F.; Trewin, A.; Wood, C. D.; Campbell, N. L.; Niu, H.; Dickinson, C.; Ganin, A. Y.; Rosseinsky, M. J.; Khimyak, Y. Z.; Cooper, A. I. *Angew. Chem., Int. Ed.* **2007**, *46*, 8574.

(12) Stockel, E.; Wu, X. F.; Trewin, A.; Wood, C. D.; Clowes, R.; Campbell, N. L.; Jones, J. T. A.; Khimyak, Y. Z.; Adams, D. J.; Cooper, A. I. *Chem. Commun.* **2009**, 212.

(13) Jiang, J. X.; Su, F.; Trewin, A.; Wood, C. D.; Niu, H.; Jones, J. T. A.; Khimyak, Y. Z.; Cooper, A. I. *J. Am. Chem. Soc.* **2008**, *130*, 7710.

(14) Feng, X.; Ding, X.; Jiang, D. *Chem. Soc. Rev.* **2012**, *41*, 6010.

(15) Ding, S. Y.; Wang, W. *Chem. Soc. Rev.* **2013**, *42*, 548.

(16) Cote, A. P.; Benin, A. I.; Ockwig, N. W.; O'Keeffe, M.; Matzger, A. J.; Yaghi, O. M. *Science* **2005**, *310*, 1166.

(17) El-Kaderi, H. M.; Hunt, J. R.; Mendoza-Cortes, J. L.; Cote, A. P.; Taylor, R. E.; O'Keeffe, M.; Yaghi, O. M. *Science* **2007**, *316*, 268.

(18) Spitler, E. L.; Dichtel, W. R. *Nat. Chem.* **2010**, *2*, 672.

(19) Nagai, A.; Guo, Z.; Feng, X.; Jin, S.; Chen, X.; Ding, X.; Jiang, D. *Nat. Commun.* **2011**, *2*, 536.

(20) Xie, Z. G.; Wang, C.; deKrafft, K. E.; Lin, W. B. *J. Am. Chem. Soc.* **2011**, *133*, 2056.

(21) Ding, S. Y.; Gao, J.; Wang, Q.; Zhang, Y.; Song, W. G.; Su, C. Y.; Wang, W. *J. Am. Chem. Soc.* **2011**, *133*, 19816.

(22) Spitler, E. L.; Koo, B. T.; Novotney, J. L.; Colson, J. W.; Uribe-Romo, F. J.; Gutierrez, G. D.; Clancy, P.; Dichtel, W. R. *J. Am. Chem. Soc.* **2011**, *133*, 19416.

(23) Ding, X.; Guo, J.; Feng, X.; Honsho, Y.; Seki, S.; Maitarad, P.; Saeki, A.; Nagase, S.; Jiang, D. *Angew. Chem., Int. Ed.* **2011**, *50*, 1289.

(24) Feng, X.; Liu, L.; Honsho, Y.; Saeki, A.; Seki, S.; Irle, S.; Dong, Y.; Nagai, A.; Jiang, D. *Angew. Chem., Int. Ed.* **2012**, *51*, 2618.

(25) Colson, J. W.; Woll, A. R.; Mukherjee, A.; Levendorf, M. P.; Spitler, E. L.; Shields, V. B.; Spencer, M. G.; Park, J.; Dichtel, W. R. *Science* **2011**, *332*, 228.

(26) Ge, P.-H.; Fu, W.; Herrmann, W. A.; Herdtweck, E.; Campana, C.; Adams, R. D.; Bunz, U. H. F. *Angew. Chem., Int. Ed.* **2000**, *39*, 3607.

(27) Miljanic, O. S.; Vollhardt, K. P. C.; Whitener, G. D. *Synlett* **2003**, 29.

(28) Zhang, W.; Moore, J. S. *J. Am. Chem. Soc.* **2004**, *126*, 12796.

(29) Zhang, W.; Brombosz, S. M.; Mendoza, J. L.; Moore, J. S. *J. Org. Chem.* **2005**, *70*, 10198.

(30) Zhang, W.; Moore, J. S. *J. Am. Chem. Soc.* **2005**, *127*, 11863.

(31) Cho, H. M.; Weissman, H.; Wilson, S. R.; Moore, J. S. *J. Am. Chem. Soc.* **2006**, *128*, 14742.

(32) Zhang, W.; Moore, J. S. *Angew. Chem., Int. Ed.* **2006**, *45*, 4416.

(33) Cho, H. M.; Weissman, H.; Moore, J. S. *J. Org. Chem.* **2008**, *73*, 4256.

(34) Finke, A. D.; Gross, D. E.; Han, A.; Moore, J. S. *J. Am. Chem. Soc.* **2011**, *133*, 14063.

(35) Jyothish, K.; Zhang, W. *Angew. Chem., Int. Ed.* **2011**, *50*, 3435.

(36) Jyothish, K.; Wang, Q.; Zhang, W. *Adv. Synth. Catal.* **2012**, *354*, 2073.

(37) Zhang, C. X.; Long, H.; Zhang, W. *Chem. Commun.* **2012**, *48*, 6172.

(38) Zhang, C.; Wang, Q.; Long, H.; Zhang, W. *J. Am. Chem. Soc.* **2011**, *133*, 20995.

(39) Novotney, J. L.; Dichtel, W. R. *Acs Macro Lett.* **2013**, *2*, 423.

(40) Yang, H.; Liu, Z.; Zhang, W. *Adv. Synth. Catal.* **2013**, *355*, 885.

(41) Zhang, W.; Moore, J. S. *Adv. Synth. Catal.* **2007**, *349*, 93.

(42) Jyothish, K.; Zhang, W. *Angew. Chem., Int. Ed.* **2011**, *50*, 8478.

(43) Wu, X. A.; Tamm, M. *Beilstein J. Org. Chem.* **2011**, *7*, 82.

(44) Schrock, R. R.; Czekelius, C. *Adv. Synth. Catal.* **2007**, *349*, 55.

(45) Weber, J.; Schmidt, J.; Thomas, A.; Bohlmann, W. *Langmuir* **2010**, *26*, 15650.

(46) Feng, J. C.; Zhang, C.; Li, Y.; Yang, M. J. *J. Appl. Polym. Sci.* **2011**, *121*, 217.

(47) McIlroy, S. P.; Clo, E.; Nikolajsen, L.; Frederiksen, P. K.; Nielsen, C. B.; Mikkelsen, K. V.; Gothelf, K. V.; Ogilby, P. R. *J. Org. Chem.* **2005**, *70*, 1134.

(48) Li, X. H.; Gibb, B. C. *Supramol. Chem.* **2003**, *15*, 495.

(49) Pandey, P.; Farha, O. K.; Spokoyny, A. M.; Mirkin, C. A.; Kanatzidis, M. G.; Hupp, J. T.; Nguyen, S. T. *J. Mater. Chem.* **2011**, *21*, 1700.

(50) Gagnon, E.; Maris, T.; Wuest, J. D. *Org. Lett.* **2010**, *12*, 404.

CHAPTER 4

Photoresponsive Porous Organic Polymers with Azobenzene Moiety

(A paper was published for this chapter: Zhu, Y.; Zhang, W. "Reversible Tuning of Pore Size and CO2 Adsorption in Azobenzene Functionalized Porous Organic Polymers" *Chem. Sci.* 2014, *5*, 4957 - 4961)

4.1 Abstract

A series of novel physiochemical stable porous organic polymers (POPs), **UCBZ-1, 2, 3, 4** comprising azobenzene moieties, have been synthesized through dynamic imine chemistry and fully characterized with solid-state ^{13}C-NMR, IR, gas adsorption isotherms, TGA, SEM, and PXRD. The resulting porous organic polymers showed permanent porosity with a BET surface area around 1000 $m^2 \cdot g^{-1}$. More importantly, these polymers exhibit fully reversible responsive pore size distribution and CO_2 adsorption capacities triggered by UV irradiation or heat treatment. We observed the transformation of some micropores of around 14 Å to the larger ones (17 Å) upon UV irradiation. Although BET surface areas remain almost constant during the isomerization process, *trans* to *cis* isomerization of azobenzene groups significantly increases CO_2 uptake (up to 29 % at 273 K and 1 atm) of the frameworks, which is largely attributed to the enhanced dipole-quadrupole interaction between CO_2 and the frameworks due to the increased dipole moment of *cis* -N=N- groups compared to *trans* -N=N-. This responsiveness differs from the previously reported responsive MOFs containing azobenzene groups, which release CO_2 upon *trans* to *cis* isomerization. These polymers thus represent a new class of porous polymers having intriguing stimuli-responsive properties for advanced applications.

4.2 Introduction

Functional polymers that are structurally adaptable in response to a single stimulus or multiple stimuli have attracted great attention due to their potential applications as stimuli-responsive 'smart' materials.[1-4] Metal-organic frameworks (MOFs), containing photochromic moieties in framework backbones as pendent groups, or physically dispersed guest molecules in the pores, have shown interesting optically responsive gas adsorption behaviors and opened a promising pathway towards cost-effective capture and release of CO_2.[5-8] Porous organic polymers (POPs), such as covalent organic frameworks (COFs),[9-13] porous aromatic frameworks (PAFs),[14] conjugated microporous polymers (CMPs),[15] or porous polymer networks (PPNs),[16] have emerged as a new class of porous materials that exhibit light weight, intrinsic porosity, high physiochemical stability, and structural tunability. POPs have been widely used in gas adsorption and separation, [17-21] heterogeneous catalysis, [22] and a range of other applications. However, to date responsive POPs have rarely been investigated. Herein, we report a series of photoresponsive purely organic porous polymers containing azobenzene moieties. The pore size distributions and CO_2 uptake are reversibly altered by the use of UV light irradiation and thermal treatment for several cycles with little change in their responsiveness. In contrast to photoresponsive MOFs containing azobenzene moieties, in which *trans*-to-*cis* isomerization induces the release of CO_2,[7] our materials show a unique inverse change, adsorbing more CO_2 upon *trans*-to-*cis* isomerization.

Typical external stimuli include light,[23,24] pH,[25,26] temperature,[27] ionic strength,[28] mechanical stress,[29-31] etc. Among these stimuli, light is the scientifically and technologically most attractive stimulus to trigger molecular change since it can be conveniently manipulated

by modern optics and seldom generates side products. Various structural motifs are known to be photoresponsive, such as azobenzene and its derivatives,[32] triphenylmethane leuco derivatives,[33,34] and spiropyrans.[35,36] Among them, azobenzene and its derivatives are arguably the most attractive systems.[37] The *trans/cis* isomerization of azobenzene provides large changes in the structure and dipole moment: much shorter distances (d4–4' ≈ 6 Å) between the aryl termini and larger dipole moment of 3.0 D in the non-planar *cis* isomer compared to 0 D dipole moment in the planar *trans* isomer (d4–4' ≈ 9 Å).[38,39] We envision that such significant geometrical and polarity changes of the azobenzene moieties during the course of photoisomerization can be translated into bulk materials and influence their properties.

4.3 Results and discussion

We introduced azobenzene moieties into organic porous materials and prepared a series of imine-linked POPs through Schiff-Base chemistry.[40,41] Diamines (1-4, **Figure 4.1**) substituted with various sterically different azobenzene groups were prepared in order to explore the effect of building block structures on the responsiveness of the porous materials. Commercially available diamine 5 with no azobenzene substituent was chosen as a control compound. 1, 3, 5-Triformylphloroglucinol (6) was selected as the complimentary aldehyde building block. It was expected that the resulting enol-imine polymers can tautomerize to form more stable β-keto-enamines,[42] thus significantly enhancing their stability.[43-47] First, we confirmed the *trans/cis* isomerization (**Figure 4.2**) of azobenzene functionalized diamine monomers by UV-Vis measurements and ^{1}H-NMR study. UV-Vis spectra of the pure diamines (1-3) in dichloromethane show a typical strong π→π* absorption band around 310 nm and a tiny broad n→π* absorption band around 415 nm from the azo functional group. Upon UV

irradiation, the intensity of the 310 nm band was decreased while the intensity of the 415 nm band was slightly increased, indicating the *trans-to-cis* isomerization of the azo functional group (**Figures 4.5, 4.6 and 4.7**). Diamine 4 with two azo groups exhibits a different UV absorption pattern, showing two strong bands around 310 nm and 360 nm, both of which were decreased upon UV irradiation (**Figure 4.8**). The ^{1}H NMR study of diamine 1 showed several new peaks after exposure to UV light, which are ascribed to the formation of *cis*-diamine 1 (**Figures 4.9 and 4.10**).

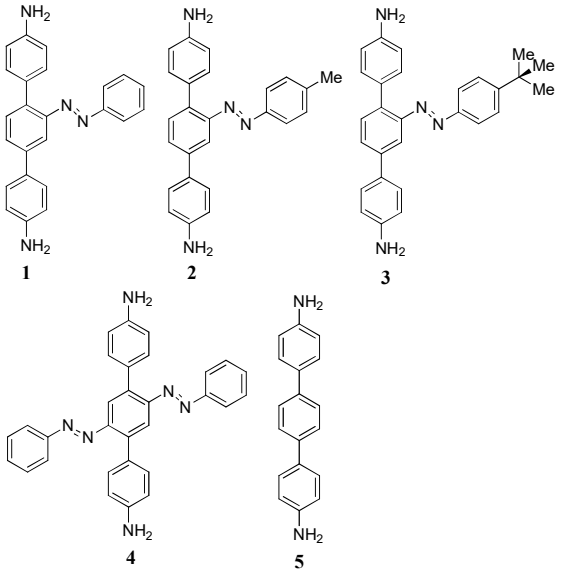

Figure 4.1. Structures of diamines.

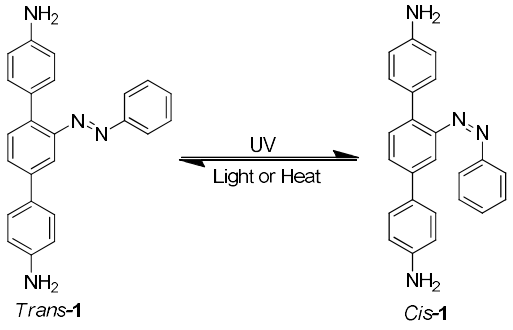

Figure 4.2. *Trans*/*cis* isomerization of diamine **1**.

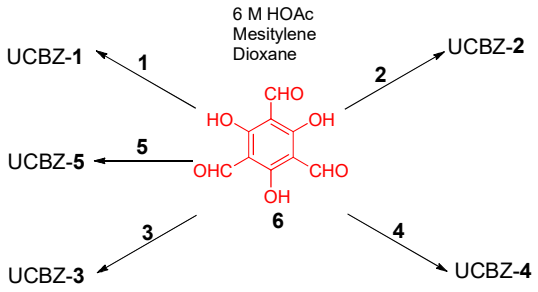

Scheme 4.1. Synthesis of UCBZ **1**-**5**.

Next, we set out to explore the imine condensation between diamines (**1-4**) and trialdehyde **6**. In order to determine the optimal conditions leading to the materials with high specific surface area, we systematically screened a series of solvothermal conditions by varying the solvent combination, catalyst concentration, and temperatures (**Table 4.1**). We used a 3:2 stoichiometric ratio of diamine 1 and trialdehyde **6** as the starting materials to form polymer **UCBZ-1**. BET specific surface areas of the products were evaluated by nitrogen adsorption/desorption isotherms of freshly activated samples at 77 K. We found reaction conditions have a drastic effect on the BET specific surface areas, ranging from 112 $m^2 \cdot g^{-1}$ to 980 $m^2 \cdot g^{-1}$. The optimum conditions require a mixture of 1, 4-dioxane and mesitylene (2:1 v/v) as the solvent, 6 M acetic acid (4 equiv.) as the catalyst, and 150 °C reaction temperature to form highly porous UCBZ-1. Under the optimized conditions, we also synthesized UCBZ- 2, 3, 4 from diamines 2-4, and aldehyde 6. UCBZ series were precipitated as orange or red solids and collected by vacuum filtration after successive washing with acetone and dichloromethane in good yields (74-92 %) (**Scheme 4.1**). The polymers were characterized by FT-IR and solid-state ^{13}C-NMR, TGA and SEM. The FT-IR spectra of the UCBZ-1, 2, 3, 4 show the characteristic N=N stretching band around 1451 cm^{-1}, indicating the azobenzene group is stable and retained in the frameworks during the solvothermal reactions. The C=O stretch of the

starting trialdehyde shifted from ~1658 cm^{-1} to ~1623 cm^{-1}, which corresponds to the characteristic stretch of β-keto-enamine (**Figure 4.12**). The solid-state ^{13}C cross polarization magic angle spinning (CP-MAS) NMR spectra showed the resonance signals around 149 ppm and 185 ppm, which correspond to the enamine and ketone groups, respectively, thus further supporting the formation of β-keto-enamine linked structure (**Figures 4.20, 4.21, 4.22, and 4.23**). The polymers (UCBZ-1, 2, 3, and 5) show some crystallinity with similar powder X-ray diffraction (PXRD) patterns (**Figures 4.13 and 4.14**). However, due to the low crystallinity, the structure simulations of the polymers were not successful. UCBZ-4 seems more disordered, showing no obvious diffraction peaks. All the materials are insoluble in common organic solvents such as dichloromethane, acetone, ethanol, THF and DMF. Thermal gravimetric analyses (TGA) show all the materials have good stability and do not decompose until 400 °C (**Figure 4.11**).

Table 4.1. The summary of synthetic conditions for UCBZ-**1** and the resulting BET specific surface areas. Diamine **1** (0.15 mmol) and aldehyde **6** (0.10 mmol) were used.

Entry	**Solvents (mL)**			**6 M HOAc (mL)**	**T (°C)**	**SA_{BET} ($m^2 \cdot g^{-1}$)**
	1,4-dioxane	Mesitylene	DMA			
1	3	3	0	0.2	150	867
2	4	2	0	0.3	150	699
3	4	3	0	0.2	120	565
4	5	2	0	0.4	120	577
5	**4**	**2**	**0**	**0.2**	**150**	**980**
6	3	3	0	0.3	150	917
7	0	0	3	0.3	100	278
8	0	3	0	0.3	100	112

9	3	0	0	0.3	120	128
10	2	2	0	0.2	150	659

Table 4.2. The summary of porosity properties of UCBZ series.

Polymer	**SA_{BET}** **$(m^2 \cdot g^{-1})^a$**	**SA_{Lang}** **$(m^2 \cdot g^{-1})^b$**	**V_{Total}** **$(cm^3 \cdot g^{-1})^c$**
UCBZ-1	980	1458	1.46
UCBZ-2	1017	1531	1.49
UCBZ-3	1014	1429	1.06
UCBZ-4	733	1104	0.87
UCBZ-5	1104	1675	1.56

[a)]Surface area ($m^2 \cdot g^{-1}$) was calculated from the nitrogen adsorption isotherms based on the BET model (P/P_0 = 0.01-0.12). [b)]Surface area ($m^2 \cdot g^{-1}$) was calculated from the nitrogen adsorption isotherms based on the Langmuir model (P/P_0 = 0.20-0.30). [c)]The total pore volume ($cm^3 \cdot g^{-1}$) was calculated at P/P_0 = 0.99.

The permanent porosities of UCBZ series were evaluated by the N_2 adsorption/desorption isotherms of the freshly activated samples at 77 K, and their pore size distributions were calculated by employing non-local density functional theory (NLDFT) (**Table 4.2**). As shown in **Figure 4.3a**, all the polymers exhibit typical type I nitrogen adsorption isotherms and BET surface areas ranging from 700 to 1000 $m^2 \cdot g^{-1}$. UCBZ-4 with two azobenzene pendent groups on the backbone exhibits a significantly lower surface area compared to other polymers. The pore size distributions of the polymers are similar, showing majority micropores in the range of around 14 Å to 17 Å and some mesopores. While the BET surface areas do not change much after UV irradiation, the ratio of larger pores (size ~17 Å) are considerably increased

compared to the smaller ones (size ~14 Å), which is consistent with the observation in the case of a MOF containing azobenzene pendent groups pointing into the pores.[7]

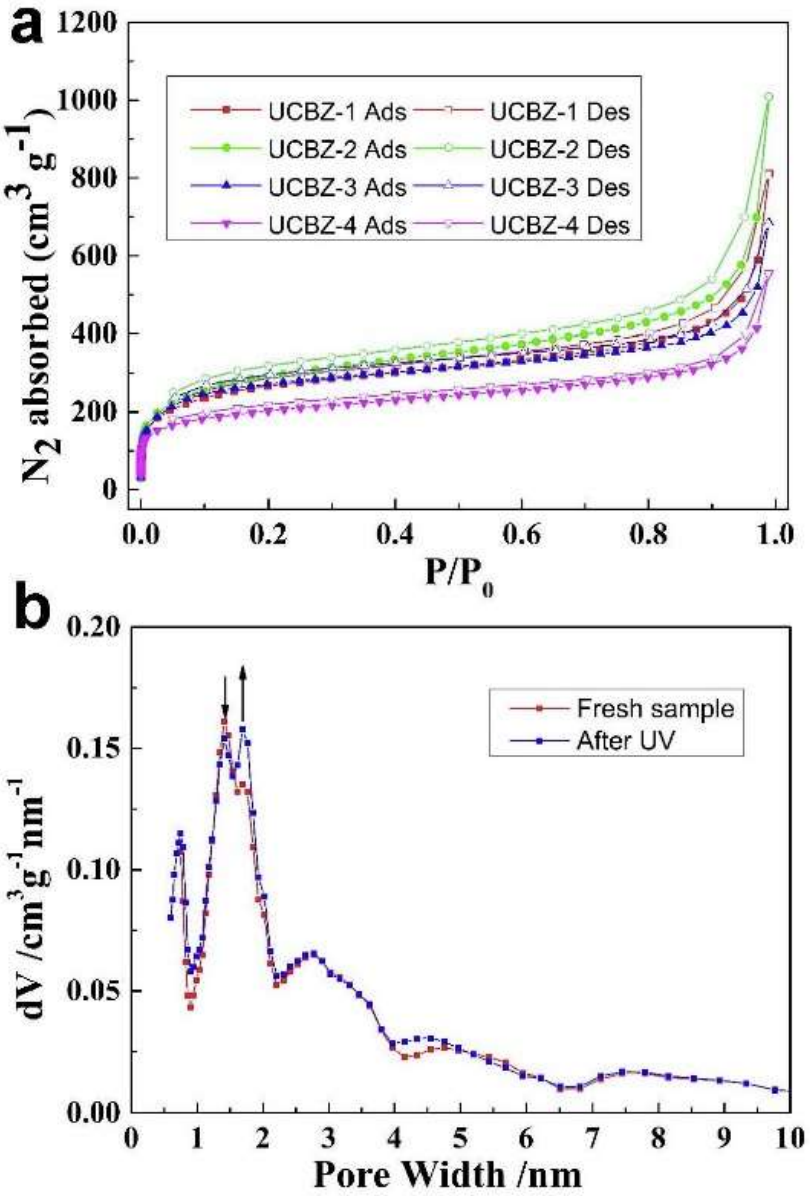

Figure 4.3. (a) Nitrogen adsorption and desorption isotherms for UCBZ series at 77 K. (b) Pore size distribution of UCBZ-4 sample, freshly activated (red) and after UV irradiation (blue).

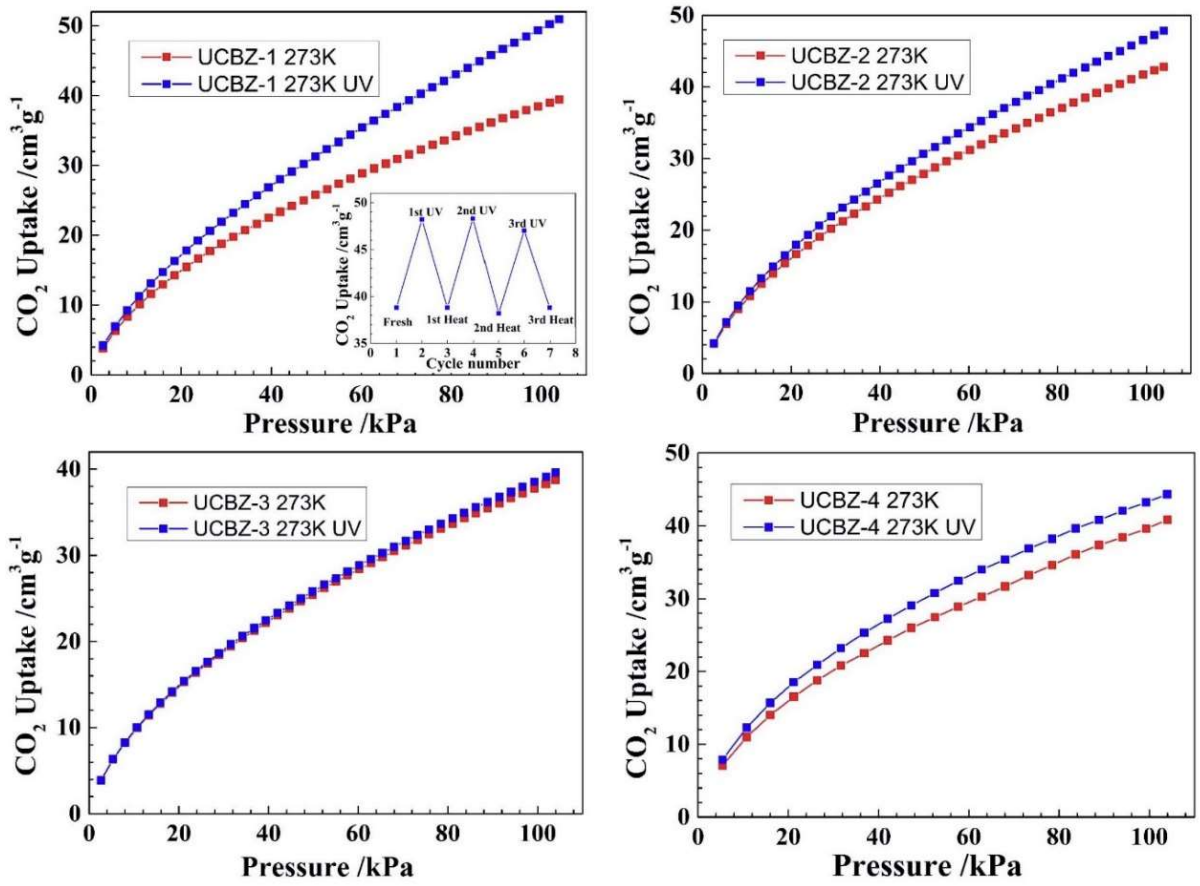

Figure 4.4. CO_2 adsorption isotherms for UCBZ-1-4 of fresh sample and after UV irradiation and reversibility of UCBZ-1 after several cycles of UV and heat treatment.

It is generally accepted that *trans/cis* isomerization of azobenzenes leads to significant geometrical as well as dipole changes. We envisioned that the enhanced polarity of the pore surface upon the conversion of *trans*-azobenzene to *cis*-azobenzene would promote the dipole-quadrupole interaction between the pore surface and CO_2 molecules, and hence increase the uptake of CO_2.[48] As expected, we observed the increase of CO_2 uptake upon UV irradiation of UCBZ series. A freshly activated sample of UCBZ-1 showed a CO_2 adsorption capacity of 39 $cm^3 \cdot g^{-1}$ at 273 K and 1 atm. In contrast, after the UV irradiation for 9 minutes, the CO_2 uptake was increased to 50 $cm^3 \cdot g^{-1}$ under the same conditions, which corresponds to a 29% increase (**Figure 4.4a**). It appears that a bulky substituent on the azobenzene moiety has a negative effect on the photo-responsiveness of the frameworks. Although the surface areas of UCBZ-**2** and UCBZ-**3** containing azobenzenes substituted with bulkier alkyl groups are comparable to that of UCBZ-**1**, they show only 12% and 2% increase of the CO_2 adsorption capacity, respectively. Presumably, the steric hindrance at the *para*-position of azobenzenes suppress the isomerization, especially within a confined space in the solid sample. UCBZ-**4** functionalized with two azobenzene groups also shows much less increase of CO_2 uptake (9% increase) after UV irradiation, likely due to the steric hindrance and/or low quantum yield of photoisomerization caused by the high density of azobenzene moieties inside the pore. Importantly, the photoresponsive behaviors of these POP materials are fully reversible. We did not observe any decay of the responsiveness during the repetitive UV irradiation and thermal regeneration. After multiple cycles of alternating external stimuli, the polymers still exhibit the similar adsorption properties, indicating the robustness and the high switchability of their pore structures (**Figure 4.4**).

It is interesting to note that although the changes in the pore size distribution (PSD) of UCBZ polymers are similar to the previously reported MOFs containing an organic linker substituted with

azobenzene groups,[7] the changes in CO_2 adsorption capacity are inverse. We observed the increase of CO_2 adsorption upon the conversion of *trans*-isomer to *cis*-isomer, while the decrease of CO_2 adsorption was observed for the MOFs.[7] It is reported that the phenyl ring of *cis*-azobenzene partially blocks the metal-oxygen center, which is the major CO_2 adsorption site. It is unclear whether the *cis*-azobenzene of UCBZ polymers blocks the keto-enamine groups, which also have favorable interaction with CO_2 and promote its adsorption. In the present case, we believe the increase of surface polarity induced by *trans*→*cis* isomerization is the major reason for the increase of the CO_2 adsorption after the UV irradiation.

In order to further confirm the azobenzene moiety indeed plays a critical role in tuning the pore size distribution and CO_2 adsorption upon UV irradiation or thermal treatment, we tested the responsiveness of UCBZ-5 without the azobenzene moiety. UCBZ-5 was prepared under the same synthetic condition with entry 5 in **Table 4.1**. It exhibits a BET surface area of 1104 $m^2 \cdot g^{-1}$ and total pore volume of 1.56 $cm^3 \cdot g^{-1}$, which are comparable to those of photoresponsive UCBZ series. The color of UCBZ-5 is light yellow instead of orange or red due to the absence of azobenzene moieties. As expected, UCBZ-5 does not exhibit a responsive character, showing almost identical CO_2 uptake and pore size distribution before and after UV irradiation at 273 K and 1 atm. These results clearly demonstrate that the azobenzene groups are responsible for the changes in the gas adsorption property in UCBZ polymers under photo or thermal stimuli.

4.4 Conclusion

In conclusion, we have successfully prepared stimuli responsive porous organic polymers whose pore size distribution and gas (e.g. CO_2) adsorption properties can be reversibly altered for multiple cycles under UV or thermal treatment. Structure-property relationship study shows that

bulky substituents on azobenzene moieties diminish the extent of responsiveness. The control experiment using an analogous porous polymer without azobenzene groups indicates the *cis*/*trans* isomerization of the azobenzene groups enables the responsiveness of the materials. Although similar azobenzene containing MOFs show decreased CO_2 uptake upon *trans*→*cis* isomerization, the UCBZ series show significant increase of CO_2 adsorption (up to 29%), which likely results from the increase of pore surface polarity caused by more polar *cis*-azobenzene groups. Our work demonstrates the first example of photoresponsive porous organic polymers, which has good stability and reversibility. Incorporation of stimuli-responsive units into the host organic frameworks would create a new class of porous polymers having intriguing stimuli-responsive properties targeting various applications, which could complement responsive metal organic frameworks reported thus far.

4.5 Experimental section

4.5.1. Materials and measurements

All chemical reagents were commercially available and used without further purification unless otherwise indicated. 2, 5-Dibromoaniline[49,50], and 1, 3, 5-triformylphloroglucinol[51] were synthesized following the published procedures. 4-Methylnitrosobenzene, and 4-tertbutylnitrosobenzene were also prepared according to the published procedures.[52]

Flash column chromatography was performed by using a 100-150 times the weight excess of flash silica gel 32-63 μm from Dynamic Absorbants Inc. Fractions were analyzed by TLC using TLC silica gel F254 250 μm precoated-plates from Dynamic Absorbants Inc.

NMR spectra were taken using Inova 400 and Inova 500 spectrometers. Solid-state cross polarization magic angle spinning (CP-MAS) NMR spectra were recorded on an Inova 400 NMR spectrometer.

Powder X-Ray Diffraction (PXRD) was obtained from a Bruker D-8 Discover diffractometer, using monochromated Cu K_α (λ = 1.542 Å) radiation.

The FT-IR spectra of starting materials and as synthesized UCBZ series were obtained from Thermo Nicolet Avatar-370 spectrometer using KBr (IR grade) pellets.

Elemental analysis was taken at an Exeter Analytical-Model CE 440 CHN Analyzer, microanalysis laboratory, University of Illinois at Urbana-Champaign.

Thermogravimetric analyses (TGA) were performed on a thermogravimetric/differential thermal analyzer by heating the samples at 10 °C min^{-1} to 600 °C under the atmosphere of nitrogen.

The Quantachrome Autosorb ASiQ automated gas sorption analyzer was used to measure N_2 and CO_2 adsorption isotherms. The sample was heated at 100 °C and kept at this temperature for at least 22 hours for the activation. Ultra high purity grade (99.999 % purity) N_2, CO_2 and He, oil-free valves and gas regulators were used for all free space corrections and measurements. For all of the gas adsorption measurements, the temperatures were controlled by using a refrigerated bath of liquid N_2 (77 K), ice water (273 K).

Scanning Electron Microscopy images (SEM) were recorded using a JSM-6480LV (LVSEM) at 5.0 kV. Samples were sputter coated with gold prior to analysis.

For the UV sources, a universal lamp supply-250 watts (model 1152/1144) was used for the diamines photoisomerization; a Hanovia mercury lamp (Model: 679A36, 450 watts) was used for the polymer photoisomerization; UV-Vis adsorption spectra of the diamines were collected in a 1 cm path length quartz cuvette by using an Agilent 8453 spectrophotometer equipped with tungsten and deuterium lamps.

4.5.2. General synthetic procedures

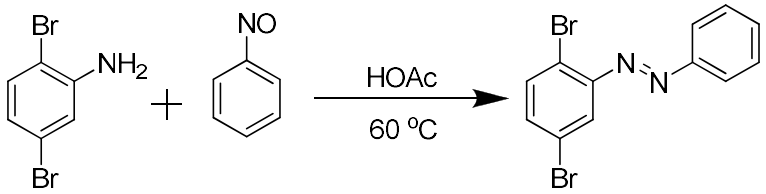

Synthesis of 1-(2,5-dibromophenyl)-2-phenyldiazene: A 100 mL Schlenk tube was charged with 2, 5-dibromoaniline (1.20 g, 4.8 mmol) and nitrosobenzene (0.90 g, 8.4 mmol). Acetic acid (15 mL) was added to this tube, and the resulting mixture was degassed and stirred at 90 °C for 36 hours. It was then cooled to room temperature, and acetic acid was neutralized by saturated sodium bicarbonate (Na_2CO_3) solution. The aqueous layer was extracted with dichloromethane (2 x 60 mL). The combined organic layer was dried over anhydrous sodium sulfate (Na_2SO_4), and the volatiles were removed under reduced pressure. The residue was purified by flash chromatography column (gradient elution, hexanes → 20% CH_2Cl_2/hexane) to yield the pure product as an orange solid (0.82 g, 51%): ^{1}H-NMR (500 MHz, $CDCl_3$) δ 8.01-7.99 (m, 2H), 7.84 (d, 1H, J = 2.5 Hz), 7.64 (d, 1H, J = 8.5 Hz), 7.58-7.54 (m, 3H), 7.45 (q, 1H, J_1 = 2.5 Hz, J_2 = 8.5 Hz); ^{13}C-NMR (100 MHz, $CDCl_3$): δ 152.3, 150.0, 134.8, 134.4, 132.1, 129.2, 124.4, 123.6, 122.0, 121.0; HR-MS (ESI) calcd. for $C_{12}H_8N_2Br_2$ ($[M+H]^+$): 340.9112. Found: 340.9107.

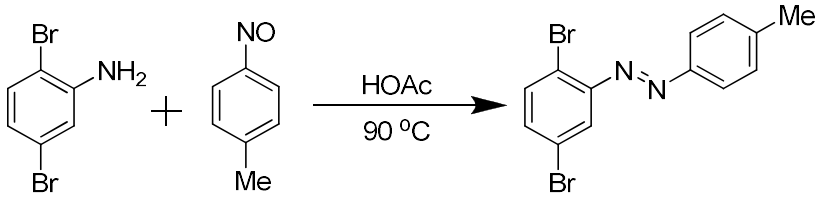

Synthesis of 1-(2, 5-dibromophenyl)-2-*p*-tolyldiazene: A 100 mL Schlenk tube was charged with 2, 5-dibromoaniline (0.82 g, 2.9 mmol) and 4-methylnitrosobenzene (0.82 g, 6.8 mmol). Acetic acid (10 mL) was added to this tube, and the resulting mixture was degassed and stirred at 90 °C for 36 hours. It was then cooled to room temperature, and acetic acid was neutralized by

saturated sodium bicarbonate solution. The aqueous layer was extracted with dichloromethane (2 x 60 mL), and the combined organic layer was dried over anhydrous sodium sulfate. The solvent was removed under reduced pressure and the residue was purified by flash chromatography column (10% dichloromethane in hexanes as the eluent) to yield the pure product as an orange solid (0.24 g, 21 %): ^{1}H-NMR (500 MHz, $CDCl_3$) δ 7.91 (d, 2H, J = 8.0 Hz), 7.83 (d, 1H, J = 2.5 Hz), 7.62 (d, 1H, J = 8.5 Hz), 7.43 (q, 1H, J_1 = 2.5 Hz, J_2 = 8.5 Hz), 7.35 (d, 2H, J = 8.0 Hz), 2.47 (s, 3H); ^{13}C-NMR (100 MHz, $CDCl_3$): δ 150.5, 150.2, 143.0, 134.8, 134.0, 129.9, 124.1, 123.6, 122.0, 121.0, 21.6; HR-MS (ESI) calcd. for $C_{13}H_{10}N_2Br_2$ ($[M+H]^+$): 354.9269. Found: 354.9274.

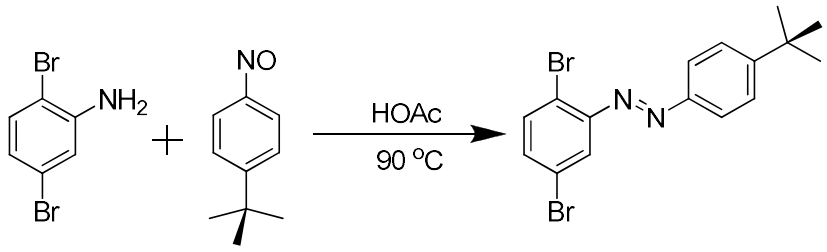

Synthesis of 4-tert-butylphenyl-1-(2,5-dibromophenyl)diazene: A 100 mL Schlenk tube was charged with 2, 5-dibromoaniline (0.73 g, 2.9 mmol) and 4-*tert*-butylnitrosobenzene (0.62 g, 3.8 mmol). Acetic acid (10 mL) and chloroform (10 mL) were added to this tube, and the resulting mixture was degassed and stirred at 90 °C for 36 hours. It was then cooled to room temperature, and acetic acid was neutralized by saturated sodium bicarbonate solution. The aqueous layer was extracted with dichloromethane (2 x 60 mL), and the combined organic layer was dried over anhydrous sodium sulfate. The solvent was removed under reduced pressure and the residue was purified by flash chromatography column (first hexanes then 10 % dichloromethane in hexanes as the eluent) to yield the pure product as an orange solid (0.37 g, 28 %): ^{1}H-NMR (500 MHz, $CDCl_3$) δ 7.94 (d, 2H, J = 9.0 Hz), 7.82 (d, 1H, J = 2.5 Hz), 7.62 (d, 1H, J = 8.5 Hz), 7.57 (d, 2H, J = 8.5 Hz), 7.43 (q, 1H, J_1 = 2.5 Hz, J_2 = 8.5 Hz), 1.40 (s, 9H); ^{13}C-NMR (100 MHz, $CDCl_3$): δ 155.9,

150.4, 150.2, 134.8, 134.0, 126.2, 124.1, 123.4, 122.0, 121.0, 35.1, 31.2; HR-MS (ESI) calcd. for $C_{16}H_{16}N_2Br_2$ ($[M+H]^+$): 396.9739. Found: 396.9738.

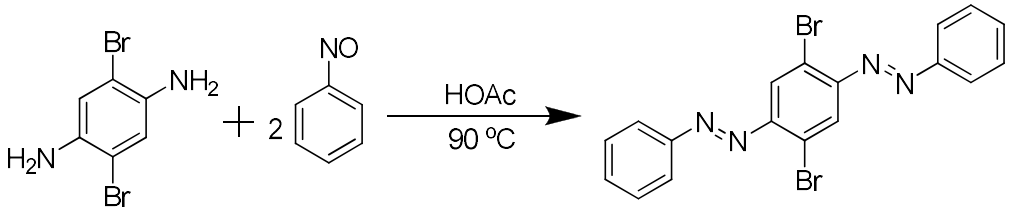

Synthesis of (1,1')-2,2'-(2,5-dibromo-1,4-phenylene)bis(1-phenyldiazene): A 100 mL Schlenk tube was charged with 2, 5-dibromo-4-aminoaniline (0.82 g, 3.1 mmol) and nitrosobenzene (1.32 g, 12.3 mmol). Acetic acid (10 mL) and chloroform (10 mL) was added to this tube, and the resulting mixture was degassed and stirred at 90 °C for 36 hours. It was then cooled to room temperature, and acetic acid was neutralized by saturated sodium bicarbonate solution. The aqueous layer was extracted with dichloromethane (2 x 60 mL), and the combined organic layer was dried over anhydrous sodium sulfate. The solvent was removed under reduced pressure and the residue was purified by flash chromatography column (gradient elution, hexanes→10 % dichloromethane in hexanes) to yield the pure product as a dark orange solid (0.11 g, 9 %): ^{1}H-NMR (500 MHz, $CDCl_3$) δ 8.11 (s, 2H), 8.04-8.06 (m, 4H,), 7.57-7.59 (m, 6H); ^{13}C-NMR (100 MHz, $CDCl_3$): δ 152.5, 150.3, 132.4, 129.3, 125.1, 123.8, 122.4; HR-MS (ESI) calcd. for $C_{18}H_{12}N_4Br_2$ ($[M+H]^+$): 444.9487. Found: 444.9488.

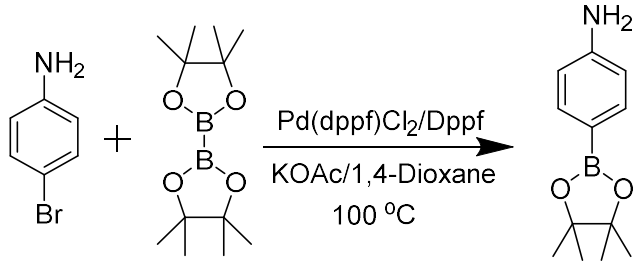

Synthesis of 4-(4,4,5,5-tetramethyl-1,3,2-dioxaborolan-2-yl)aniline: A 100 mL Schlenk tube was charged with 4-bromoaniline (1.72 g, 10.0 mmol), bis(pinacolato)diboron (3.05 g, 12.0 mmol) and potassium acetate (3.00 g, 30.6 mmol). To this mixture, catalyst [1, 1′-Bis(diphenylphosphino)ferrocene]dichloropalladium ($PdCl_2dppf$) (210 mg, 0.29 mmol) and ligand 1,1'-Bis(diphenylphosphino)ferrocene (dppf) (160 mg, 0.30 mmol) were added, followed by anhydrous 1, 4-dioxane (50 mL). The resulting solution was degassed three times and stirred at 100 °C for 2 days. After cooled to room temperature, water (150 mL) was added. The aqueous layer was extracted with dichloromethane (2 x 150 mL), and the combined organic layer was dried over anhydrous sodium sulfate. The solvent was removed under reduced pressure, and the residue was purified by flash chromatography column (gradient elution, dichloromethane→10 % ethyl acetate in dichloromethane). After removing a small amount of the bis(pinacolato)diboron contaminant by washing with a mixture of methanol/hexanes, the pure product was obtained as a white solid (1.44 g, 66 %): ^{1}H-NMR (500 MHz, $CDCl_3$) δ 7.62 (d, 2H, J = 8.5 Hz), 6.66 (d, 2H, J = 8.5 Hz), 3.86 (s, 2H), 1.33 (s, 12H); ^{13}C-NMR (100 MHz, $CDCl_3$): δ 149.3, 136.4, 114.0, 83.3, 24.8. The NMR data is consistent with the literature report.[53]

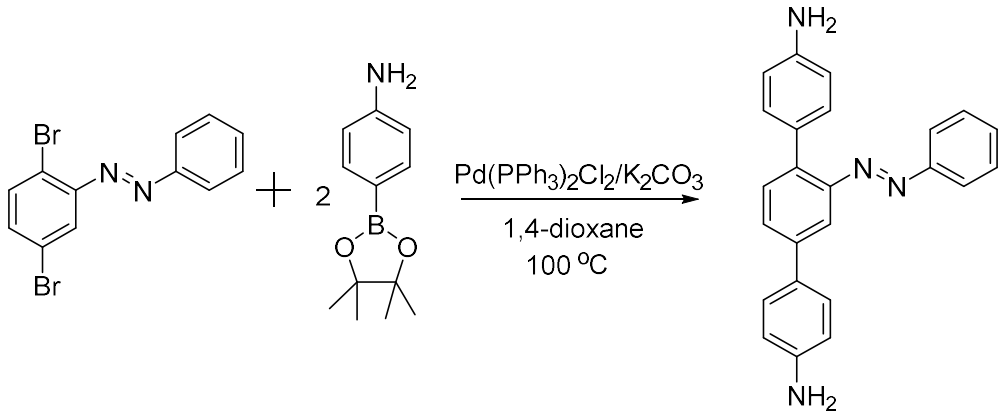

diamine **1**

Synthesis of diamine 1: A 100 mL Schlenk tube was charged with 2,5-dibromophenyl-2-phenyldiazene (340 mg, 1.0 mmol) and 4-(4,4,5,5-tetramethyl-1,3,2-dioxaborolan-2-yl)aniline (550 mg, 2.6 mmol). The catalyst $Pd(PPh_3)_2Cl_2$ (180 mg, 0.2 mmol) and K_2CO_3 (400 mg) were added followed by 1, 4-dioxane (20 mL) and water (4 mL). The resulting mixture was stirred at 100 ˚C for 36 hours. After cooled to room temperature, water (50 mL) was added. The product was extracted with dichloromethane (2 x 50 mL), and the combined organic layer was dried over anhydrous sodium sulfate (Na_2SO_4). The volatiles were removed under reduced pressure, and the residue was purified by flash column chromatography (gradient elution, dichloromethane→10% ethyl acetate in dichloromethane) to yield the pure product as a red orange solid (215 mg, 59%): ^{1}H-NMR (500 MHz, $CDCl_3$) δ 7.90 (d, 1H, J = 2.0 Hz), 7.88 (d, 2H, J = 7.0 Hz), 7.72 (q, 1H, J_1 = 2.0 Hz, J_2 = 8.0 Hz), 7.61 (d, 1H, J = 8.0 Hz), 7.55 (d, 2H, J = 8.0 Hz), 7.49 (m, 3H), 7.33 (d, 2H, J = 8.5 Hz), 6.80 (t, 4H, J_1 = 8.0 Hz, J_2 = 8.0 Hz), 3.80 (s, 2H), 3.78 (s, 2H); ^{13}C-NMR (100 MHz, $CDCl_3$): δ 152.9, 149.7, 146.0, 145.7, 140.0, 138.9, 132.0, 130.75, 130.69, 130.6, 129.0, 128.8, 128.6, 128.0, 123.3, 115.4, 114.4, 113.4; HR-MS (ESI) calcd. for $C_{24}H_{20}N_4$ ($[M+H]^+$): 365.1766. Found: 365.1769.

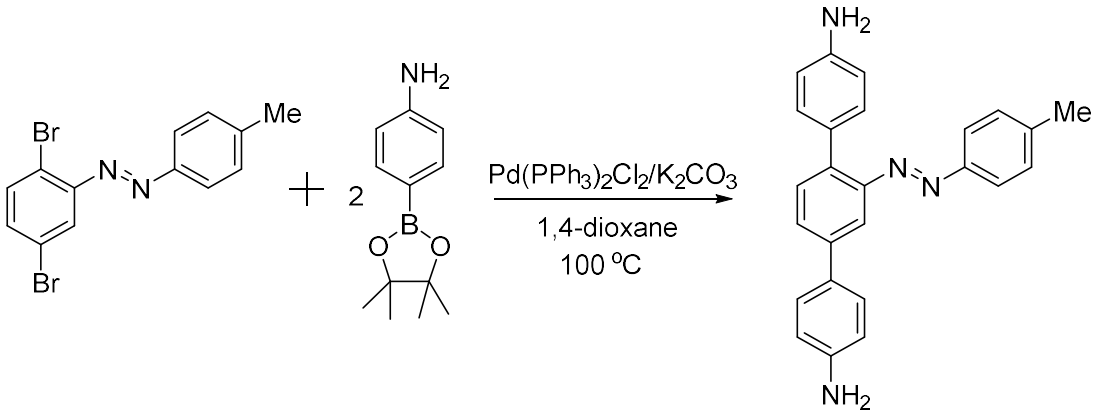

diamine **2**

Synthesis of diamine 2: A 100 mL Schlenk tube was charged with 2,5-dibromophenyl-2-*p*-tolyldiazene (240 mg, 0.68 mmol) and 4-(4,4,5,5-tetramethyl-1,3,2-dioxaborolan-2-yl)aniline (590 mg, 2.7 mmol). The catalyst $Pd(PPh_3)_2Cl_2$ (130 mg, 0.14 mmol) and K_2CO_3 (300 mg, 2.2 mmol) were added followed by 1, 4-dioxane (15 mL) and water (3 mL). The resulting mixture was stirred at 100 ˚C for 36 hours, and then cooled to room temperature. Water (50 mL) was added and the mixture was extracted with dichloromethane (2 x 50 mL). The combined organic layer was dried over anhydrous sodium sulfate (Na_2SO_4), and concentrated under reduced pressure. The residue was purified by flash column chromatography (gradient elution, dichloromethane→10 % ethyl acetate in dichloromethane) to yield the pure compound as a red orange solid (160 mg, 62 %): ^{1}H-NMR (500 MHz, $CDCl_3$) δ 7.86 (d, 1H, J = 1.5 Hz), 7.76 (d, 2H, J = 8.5 Hz), 7.69 (q, 1H, J_1 = 2.0 Hz, J_2 = 8.0 Hz), 7.59 (d, 1H, J = 8.0 Hz), 7.53 (d, 2H, J = 8.5 Hz), 7.31 (d, 2H, J = 8.5 Hz), 7.28 (d, 2H, J = 8.0 Hz), 6.78 (d, 2H, J = 8.5 Hz), 6.76 (d, 2H, J = 8.5 Hz), 3.76 (s, 4H), 2.42 (s, 3H); ^{13}C-NMR (100 MHz, $CDCl_3$): δ 151.0, 149.7, 145.9, 145.6, 141.1, 139.9, 138.5, 136.3, 131.9, 130.6, 129.6, 128.8, 128.2, 127.9, 123.2, 115.3, 114.3, 113.3, 21.4; HR-MS (ESI) calcd. for $C_{25}H_{22}N_4$ ($[M+H]^+$): 379.1923. Found: 379.1922.

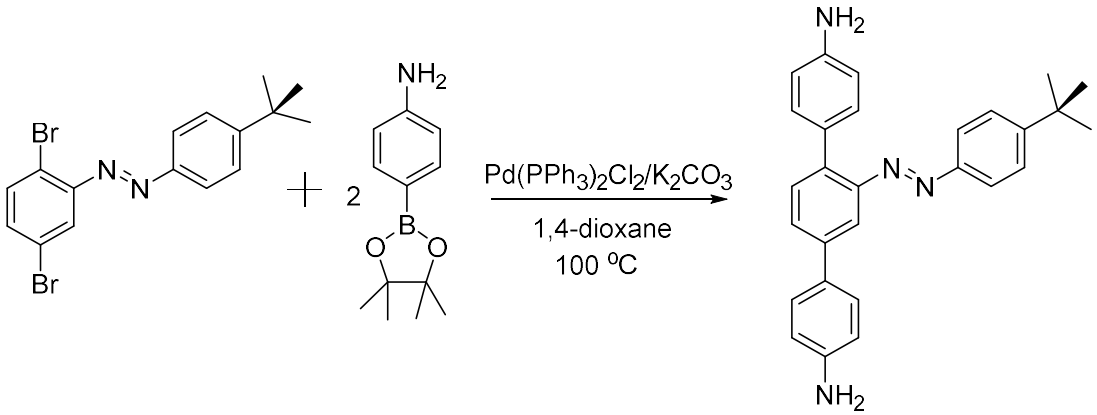

diamine **3**

Synthesis of diamine 3: A 100 mL Schlenk tube was charged with 4-tert-butylphenyl-2-(2,5-dibromophenyl)diazene (500 mg, 1.3 mmol) and 4-(4,4,5,5-tetramethyl-1,3,2-dioxaborolan-2-yl)aniline (740 mg, 3.4 mmol). The catalyst $Pd(PPh_3)_2Cl_2$ (200 mg, 0.22 mmol) and K_2CO_3 (480 mg, 3.5 mmol) were added, followed by 1, 4-dioxane (24 mL) and water (5 mL). The resulting mixture was stirred at 100 ˚C for 36 hours, and cooled to room temperature. Water (50 mL) was added and the mixture was extracted with dichloromethane (2 x 50 mL). The combined organic layer was dried over anhydrous sodium sulfate, and the volatiles were removed under reduced pressure. The residue was purified by flash column chromatography (gradient elution, dichloromethane→10% ethyl acetate in dichloromethane) to yield the pure product as a red orange solid (160 mg, 30%): ^{1}H-NMR (500 MHz, $CDCl_3$) δ 7.87 (d, 1H, J = 2.0 Hz), 7.82 (d, 2H, J = 8.5 Hz), 7.70 (q, 1H, J_1 = 2.0 Hz, J_2 = 8.0 Hz), 7.61 (d, 1H, J = 8.0 Hz), 7.55 (d, 2H, J = 8.5 Hz), 7.52 (d, 2H, J = 8.5 Hz), 7.33 (d, 2H, J = 8.5 Hz), 6.81 (d, 2H, J = 8.5 Hz), 6.78 (d, 2H, J = 8.5 Hz), 3.78 (d, 4H); ^{13}C-NMR (100 MHz, $CDCl_3$): δ 154.2, 150.9, 149.9, 146.0, 145.6, 140.0, 138.6, 132.0, 130.7, 128.8, 128.3, 128.0, 125.9, 125.3, 123.0, 115.3, 114.4, 113.4, 35.0, 31.3; HR-MS (ESI) calcd. for $C_{28}H_{28}N_4$ ([M+H]$^+$): 421.2392. Found: 421.2381.

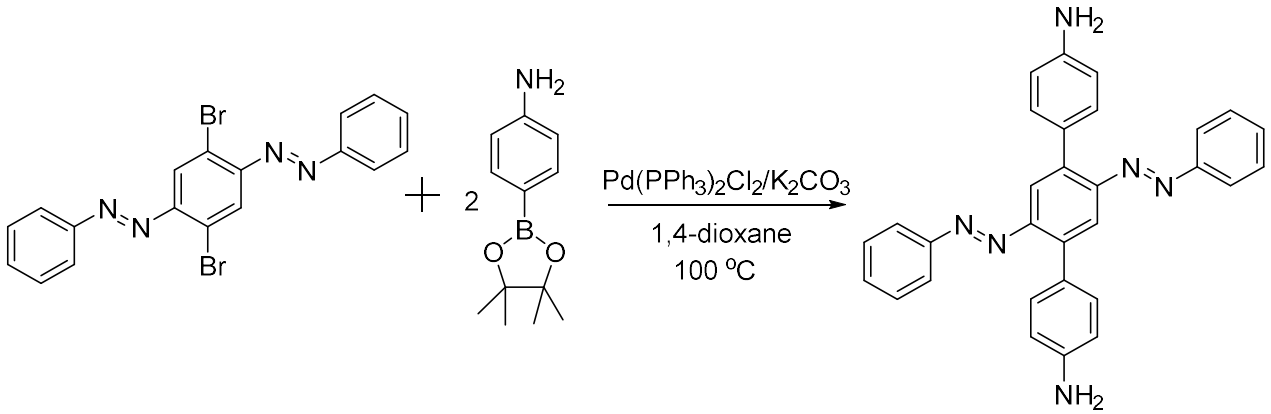

diamine **4**

Synthesis of diamine 4: A 100 mL Schlenk tube was charged with 2,2'-(2,5-dibromo-1,4-phenylene)bis(1-phenyldiazene) (150 mg, 0.34 mmol) and 4-(4,4,5,5-tetramethyl-1,3,2-dioxaborolan-2-yl)aniline (280 mg, 1.3 mmol). The catalyst $Pd(PPh_3)_2Cl_2$ (70 mg, 0.08 mmol) and K_2CO_3 (150 mg, 1.1) were added followed by 1, 4-dioxane (8 mL) and water (1.5 mL). The resulting mixture was stirred at 100 °C for 36 hours, and cooled to room temperature. Water (50 mL) was added and the mixture was extracted with dichloromethane (2 x 50 mL). The combined organic layer was dried over anhydrous sodium sulfate and the volatiles were removed under reduced pressure. The residue was purified by flash column chromatography (gradient elution, dichloromethane→10% ethyl acetate in dichloromethane) to yield the pure product as a red orange solid (63 mg, 40%): ^{1}H-NMR (500 MHz, $CDCl_3$) δ 7.92 (s, 2H), 7.89 (d, 4H, *J*= 8.5 Hz), 7.50 (m, 6H), 7.39 (d, 4H, *J* = 8.0 Hz), 6.80 (d, 4H, *J* = 8.0 Hz), 3.82 (s, 4H); ^{13}C-NMR (100 MHz, DMSO-d_6): δ 152.9, 150.3, 149.1, 139.6, 132.0, 131.9, 130.0, 124.9, 123.3, 117.5, 113.8; HR-MS (ESI) calcd. for $C_{30}H_{24}N_6$ ($[M+H]^+$): 469.2141. Found: 469.2161.

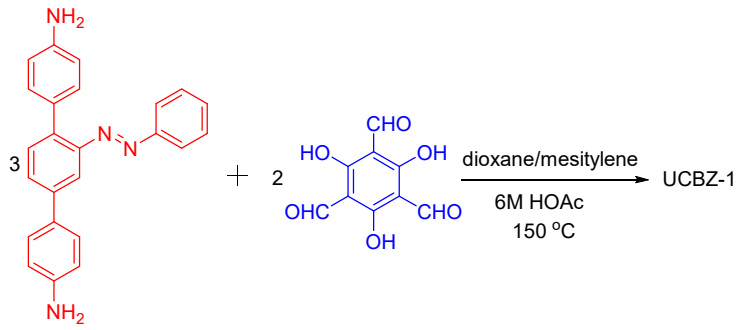

Synthesis of UCBZ-1: A customized glass tube (the outer diameter is 10 mm and the inner diameter is 8 mm) was charged with 1, 3, 5-triformylphloroglucinol (21 mg, 0.1 mmol), diamine **1** (54 mg, 0.15 mmol), 1,4-dioxane (4 mL), mesitylene (2 mL) and 6 M acetic acid (0.2 mL). The tube was flash frozen at 77 K in liquid nitrogen bath and evacuated to the internal pressure about 100 mtorr, and then the tube was sealed under the frame. The mixture was warmed to room

temperature, and the reaction temperature was slowly raised to 150 °C over 2 hours. The reaction was kept at this temperature for 3 days and cooled to room temperature over 12 hours. The orange precipitate was collected by vacuum filtration, washed with large amount of dichloromethane and acetone, and dried under vacuum to yield UCBZ-**1** (62 mg, 88 %): Elemental analysis calcd (%) for $(C_{28}H_{20}N_4O_4)_n$: C, 70.58; H, 4.23; N, 11.76. Found: C, 71.67; H, 4.02; N, 10.85. (Since the materials are polymers instead of pure compounds, their elemental analysis results are just used as a reference, not to determine their purity.)

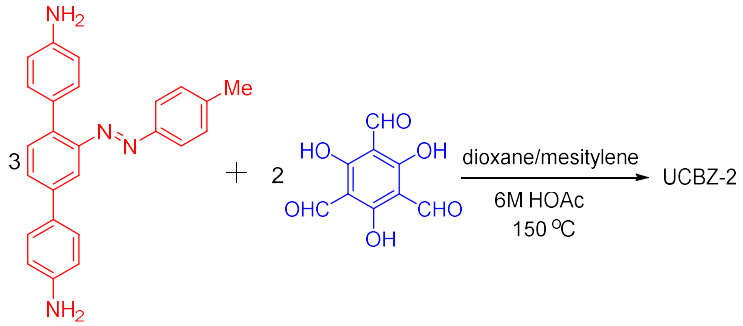

Synthesis of UCBZ-2: The above polymerization procedure for **UCBZ-1** was followed. Using 1, 3, 5-triformylphloroglucinol (21 mg, 0.1 mmol), diamine **2** (57 mg, 0.15 mmol), 1,4-dioxane (4 mL), mesitylene (2 mL), and 6 M acetic acid (0.2 mL), **UCBZ-2** was obtained as an orange precipitate (69 mg, 92 %): Elemental analysis calcd (%) for $(C_{29}H_{22}N_4O_4)_n$: C, 71.01; H, 4.52; N, 11.42. Found: C, 73.16; H, 4.03; N, 11.12. (Since the materials are polymers instead of pure compounds, their elemental analysis results are just used as a reference, not to determine their purity.)

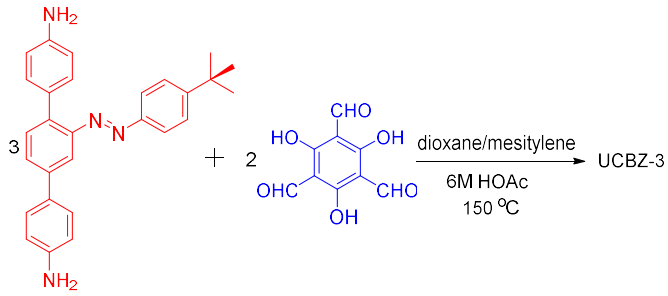

Synthesis of UCBZ-3: The above polymerization procedure for **UCBZ-1** was followed. Using 1, 3, 5-triformylphloroglucinol (21 mg, 0.1 mmol), diamine **3** (63 mg, 0.15 mmol), 1,4-dioxane (4 mL), mesitylene (2 mL), and 6 M acetic acid (0.2 mL), **UCBZ-3** was obtained as an orange precipitate (66 mg, 79 %): Elemental analysis calcd (%) for $(C_{32}H_{28}N_4O_4)_n$: C, 72.16; H, 5.30; N, 10.52. Found: C, 74.76; H, 5.11; N, 9.92. (Since the materials are polymers instead of pure compounds, their elemental analysis results are just used as a reference, not to determine their purity.)

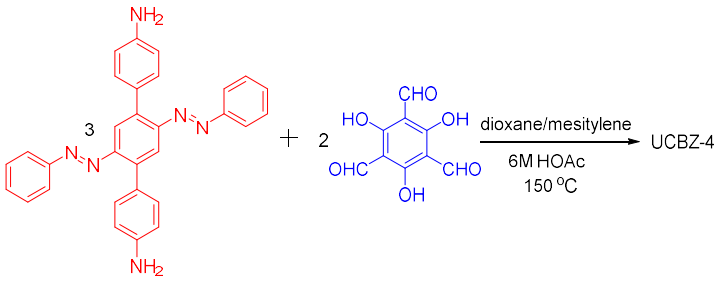

Synthesis of UCBZ-4: The above polymerization procedure for **UCBZ-1** was followed. Using 1, 3, 5-triformylphloroglucinol (18 mg, 0.086 mmol), diamine **4** (61 mg, 0.13 mmol), 1,4-dioxane (4 mL), mesitylene (2 mL), and 6 M acetic acid (0.2 mL), **UCBZ-4** was obtained as an orange precipitate (57 mg, 74%): Elemental analysis calcd (%) for $(C_{34}H_{24}N_6O_4)_n$: C, 70.29; H, 4.17; N, 14.48. Found: C, 68.91; H, 3.85; N, 11.30. (Since the materials are polymers instead of pure compounds, their elemental analysis results are just used as a reference, not to determine their purity.)

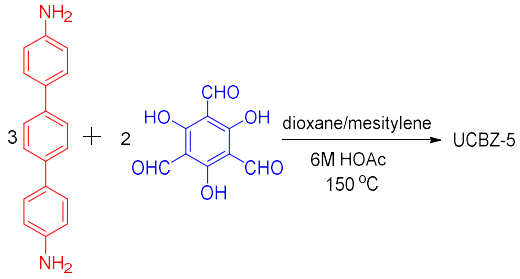

Synthesis of UCBZ-5: The above polymerization procedure for **UCBZ-1** was followed. Using 1, 3, 5-triformylphloroglucinol (21 mg, 0.1 mmol), 4, 4''-diamino-*p*-terphenyl (39 mg, 0.15 mmol), 1,4-dioxane (4 mL), mesitylene (2 mL), and 6 M acetic acid (0.2 mL), **UCBZ-5** was obtained as an orange precipitate (49 mg, 86%): Elemental analysis calcd (%) for $(C_{22}H_{16}N_2O_4)_n$: C, 70.96; H, 4.33; N, 7.52. Found: C, 75.75; H, 4.20; N, 7.48. (Since the materials are polymers instead of pure compounds, their elemental analysis results are just used as a reference, not to determine their purity.)

4.5.3. UV spectra of the azobenzene derivatives diamines

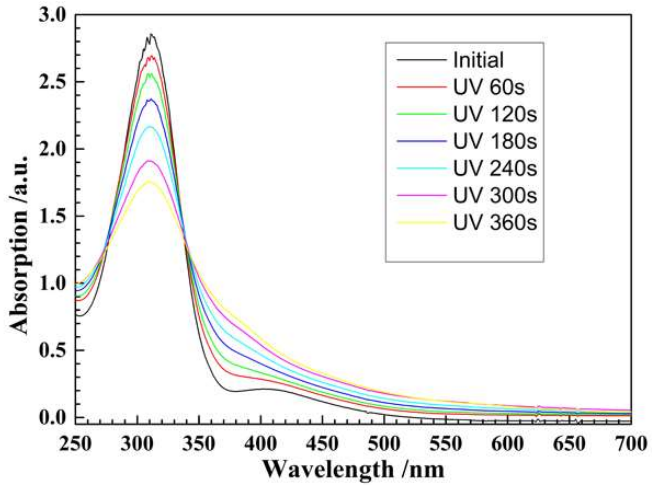

Figure 4.5. Changes in the adsorption spectra of diamine **1** in CH_2Cl_2 over the time during the irradiation with 320 nm light.

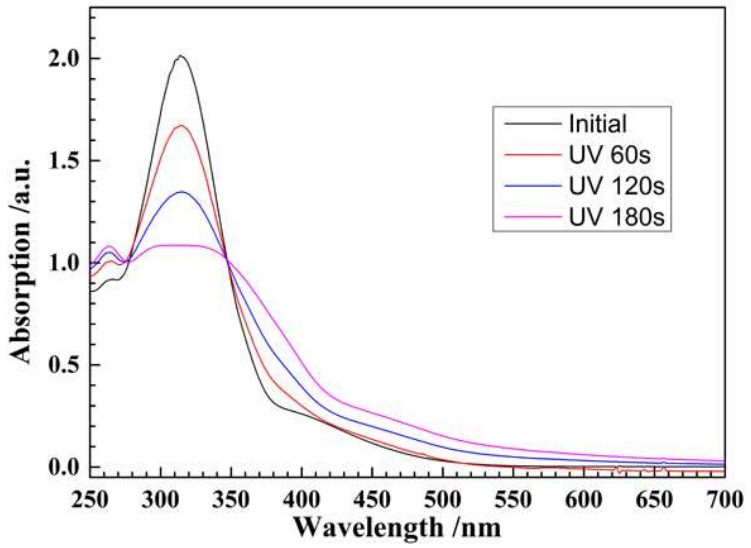

Figure 4.6. Changes in the adsorption spectrum of diamine **2** in dichloromethane over the time during the irradiation with 320 nm light.

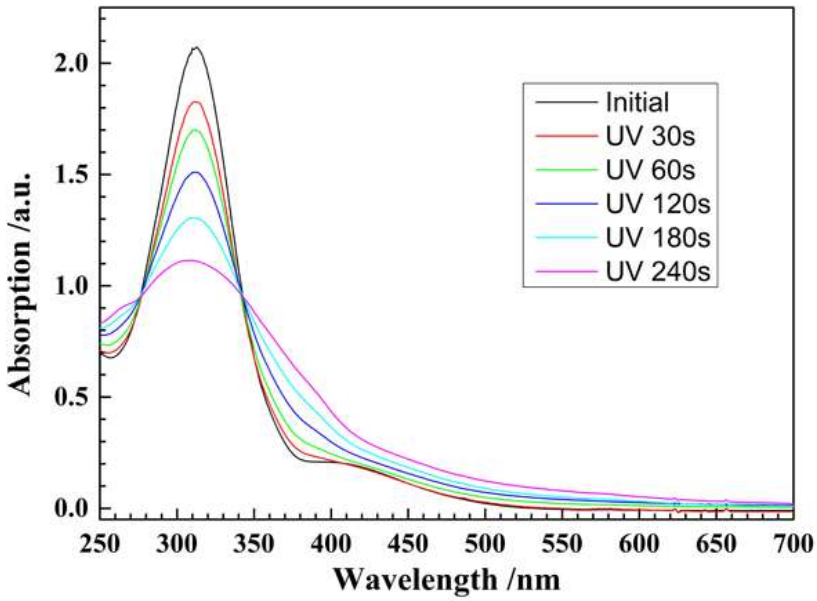

Figure 4.7. Changes in the adsorption spectrum of diamine **3** in dichloromethane over the time during the irradiation with 320 nm light.

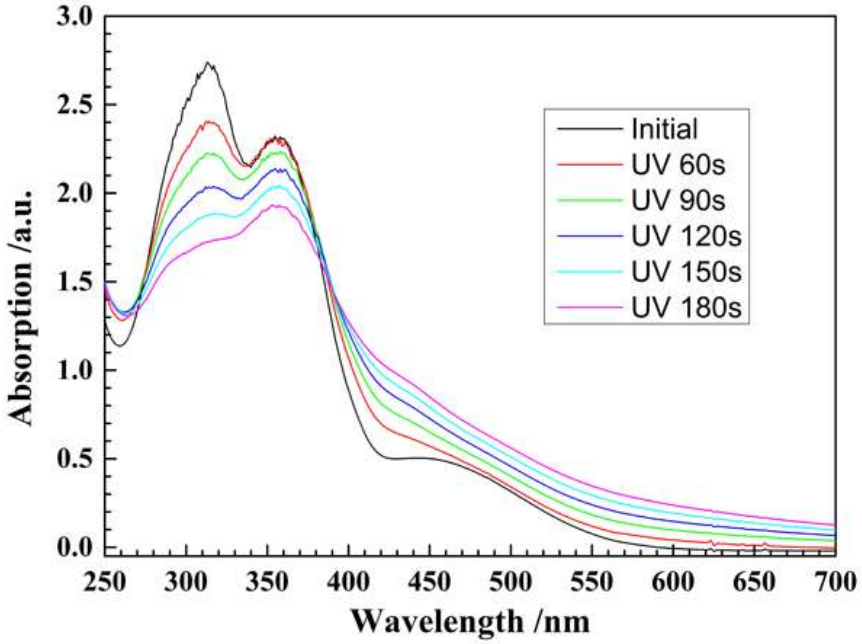

Figure 4.8. Changes in the adsorption spectrum of diamine **4** in dichloromethane over the time upon irradiation with 254 nm light.

4.5.4. NMR study of diamine 1

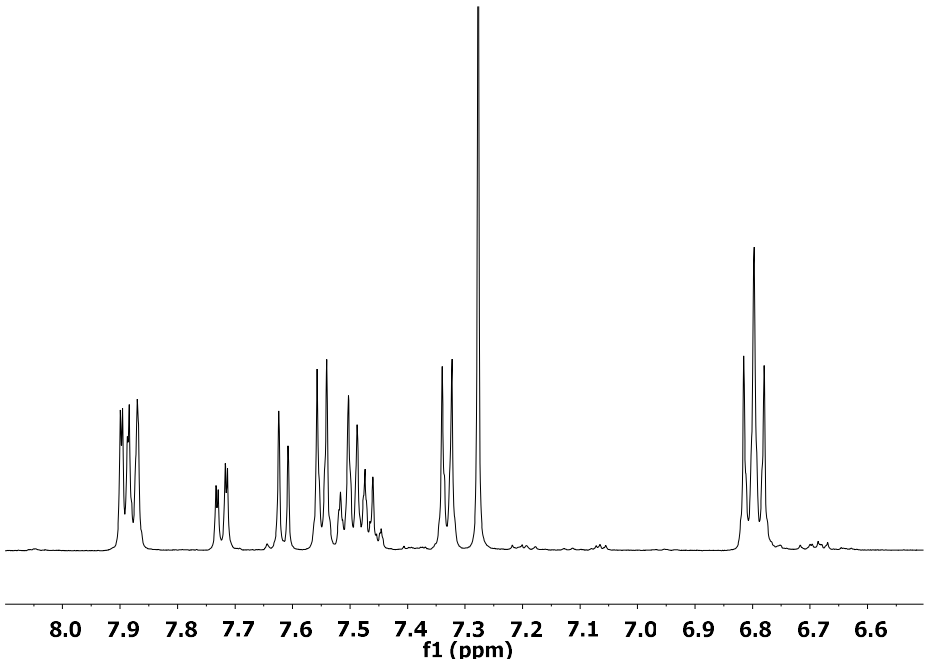

Figure 4.9. The ^{1}H NMR spectrum of as-synthesized diamine **1.**

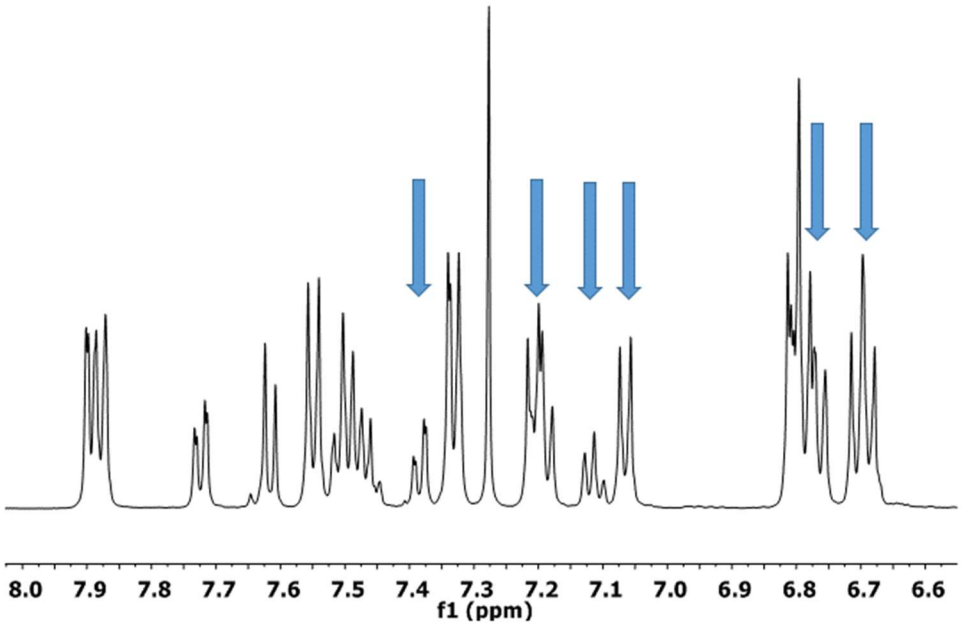

Figure 4.10. The ^{1}H NMR spectrum of diamine **1** after UV irradiation for 3 minutes.

4.5.5. TGA of UCBZ series

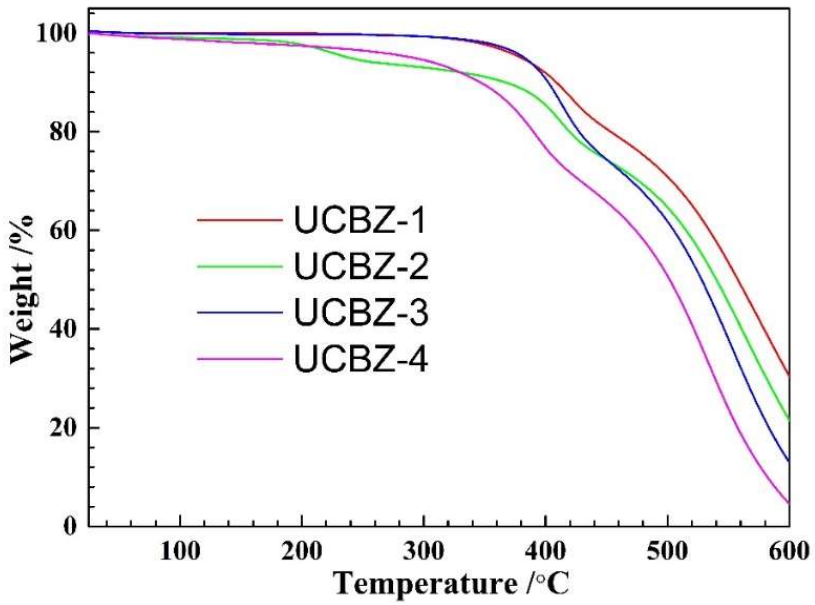

Figure 4.11. TGA curves of UCBZ series.

4.5.6. FT-IR of the UCBZ series

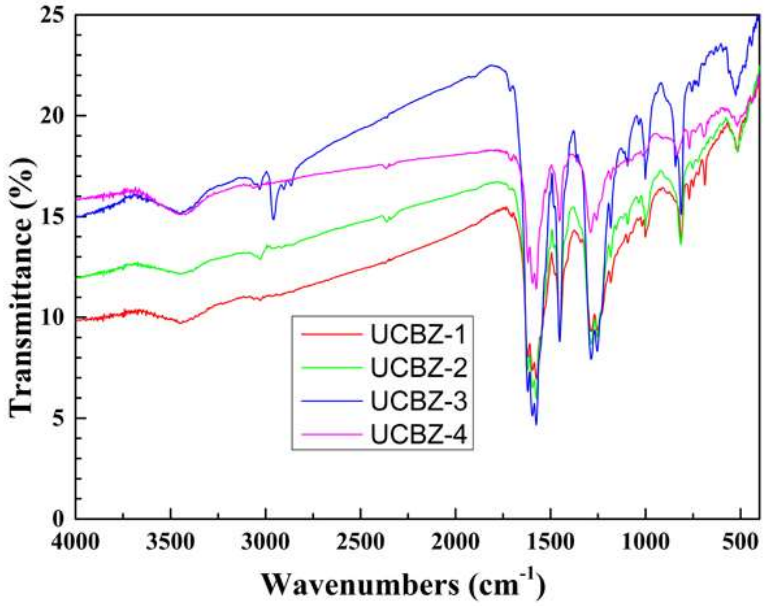

Figure 4.12. IR spectra of the UCBZ series.

4.5.7. Powder X-Ray diffraction of the UCBZ series

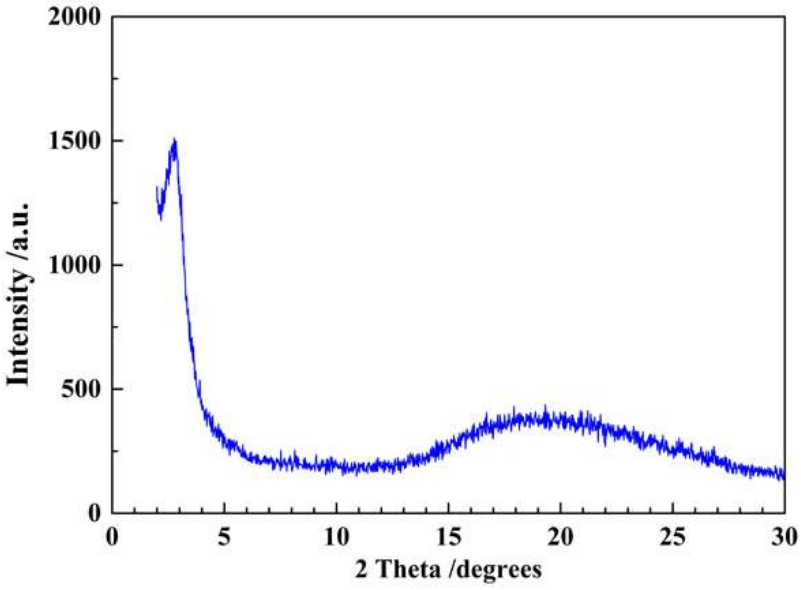

Figure 4.13. Powder X-ray diffraction pattern of UCBZ-**1**.

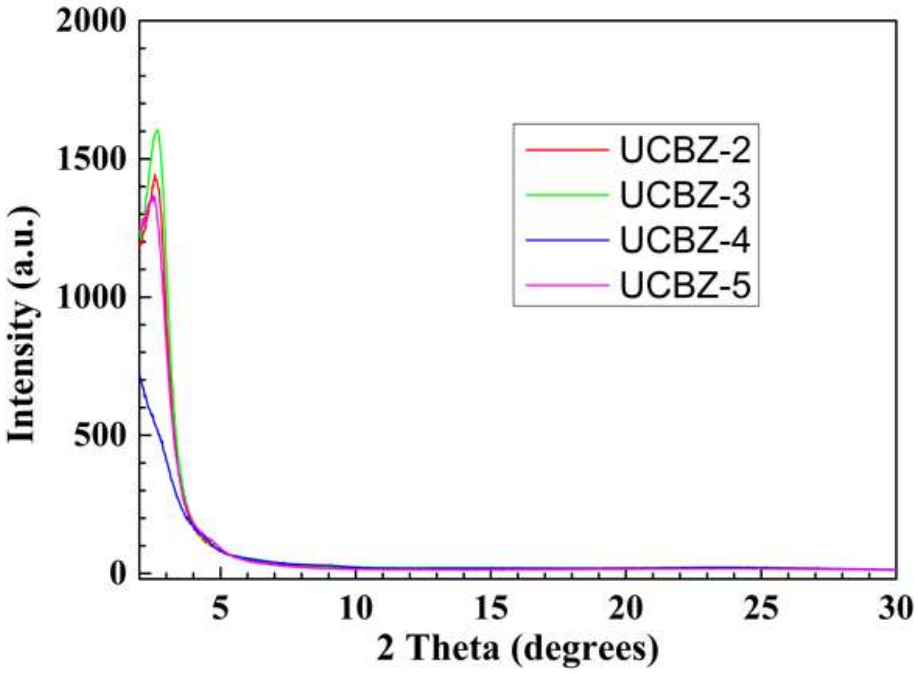

Figure 4.14. Powder X-ray diffraction pattern of UCBZ-**2, 3, 4,** and **5**.

4.5.8. Additional gas adsorption data for the UCBZ series

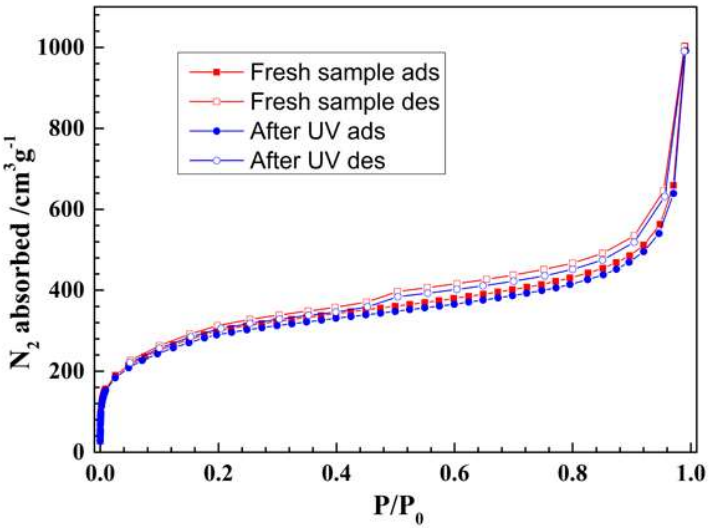

Figure 4.15. N_2 adsorption and desorption of UCBZ-**5** before and after UV irradiation.

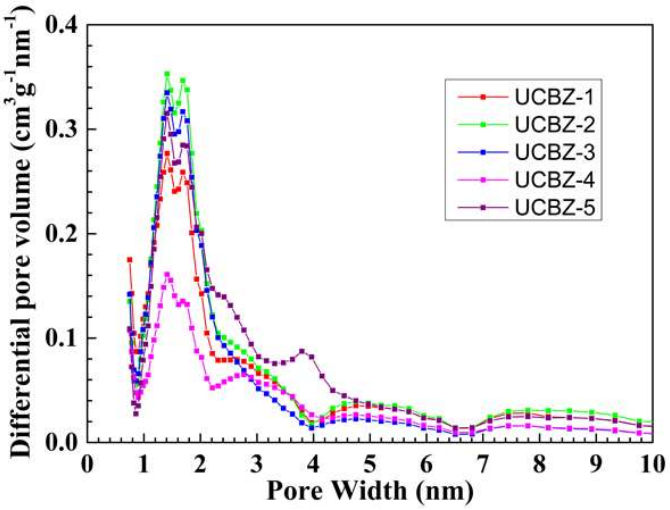

Figure 4.16. Pore size distribution of the UCBZ series.

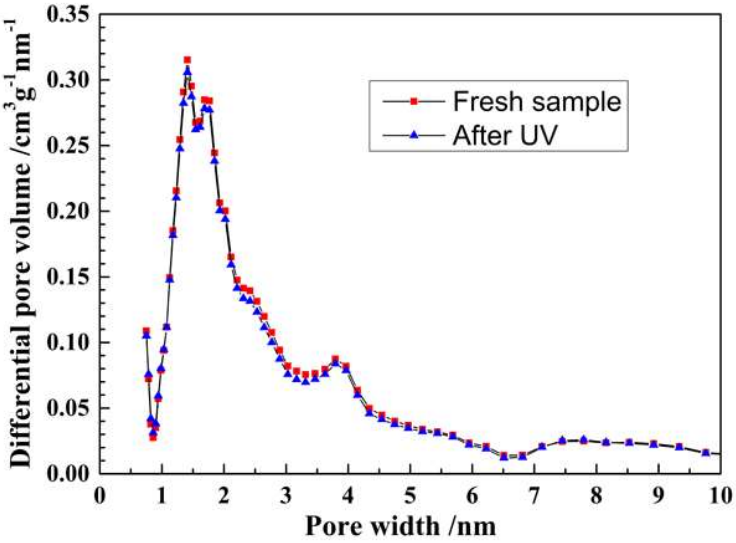

Figure 4.17. Pore size distribution of UCBZ-**5** before and after UV irradiation.

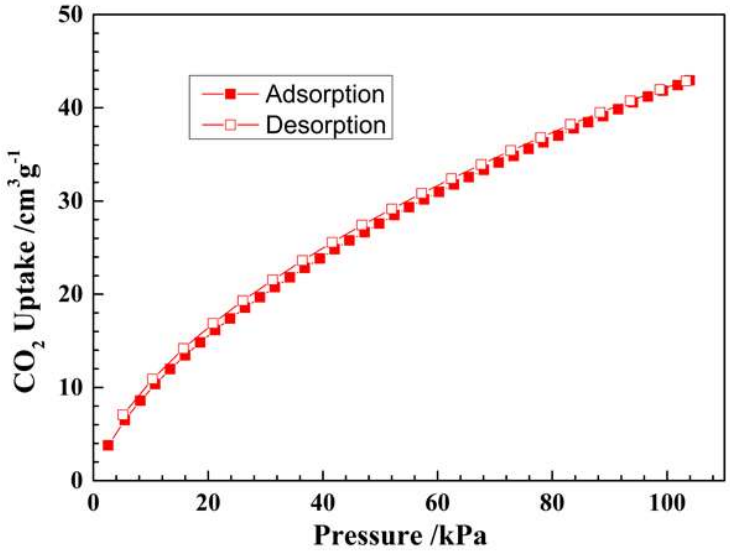

Figure 4.18. CO_2 adsorption isotherms for UCBZ-**5** of the fresh activated sample.

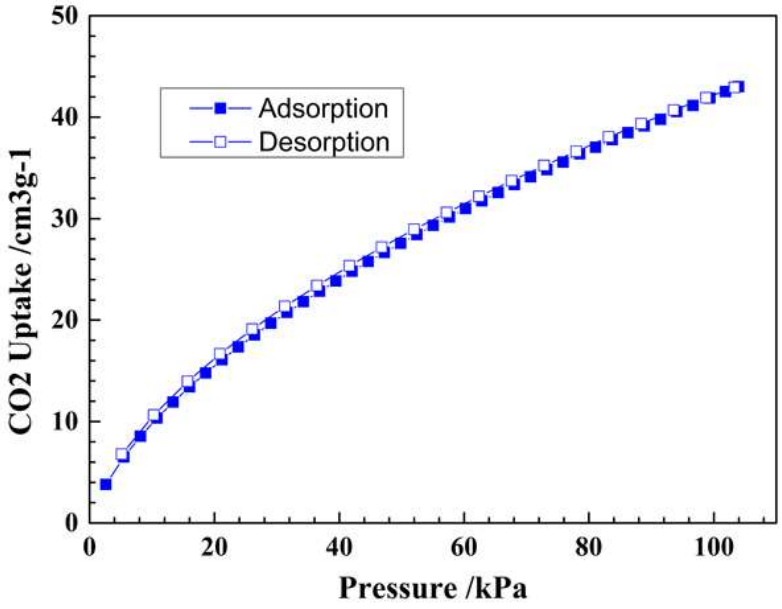

Figure 4.19. CO_2 adsorption isotherms for UCBZ-**5** after UV irradiation.

4.5.9. Solid-State ^{13}C CP-MAS data

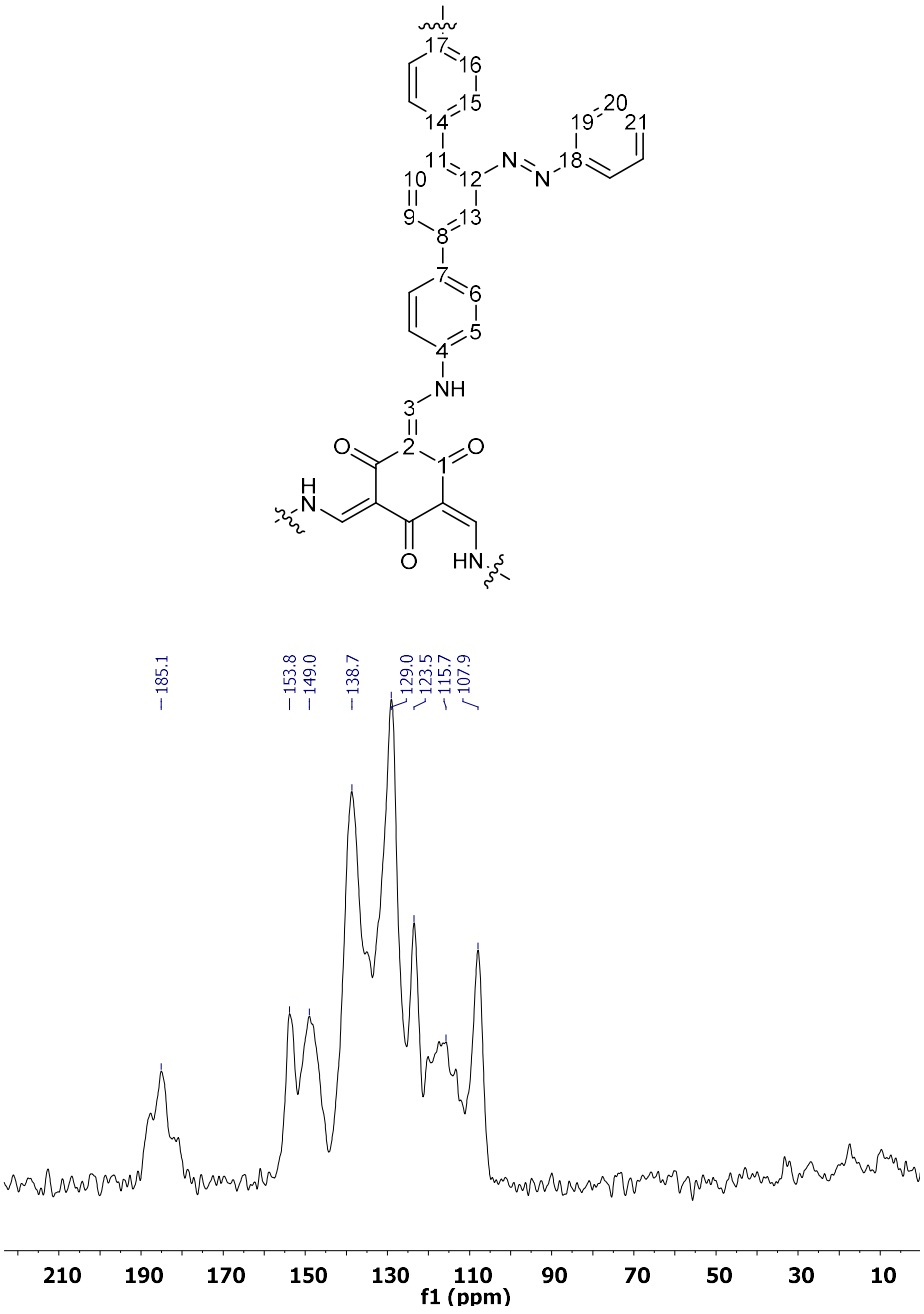

Figure 4.20. Solid State ^{13}C CP-MAS NMR spectrum of UCBZ-**1**.

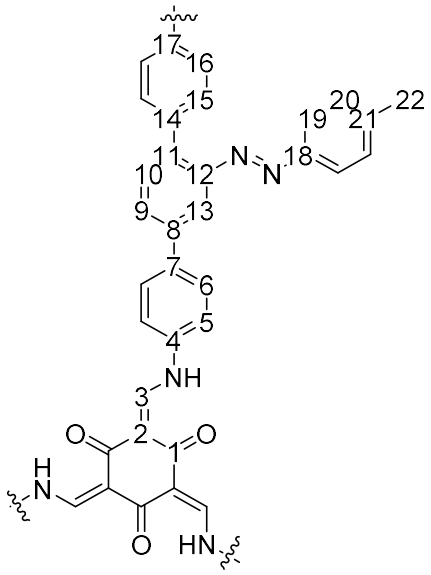

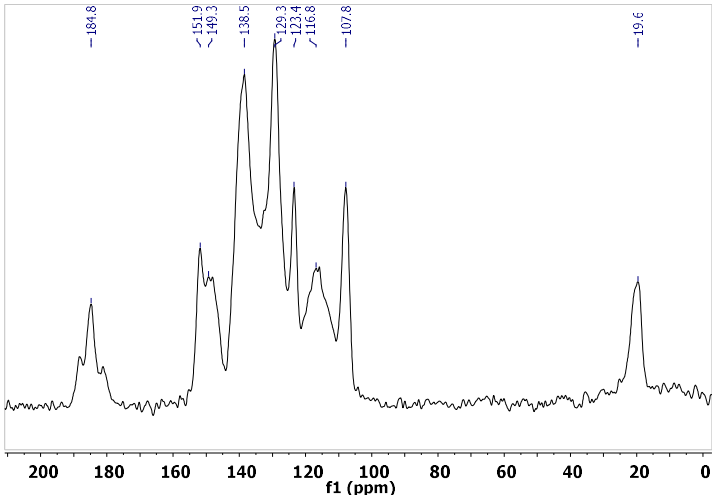

Figure 4.21. Solid State ^{13}C CP-MAS NMR spectrum of UCBZ-**2**.

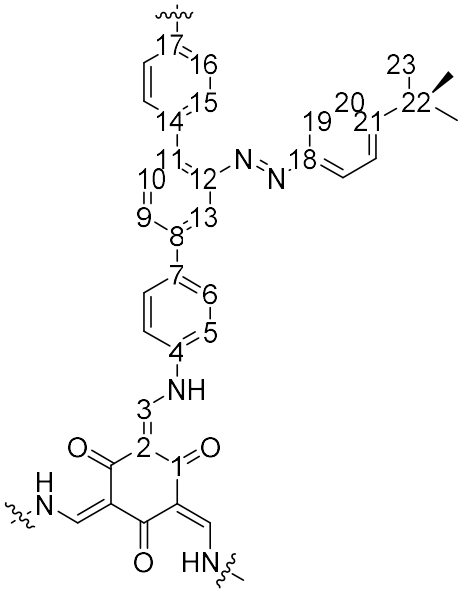

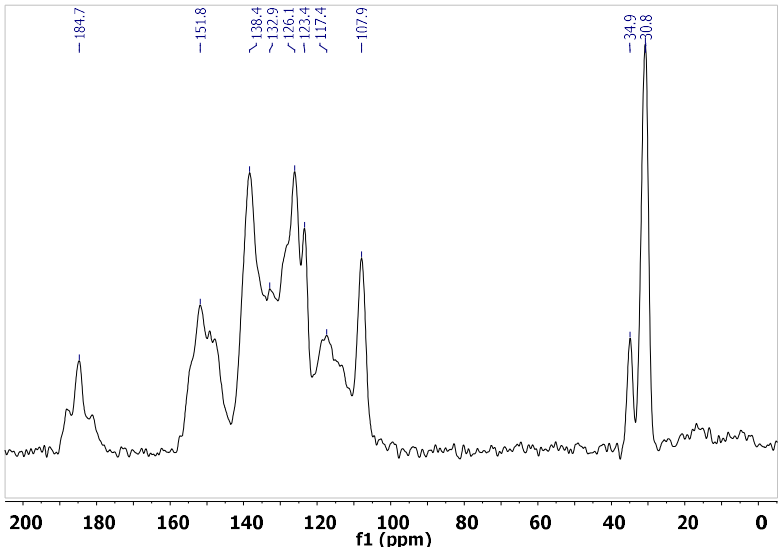

Figure 4.22. Solid State ^{13}C CP-MAS NMR spectrum of UCBZ-**3**.

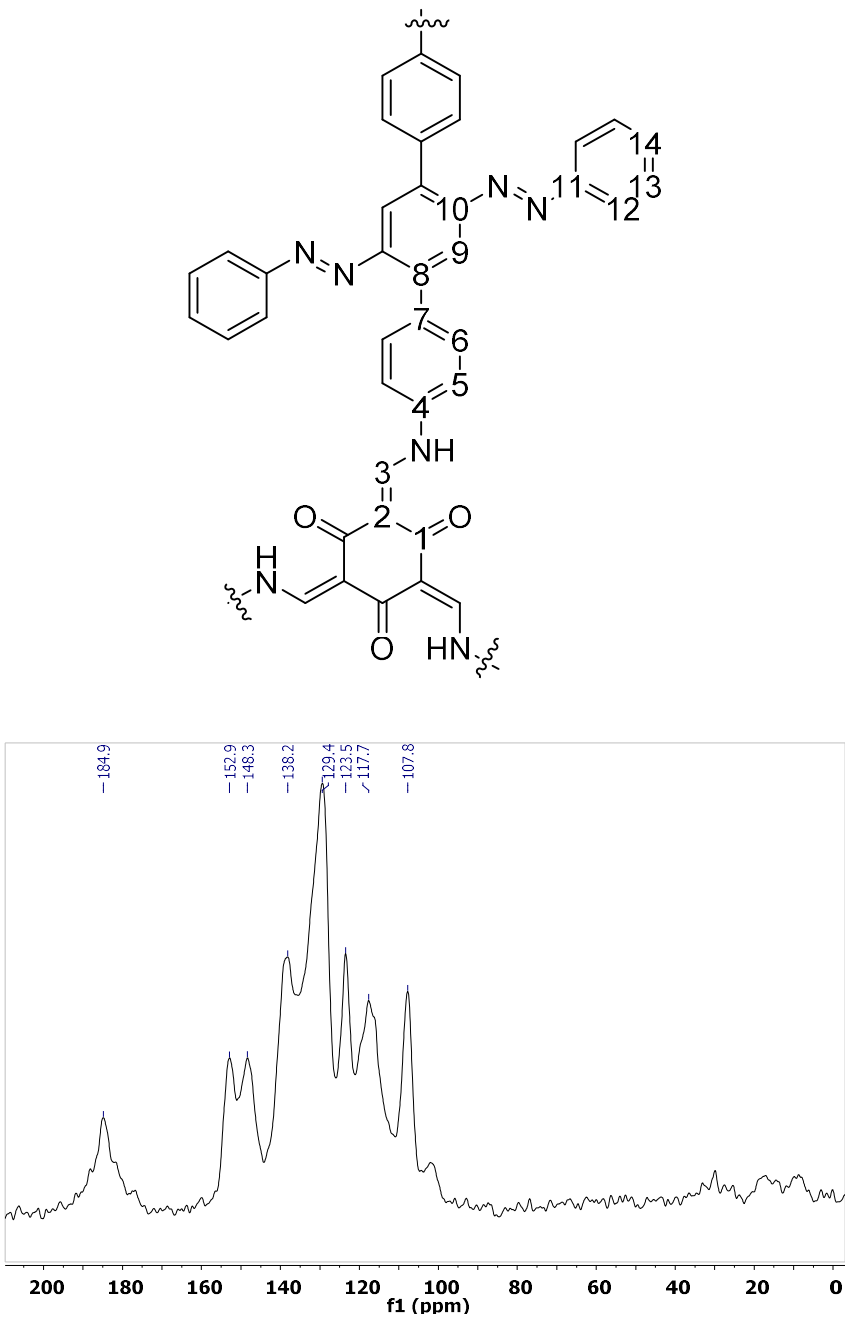

Figure 4.23. Solid State ^{13}C CP-MAS NMR spectrum of UCBZ-**4**.

4.5.10. SEM images of UCBZ series

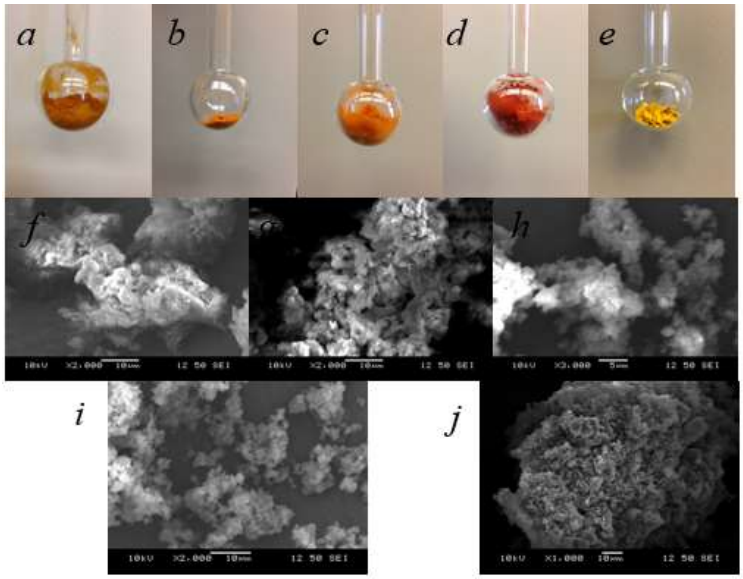

Figure 4.24. SEM images of the UCBZ series.

4.6. References

(1) Wojtecki, R. J.; Meador, M. A.; Rowan, S. J. *Nat. Mater.* **2011**, *10*, 14.

(2) Liu, F.; Urban, M. W. *Prog. Polym. Sci.* **2010**, *35*, 3.

(3) Stuart, M. A. C.; Huck, W. T. S.; Genzer, J.; Muller, M.; Ober, C.; Stamm, M.; Sukhorukov, G. B.; Szleifer, I.; Tsukruk, V. V.; Urban, M.; Winnik, F.; Zauscher, S.; Luzinov, I.; Minko, S. *Nat. Mater.* **2010**, *9*, 101.

(4) Kundu, P. K.; Olsen, G. L.; Kiss, V.; Klajn, R. *Nat. Commun.* **2014**, *6*, doi: 10.1038/ncomms4588.

(5) Luo, F.; Fan, C. B.; Luo, M. B.; Wu, X. L.; Zhu, Y.; Pu, S. Z.; Xu, W. Y.; Guo, G. C. *Angew. Chem., Int. Ed.* **2014**, *53*, In press.

(6) Lyndon, R.; Konstas, K.; Ladewig, B. P.; Southon, P. D.; Kepert, C. J.; Hill, M. R. *Angew. Chem., Int. Ed.* **2013**, *52*, 3695.

(7) Park, J.; Yuan, D. Q.; Pham, K. T.; Li, J. R.; Yakovenko, A.; Zhou, H. C. *J. Am. Chem. Soc.* **2012**, *134*, 99.

(8) Yanai, N.; Uemura, T.; Inoue, M.; Matsuda, R.; Fukushima, T.; Tsujimoto, M.; Isoda, S.; Kitagawa, S. *J. Am. Chem. Soc.* **2012**, *134*, 4501.

(9) Cote, A. P.; Benin, A. I.; Ockwig, N. W.; O'Keeffe, M.; Matzger, A. J.; Yaghi, O. M. *Science* **2005**, *310*, 1166.

(10) El-Kaderi, H. M.; Hunt, J. R.; Mendoza-Cortes, J. L.; Cote, A. P.; Taylor, R. E.; O'Keeffe, M.; Yaghi, O. M. *Science* **2007**, *316*, 268.

(11) Feng, X.; Ding, X. S.; Jiang, D. L. *Chem. Soc. Rev.* **2012**, *41*, 6010.

(12) Ding, S. Y.; Wang, W. *Chem. Soc. Rev.* **2013**, *42*, 548.

(13) Colson, J. W.; Dichtel, W. R. *Nat. Chem.* **2013**, *5*, 453.

(14) Ben, T.; Ren, H.; Ma, S. Q.; Cao, D. P.; Lan, J. H.; Jing, X. F.; Wang, W. C.; Xu, J.; Deng, F.; Simmons, J. M.; Qiu, S. L.; Zhu, G. S. *Angew. Chem., Int. Ed.* **2009**, *48*, 9457.

(15) Cooper, A. I. *Adv. Mater.* **2009**, *21*, 1291.

(16) Lu, W. G.; Yuan, D. Q.; Zhao, D.; Schilling, C. I.; Plietzsch, O.; Muller, T.; Brase, S.; Guenther, J.; Blumel, J.; Krishna, R.; Li, Z.; Zhou, H. C. *Chem. Mater.* **2010**, *22*, 5964.

(17) Han, S. S.; Furukawa, H.; Yaghi, O. M.; Goddard, W. A. *J. Am. Chem. Soc.* **2008**, *130*, 11580.

(18) Wood, C. D.; Tan, B.; Trewin, A.; Su, F.; Rosseinsky, M. J.; Bradshaw, D.; Sun, Y.; Zhou, L.; Cooper, A. I. *Adv. Mater.* **2008**, *20*, 1916.

(19) Dawson, R.; Adams, D. J.; Cooper, A. I. *Chem. Sci.* **2011**, *2*, 1173.

(20) Yuan, D. Q.; Lu, W. G.; Zhao, D.; Zhou, H. C. *Adv. Mater.* **2011**, *23*, 3723.

(21) Chang, Z.; Zhang, D. S.; Chen, Q.; Bu, X. H. *Phys. Chem. Chem. Phys.* **2013**, *15*, 5430.

(22) Kaur, P.; Hupp, J. T.; Nguyen, S. T. *ACS Catal.* **2011**, *1*, 819.

(23) Yagai, S.; Kitamura, A. *Chem. Soc. Rev.* **2008**, *37*, 1520.

(24) Ercole, F.; Davis, T. P.; Evans, R. A. *Polym. Chem.* **2010**, *1*, 37.

(25) Murthy, N.; Campbell, J.; Fausto, N.; Hoffman, A. S.; Stayton, P. S. *Bioconjugate Chem* **2003**, *14*, 412.

(26) Dai, S.; Ravi, P.; Tam, K. C. *Soft Matter* **2008**, *4*, 435.

(27) Dimitrov, I.; Trzebicka, B.; Muller, A. H. E.; Dworak, A.; Tsvetanov, C. B. *Prog. Polym. Sci.* **2007**, *32*, 1275.

(28) Magnusson, J. P.; Khan, A.; Pasparakis, G.; Saeed, A. O.; Wang, W. X.; Alexander, C. *J. Am. Chem. Soc.* **2008**, *130*, 10852.

(29) Weder, C. *Nature* **2009**, *459*, 45.

(30) Brantley, J. N.; Wiggins, K. M.; Bielawski, C. W. *Science* **2011**, *333*, 1606.

(31) Davis, D. A.; Hamilton, A.; Yang, J.; Cremar, L. D.; Van Gough, D.; Potisek, S. L.; Ong, M. T.; Braun, P. V.; Martinez, T. J.; White, S. R.; Moore, J. S.; Sottos, N. R. *Nature* **2009**, *459*, 68.

(32) Bandara, H. M. D.; Burdette, S. C. *Chem. Soc. Rev.* **2012**, *41*, 1809.

(33) Irie, M.; Kunwatchakun, D. *Macromolecules* **1986**, *19*, 2476.

(34) Mamada, A.; Tanaka, T.; Kungwatchakun, D.; Irie, M. *Macromolecules* **1990**, *23*, 1517.

(35) Berkovic, G.; Krongauz, V.; Weiss, V. *Chem. Rev.* **2000**, *100*, 1741.

(36) Minkin, V. I. *Chem. Rev.* **2004**, *104*, 2751.

(37) Dou, Y. S.; Hu, Y.; Yuan, S. A.; Wu, W. F.; Tang, H. *Mol. Phys.* **2009**, *107*, 181.

(38) Borisenko, V.; Burns, D. C.; Zhang, Z. H.; Woolley, G. A. *J. Am. Chem. Soc.* **2000**, *122*, 6364.

(39) Liu, N. G.; Chen, Z.; Dunphy, D. R.; Jiang, Y. B.; Assink, R. A.; Brinker, C. J. *Angew. Chem., Int. Ed.* **2003**, *42*, 1731.

(40) Belowich, M. E.; Stoddart, J. F. *Chem. Soc. Rev.* **2012**, *41*, 2003.

(41) Jin, Y.; Zhu, Y.; Zhang, W. *CrystEngComm* **2013**, *15*, 1484.

(42) Chong, J. H.; Sauer, M.; Patrick, B. O.; MacLachlan, M. J. *Org. Lett.* **2003**, *5*, 3823.

(43) Kandambeth, S.; Mallick, A.; Lukose, B.; Mane, M. V.; Heine, T.; Banerjee, R. *J. Am. Chem. Soc.* **2012**, *134*, 19524.

(44) Biswal, B. P.; Chandra, S.; Kandambeth, S.; Lukose, B.; Heine, T.; Banerjeet, R. *J. Am. Chem. Soc.* **2013**, *135*, 5328.

(45) DeBlase, C. R.; Silberstein, K. E.; Truong, T. T.; Abruna, H. D.; Dichtel, W. R. *J. Am. Chem. Soc.* **2013**, *135*, 16821.

(46) Biswal, B. P.; Chandra, S.; Kandambeth, S.; Lukose, B.; Heine, T.; Banerjee, R. *J. Am. Chem. Soc.* **2013**, *135*, 5328.

(47) Zhu, Y.; Long, H.; Zhang, W. *Chem. Mater.* **2013**, *25*, 1630.

(48) Li, J. R.; Kuppler, R. J.; Zhou, H. C. *Chem. Soc. Rev.* **2009**, *38*, 1477.

(49) Maya, F.; Tour, J. M. *Tetrahedron* **2004**, *60*, 81.

(50) Kosynkin, D. V.; Tour, J. M. *Org. Lett.* **2001**, *3*, 993.

(51) Yelamaggad, C. V.; Achalkumar, A. S.; Rao, D. S. S.; Prasad, S. K. *J. Org. Chem.* **2009**, *74*, 3168.

(52) Zhao, D. B.; Johansson, M.; Backvall, J. E. *Eur. J. Org. Chem.* **2007**, 4431.

(53) Mallagaray, A.; Canales, A.; Dominguez, G.; Jimenez-Barbero, J.; Perez-Castells, J. *Chem. Commun.* **2011**, *47*, 7179.

CHAPTER 5

Desymmetrized Vertex Design for the Synthesis of Covalent Organic Frameworks (COFs) with Heterogeneous Pore Structures

(A paper was published for this chapter: Zhu, Y.; Wan, S.; Jin, Y.; Zhang, W. "Desymmetrized Vertex Design for the Synthesis of Covalent Organic Frameworks with Periodically Heterogeneous Pore Structures" *J. Am. Chem. Soc.* 2015, 137, 13772–13775)

5.1 Abstract

Conventionally, COFs are synthesized with only one kind of pore size, in this chapter, two novel porous 2D covalent organic frameworks (COF) with periodically heterogeneous pore structures were successfully synthesized through the desymmetrized vertex design strategy. Condensation of C_{2v} symmetric 5-(4-formylphenyl)isophthalaldehyde or 5-((4-formylphenyl)ethylene)isophthalaldehyde with linear hydrazine linker under the solvothermal or microwave heating conditions yield crystalline 2D COFs, **HP-COF-1** and **HP-COF-2** with high specific surface area. PXRD patterns and computer modelling study together with pore size distribution (PSD) analysis show each of the resulting COFs exhibits two distinctively different hexagonal pore structures. The structures were fully characterized by FT-IR, solid state ^{13}C-NMR, gas adsorption, FT-SEM, TEM and theoretical simulations. Such rational design and synthetic strategy provide new possibilities for preparing highly ordered porous polymers with heterogeneous pore structures.

5.2 Introduction

In the past decade, covalent organic frameworks (COFs)[1-3] have emerged as a new class of highly ordered crystalline organic porous polymers and have attracted tremendous research interests due to their unique structures and various potential applications in gas storage and separation, heterogeneous catalysis,

and optoelectronic materials.[2-15] COFs are constructed through reticular synthesis[16] involving dynamic covalent reactions.[17] Such approach provides precise periodicity control in skeleton, customizable pore surface, structural diversity, as well as high physiochemical stability. A large number of COFs have been synthesized and characterized within the past decade. However, they are mainly limited to uniform pore structures with homogeneous pore environments. Introduction of pore heterogeneity within ordered COFs is desirable to tailor materials characteristics, such as electronic, magnetic, mechanical, and sorption properties. Structural disorders and heterogeneities have been widely investigated in hierarchical porous polymers (HPPs)[18-20] and metal organic frameworks (MOFs),[21-26] which have shown intriguing applications in catalysis and separation technology. In most cases, such structural "defects" are randomly distributed and their spatial arrangement are hard to identify. Complex COFs with intentionally created heterogeneities are rare.[27-29] One such example was recently reported by Zhao and coworkers, demonstrating the synthesis of a 2D COF with dual pores.[27] Our group also attempted to prepare COFs with dual pores through "macrocycle-to-framework" strategy using a preporous shape-persistent macrocycle as building block.[29] However, due to the small internal cavity of the macrocycle, it was difficult to identify and characterize the small pores. Herein we describe a facile and conceptual approach which can produce COFs with predesigned periodic "defects" in the ordered framework.

5.3 Results and discussion

Conventionally, COFs are synthesized from highly symmetric building blocks in order to form well-ordered, easily predictable crystalline structures. Multitopic building blocks with C_3/D_{3h} or C_4/D_{4h} symmetry are the most commonly used.[30] By using these types of building blocks as vertices along with ditopic linear linkers, the extended topological structures with high symmetry can be achieved. Such approach creates COFs with uniform pore structures (e.g., hexagonal or tetragonal). We envision that introducing asymmetric elements into building block design could create COFs with heterogeneous pore

structures (HP-COFs). For example, desymmetrization of a D_{3h} vertex to C_{2v} would generate a 2D framework structure possessing two different hexagonal pores, as shown in **Scheme 5.1**.

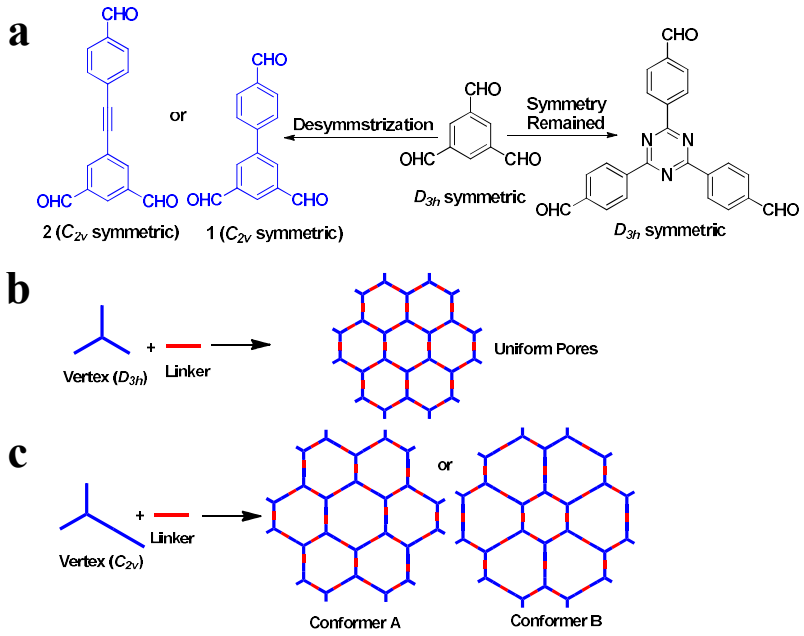

Scheme 5.1. Design strategy for the synthesis of heterogeneous COFs.

Following the desymmetrized vertex design strategy, we designed and synthesized C_{2v} symmetric 5-(4-formylphenyl)isophthalaldehyde (**1**) and 5-((4-formylphenyl)ethylene)isophthalaldehyde (**2**) as the tritopic vertex to form 2D covalent organic frameworks with two different kinds of hexagonal honey comb pores. We chose hydrazine, which is the smallest diamine, as the ditopic linear linker. Condensation of hydrazine and aldehydes can form stable diazabutadiene (-C=N-N=C-) linkage in the COFs.[31] The reaction was carried out under solvothermal conditions by using 1,4-dioxane and 1,2-dichlorobenzene (*o*-DCB) as the co-solvents in the presence of acetic acid (6 M). We screened the synthetic conditions by varying the solvent combination/ratio, reaction temperature/time, and catalyst loading in order to optimize the porosity and crystallinity of the materials. Under the optimal synthetic conditions, 10/5/1 (*v/v/v*) ratio of 1,4-dioxane, *o*-DCB and 6M acetic acid at 150 °C for 4 days, we obtained HP-COF-1 and HP-COF-2 as light yellow microcrystalline solids. As an alternative approach, the microwave heating method[32,33] was also utilized to synthesize both COFs, which show similar powder X-ray diffraction (PXRD) patterns as

those obtained under solvothermal conditions. The resulting HP-COFs are stable in common organic solvents, such as dimethylformamide (DMF), tetrahydrofuran (THF), chloroform, acetone and dichloromethane.

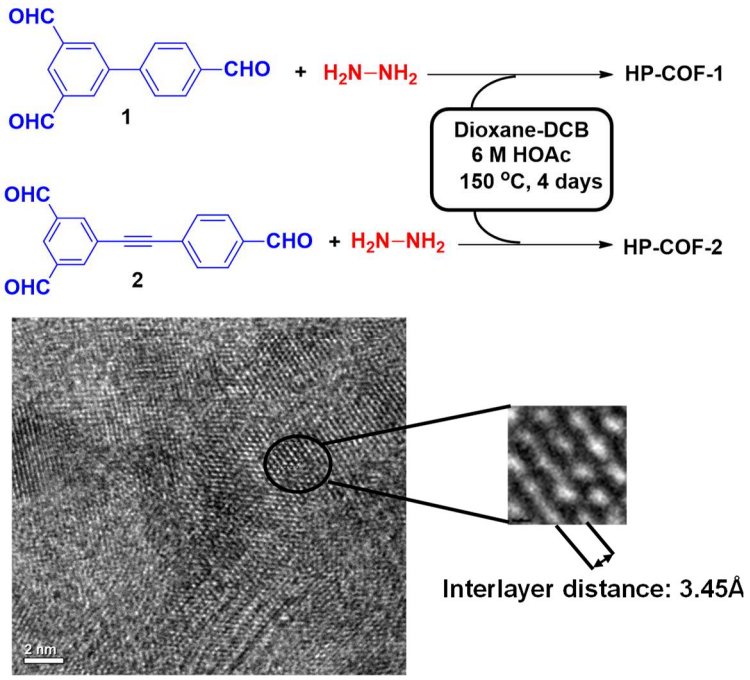

Figure 5.1. Synthesis of HP-COFs and TEM images of HP-COF-1.

The as-synthesized HP-COFs were characterized by Fourier transform infrared spectroscopy (FT-IR). The spectra of HP-COFs show the nearly complete disappearance of C=O resonance, indicating the aldehydes are mostly consumed during the reaction. In addition, the strong stretching vibration band at 1622 cm^{-1} was observed, confirming the formation of C=N linkage (**Figure 5.5**). The ^{13}C CP-MAS NMR spectrum shows the characteristic signal for the C=N group at about 161 ppm. The aldehyde carbon peak was barely observed. The chemical shifts of other fragments are in good agreement with those of the monomers (**Figure 5.12 and 5.13**). Thermal gravimetric analysis (TGA) revealed that the HP-COF-1 and HP-COF-2 are stable up to 300 °C, with around 20% weight loss at 400 °C (**Figure 5.4**). Field emission scanning electron microscopy (FE-SEM) images show that both COFs have sponge-like morphology (**Figure 5.14 and 5.15**). Transmission Electron Microscopy (TEM) characterization reveals their layered

structures with the interlayer distance around 3.45 Å (**Figure 5.1**). Our observation is consistent with the previous literature report,[4,13-15,34,35] further supporting the two dimensional nature of these frameworks.

The porosity of each COF was assessed by measuring N_2 adsorption/desorption isotherms at 77 K on the fully activated samples. The adsorption curves of HP-COFs (**Figure 5.2a**) show typical type I isotherms according the IUPAC notation,[36] which is the characteristic of microporous materials. Employing the Brunauer–Emmett–Teller (BET) model over the $0.01 < P/P_0 < 0.10$ range of the isotherms, we obtained a specific surface area of 1197 $m^2\ g^{-1}$ for HP-COF-1 and 804 $m^2\ g^{-1}$ for HP-COF-2, respectively, which are comparable with that of the recently reported azine based COFs.[31,37] We also measured the CO_2 and N_2 adsorption isotherms of HP-COF-1 at 273 K. It shows that HP-COF-1 exhibits a good a selectivity (24.8, Henry's method[38]) for adsorption of CO_2 over N_2 with a CO_2 adsorption capacity of 54 $cm^3\ g^{-1}$ at 1 atm.

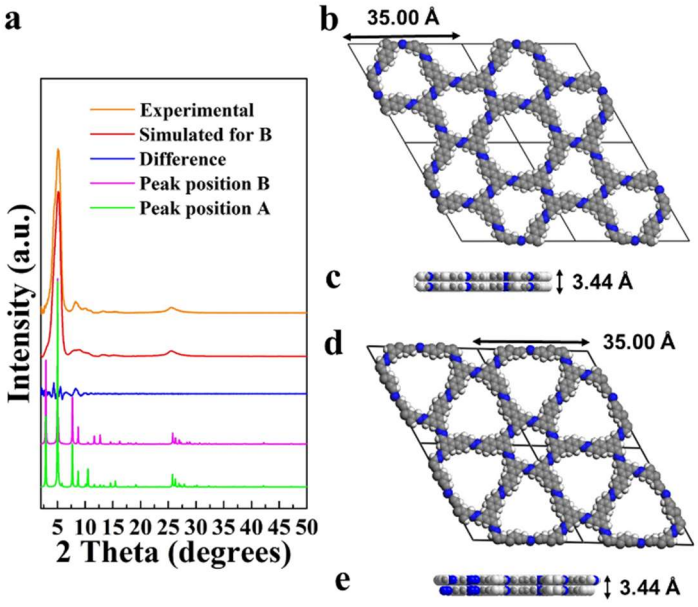

Figure 5.2. (a) PXRD patterns of HP-COF-1; (b), (c) the unit cell structure of structural isomeric form A of HP-COF-1 in AA stacking (b), and the view along the Z axis (c); (c), (d) the unit cell structure of structural isomeric form B of HP-COF-1 in AA stacking (c) and the view along the Z axis (d).

The crystallinity of HP-COF-1 and HP-COF-2 was determined by PXRD analysis. The diffraction data clearly indicate the crystalline feature of HP-COF-1 and HP-COF-2. Higher-quality diffraction data was obtained for HP-COF-1 (**Figure 5.2a)**, which were indexed on the basis of a primitive hexagonal lattice. We observed diffraction peaks of HP-COF-1 at 5.12 and 8.30°, which can be assigned to the 110 and 210 plane diffraction, respectively. In addition, a peak at 25.56° correlating to the value of the interlayer distance was observed. The *d* spacing of HP-COF-1 was calculated to be 3.44 Å, which is consistent with the TEM characterization (**Figure 5.1**). We did not observe diffraction peaks that are characteristic for the starting materials. In order to determine the periodic structure, the theoretical simulation study was performed on the hexagonal system, with layers lying on the *ab* plane. The *Reflex* module in Material Studio software package was used in conjugation with the PXRD data.

It should be noted that the combination of C_{2v} symmetric vertex and linear linker would generate two possible structural isomeric forms (A and B, Scheme 5.1c) with symmetric infinite honeycomb periodic structures. Both of them contain two different kinds of hexagonal pores. By using Material Studio software package, we evaluated these two possible structural isomeric forms. For simplicity, we only built the eclipsed models, which are the most commonly observed in 2D COFs. A geometrical energy minimization was performed, using the universal force-field implemented in the *forcite* module, to optimize the geometry of the building blocks, as well as the unit cell parameters. A full profile pattern matching (Pawley) refinement in the Reflex module produced unit cell parameters for HP-COF-1: $a = b = 35.00$ Å, $c = 3.44$ Å (residuals: $R_p = 9.76\%$ and $R_{wp} = 5.14\%$); and HP-COF-2: $a = b = 39.89$ Å, $c = 3.47$ Å (residuals: $R_p = 1.92\%$ and $R_{wp} = 1.47\%$), which agree well with the observed reflections. The same unit cell parameters were obtained for both structural isomeric forms of HP-COF-1 and HP-COF-2. The powder diffraction patterns for the models were then calculated and compared with the experimental ones. We found the simulated PXRD patterns of both structural isomeric forms of HP-COF-1 are in agreement with experimental results, supporting the eclipsed stacking of the layers (**Figure 5.1**). Since

structural isomers A and B have similar cell parameters and simulated diffraction patterns, in order to assign the exact structure isomer structure, we performed theoretical energy calculations and analyzed the pore size distribution of these COFs.

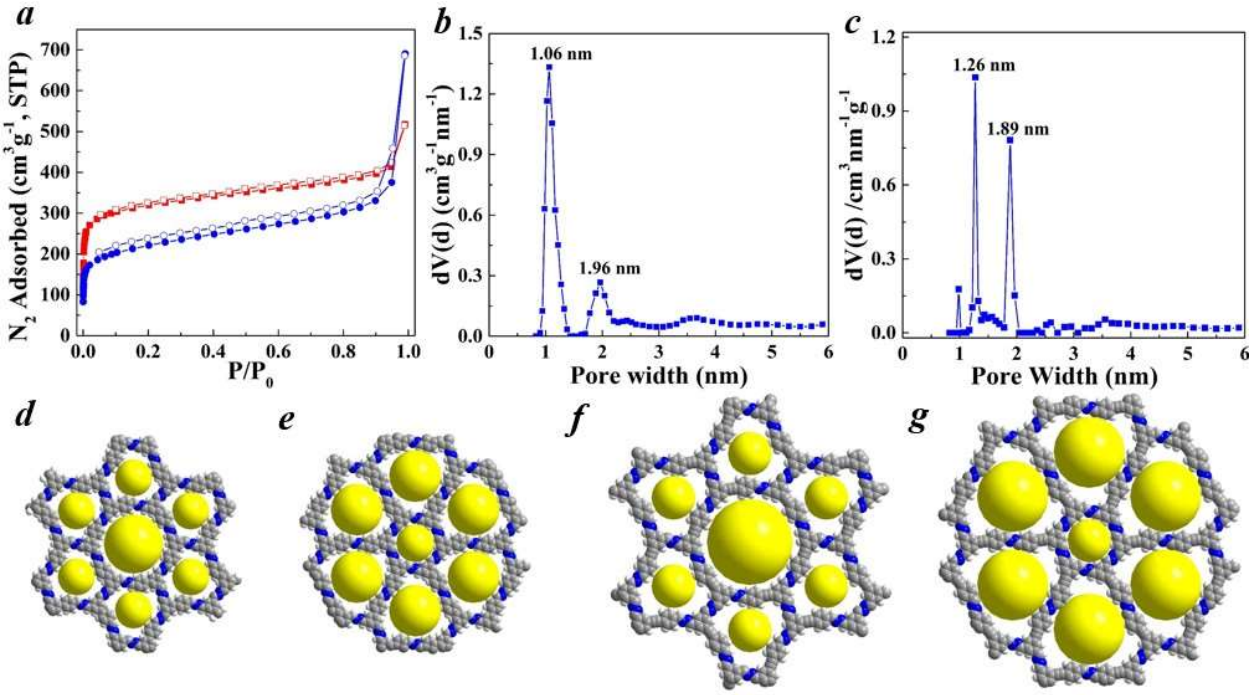

Figure 5.3. (a) N_2 adsorption and desorption isotherms of HP-COF-1 (red) and HP-COF-2 (blue); (b), (c) pore size distributions of HP-COF-1 (b), and HP-COF-2 (c); (d), (e) the pore structure models of HP-COF-1 in structural isomer A (d) and structural isomer B (e); (f), (g) the pore structure models of HP-COF-2 in structural isomer A (f) and structural isomer B (g).

Table 5.1. Gas adsorption properties and pore size distribution of HP-COFs.

COFs	SA_{BET}[a]	V_{Total}[b]	Pore size (nm)		
			Predicted[c]		Experimental[d]
			structural isomer A	structural isomer B	
HP-COF-**1**	1197	0.80	1.11 and 1.93	1.08 and 1.56	1.06 and 1.96
HP-COF-**2**	804	1.07	1.16 and 2.34	1.09 and 1.81	1.26 and 1.89

[a]Surface area ($m^2 \cdot g^{-1}$) calculated from the nitrogen adsorption based on the BET model; [b]The total pore volume ($cm^3 \cdot g^{-1}$) calculated at P/P_0 = 0.99; [c]Predicted pore size based on the eclipsed stacking of layers; [d]Calculated pore size from nitrogen adsorption isotherms using NLDFT-N_2-carbon adsorption branch kernel at 77 K based on a slit/cylindrical pore model.

The total energy of each structural isomeric form was estimated and compared to get some insightful information on their thermodynamic stabilities. For both HP-COF-1 and HP-COF-2, the relative total energy of two structural isomers are quite close: 117.19 kcal/mol and 117.16 kcal/mol for structural isomer form A and structural isomer form B of HP-COF-1, and 40.52 kcal/mol and 40.50 kcal/mol for structural isomer form A and structural isomer form B of HP-COF-2, respectively. Therefore, it was difficult to distinguish the two isomers from a thermodynamic point of view.

Next, the pore size distribution (PSD) of HP-COFs was analyzed by using nonlocal density functional theory (NL-DFT) model (**Figure 5.3, Table 5.2**). It reveals that HP-COF-1 exhibit two major pores around 1.06 nm and 1.96 nm, with greater abundance of smaller pores. The experimental result thus agrees better with the simulated structural isomer form A, in which one large pore with the size of 1.93 is surrounded by six small pores with the size of 1.11 nm. For HP-COF-2, the PSD analysis shows two major peaks around 1.26 nm and 1.89 nm with more abundant

larger pores. These results suggest the formation of structural isomer form B in the case of HP-COF-2, whose simulated structure shows two pores of sizes around 1.09 and 1.81 nm, closely matching with the experimental result. The total pore volumes of HP-COF-1 and HP-COF-2 were estimated to be V_p = 0.80 and 1.07 $cm^3\ g^{-1}$ at P/P_0 = 0.99, respectively.

5.4 Conclusion

In conclusion, we have successfully synthesized two COFs with heterogeneous pore structures through the desymmetrized vertex design strategy. Pore size distribution analysis revealed that two distinctive micropores (1.06-1.96 nm) were incorporated into the resulting COFs. The structure assignment is supported by both the PSD experimental data and theoretical simulation. Our design strategy opens new possibilities for developing COFs with heterogeneous pore structures targeting specified material properties.

5.5 Experimental section

5.5.1. Materials and measurements

All chemical reagents and solvents were commercially available and used without further purification unless otherwise indicated. 5-Bromoisophthalaldehyde,[39] 4-Ethynylbenzaldehyde,[40] 5-((4-formylphenyl)ethynyl)isophthalaldehyde,[41] and 5-(4-formylphenyl)isophthalaldehyde[41] were synthesized according to the published procedure.

Flash column chromatography was performed using a 100-150 times the weight excess of flash silica gel 32-63 μm from Dynamic Absorbants, Inc. Fractions were analyzed by TLC using TLC silica gel F254 250 μm precoated-plates from Dynamic Absorbants Inc.

NMR spectra were taken using Inova 400 and Inova 500 spectrometers. Solid-state cross polarization magic angle spinning (CP-MAS) NMR spectra were recorded on an Inova 400 NMR spectrometer.

Powder X-Ray Diffraction (PXRD) was obtained from a Bruker D-8 Discover diffractometer, using monochromated Cu K_α (λ = 1.542 Å) radiation.

The FT-IR spectra of starting materials and as synthesized HP-COFs were obtained from Agilent Technologies Cary 630 FT-IR.

Elemental analysis was taken at an Exeter Analytical-Model CE 440 CHN Analyzer, microanalysis laboratory, University of Illinois at Urbana-Champaign.

Thermogravimetric analyses (TGA) were performed on a thermogravimetric/differential thermal analyzer by heating the samples to 800 °C at 10 °C min^{-1} under the atmosphere of nitrogen.

The Quantachrome Autosorb ASiQ automated gas sorption analyzer was used to measure N_2 and CO_2 adsorption isotherms. The samples were heated at 120 °C and kept at this temperature for at least 20 hours under vacuum for activation. Ultra high purity grade (99.999 % purity) N_2, CO_2 and He, oil-free valves and gas regulators were used for all free space corrections and measurements. For all of the gas adsorption measurements, the temperatures were controlled by using a refrigerated bath of liquid N_2 (77 K), and ice water (273 K).

Scanning Electron Microscopy images (SEM) were recorded using a JSM-6480LV (LVSEM) at 5.0 kV. Samples were sputter coated with gold prior to analysis.

5.5.2. General synthetic procedures

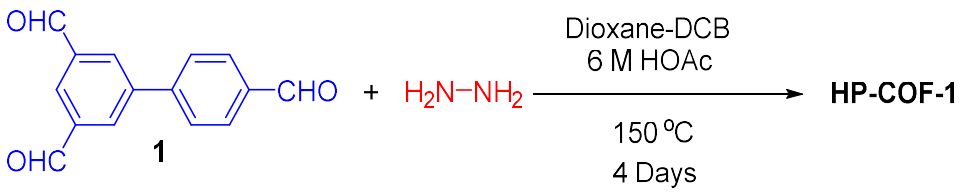

Synthesis of HP-COF-1: A customized glass tube (the outer diameter is 10 mm and the inner diameter is 8 mm) was charged with 5-(4-formylphenyl)isophthalaldehyde (**1**, 23.8 mg, 0.1 mmol), hydrazine monohydrate (9.4 μL, 0.15 mmol, injected by using micropipet), 1,4-dioxane (2 mL), *o*-Dichlorobenzene (1 mL), and 6 M acetic acid (0.2 mL). The mixture was sonicated for a few minutes. The tube was then flash frozen at 77 K under liquid nitrogen bath, evacuated to the internal pressure about 100 mtorr, and sealed under the frame. The mixture was warmed to room temperature, and the reaction temperature was slowly raised to 150 °C over 2 hours. The reaction was kept at this temperature for 4 days and cooled to room temperature over 12 hours. The light yellow precipitate was collected by vacuum filtration, washed with large amount of dichloromethane and acetone, and dried under vacuum to yield HP-COF-**1** (20 mg, 87 %): Elemental analysis calcd (%) for $(C_{15}H_{10}N_3)_n$: C, 77.57; H, 4.34; N, 18.09. Found: C, 72.61; H, 4.02; N, 15.09. (Since the materials are polymers instead of pure compounds, their elemental analysis results are just used as a reference, not to determine their purity.)

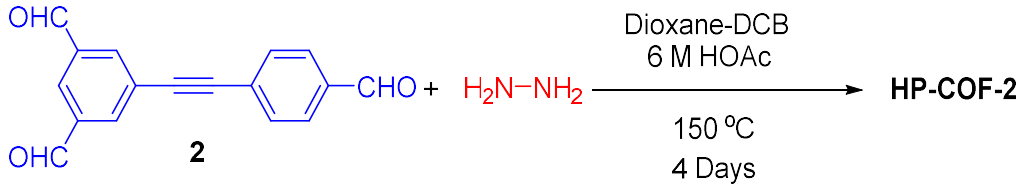

Synthesis of HP-COF-2: The above synthetic procedure for **HP-COF-1** was followed. Using 5-((4-formylphenyl)ethynyl)isophthalaldehyde (**2**, 26.2 mg, 0.1 mmol), hydrazine monohydrate (9.4 μL, 0.15 mmol), 1,4-dioxane (2 mL), mesitylene (1 mL), and 6 M acetic acid (0.2 mL), **HP-COF-2** was obtained as a yellow precipitate. The color was a little dark compared to HP-COF-1 (22 mg, 86 %): Elemental analysis calcd (%) for $(C_{17}H_{10}N_3)_n$: C, 79.67; H, 3.93; N, 16.40. Found: C, 75.38;

H, 3.95; N, 14.21. (Since the materials are polymers instead of pure compounds, their elemental analysis results are just used as a reference, not to determine their purity.)

5.5.3. TGA of HP-COFs

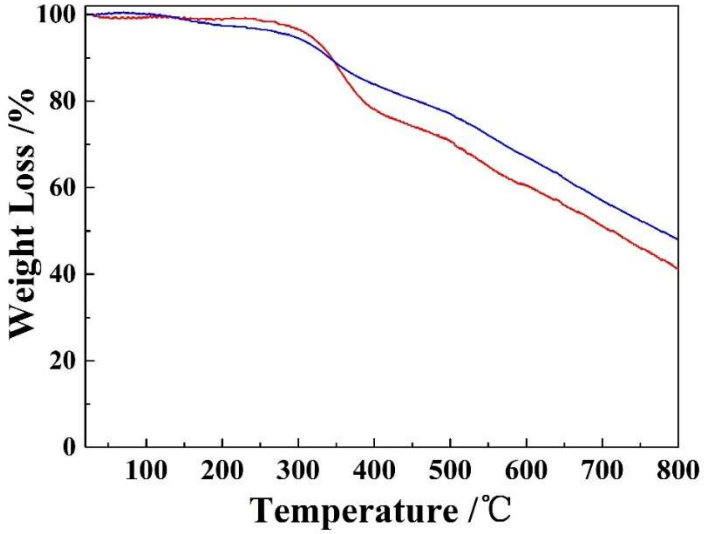

Figure 5.4. TGA curves of HP-COF-1 (red) and HP-COF-2 (blue).

5.5.4. FT-IR spectra of HP-COFs and aldehydes

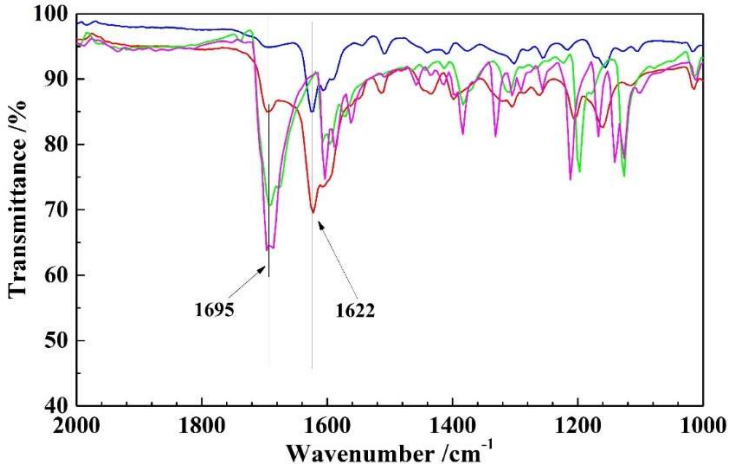

Figure 5.5. IR spectra of monomers and HP-COFs: HP-COF-1 (red), HP-COF-2 (blue), monomer **1** (green), and monomer **2** (magenta).

5.5.5. Structural Modeling and X-ray Diffraction Analyses.

All the models, including cell parameters and atomic positions were generated using the *Materials Studio* software package, employing the *Materials Visualizer* module. All the models were constructed in the hexagonal system, with the layers lying on the **ab** plane. The space groups with the maximum possible symmetry were selected. An energy minimization was performed to optimize the geometry of the building units, employing the *universal force field* implemented in the *Forcite* module of *Materials Studio*. During this process, the unit cell parameters for each model were also optimized. In **Table 5.2**, the values of the optimized unit cell parameters and the space group for the models constructed are summarized.

Table 5.2. Optimized unit cell parameters of the constructed models for HP-COF-**1** and HP-COF-**2**.

	HP-COF-**1**		HP-COF-**2**	
	Structural isomer A	Structural isomer B	Structural isomer A	Structural isomer B
Space group	*P6*/*m*	*P6*/*m*	*P6*/*m*	*P6*/*m*
***a* (Å)**	35.00	35.00	39.89	39.89
***c* (Å)**	3.44	3.44	3.47	3.47
Total Energy (kcal/mol)	117.19	117.16	40.52	40.50

The corresponding powder patterns for the four models were calculated and compared with the experimental patterns, finding the best agreement for the eclipsed models. With them, full profile pattern (Pawley) refinements were performed against the experimental powder patterns obtaining the refined unit cell parameters. **Tables 5.3** and **5.4** show the refined cell parameters and the fractional atomic coordinates of the two final models.

Table 5.3. Refined unit cell parameters and fractional atomic coordinates for HP-COF-**1**.

Name	HP-COF-1		
Space group	*P6/m*		
***a* (Å)**	35.00		
***c* (Å)**	3.44		
Atom name	***x***	***y***	***z***
H1	0.68877	0.82235	1.00000
C2	0.72279	0.82975	1.00000
N3	0.75428	0.87048	1.00000
N4	0.74473	0.90482	1.00000
H5	0.81017	0.95318	1.00000
C6	0.77610	0.94560	1.00000
C7	0.76630	0.98206	1.00000
C8	0.72267	0.97389	1.00000
H9	0.69691	0.93995	1.00000
C10	0.66587	0.99971	1.00000
H11	0.63285	0.92734	1.00000
C12	0.62934	0.95614	1.00000
C13	0.58599	0.94801	1.00000
H14	0.55907	0.91419	1.00000
C15	0.57729	0.98282	1.00000
C16	0.53115	0.97322	1.00000

H17	0.50458	0.93918	1.00000
N18	0.47807	0.99528	1.00000
H19	0.39296	0.94618	1.00000
C20	0.38725	0.97386	1.00000
C21	0.34382	0.96551	1.00000
H22	0.31870	0.93128	1.00000
C23	0.28693	0.99130	1.00000
H24	0.25483	0.91939	1.00000
C25	0.25051	0.94772	1.00000
C26	0.20688	0.93921	1.00000
C27	0.19875	0.97379	1.00000
H28	0.16515	0.96826	1.00000

Table 5.4. Refined unit cell parameters and fractional atomic coordinates for HP-COF-**2**.

Name	HP-COF-2		
Space group	*P6/m*		
***a* (Å)**	39.89		
***c* (Å)**	3.47		
Atom name	***x***	***y***	***z***
H1	0.72600	0.84920	1.00000
C2	0.75564	0.85506	1.00000
N3	0.78383	0.89053	1.00000
N4	0.77644	0.92133	1.00000

H5	0.83428	0.96262	1.00000
C6	0.80464	0.95679	1.00000
C7	0.79719	0.98949	1.00000
C8	0.75929	0.98333	1.00000
H9	0.73468	0.95418	1.00000
C10	0.64265	0.99613	1.00000
H11	0.61594	0.93382	1.00000
C12	0.61122	0.95830	1.00000
C13	0.57340	0.95185	1.00000
H14	0.54941	0.92238	1.00000
C15	0.56663	0.98315	1.00000
C16	0.52644	0.97558	1.00000
H17	0.50272	0.94593	1.00000
N18	0.48089	0.99626	1.00000
H19	0.40595	0.95417	1.00000
C20	0.40163	0.97888	1.00000
C21	0.36383	0.97249	1.00000
H22	0.33968	0.94310	1.00000
C23	0.31847	0.99726	1.00000
C24	0.28589	0.99174	1.00000
C25	0.24703	0.98520	1.00000
H26	0.22074	0.92315	1.00000

C27	0.21560	0.94739	1.00000
C28	0.17760	0.94075	1.00000
C29	0.17142	0.97250	1.00000
H30	0.14220	0.96774	1.00000

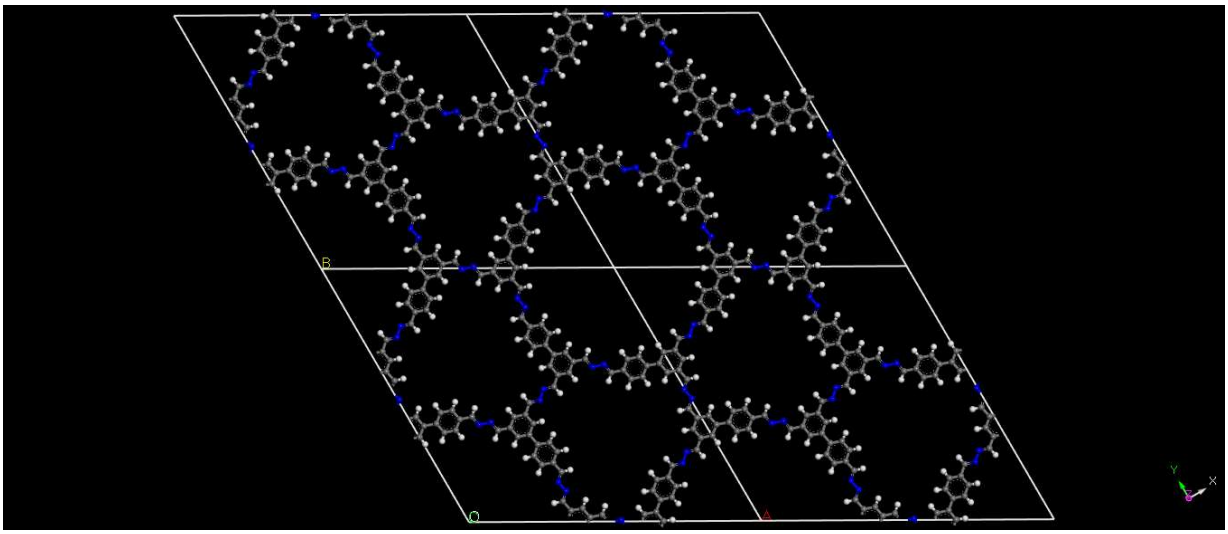

Figure 5.6. The stick model of structural isomeric form A of HP-COF-1.

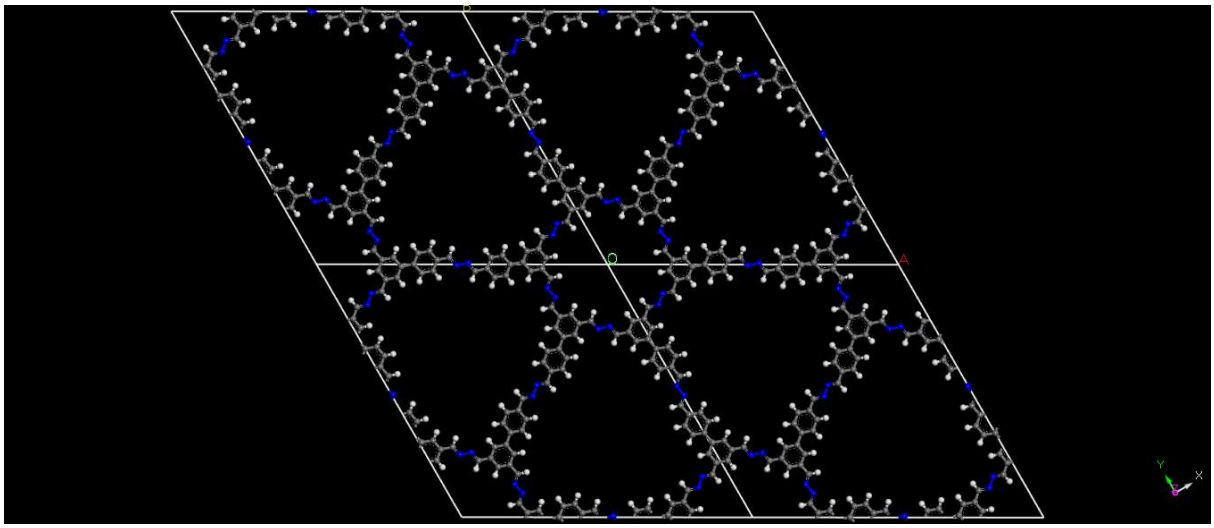

Figure 5.7. The stick model of structural isomeric form B of HP-COF-1.

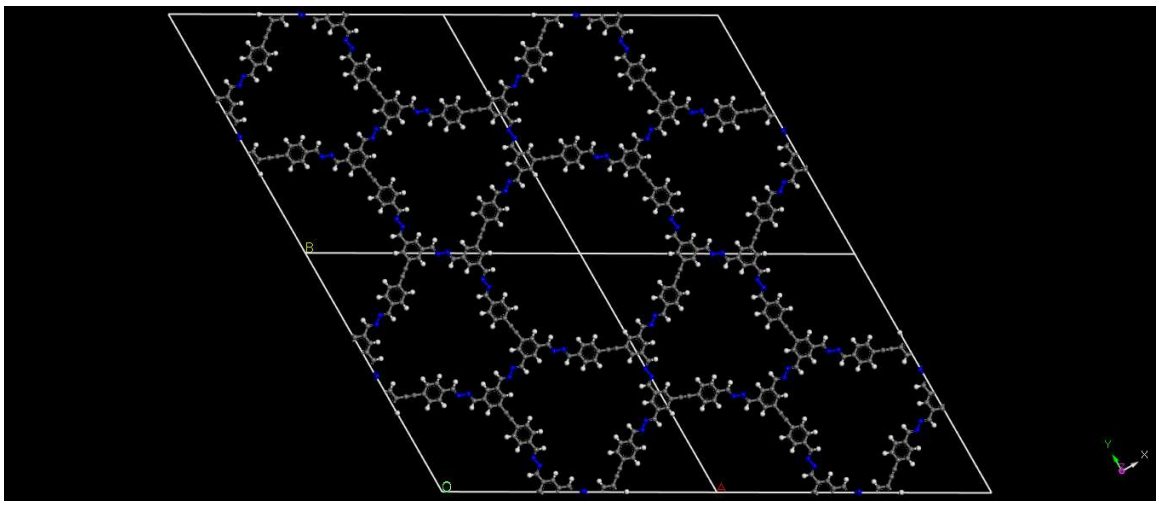

Figure 5.8. The stick model of structural isomeric form A of HP-COF-2.

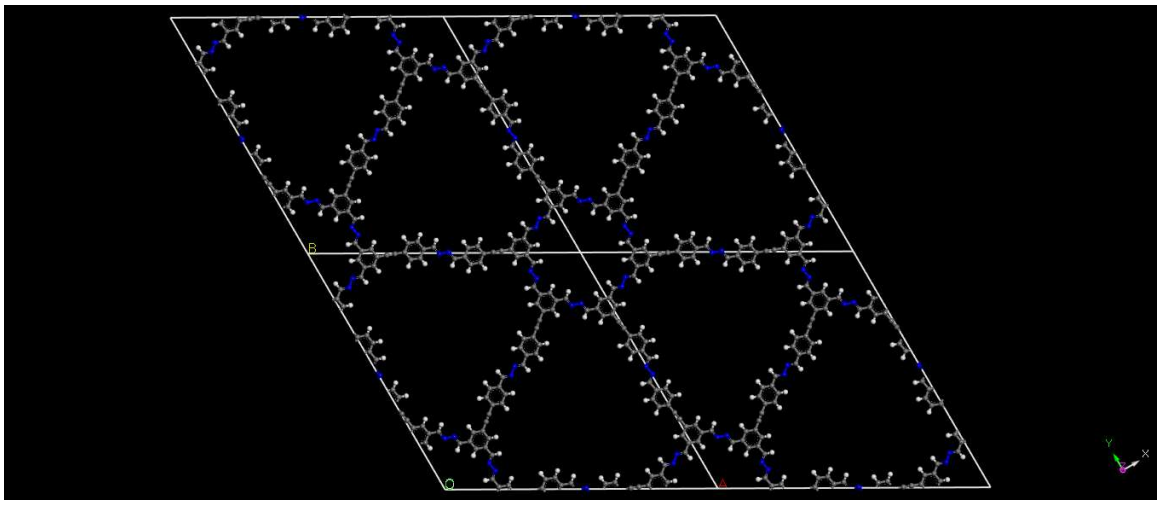

Figure 5.9. The stick model of structural isomeric form B of HP-COF-2.

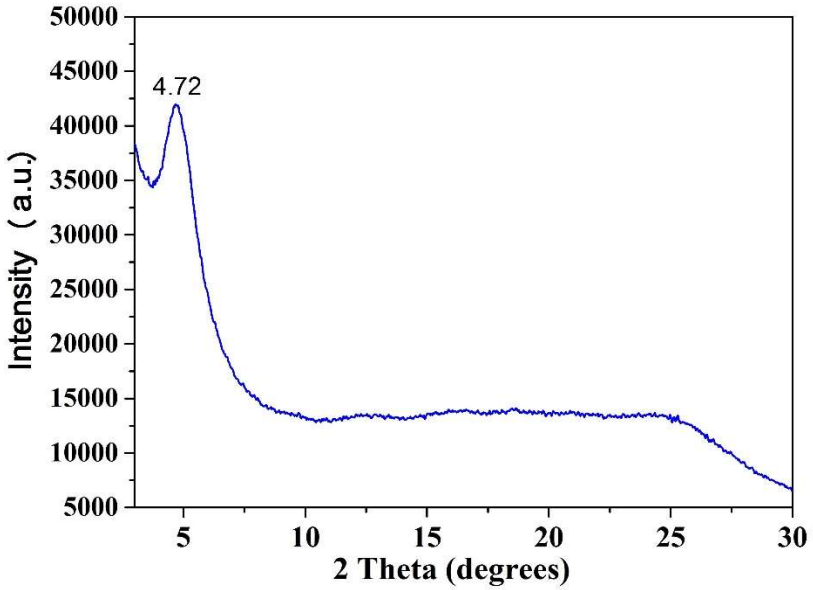

Figure 5.10. PXRD patterns of HP-COF-2.

5.5.6. Additional gas adsorption data for HP-COFs

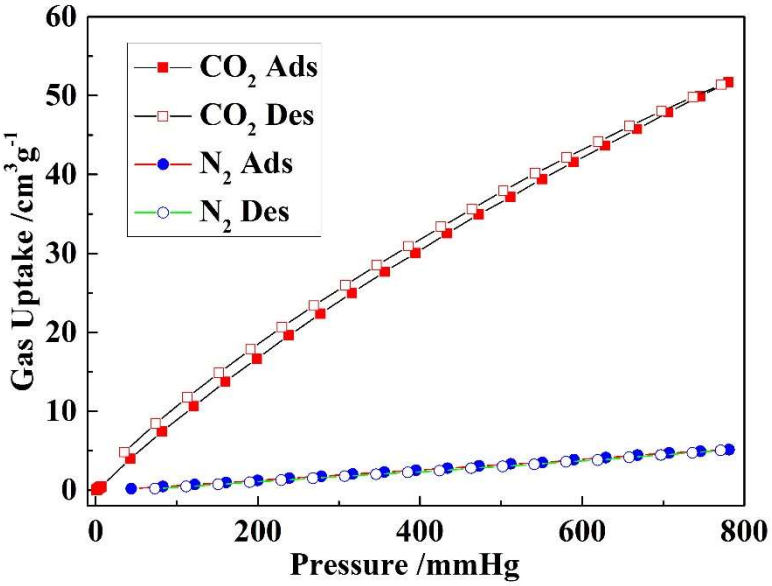

Figure 5.11. CO_2 and N_2 adsorption isotherms of HP-COF-1 at 273 K.

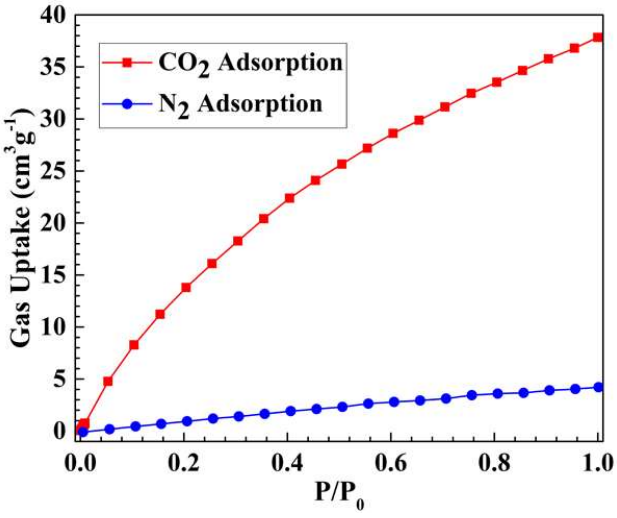

Figure 5.12. CO_2 and N_2 sorption isotherms of HP-COF-2 at 273 K.

5.5.7. Solid-State ^{13}C CP-MAS

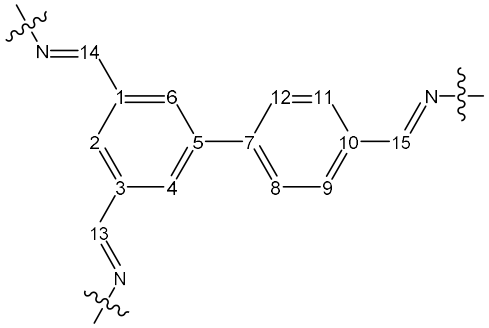

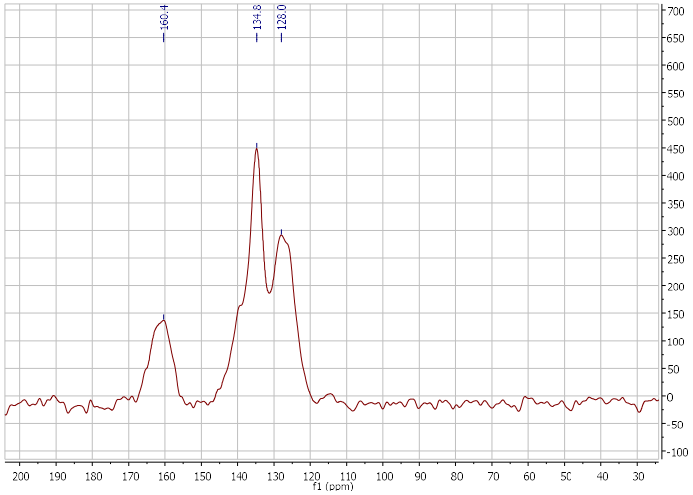

Figure 5.13. Solid State ^{13}C CP-MAS NMR spectrum of HP-COF-**1**.

Peak	Assignments
160.4	13, 14, 15
134.8	1, 2, 3, 4, 6, 9, 10, 11
128.0	5, 7, 8, 12

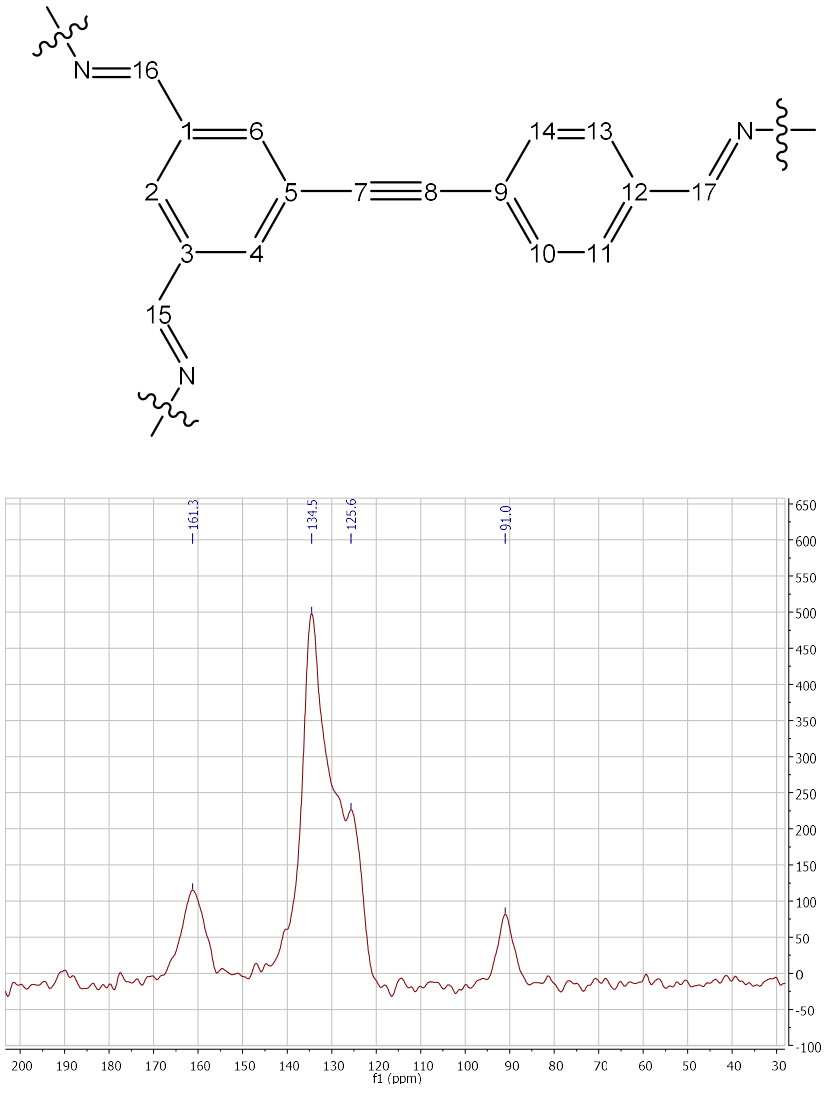

Figure 5.14. Solid State ^{13}C CP-MAS NMR spectrum of HP-COF-**2**.

Peak	Assignments
161.3	15, 16, 17
134.8	1, 2, 3, 4, 6, 11, 12, 13
128.0	5, 9, 10, 14
91.0	7, 8

5.5.8. SEM images of HP-COF series

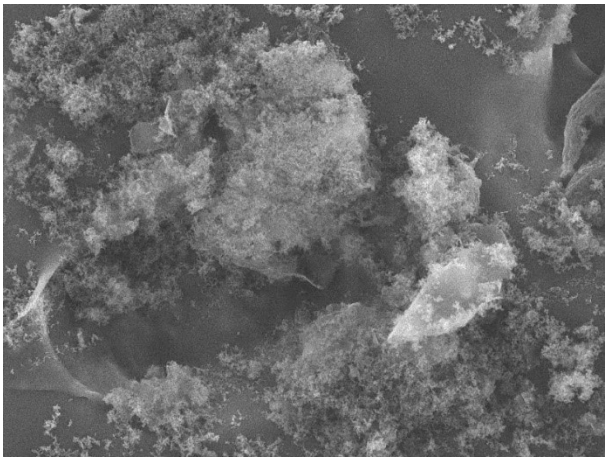

Figure 5.15. SEM image of HP-COF-1 (20 kV, ×400).

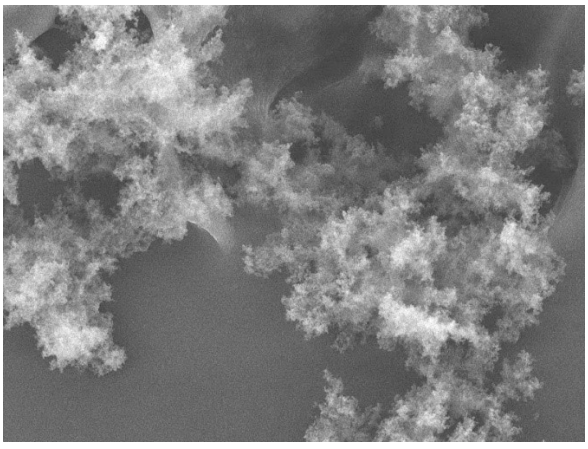

Figure 5.16. SEM image of HP-COF-2 (20 kV, ×400).

5.5.9. TEM images of HP-COF series

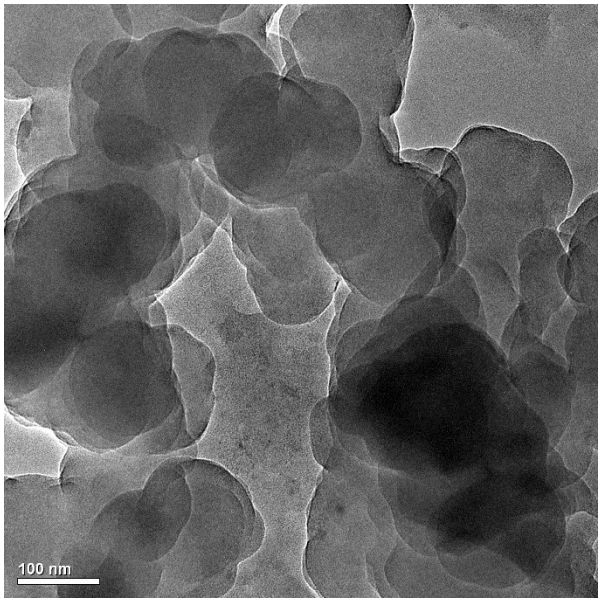

Figure 5.17. TEM image of HP-COF-1.

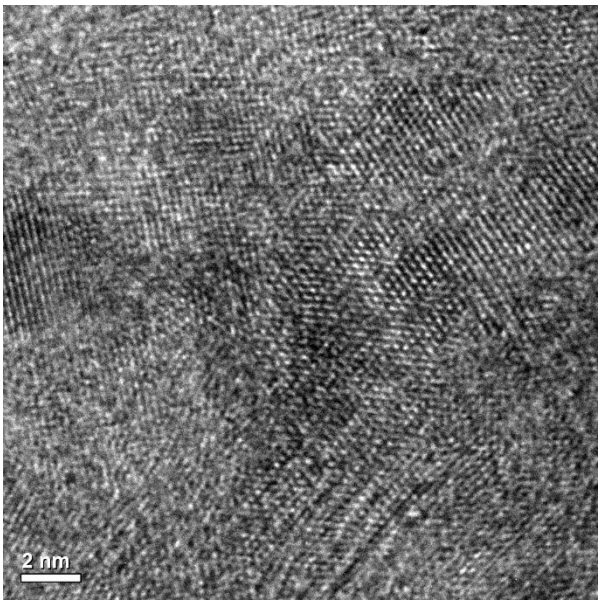

Figure 5.18. TEM image of HP-COF-2 (layer by layer structure).

5.6 References

(1) Cote, A. P.; Benin, A. I.; Ockwig, N. W.; O'Keeffe, M.; Matzger, A. J.; Yaghi, O. M. *Science* **2005**, *310*, 1166.

(2) Feng, X.; Ding, X. S.; Jiang, D. L. *Chem. Soc. Rev.* **2012**, *41*, 6010.

(3) Ding, S. Y.; Wang, W. *Chem. Soc. Rev.* **2013**, *42*, 548.

(4) Cote, A. P.; Benin, A. I.; Ockwig, N. W.; O'Keeffe, M.; Matzger, A. J.; Yaghi, O. M. *Science* **2005**, *310*, 1166.

(5) El-Kaderi, H. M.; Hunt, J. R.; Mendoza-Cortes, J. L.; Cote, A. P.; Taylor, R. E.; O'Keeffe, M.; Yaghi, O. M. *Science* **2007**, *316*, 268.

(6) Tilford, R. W.; Mugavero, S. J.; Pellechia, P. J.; Lavigne, J. J. *Adv. Mater.* **2008**, *20*, 2741.

(7) Han, S. S.; Furukawa, H.; Yaghi, O. M.; Goddard, W. A. *J. Am. Chem. Soc.* **2008**, *130*, 11580.

(8) Wan, S.; Guo, J.; Kim, J.; Ihee, H.; Jiang, D. L. *Angew. Chem., Int. Ed.* **2008**, *47*, 8826.

(9) Furukawa, H.; Yaghi, O. M. *J. Am. Chem. Soc.* **2009**, *131*, 8875.

(10) Colson, J. C., J. W.; Woll, A. R.; Mukherjee, A.; Levendorf, M. P.; Spitler, E. L.; Shields, V. B.; Spencer, M. G.; Park, J.; Dichtel, W. R. *Science* **2011**, *332*, 228.

(11) Wan, S.; Gandara, F.; Asano, A.; Furukawa, H.; Saeki, A.; Dey, S. K.; Liao, L.; Ambrogio, M. W.; Botros, Y. Y.; Duan, X. F.; Seki, S.; Stoddart, J. F.; Yaghi, O. M. *Chem. Mater.* **2011**, *23*, 4094.

(12) Ding, S. Y.; Gao, J.; Wang, Q.; Zhang, Y.; Song, W. G.; Su, C. Y.; Wang, W. *J. Am. Chem. Soc.* **2011**, *133*, 19816.

(13) Kandambeth, S.; Mallick, A.; Lukose, B.; Mane, M. V.; Heine, T.; Banerjee, R. *J. Am. Chem. Soc.* **2012**, *134*, 19524.

(14) Biswal, B. P.; Chandra, S.; Kandambeth, S.; Lukose, B.; Heine, T.; Banerjee, R. *J. Am. Chem. Soc.* **2013**, *135*, 5328.

(15) DeBlase, C. R.; Silberstein, K. E.; Truong, T. T.; Abruna, H. D.; Dichtel, W. R. *J. Am. Chem. Soc.* **2013**, *135*, 16821.

(16) O'Keeffe, M.; Peskov, M. A.; Ramsden, S. J.; Yaghi, O. M. *Accounts Chem Res* **2008**, *41*, 1782.

(17) Jin, Y. H.; Yu, C.; Denman, R. J.; Zhang, W. *Chem. Soc. Rev.* **2013**, *42*, 6634.

(18) Sai, H.; Tan, K. W.; Hur, K.; Asenath-Smith, E.; Hovden, R.; Jiang, Y.; Riccio, M.; Muller, D. A.; Elser, V.; Estroff, L. A.; Gruner, S. M.; Wiesner, U. *Science* **2013**, *341*, 530.

(19) Seo, M.; Kim, S.; Oh, J.; Kim, S. J.; Hillmyer, M. A. *J. Am. Chem. Soc.* **2015**, *137*, 600.

(20) Ning, Y.; Yang, Y.; Wang, C. Y.; Ngai, T.; Tong, Z. *Chem. Commun.* **2013**, *49*, 8761.

(21) Wong-Foy, A. G.; Lebel, O.; Matzger, A. J. *J. Am. Chem. Soc.* **2007**, *129*, 15740.

(22) Schnobrich, J. K.; Lebel, O.; Cychosz, K. A.; Dailly, A.; Wong-Foy, A. G.; Matzger, A. J. *J. Am. Chem. Soc.* **2010**, *132*, 13941.

(23) Xie, Y. B.; Yang, H.; Wang, Z. Y. U.; Liu, Y. Y.; Zhou, H. C.; Li, J. R. *Chem. Commun.* **2014**, *50*, 563.

(24) Fang, Z. L.; Bueken, B.; De Vos, D. E.; Fischer, R. A. *Angew. Chem., Int. Ed.* **2015**, *54*, 7234.

(25) Furukawa, H.; Muller, U.; Yaghi, O. M. *Angew. Chem., Int. Ed.* **2015**, *54*, 3417.

(26) Choi, K. M.; Jeon, H. J.; Kang, J. K.; Yaghi, O. M. *J. Am. Chem. Soc.* **2011**, *133*, 11920.

(27) Zhou, T. Y.; Xu, S. Q.; Wen, Q.; Pang, Z. F.; Zhao, X. *J. Am. Chem. Soc.* **2014**, *136*, 15885.

(28) Feng, X.; Dong, Y. P.; Jiang, D. L. *CrystEngComm* **2013**, *15*, 1508.

(29) Yang, H. S.; Du, Y.; Wan, S.; Trahan, G. D.; Jin, Y. H.; Zhang, W. *Chem. Sci.* **2015**, *6*, 4049.

(30) Colson, J. W.; Dichtel, W. R. *Nat. Chem.* **2013**, *5*, 453.

(31) Dalapati, S.; Jin, S. B.; Gao, J.; Xu, Y. H.; Nagai, A.; Jiang, D. L. *J. Am. Chem. Soc.* **2013**, *135*, 17310.

(32) Campbell, N. L.; Clowes, R.; Ritchie, L. K.; Cooper, A. I. *Chem. Mater.* **2009**, *21*, 204.

(33) Ritchie, L. K.; Trewin, A.; Reguera-Galan, A.; Hasell, T.; Cooper, A. I. *Micropor. Mesopor. Mat.* **2010**, *132*, 132.

(34) Wan, S.; Guo, J.; Kim, J.; Ihee, H.; Jiang, D. L. *Angew. Chem., Int. Ed.* **2009**, *48*, 5439.

(35) Kuhn, P.; Antonietti, M.; Thomas, A. *Angew. Chem., Int. Ed.* **2008**, *47*, 3450.

(36) Rouquerol, J.; Avnir, D.; Fairbridge, C. W.; Everett, D. H.; Haynes, J. H.; Pernicone, N.; Ramsay, J. D. F.; Sing, K. S. W.; Unger, K. K. *Pure. Appl. Chem.* **1994**, *66*, 1739.

(37) Li, Z. P.; Feng, X.; Zou, Y. C.; Zhang, Y. W.; Xia, H.; Liu, X. M.; Mu, Y. *Chem. Commun.* **2014**, *50*, 13825.

(38) Zhou, D. D.; He, C. T.; Liao, P. Q.; Xue, W.; Zhang, W. X.; Zhou, H. L.; Zhang, J. P.; Chen, X. M. *Chem. Commun.* **2013**, *49*, 11728.

(39) Drewry, J. A.; Duodu, E.; Mazouchi, A.; Spagnuolo, P.; Burger, S.; Gradinaru, C. C.; Ayers, P.; Schimmer, A. D.; Gunning, P. T. *Inorg. Chem.* **2012**, *51*, 8284.

(40) de Miguel, G.; Wielopolski, M.; Schuster, D. I.; Fazio, M. A.; Lee, O. P.; Haley, C. K.; Ortiz, A. L.; Echegoyen, L.; Clark, T.; Guldi, D. M. *J. Am. Chem. Soc.* **2011**, *133*, 13036.

(41) Catala, L.; Le Moigne, J.; Gruber, N.; Novoa, J. J.; Rabu, P.; Belorizky, E.; Turek, P. *Chem.Eur. J.* **2005**, *11*, 2440.

CHAPTER 6

Conclusions and future work

6.1 Overview of objectives

The overall objective of this dissertation was to use different dynamic covalent chemical reactions in synthesizing porous organic polymers (POPs), incorporating various functional groups to the POPs, and developing new synthetic strategies for the synthesis of covalent organic frameworks (COFs) with heterogeneous pore structures. We further explored their structure-property relationships by studying their gas adsorption and separation behaviors. Specifically, a series of imine-linked POPs was synthesized by using imine condensation/metathesis, and the resulting porous polymers exhibited high specific surface area, high small gas (e.g., H_2, CH_4, CO_2, C_2H_2) uptake, and good CO_2/N_2 adsorption selectivity. Alkyne metathesis is a recently developed dynamic covalent chemistry, and by using this method, two POPs were synthesized with high specific surface area. More importantly, this method is advantageous over the traditional irreversible Sonogashira cross coupling reaction for the synthesis of POPs. In addition, by using a porphyrin-based monomer, we were able to use alkyne metathesis to synthesize a 2D porous polymer that exhibits good electrocatalytical performance for oxygen reduction reaction, a very important reaction running in fuel cells.

Besides using different dynamic covalent chemical reactions to synthesize POPs, introducing various functional groups into the POPs was also explored in order to prepare responsive POPs. Responsive polymers can adapt to environmental change and convert chemical or biochemical signals to thermal, optical, or mechanical signals, and vice versa. Azobenzene is a very classical photoresponsive molecule, and it can undergo *trans*↔*cis* isomerization under UV light irradiation or thermal treatment. With this in mind, we designed and synthesized a series of azobenzene functionalized diamine, which were further reacted with trialdehydes to form photoresponsive POPs. Pore size distribution and CO_2

adsorption experiments confirm their photoresponsiveness, as they can reversibly change the pore size distribution and CO_2 adsorption. Therefore, a series of photoresponsive POPs were successfully synthesized.

Design/synthetic strategy is always central for the development of POPs and COFs. Generally, COFs are synthesized from highly symmetric building blocks. On the other hand, using building blocks with low symmetry could create novel topological structures and may lead to new applications for COFs. Under such design principle, we desymmetrized the D_{3h} building blocks to C_{2v} building blocks in COF synthesis, and two COFs with heterogeneous hexagonal pore structures were obtained through such desymmetrized synthetic strategy. Both the pore size distribution and theoretical modelling confirm the dual-pore COF structures. Such design strategy would allow the synthesis of COFs with more complicated structure and may lead to new properties for COFs.

6.2 Abstract

Covalent organic frameworks (COFs) with new topological and structural complexity may lead to unprecedented properties and applications. In this chapter, we are using desymmetrized vertex design strategy and topology-directed synthetic strategy to prepare COFs with novel pore structures. The preliminary results indeed show some promise. Currently, further optimization of the synthetic conditions is being pursed.

6.3 Introduction

Covalent organic frameworks (COFs)[1-3] have great potential application in many fields, such as gas storage[4], CO_2 capture[5], chemical sensing[6], heterogeneous catalysis[7], energy storage[8], etc. In general,

COFs are synthesized from highly symmetric building blocks at their very beginning, and uniform hexagonal or tetragonal pore structures are formed. With the development of new building blocks and synthetic strategies, COFs with more complicated structures are reported. It is generally accepted that the topology of COFs can affect their properties. Therefore, the synthesis of COFs with novel topology may lead to new properties and diversify their structure library. COFs with more than one kind of pore are rare, until recently, a few examples with two or three different kinds of pores have been synthesized[9-13]. It is desired to develop new synthetic strategies and novel building blocks for the synthesis of COFs with novel topology. Herein, we describe some new design strategies for the synthesis of COFs with novel pore structures.

6.4 Results and discussion

In chapter 5, we developed a desymmetrized vertex design strategy for the synthesis of COFs with heterogeneous hexagonal pore structures. Continuing our efforts on the synthesis of COFs with novel structures, in this chapter, we explored some new synthetic strategies to construct COFs with novel pore structures. In the last chapter, D_{3h} building blocks were desymmetrized to C_{2v} building blocks. In this chapter, the C_{2v} building blocks are further desymmetrized to form non-symmetric building blocks. By using this non-symmetric building together with linear linker, the COFs may bear three different hexagonal pore structures, as shown in **Scheme 6.1**.

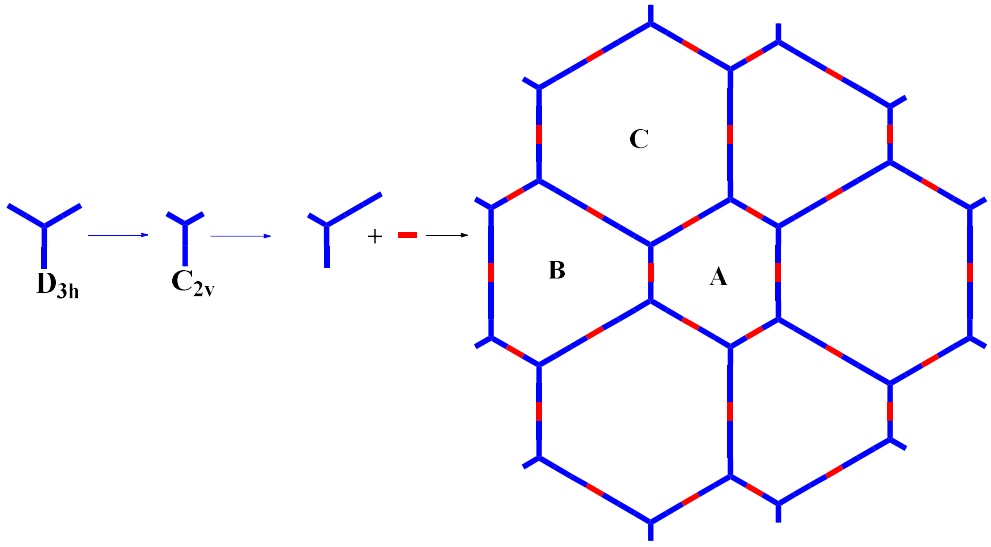

Scheme 6.1. Design strategy for the synthesis of heterogeneous COFs with three different hexagonal pore structures.

Another strategy for the synthesis of COFs with heterogeneous pore structures is what we call topology directed synthetic strategy, in which the topological structure is dissected into small pieces, then we can design building blocks that match the geometry requirements. As shown in **scheme 6.2**, a 2D topological structure with alternating tetragonal and octagonal pore structure can be formed from very simple building blocks.

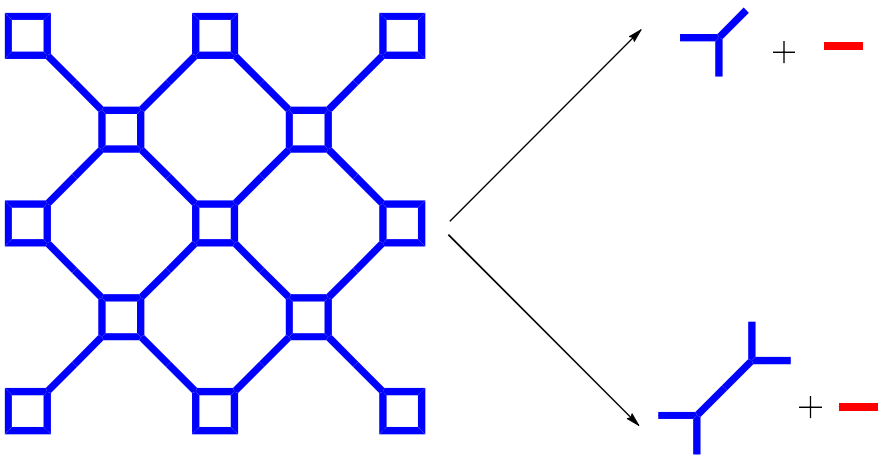

Scheme 6.2. Design strategy for the synthesis of heterogeneous COFs with alternating tetragonal and octagonal pore structures.

Following the above design strategies, we designed and synthesized a few building blocks that can match the geometry requirements for the synthesis of COFs with desired topology. Then, we used these building blocks to condense with linear linkers hydrazine or glyoxal to prepare the COFs. The reaction was carried out under solvothermal conditions by using 1,4-dioxane and 1,2-dichlorobenzene (*o*-DCB) as the co-solvents in the presence of acetic acid (6 M). We screened many reaction conditions by varying the solvent combination, reaction temperature, reaction time, and catalyst concentration, although at this stage we still have not found the optimal synthetic conditions for the synthesis of highly crystalline COFs with high surface area.

6.5 Conclusion

In conclusion, by using desymmetrized vertex design and topology-directed synthetic strategy, we were able to synthesize COFs with designed heterogeneous pore structures, based on preliminary experimental results. Although at this stage the COFs that we synthesized are still not highly crystalline and the surface area is not very high, further optimization on the reaction condition is being pursued. The synthetic conditions play an important role in the synthesis of COFs, and we will continue to optimize the synthetic conditions in order to get more crystalline and higher surface area COFs.

6.6 Experimental section

6.6.1. Materials and measurements

All chemical reagents and solvents were commercially available and used without further purification unless otherwise indicated. 3,5-Dibromobenzaldehyde[14], 4-ethynylbenzaldehyde[15], 3, 6-dibromo-9-(4-bromophenyl)-carbazole[16], and 3,6-dinitrocarbazole[17] were synthesized according to the published procedure.

Flash column chromatography was performed using a 100-150 times the weight excess of flash silica gel 32-63 μm from Dynamic Absorbants, Inc. Fractions were analyzed by TLC using TLC silica gel F254 250 μm precoated-plates from Dynamic Absorbants Inc.

NMR spectra were taken using Inova 400 and Inova 500 spectrometers. Solid-state cross polarization magic angle spinning (CP-MAS) NMR spectra were recorded on an Inova 400 NMR spectrometer.

The Quantachrome Autosorb ASiQ automated gas sorption analyzer was used to measure N_2 and CO_2 adsorption isotherms. The samples were heated at 120 °C and kept at this temperature for at least 20 hours under vacuum for activation. Ultra high purity grade (99.999 % purity) N_2, CO_2 and He, oil-free valves and gas regulators were used for all free space corrections and measurements. For all of the gas adsorption measurements, the temperatures were controlled by using a refrigerated bath of liquid N_2 (77 K).

6.7 References

(1) Cote, A. P.; Benin, A. I.; Ockwig, N. W.; O'Keeffe, M.; Matzger, A. J.; Yaghi, O. M. *Science* **2005**, *310*, 1166.

(2) Cote, A. P.; El-Kaderi, H. M.; Furukawa, H.; Hunt, J. R.; Yaghi, O. M. *J. Am. Chem. Soc.* **2007**, *129*, 12914.

(3) Feng, X.; Ding, X. S.; Jiang, D. L. *Chem. Soc. Rev.* **2012**, *41*, 6010.

(4) Furukawa, H.; Yaghi, O. M. *J. Am. Chem. Soc.* **2009**, *131*, 8875.

(5) Huang, N.; Chen, X.; Krishna, R.; Jiang, D. L. *Angew. Chem., Int. Ed.* **2015**, *54*, 2986.

(6) Ding, S. Y.; Dong, M.; Wang, Y. W.; Chen, Y. T.; Wang, H. Z.; Su, C. Y.; Wang, W. *J. Am. Chem. Soc.* **2016**, *138*, 3031.

(7) Ding, S. Y.; Gao, J.; Wang, Q.; Zhang, Y.; Song, W. G.; Su, C. Y.; Wang, W. *J. Am. Chem. Soc.* **2011**, *133*, 19816.

(8) DeBlase, C. R.; Silberstein, K. E.; Truong, T. T.; Abruna, H. D.; Dichtel, W. R. *J. Am. Chem. Soc.* **2013**, *135*, 16821.

(9) Zhou, T. Y.; Xu, S. Q.; Wen, Q.; Pang, Z. F.; Zhao, X. *J. Am. Chem. Soc.* **2014**, *136*, 15885.

(10) Yang, H. S.; Du, Y.; Wan, S.; Trahan, G. D.; Jin, Y. H.; Zhang, W. *Chem. Sci.* **2015**, *6*, 4049.

(11) Zhu, Y. L.; Wan, S.; Jin, Y. H.; Zhang, W. *J. Am. Chem. Soc.* **2015**, *137*, 13772.

(12) Xu, S. Q.; Zhan, T. G.; Wen, Q.; Pang, Z. F.; Zhao, X. *Acs Macro Lett* **2016**, *5*, 99.

(13) Pang, Z. F.; Xu, S. Q.; Zhou, T. Y.; Liang, R. R.; Zhan, T. G.; Zhao, X. *J. Am. Chem. Soc.* **2016**, *138*, 4710.

(14) Laughrey, Z. R.; Gibb, C. L. D.; Senechal, T.; Gibb, B. C. *Chem.-Eur. J.* **2003**, *9*, 130.

(15) de Miguel, G.; Wielopolski, M.; Schuster, D. I.; Fazio, M. A.; Lee, O. P.; Haley, C. K.; Ortiz, A. L.; Echegoyen, L.; Clark, T.; Guldi, D. M. *J. Am. Chem. Soc.* **2011**, *133*, 13036.

(16) Shi, H. P.; Xin, D. H.; Dong, X. Q.; Dai, J. X.; Wu, X. H.; Miao, Y. Q.; Fang, L.; Wang, H.; Choi, M. M. F. *J. Mater. Chem. C* **2014**, *2*, 2160.

(17) Chen, J. P.; Labarthet, F. L.; Natansohn, A.; Rochon, P. *Macromolecules* **1999**, *32*, 8572.

Bibliography

(1) Cote, A. P.; Benin, A. I.; Ockwig, N. W.; O'Keeffe, M.; Matzger, A. J.; Yaghi, O. M. *Science* **2005**, *310*, 1166.

(2) El-Kaderi, H. M.; Hunt, J. R.; Mendoza-Cortes, J. L.; Cote, A. P.; Taylor, R. E.; O'Keeffe, M.; Yaghi, O. M. *Science* **2007**, *316*, 268.

(3) Jiang, J. X.; Su, F.; Trewin, A.; Wood, C. D.; Campbell, N. L.; Niu, H.; Dickinson, C.; Ganin, A. Y.; Rosseinsky, M. J.; Khimyak, Y. Z.; Cooper, A. I. *Angew. Chem., Int. Ed.* **2007**, *46*, 8574.

(4) Cooper, A. I. *Adv. Mater.* **2009**, *21*, 1291.

(5) Cote, A. P.; El-Kaderi, H. M.; Furukawa, H.; Hunt, J. R.; Yaghi, O. M. *J. Am. Chem. Soc.* **2007**, *129*, 12914.

(6) Lino, M. A.; Lino, A. A.; Mazzoni, M. S. C. *Chem. Phys. Lett.* **2007**, *449*, 171.

(7) Babarao, R.; Jiang, J. W. *Energy Environ. Sci.* **2008**, *1*, 139.

(8) Han, S. S.; Furukawa, H.; Yaghi, O. M.; Goddard, W. A. *J. Am. Chem. Soc.* **2008**, *130*, 11580.

(9) Hunt, J. R.; Doonan, C. J.; LeVangie, J. D.; Cote, A. P.; Yaghi, O. M. *J. Am. Chem. Soc.* **2008**, *130*, 11872.

(10) Mastalerz, M. *Angew. Chem., Int. Ed.* **2008**, *47*, 445.

(11) Tilford, R. W.; Mugavero, S. J.; Pellechia, P. J.; Lavigne, J. J. *Adv. Mater.* **2008**, *20*, 2741.

(12) Zwaneveld, N. A. A.; Pawlak, R.; Abel, M.; Catalin, D.; Gigmes, D.; Bertin, D.; Porte, L. *J. Am. Chem. Soc.* **2008**, *130*, 6678.

(13) Campbell, N. L.; Clowes, R.; Ritchie, L. K.; Cooper, A. I. *Chem. Mater.* **2009**, *21*, 204.

(14) Cao, D. P.; Lan, J. H.; Wang, W. C.; Smit, B. *Angew. Chem., Int. Ed.* **2009**, *48*, 4730.

(15) Furukawa, H.; Yaghi, O. M. *J. Am. Chem. Soc.* **2009**, *131*, 8875.

(16) Gutzler, R.; Walch, H.; Eder, G.; Kloft, S.; Heckl, W. M.; Lackinger, M. *Chem. Commun.* **2009**, 4456.

(17) Ben, T.; Ren, H.; Ma, S. Q.; Cao, D. P.; Lan, J. H.; Jing, X. F.; Wang, W. C.; Xu, J.; Deng, F.; Simmons, J. M.; Qiu, S. L.; Zhu, G. S. *Angew. Chem., Int. Ed.* **2009**, *48*, 9457.

(18) Ren, H.; Ben, T.; Wang, E. S.; Jing, X. F.; Xue, M.; Liu, B. B.; Cui, Y.; Qiu, S. L.; Zhu, G. S. *Chem. Commun.* **2010**, *46*, 291.

(19) Yuan, Y.; Sun, F. X.; Ren, H.; Jing, X. F.; Wang, W.; Ma, H. P.; Zhao, H. J.; Zhu, G. S. *J. Mater. Chem.* **2011**, *21*, 13498.

(20) Dawson, R.; Laybourn, A.; Clowes, R.; Khimyak, Y. Z.; Adams, D. J.; Cooper, A. I. *Macromolecules* **2009**, *42*, 8809.

(21) Schmidt, J.; Werner, M.; Thomas, A. *Macromolecules* **2009**, *42*, 4426.

(22) Xu, Y. H.; Jin, S. B.; Xu, H.; Nagai, A.; Jiang, D. L. *Chem. Soc. Rev.* **2013**, *42*, 8012.

(23) Lu, W. G.; Yuan, D. Q.; Zhao, D.; Schilling, C. I.; Plietzsch, O.; Muller, T.; Brase, S.; Guenther, J.; Blumel, J.; Krishna, R.; Li, Z.; Zhou, H. C. *Chem. Mater.* **2010**, *22*, 5964.

(24) Lu, W. G.; Yuan, D. Q.; Sculley, J. L.; Zhao, D.; Krishna, R.; Zhou, H. C. *J. Am. Chem. Soc.* **2011**, *133*, 18126.

(25) Yuan, D. Q.; Lu, W. G.; Zhao, D.; Zhou, H. C. *Adv. Mater.* **2011**, *23*, 3723.

(26) Lu, W. G.; Sculley, J. P.; Yuan, D. Q.; Krishna, R.; Wei, Z. W.; Zhou, H. C. *Angew. Chem., Int. Ed.* **2012**, *51*, 7480.

(27) McKeown, N. B.; Makhseed, S.; Budd, P. M. *Chem. Commun.* **2002**, 2780.

(28) Budd, P. M.; Ghanem, B. S.; Makhseed, S.; McKeown, N. B.; Msayib, K. J.; Tattershall, C. E. *Chem. Commun.* **2004**, 230.

(29) McKeown, N. B.; Budd, P. M.; Msayib, K. J.; Ghanem, B. S.; Kingston, H. J.; Tattershall, C. E.; Makhseed, S.; Reynolds, K. J.; Fritsch, D. *Chem.-Eur. J.* **2005**, *11*, 2610.

(30) McKeown, N. B.; Budd, P. M. *Chem. Soc. Rev.* **2006**, *35*, 675.

(31) McKeown, N. B.; Budd, P. M.; Book, D. *Macromol. Rapid Comm.* **2007**, *28*, 995.

(32) Wood, C. D.; Tan, B.; Trewin, A.; Niu, H. J.; Bradshaw, D.; Rosseinsky, M. J.; Khimyak, Y. Z.; Campbell, N. L.; Kirk, R.; Stockel, E.; Cooper, A. I. *Chem. Mater.* **2007**, *19*, 2034.

(33) Jiang, J. X.; Su, F.; Trewin, A.; Wood, C. D.; Niu, H.; Jones, J. T. A.; Khimyak, Y. Z.; Cooper, A. I. *J. Am. Chem. Soc.* **2008**, *130*, 7710.

(34) Kuhn, P.; Antonietti, M.; Thomas, A. *Angew. Chem., Int. Ed.* **2008**, *47*, 3450.

(35) Rose, M.; Bohlmann, W.; Sabo, M.; Kaskel, S. *Chem. Commun.* **2008**, 2462.

(36) Fritsch, J.; Rose, M.; Wollmann, P.; Bohlmann, W.; Kaskel, S. *Materials* **2010**, *3*, 2447.

(37) Uribe-Romo, F. J.; Hunt, J. R.; Furukawa, H.; Klock, C.; O'Keeffe, M.; Yaghi, O. M. *J. Am. Chem. Soc.* **2009**, *131*, 4570.

(38) Chen, L.; Yang, Y.; Jiang, D. L. *J. Am. Chem. Soc.* **2010**, *132*, 9138.

(39) Yuan, S. W.; Dorney, B.; White, D.; Kirklin, S.; Zapol, P.; Yu, L. P.; Liu, D. J. *Chem. Commun.* **2010**, *46*, 4547.

(40) Dawson, R.; Adams, D. J.; Cooper, A. I. *Chem. Sci.* **2011**, *2*, 1173.

(41) Dogru, M.; Sonnauer, A.; Gavryushin, A.; Knochel, P.; Bein, T. *Chem. Commun.* **2011**, *47*, 1707.

(42) Kaur, P.; Hupp, J. T.; Nguyen, S. T. *ACS Catal.* **2011**, *1*, 819.

(43) Peng, Y.; Ben, T.; Xu, J.; Xue, M.; Jing, X. F.; Deng, F.; Qiu, S. L.; Zhu, G. S. *Dalton Trans.* **2011**, *40*, 2720.

(44) Rabbani, M. G.; El-Kaderi, H. M. *Chem. Mater.* **2011**, *23*, 1650.

(45) Zhao, H. Y.; Jin, Z.; Su, H. M.; Jing, X. F.; Sun, F. X.; Zhu, G. S. *Chem. Commun.* **2011**, *47*, 6389.

(46) Chen, Q.; Luo, M.; Hammershoj, P.; Zhou, D.; Han, Y.; Laursen, B. W.; Yan, C. G.; Han, B. H. *J. Am. Chem. Soc.* **2012**, *134*, 6084.

(47) Jin, Y. H.; Voss, B. A.; McCaffrey, R.; Baggett, C. T.; Noble, R. D.; Zhang, W. *Chem. Sci.* **2012**, *3*, 874.

(48) Konstas, K.; Taylor, J. W.; Thornton, A. W.; Doherty, C. M.; Lim, W. X.; Bastow, T. J.; Kennedy, D. F.; Wood, C. D.; Cox, B. J.; Hill, J. M.; Hill, A. J.; Hill, M. R. *Angew. Chem., Int. Ed.* **2012**, *51*, 6639.

(49) Berlanga, I.; Ruiz-Gonzalez, M. L.; Gonzalez-Calbet, J. M.; Fierro, J. L. G.; Mas-Balleste, R.; Zamora, F. *Small* **2011**, *7*, 1207.

(50) Choi, Y. J.; Choi, J. H.; Choi, K. M.; Kang, J. K. *J. Mater. Chem.* **2011**, *21*, 1073.

(51) Ding, X. S.; Guo, J.; Feng, X. A.; Honsho, Y.; Guo, J. D.; Seki, S.; Maitarad, P.; Saeki, A.; Nagase, S.; Jiang, D. L. *Angew. Chem., Int. Ed.* **2011**, *50*, 1289.

(52) Ding, X. S.; Chen, L.; Honsho, Y.; Feng, X.; Saenpawang, O.; Guo, J. D.; Saeki, A.; Seki, S.; Irle, S.; Nagase, S.; Parasuk, V.; Jiang, D. L. *J. Am. Chem. Soc.* **2011**, *133*, 14510.

(53) Ding, X. S.; Feng, X.; Saeki, A.; Seki, S.; Nagai, A.; Jiang, D. L. *Chem. Commun.* **2012**, *48*, 8952.

(54) Dogru, M.; Bein, T. *Nat. Nanotechnol.* **2011**, *6*, 333.

(55) Feng, X. A.; Chen, L.; Dong, Y. P.; Jiang, D. L. *Chem. Commun.* **2011**, *47*, 1979.

(56) Lanni, L. M.; Tilford, R. W.; Bharathy, M.; Lavigne, J. J. *J. Am. Chem. Soc.* **2011**, *133*, 13975.

(57) Lukose, B.; Kuc, A.; Heine, T. *Chem.-Eur. J.* **2011**, *17*, 2388.

(58) Colson, J. W.; Dichtel, W. R. *Nat. Chem.* **2013**, *5*, 453.

(59) Nagai, A.; Guo, Z. Q.; Feng, X.; Jin, S. B.; Chen, X.; Ding, X. S.; Jiang, D. L. *Nat Commun* **2011**, *2*, 536.

(60) Bunck, D. N.; Dichtel, W. R. *Chem.-Eur. J.* **2013**, *19*, 818.

(61) Uribe-Romo, F. J.; Doonan, C. J.; Furukawa, H.; Oisaki, K.; Yaghi, O. M. *J. Am. Chem. Soc.* **2011**, *133*, 11478.

(62) Zhang, Y. G.; Tan, M. X.; Li, H.; Zheng, Y. G.; Gao, S. J.; Zhang, H.; Ying, J. Y. *Chem. Commun.* **2011**, *47*, 7365.

(63) Du, Y.; Mao, K. M.; Kamakoti, P.; Ravikovitch, P.; Paur, C.; Cundy, S.; Li, Q. C.; Calabro, D. *Chem. Commun.* **2012**, *48*, 4606.

(64) Feng, X.; Ding, X. S.; Jiang, D. L. *Chem. Soc. Rev.* **2012**, *41*, 6010.

(65) Jiang, J. X.; Trewin, A.; Adams, D. J.; Cooper, A. I. *Chem. Sci.* **2011**, *2*, 1777.

(66) Dawson, R.; Laybourn, A.; Khimyak, Y. Z.; Adams, D. J.; Cooper, A. I. *Macromolecules* **2010**, *43*, 8524.

(67) Cheng, G.; Hasell, T.; Trewin, A.; Adams, D. J.; Cooper, A. I. *Angew. Chem., Int. Ed.* **2012**, *51*, 12727.

(68) Liu, X. M.; Zhang, Y. W.; Li, H.; Sigen, A.; Xia, H.; Mu, Y. *Rsc Adv* **2013**, *3*, 21267.

(69) Kuhn, P.; Forget, A.; Su, D. S.; Thomas, A.; Antonietti, M. *J. Am. Chem. Soc.* **2008**, *130*, 13333.

(70) Rabbani, M. G.; El-Kaderi, H. M. *Chem. Mater.* **2012**, *24*, 1511.

(71) Ren, S. J.; Bojdys, M. J.; Dawson, R.; Laybourn, A.; Khimyak, Y. Z.; Adams, D. J.; Cooper, A. I. *Adv. Mater.* **2012**, *24*, 2357.

(72) Yan, Z. J.; Ren, H.; Ma, H. P.; Yuan, R. R.; Yuan, Y.; Zou, X. Q.; Sun, F. X.; Zhu, G. S. *Micropor. Mesopor. Mat.* **2013**, *173*, 92.

(73) Spitler, E. L.; Colson, J. W.; Uribe-Romo, F. J.; Woll, A. R.; Giovino, M. R.; Saldivar, A.; Dichtel, W. R. *Angew. Chem., Int. Ed.* **2012**, *51*, 2623.

(74) Wood, C. D.; Tan, B.; Trewin, A.; Su, F.; Rosseinsky, M. J.; Bradshaw, D.; Sun, Y.; Zhou, L.; Cooper, A. I. *Adv. Mater.* **2008**, *20*, 1916.

(75) Zhou, H. C.; Long, J. R.; Yaghi, O. M. *Chem. Rev.* **2012**, *112*, 673.

(76) Wu, D. C.; Xu, F.; Sun, B.; Fu, R. W.; He, H. K.; Matyjaszewski, K. *Chem. Rev.* **2012**, *112*, 3959.

(77) Xiong, M.; Ding, H. M.; Li, B. J.; Zhou, T. L.; Wang, C. *Curr. Org. Chem.* **2014**, *18*, 1965.

(78) Liu, Q. Q.; Tang, Z.; Wu, M. D.; Zhou, Z. H. *Polym. Int.* **2014**, *63*, 381.

(79) Colson, J. W.; Woll, A. R.; Mukherjee, A.; Levendorf, M. P.; Spitler, E. L.; Shields, V. B.; Spencer, M. G.; Park, J.; Dichtel, W. R. *Science* **2011**, *332*, 228.

(80) Spitler, E. L.; Koo, B. T.; Novotney, J. L.; Colson, J. W.; Uribe-Romo, F. J.; Gutierrez, G. D.; Clancy, P.; Dichtel, W. R. *J. Am. Chem. Soc.* **2011**, *133*, 19416.

(81) Stuart, M. A. C.; Huck, W. T. S.; Genzer, J.; Muller, M.; Ober, C.; Stamm, M.; Sukhorukov, G. B.; Szleifer, I.; Tsukruk, V. V.; Urban, M.; Winnik, F.; Zauscher, S.; Luzinov, I.; Minko, S. *Nat. Mater.* **2010**, *9*, 101.

(82) Liu, F.; Urban, M. W. *Prog. Polym. Sci.* **2010**, *35*, 3.

(83) Kundu, P. K.; Olsen, G. L.; Kiss, V.; Klajn, R. *Nat Commun* **2014**, *5*, 3588.

(84) Luo, F.; Fan, C. B.; Luo, M. B.; Wu, X. L.; Zhu, Y.; Pu, S. Z.; Xu, W. Y.; Guo, G. C. *Angew. Chem., Int. Ed.* **2014**, *53*, 9298.

(85) Lyndon, R.; Konstas, K.; Ladewig, B. P.; Southon, P. D.; Kepert, C. J.; Hill, M. R. *Angew. Chem., Int. Ed.* **2013**, *52*, 3695.

(86) Park, J.; Yuan, D. Q.; Pham, K. T.; Li, J. R.; Yakovenko, A.; Zhou, H. C. *J. Am. Chem. Soc.* **2012**, *134*, 99.

(87) Yanai, N.; Uemura, T.; Inoue, M.; Matsuda, R.; Fukushima, T.; Tsujimoto, M.; Isoda, S.; Kitagawa, S. *J. Am. Chem. Soc.* **2012**, *134*, 4501.

(88) Yagai, S.; Kitamura, A. *Chem. Soc. Rev.* **2008**, *37*, 1520.

(89) Ercole, F.; Davis, T. P.; Evans, R. A. *Polym. Chem.* **2010**, *1*, 37.

(90) Murthy, N.; Campbell, J.; Fausto, N.; Hoffman, A. S.; Stayton, P. S. *Bioconjugate Chem* **2003**, *14*, 412.

(91) Dai, S.; Ravi, P.; Tam, K. C. *Soft Matter* **2008**, *4*, 435.

(92) Dimitrov, I.; Trzebicka, B.; Muller, A. H. E.; Dworak, A.; Tsvetanov, C. B. *Prog. Polym. Sci.* **2007**, *32*, 1275.

(93) Magnusson, J. P.; Khan, A.; Pasparakis, G.; Saeed, A. O.; Wang, W. X.; Alexander, C. *J. Am. Chem. Soc.* **2008**, *130*, 10852.

(94) Brantley, J. N.; Wiggins, K. M.; Bielawski, C. W. *Science* **2011**, *333*, 1606.

(95) Bandara, H. M. D.; Burdette, S. C. *Chem. Soc. Rev.* **2012**, *41*, 1809.

(96) Irie, M.; Kunwatchakun, D. *Macromolecules* **1986**, *19*, 2476.

(97) Berkovic, G.; Krongauz, V.; Weiss, V. *Chem. Rev.* **2000**, *100*, 1741.

(98) Minkin, V. I. *Chem. Rev.* **2004**, *104*, 2751.

(99) Dou, Y. S.; Hu, Y.; Yuan, S. A.; Wu, W. F.; Tang, H. *Mol. Phys.* **2009**, *107*, 181.

(100) Borisenko, V.; Burns, D. C.; Zhang, Z. H.; Woolley, G. A. *J. Am. Chem. Soc.* **2000**, *122*, 6364.

(101) Liu, N. G.; Chen, Z.; Dunphy, D. R.; Jiang, Y. B.; Assink, R. A.; Brinker, C. J. *Angew. Chem., Int. Ed.* **2003**, *42*, 1731.

(102) Kandambeth, S.; Mallick, A.; Lukose, B.; Mane, M. V.; Heine, T.; Banerjee, R. *J. Am. Chem. Soc.* **2012**, *134*, 19524.

(103) Biswal, B. P.; Chandra, S.; Kandambeth, S.; Lukose, B.; Heine, T.; Banerjeet, R. *J. Am. Chem. Soc.* **2013**, *135*, 5328.

(104) Wan, S.; Guo, J.; Kim, J.; Ihee, H.; Jiang, D. L. *Angew. Chem., Int. Ed.* **2008**, *47*, 8826.

(105) Wan, S.; Gandara, F.; Asano, A.; Furukawa, H.; Saeki, A.; Dey, S. K.; Liao, L.; Ambrogio, M. W.; Botros, Y. Y.; Duan, X. F.; Seki, S.; Stoddart, J. F.; Yaghi, O. M. *Chem. Mater.* **2011**, *23*, 4094.

(106) Dalapati, S.; Addicoat, M.; Jin, S. B.; Sakurai, T.; Gao, J.; Xu, H.; Irle, S.; Seki, S.; Jiang, D. L. *Nat Commun* **2015**, *6*, 7786.

(107) Ding, S. Y.; Gao, J.; Wang, Q.; Zhang, Y.; Song, W. G.; Su, C. Y.; Wang, W. *J. Am. Chem. Soc.* **2011**, *133*, 19816.

(108) Sai, H.; Tan, K. W.; Hur, K.; Asenath-Smith, E.; Hovden, R.; Jiang, Y.; Riccio, M.; Muller, D. A.; Elser, V.; Estroff, L. A.; Gruner, S. M.; Wiesner, U. *Science* **2013**, *341*, 530.

(109) Evans, J. D.; Sumby, C. J.; Doonan, C. J. *Chem. Lett.* **2015**, *44*, 582.

(110) Jin, Y. H.; Yu, C.; Denman, R. J.; Zhang, W. *Chem. Soc. Rev.* **2013**, *42*, 6634.

(111) Ning, Y.; Yang, Y.; Wang, C. Y.; Ngai, T.; Tong, Z. *Chem. Commun.* **2013**, *49*, 8761.

(112) Seo, M.; Kim, S.; Oh, J.; Kim, S. J.; Hillmyer, M. A. *J. Am. Chem. Soc.* **2015**, *137*, 600.

(113) Schnobrich, J. K.; Lebel, O.; Cychosz, K. A.; Dailly, A.; Wong-Foy, A. G.; Matzger, A. J. *J. Am. Chem. Soc.* **2010**, *132*, 13941.

(114) Wong-Foy, A. G.; Lebel, O.; Matzger, A. J. *J. Am. Chem. Soc.* **2007**, *129*, 15740.

(115) Xie, Y. B.; Yang, H.; Wang, Z. Y. U.; Liu, Y. Y.; Zhou, H. C.; Li, J. R. *Chem. Commun.* **2014**, *50*, 563.

(116) Fang, Z. L.; Bueken, B.; De Vos, D. E.; Fischer, R. A. *Angew. Chem., Int. Ed.* **2015**, *54*, 7234.

(117) Furukawa, H.; Muller, U.; Yaghi, O. M. *Angew. Chem., Int. Ed.* **2015**, *54*, 3417.

(118) Choi, K. M.; Jeon, H. J.; Kang, J. K.; Yaghi, O. M. *J. Am. Chem. Soc.* **2011**, *133*, 11920.

(119) Feng, X.; Dong, Y. P.; Jiang, D. L. *CrystEngComm* **2013**, *15*, 1508.

(120) Zhou, T. Y.; Xu, S. Q.; Wen, Q.; Pang, Z. F.; Zhao, X. *J. Am. Chem. Soc.* **2014**, *136*, 15885.

(121) Yang, H. S.; Du, Y.; Wan, S.; Trahan, G. D.; Jin, Y. H.; Zhang, W. *Chem. Sci.* **2015**, *6*, 4049.

(122) Ritchie, L. K.; Trewin, A.; Reguera-Galan, A.; Hasell, T.; Cooper, A. I. *Micropor. Mesopor. Mat.* **2010**, *132*, 132.

(123) Rouquerol, J.; Avnir, D.; Fairbridge, C. W.; Everett, D. H.; Haynes, J. H.; Pernicone, N.; Ramsay, J. D. F.; Sing, K. S. W.; Unger, K. K. *Pure. Appl. Chem.* **1994**, *66*, 1739.

(124) Zhou, D. D.; He, C. T.; Liao, P. Q.; Xue, W.; Zhang, W. X.; Zhou, H. L.; Zhang, J. P.; Chen, X. M. *Chem. Commun.* **2013**, *49*, 11728.

(125) Li, Z. P.; Feng, X.; Zou, Y. C.; Zhang, Y. W.; Xia, H.; Liu, X. M.; Mu, Y. *Chem. Commun.* **2014**, *50*, 13825.

(126) Jin, Y. H.; Voss, B. A.; Noble, R. D.; Zhang, W. *Angew. Chem., Int. Ed.* **2010**, *49*, 6348.

(127) Dawson, R.; Stevens, L. A.; Drage, T. C.; Snape, C. E.; Smith, M. W.; Adams, D. J.; Cooper, A. I. *J. Am. Chem. Soc.* **2012**, *134*, 10741.

(128) Stockel, E.; Wu, X. F.; Trewin, A.; Wood, C. D.; Clowes, R.; Campbell, N. L.; Jones, J. T. A.; Khimyak, Y. Z.; Adams, D. J.; Cooper, A. I. *Chem. Commun.* **2009**, 212.

(129) Spitler, E. L.; Dichtel, W. R. *Nat. Chem.* **2010**, *2*, 672.

(130) Xie, Z. G.; Wang, C.; deKrafft, K. E.; Lin, W. B. *J. Am. Chem. Soc.* **2011**, *133*, 2056.

(131) Feng, X.; Liu, L. L.; Honsho, Y.; Saeki, A.; Seki, S.; Irle, S.; Dong, Y. P.; Nagai, A.; Jiang, D. L. *Angew. Chem., Int. Ed.* **2012**, *51*, 2618.

(132) Zhang, C. X.; Wang, Q.; Long, H.; Zhang, W. *J. Am. Chem. Soc.* **2011**, *133*, 20995.

(133) Zhang, C. X.; Long, H.; Zhang, W. *Chem. Commun.* **2012**, *48*, 6172.

(134) Jyothish, K.; Zhang, W. *Angew. Chem., Int. Ed.* **2011**, *50*, 3435.

(135) Jyothish, K.; Wang, Q.; Zhang, W. *Adv. Synth. Catal.* **2012**, *354*, 2073.

(136) Yang, H. S.; Liu, Z. N.; Zhang, W. *Adv. Synth. Catal.* **2013**, *355*, 885.

(137) Zhang, W.; Moore, J. S. *Adv. Synth. Catal.* **2007**, *349*, 93.

(138) Wu, X. A.; Tamm, M. *Beilstein. J. Org. Chem.* **2011**, *7*, 82.

(139) Schrock, R. R.; Czekelius, C. *Adv. Synth. Catal.* **2007**, *349*, 55.

(140) Weber, J.; Schmidt, J.; Thomas, A.; Bohlmann, W. *Langmuir* **2010**, *26*, 15650.

(141) Zhu, Y. L.; Wan, S.; Jin, Y. H.; Zhang, W. *J. Am. Chem. Soc.* **2015**, *137*, 13772.

(142) Pang, Z. F.; Xu, S. Q.; Zhou, T. Y.; Liang, R. R.; Zhan, T. G.; Zhao, X. *J. Am. Chem. Soc.* **2016**, *138*, 4710.